DEVELOPMENT OF FERRITE BASED HETEROGENEOUS NANOCATALYSTS FOR ORGANIC TRANSFORMATIONS

A THESIS SUBMITTED TO

NATIONAL INSTITUTE OF TECHNOLOGY

WARANGAL

In partial fulfilment of the requirements for the award of degree of

DOCTOR OF PHILOSOPHY

IN

CHEMISTRY

BY

BANDA PRASHANTH GOUD

(Roll No. 719113)

Under the supervision of

Dr. MUCHERLA RAGHASUDHA

Assistant Professor

DEPARTMENT OF CHEMISTRY

NATIONAL INSTITUTE OF TECHNOLOGY

WARANGAL-506004, TELANGANA, INDIA,

(NOVEMBER -2023)

Dr. M. Raghasudha
Assistant Professor
Department of Chemistry
National Institute of Technology
Warangal - 506 004
Telangana, India

Mobile: +91-9550083100
Email: raghas13chem@nitw.ac.in

CERTIFICATE

This is to certify that the research work presented in this thesis entitled **"Development of Ferrite Based Heterogeneous Nanocatalysts for Organic Transformations"** submitted by **Mr. Banda Prashanth Goud** for the degree of Doctor of Philosophy in Chemistry, National Institute of Technology, Warangal (Telangana), under my supervision and that the same has not been submitted elsewhere for any degree.

Date: 29-11-2023
Place: NIT Warangal

Dr. M. Raghasudha
Thesis Supervisor

DECLARATION

I hereby declare that the matter embodied in this thesis entitled **"Development of Ferrite Based Heterogeneous Nanocatalysts for Organic Transformations"** is based entirely on the results of the investigations and research work carried out by me under the supervision of **Dr. M. Raghasudha**, Department of Chemistry, National Institute of Technology, Warangal. I declare that this work is original and has not been submitted in part or full, for any degree or diploma to this or any other University.

Date: 29-11-2023 (**Banda Prashanth Goud)**

Place: NIT Warangal

This Thesis is Dedicated
To My Beloved
Brother
Mr. Banda Praveen Goud

ACKNOWLEDGEMENTS

The work presented in this thesis would not have been possible without my close association with many people. I take this opportunity to express my heartfelt thanks and deep sense of gratitude to all the people mentioned here and others, whose names might have omitted unintentionally.

First and foremost, I would like to convey my sincere gratitude to my research supervisor ***Dr. M. Raghasudha***, Department of Chemistry, National Institute of Technology Warangal, for her invaluable knowledge and wise counsel. I have very much enjoyed the scientific freedom, excellent working conditions and an amicable atmosphere under her guidance. She has always been a pivotal and illuminating source of inspiration for me during the entire period of my research work and it has resulted in the form of my thesis. She gave me invaluable advice and never-ending support, and I will always be grateful to her.

I am greatly indebted to ***Prof. Bidyadhar Subudhi***, Director, National Institute of Technology Warangal, allowing me to submit my research work in the form of a thesis. I express my gratitude to ***Prof. N. V. Ramana Rao***, former Director, National Institute of Technology Warangal, for permitting me to carry out my research and for providing the required instrumentation facilities. I am really grateful for the financial assistance provided in the form of a fellowship from the Ministry of Education, Government of India.

I wish to thank the members of Doctoral Scrutiny Committee, NIT Warangal, ***Prof. D. Kashinath***, Chairman and Head, Department of Chemistry; ***Prof. A. Ramachandraiah*** (former member), Department of Chemistry; ***Dr. Raghu Chitta***, Department of Chemistry; ***Dr. S. Nagarajan***, Department of Chemistry; and ***Prof. N. Narasaih***, Department of Metallurgical and Materials Engineering, committee members for their thorough review, and helpful suggestions throughout the course of this research work.

My sincere thanks to ***Prof. P.V. Srilakshmi***, and ***Prof. Vishnu shanker***, Former Heads of Chemistry Department during the period of my research work. I would like to thank all the faculty members from Chemistry Department, ***Prof. B. Venkata Appa Rao (Retd), Prof. K. Laxma Reddy (Retd), Prof. V. Rajeswar Rao (Retd), Prof. K. V. Gobi***, ***Prof. N. Venkatathri***, ***Dr. K. Hari Prasad***, ***Dr. B. Srinivas, Dr. P. Santhosh***, ***Dr. CH. Jugun Prakash, Dr. Ravinder Pawar, Dr. Mukul Pradhan, Dr. Rajesh khanna Gaddam, Dr. V. Rajesh kumar,*** for their suggestions and encouragement.

I would like to convey my sincere gratitude to my teachers who helped to build my career from an early age, ***Dr. D. Nagaraju***, ***Mr. B. Sandeep***.

I would especially want to extend my heartfelt gratitude to my seniors, ***Dr. A. Bhargava sai***, ***Dr. T. Dhanunjay Rao, Dr. G. Sivaparvathi, Dr. A. Naveen Reddy, Mr. K. Narender, Dr. K. Vimal Kumar, Dr. S. Suresh, Dr. K. Vijender Reddy and Dr. G. Ambedkar*** for their unwavering support and motivation throughout every phase of my research effort.

I am highly thankful to my best friends ***Mrs. B. Ramya Reddy (Binnu), Ms. Aarti Gautam, Dr. M. Shireesha, Mr. K. Madhu,*** for being with me through all the good and bad times and for their everlasting support and encouragement throughout my studies.

It gives me great pleasure to thank my research group ***Mrs. B. Gayathri***, ***Mr. P. Kombaiah***, ***Mrs. G. Swathi*** for their help and kind cooperation.

The enduring moral support and unwavering affection that my friends and sisters have shown me over the years and during Ph. D, ***Mr. R. Naik, Mr. B. Anjaiah, Mr. Ch. Vijay, Ms. Sharanya, Mr. R. Arun kumar, Mr. R. Vara prasad, Mr. N. Nagaraju Yadav, Mr. B. Srikanth Goud, Mrs. B. Gayathri, Ms. Nitika, Ms. C. Shruthilaya, Ms. Khushboo Agarwala*** are gratefully acknowledged. Without the love, concern, and encouragement of these lovely friends, I would not have progressed this far.

Throughout these trying years, a lot of colleagues have supported me and kept me sane. I'm grateful for the jovial help from all of my research colleagues, whom I appreciate with great pleasure, ***Dr. Suman Chirra, Dr. T. Sanjeeva, Dr. K. Sujatha, Dr. K. Ramaiah, Dr. P. Vinay, Dr. K. Sathish, Dr. P. Sowmya, Dr. N. Satyanarayana, Dr. J. Parameshwara Chary, Dr. A. Varun, Dr. P. Babji, Dr. M. Srikanth, Dr. Ch. Raju, Mr. G. Srinath, Mr. G. Sripal Reddy, Mr. K. Sampath, Mrs. T. Shirisha, Mrs. B. Sravanthi, Mr. P. Venkatesham, Ms. Akanksha, Ms. Tohira Banoo, , Mr. Vijay, Mr. Subir, Ms. Sasi Sree, Ms. Pooja, Mr. Avinash Sharma, Mr. Akash, Mr. B. Apurba, Mr. Faizan, Mr. Arokiaraj. Mr. K. Ramakrishna, Mr. N. Sumit, Mr. B. Thirupathi, Mr. Anindya Roy, Mr. Yogendra Kumar, Mr. I. Madhu, Mr. K. Rambabu, Ms. Anshu Kari***, ***Ms. P. Amala***, ***Ms. Amulya, Mr. D. Ravinder*** and research scholars of various departments

My special thanks to non-teaching and technical supporting staff of chemistry department ***K. Sreenivas, P. S. Suni Kumar, G. Santhosh, Atanu Sahoo, P. Abhivardhan, A.***

Rajini, K. Keshavulu, J. Praveen, P. Heerulal, B. Sadanandam, T. Kiran Kumar, Ch. Ramesh Babu, Md. Shaheen begum, for their help in every time needed.

I wouldn't have come this far without the love, care, encouragement of some of the wonderful friends during my journey of life. I would like to thank each of them including ***Mr. Ankush, Mr. Ramesh, Mr. Shyam, Mr. Shiva, Mr. Linga, Mrs. Padhma, Mrs. Pranavi, Mr. Shekar, Mr. Sai Charan, Mr. Balu, Mr. Balesh, Mr. Basheer, Mr. Praveen, Mr. Naresh, Mr. Narsimlu, Mr. Laxman, Mr. Komresh, Mrs. Madhavi, Mr. Madhu, Mr. Kiran, Mr. Khadheer, Mr. Pavan, Mr. Bhasker***, ***Mr. Ahemed (Laddu)***, for lighting up my life with their friendship.

The greatest part about this acknowledgement is that it provides me with a special chance to express gratitude to my parents ***Late Shri. Banda Durga Goud*** and ***Smt. Banda Laxmi***, my beloved brother ***Mr. Banda. Praveen Goud,*** and sisters, ***Mrs. E. Pavani***, ***Mrs. A. Lahari,*** and ***Mrs. P. Sunitha.*** I am grateful to thank my grandparent***s Late Shri. B. Papa Goud*** *and* ***Late Smt. B. Ramulamma,*** because of whose love and sacrifice I have come this far. My sincere gratitude is extended to my family and friends for their unwavering love and support throughout my life and academic endeavours.

(Banda Prashanth Goud)

ABBREVIATIONS & SYMBOLS

Ag(OAc)	:	Silver(I) acetate
$AgNO_3$	:	Silver(I) nitrate
Ag_2O	:	Silver(I) oxide
Ag_2CO_3	:	Silver(I) carbonate
AcOH	:	Acetic acid
AO	:	Ammonium oxalate
cm	:	Centimetre
CB	:	Conduction Band
$CDCl_3$	:	Deuterated chloroform
CH_2Cl_2	:	Dichloromethane
CH_3CN	:	Acetonitrile
Cs_2CO_3	:	Cesium carbonate
$Cu(OAc)_2.H_2O$	:	Copper(II) acetate
Cu_2O	:	Copper(I) oxide
DMF	:	N,N-Dimethylformamide
DMSO	:	Dimethyl sulfoxide
DMSO-d_6	:	Deuterated dimethyl sulfoxide
EtOAc	:	Ethyl acetate
EtOH	:	Ethanol
EDAX	:	Energy Dispersive X-ray Spectroscopy
$Fe(NO_3)_3.9H_2O$	:	Iron(III) nitrate nonahydrate
$FeCl_2.\ 4H_2O$	:	Iron(II) chloride tetrahydrate
FE-SEM	:	Field Emission-Scanning Electron Microscopy
FT-IR	:	Fourier Transform Infra-Red
g	:	Grams
H_2O	:	Water
HNO_3	:	Nitric acid
HZ	:	Hertz
h	:	Hour
ICP-OES	:	Inductively coupled plasma optical emission spectroscopy
J	:	Coupling constant
K_2CO_3	:	Potassium carbonate

$K_2S_2O_8$	:	Potassium persulfate
MeOH	:	Methanol
mg	:	Milligram
min	:	Minutes
mL	:	Millilitre
mmol	:	Milli mole
µL	:	micro Litre
M	:	Molarity
mM	:	milli Molar
MW	:	Microwaves
nm	:	Nanometre
$N_2H_4.H_2O$	:	Hydrazine Hydrate
Na_2CO_3	:	Sodium carbonate
$NaBH_4$	:	Sodium borohydride
NaOAc	:	Sodium acetate
NaOH	:	Sodium hydroxide
$Ni(NO_3)_2.\ 6H_2O$	:	Nickel(II) nitrate hexahydrate
NMR	:	Nuclear Magnetic Resonance
NHE	:	Normal Hydrogen Electrode
pH	:	Potential of hydrogen
$PdCl_2$	:	Palladium(II) chloride
$Pd(OAc)_2$	:	Palladium(II) acetate
PXRD	:	Powder X-ray Diffraction
PDA	:	Polydopamine
RT	:	Room temperature
R	:	Reflectance
s	:	Singlet
SEM	:	Scanning Electron Microscopy
t	:	Triplet
TiO_2	:	Titanium dioxide
TTIP	:	Titanium tetraisopropoxide
TLC	:	Thin Layer Chromatography
TMS	:	Tetramethylsilane
TEM	:	Transmission Electron Microscopy

UV-Vis DRS	:	Ultra violet-Visible Diffuse Reflectance Spectroscopy
VB	:	Valence Band
VSM	:	Vibrating Sample Magnetometer
W	:	Watts
XPS	:	X-Ray Photoelectron Spectroscopy
Å	:	Angstrom
θ	:	Theta (Angle)
λ	:	Lambda (Wavelength)
β	:	Beta
eV	:	Electron volt
ε	:	Epsilon
υ	:	Nu
^{o}C	:	Degree centigrade
K	:	Kelvin
k	:	Degradation rate constant
KOe	:	Kilooersted
h^{+}	:	Hole
e^{-}	:	Electron
$O_2^{\bullet-}$	:	Superoxide anion radical
$^{\bullet}OH$	:	Hydroxyl radical

CONTENTS

Table of Contents

CHAPTER-I

Introduction

Chapter-I

Introduction

1.1. Background

In synthetic organic chemistry, catalysis plays a significant role in organic transformations synthesizing novel compounds with a wide range of applications that benefit society such as the production of medicines, vitamins, other nutritious products, cosmetics, polymers, plastics, high-energy fuels, and high-tech materials, etc. Researchers are attempting to develop novel catalysts, that either have advantages over currently available catalytic systems or that can be utilized to improve developing processes in terms of cost-effectiveness and reaction ease. In the past several decades, many catalysts have been developed for organic transformations. Despite great success in achieving this, there are a few challenges such as loss of catalytic activity over usage cycles, leaching of the active species of the catalyst under harsh reaction conditions, non-recovery of the catalyst and its non-reusability, usage of toxic solvents, inadvertent production of byproducts, use of expensive chemicals, high reaction temperatures, more reaction time, etc. To address these challenges, innovative catalytic systems are highly demanding. Innovative catalytic systems are the new catalysts and processes that reduce energy consumption and minimize environmental pollution in chemical synthesis and thus follow the principles of Green Chemistry. It is well-established that catalysts in nano size show enhanced efficiency and activity as they offer a large surface area for the reaction to occur. Hence, in recent years, researchers made significant advances in the development of nanocatalysts and nanocatalysis, which has emerged as an important research area.[1]

1.1.1. Nanocatalysis for organic synthesis

Green chemistry is one of the major areas of applied significances for catalysis, which is the scientific discipline that aims to generate products and minimize the production of hazardous substances. Catalysis has recently been recognized as an advanced field of study with established concepts and explanations. The design and development of new catalytic systems is achieving the sustainable goals of environmental protection and economic benefit. Researchers are working toward designing new catalysts that either outperform already available catalytic systems or can be used to enhance newly developing processes in terms of cost effectiveness and reaction ease. Nanocatalysts (catalysts in the nanoscale range ~1-100 nm in at least one dimension) have unique features due to the electronic and structural changes that set them apart from bulk materials. They show enhanced efficiency and activity as they offer a large surface area for the reaction to occur and are essential for sustainable and green

chemistry. Nanocatalysts facilitates the use of green reagents, solvent free reaction conditions, ambient reaction conditions, catalyst's reusability and avoid the use of toxic chemicals, needs less reaction time. These characteristics of the nanocatalysts have resulted in their wide range of applications in several organic transformations.[2,3] Furthermore, it is prevalent that these nanocatalysts provide straightforward, ecofriendly processes for various synthetic organic transformations with enhanced yields and selectivity.[4,5] In last few years, numerous nanocatalysts have emerged for various organic transformations.[6,7,8]

1.1.2. Need for heterogeneous nanocatalyst

It is well-known fact that, a homogeneous catalyst shows good activity, good stability due to its complete solubility in the medium. However, on industrial scale, homogeneous catalysts are considered to be expensive as they are associated with laborious work-up procedure thus minimizing their scope. Besides this, it is difficult to separate and recover the catalyst from the reaction mixture due to its contamination by products or formation of metal-complexes. Thus, it increases the economic cost and environmental pollution. To overcome these limitations, researchers have explored different strategies and the use of heterogeneous catalyst systems appears to be the most effective one. Recoverability and reusability of the homogeneous catalyst without affecting its active catalytic sites can be achieved by supporting the catalyst on NPs. It is also realized that the heterogeneous catalyst is less efficient relative to homogeneous catalyst, but it can be recovered by simple filtration and centrifugation. Thus, heterogeneous nanocatalysts are preferred over homogeneous nanocatalysts.

1.1.3. Need for heterogeneous magnetic nanocatalyst

Filtration is not advisable for nanocatalysts because the small size nanoparticles (NPs) pass through filter paper whereas centrifugation is not an economic process. But, one of the key aspects of the sustainable approach is the recovery of expensive catalysts after their use, enabling the catalyst to be reused after recovery. Magnetic separation is an alternative recovery method to the filtration and centrifugation, which is effective in terms of time, energy, and efficiency of catalysis as mentioned in **Table 1.1.**[9] Magnetic separation results in the efficient recovery of the catalyst for further use and enhances the catalyst's ability to be used as green catalysts. Hence, utilization of magnetically retrievable nanocatalyst (magnetic nanocatalyst-MNC) in synthetic organic chemistry has been extensively researched in recent years.

Table 1.1 *Difference among various recovery methods*

RECOVERY METHODS	HIGH EFFICIENCY	LOW ENERGY CONSUMPTION	LOW TIME CONSUMPTION
FILTRATION 	✗	✓	✗
CENTRIFUGATION 	✓	✗	✓
MAGNETIC SEPARATION 	✓	✓	✓

Hence, the development of heterogeneous MNC is one of the best innovative catalytic system with a sustainable greener approach in synthetic organic chemistry for a variety of chemical transformations. Currently, they have gained considerable attention in organic synthesis which confirms to the principles of green chemistry such as low reaction time, high product yield, atom economy of the reaction, recovery and recyclability of the catalyst. The catalyst in the form of magnetic NPs (MNPs) either can directly catalyse the organic transformation or can assist as a good support for the immobilization of active catalyst.

Figure 1.1. *Schematic of magnetic separation of the catalyst*

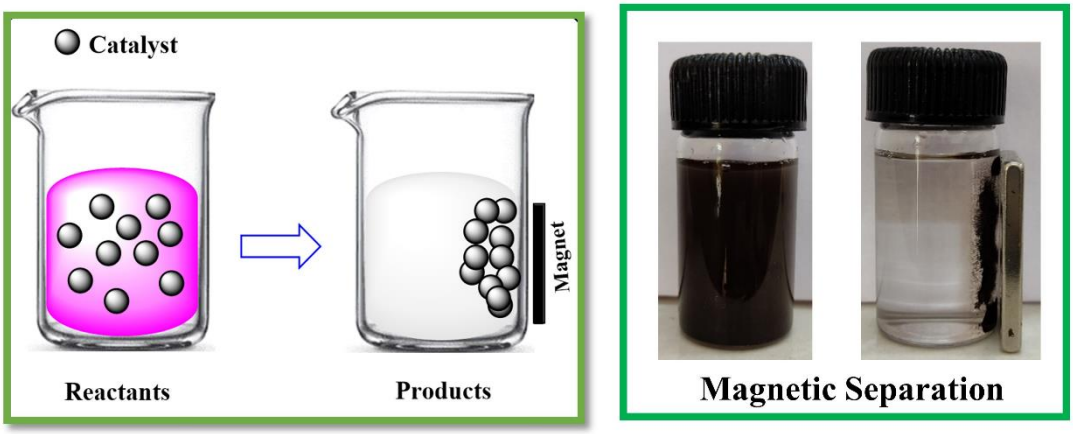

MNPs are best suited to support the active catalyst over its surface due to their high surface/mass ratio and easy dispersion in the reaction mixture. Due to large surface area, the contact between substrate and catalyst increases to a large extent and achieves reaction rate close to homogeneous counterpart. The added advantage of MNPs is their easy separation from

the reaction mixture using moderate magnetic field produced by simple external magnet. On laboratory scale, an inexpensive permanent magnet is enough for magnetic recovery, whereas electromagnet can be deployed on large scale.[10] Just keeping the magnet externally on to the MNPs allows to hold back the catalyst and decant the reaction mixture for further workup procedure as shown in the **Figure 1.1.** The separated catalyst can be reused as long as it is active.

Over the past several years, development of ferrite NPs supported catalysts have gained great attention in the field of magnetic nanocatalysis due to the excellent magnetic property of ferrite NPs.[11] These are iron-oxide based materials with low cost, easy method of preparation,[12] good stability over wide range of conditions. Additionally, the strong thermal and chemical stability,[13] broad surface area,[14] and mild magnetization of ferrite NPs with spinel structure make them ideal catalytic supports in the development of MNC for a particular application in organic synthesis.[15] Thus, ferrite based heterogeneous nanocatalysts became the fascinating materials in organic transformations.

1.1.4. Ferrites and ferrite based materials as heterogeneous magnetic nanocatalyst

1.1.4.1. Ferrites and their magnetic properties

As on date, ferrite NPs are the most explored MNPs and are of great interest in a variety of applications. Ferrites are mixed metal oxides comprising of iron (III) oxides as their key component. They crystallize into three forms *viz.*,

- Spinel ferrite (MFe_2O_4)
- Hexagonal ferrite ($MFe_{12}O_{19}$)
- Garnet ferrite ($M_3Fe_5O_{12}$)

where M stands for bivalent transition metal (Fe, Cu, Zn, Ni, Co, Mn, etc.)

Among all these, spinel ferrites are gaining recognition due to their attractive properties and applications. Moreover, majority of important ferrites that have extraordinary applications are spinel ferrites as shown in **Figure 1.2**

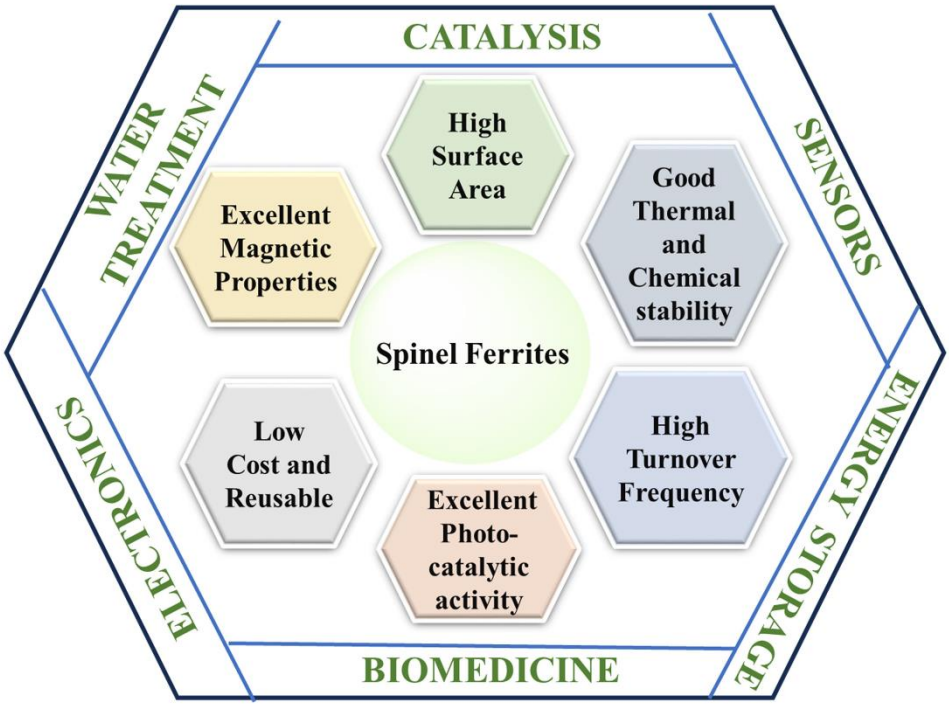

Figure 1.2 *Properties and applications of spinel ferrites*

The general formula for substances that crystallize in the spinel structure is AB_2O_4 where 'A' represents tetrahedral and 'B' represents octahedral cation sites respectively and 'O' represents oxygen anion site. Thus, spinel ferrites are represented with the general formula MFe_2O_4 where M is Fe, Mn, Co, Ni, Cu, Zn, Cd, Mg, a divalent metal cation. The spinel ferrites' unit cell belongs to the cubic structure with a space group Oh7-F3dm. There are two different types of interstitial spaces between the oxygen anions, namely tetrahedrally co-ordinated A sites (that are surrounded by 4 oxygen ions) and octahedrally coordinated B sites (that are surrounded by 6 oxygen ions), as shown in the face-centered cubic arrangement of the oxygen anions in the **Figure 1.3.**[16]

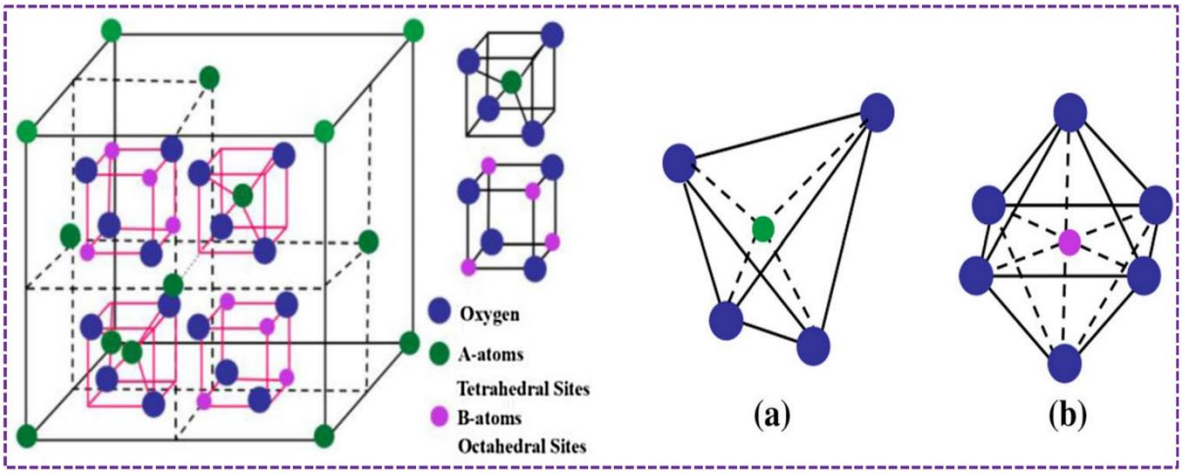

Figure 1.3 *Structure of spinel ferrites a). tetrahedrally coordinated A sites b). octahedrally coordinated b sites*

For the past few decades, Ferrite NPs (spinel ferrites-MFe_2O_4, M=divalent metal ions**,** such as Fe, Cu, Zn, Ni, Co, Mn, etc**.**) in bare unmodified form as such have gained attention. It is found that they have been used in diverse applications as shown in the **Figure 1.2** due to their extraordinary magnetic and photocatalytic properties, less cost, good stability, and high surface area. There are eight formula units of MFe_2O_4 in a unit cell. Thus, unit cell of a spinel ferrite contains 32 oxygen ions (O^{2-}) , 16 trivalent iron ions (Fe^{3+}) and 8 divalent metal cations (M^{2+}). A total of 24 metal cations (16 Fe^{3+} and 8 M^{2+}) are distributed into tetrahedral (A) sites and octahedral (B) sites. In a single unit cell of 32 oxygen anions, there are 64 A sites and 32 B sites available for cations and are partially populated by Fe^{3+} and M^{2+} ions. It turns out that, of the 64 A sites only 8 are occupied and of 32 B sites only 16 are occupied.[17] The general cation distribution in spinel ferrites can be represented as[18]

$$[M_{1-i}Fe_i]^A[M_iFe_{2-i}]^BO_4$$

Where M = divalent cation which shares A and B sites with Fe^{3+} cation and i = inversion parameter. Inversion parameter depends on the type of constituents in the ferrites and method of synthesis. Spinel ferrites can be divided into three categories according to the distribution of metal cations between the A and B sites, which is dependent on the degree of inversion.

i. When i = 0, they are named as **normal spinel** where divalent cations (M^{2+}) reside in A sites and trivalent cations (Fe^{3+}) occupy B sites with the structural formula $[M]^A[Fe_2]^BO_4$
   Ex: $ZnFe_2O_4$, $CdFe_2O_4$

ii. When i = 1, they are named as **inverse spinel** where M^{2+} occupy B sites and one half of the Fe^{3+} occupy B sites and other half of the Fe^{3+} occupy A sites with the structural formula $[Fe]^A[MFe]^BO_4$
   Ex: Fe_3O_4, $CoFe_2O_4$, $NiFe_2O_4$, $CuFe_2O_4$, $MgFe_2O_4$

iii. When 0<i<1, they are named as **mixed spinel** where the M^{2+} and Fe^{3+} are spread on both A and B sites
   Ex: $MnFe_2O_4$

Most important properties of ferrites includes high magnetic permeability, low magnetic loss and high electrical resistance. Various properties of ferrites which make them a good catalytic support are low cost, hardness, chemical stability, and good magnetic property. Important property of ferrites is ferrimagnetism due to the exchange phenomenon between metal

electrons and oxygen ions. That is there is a net magnetic moment at molecular level as a result of electronic exchange between metal and oxygen ions called as super exchange. A ferrimagnetic material does not lose its magnetism even in the absence of external magnetic field. In ferrimagnetic materials atoms have opposing magnetic field strengths/moments, but they are unequal. Thus, there exists some net magnetic moment.

A very good characteristic feature of ferrite is that its composition can be modified by keeping the basic crystalline structure same. This enables the retention of structural properties and enhancement of other properties by modifying the composition. This property of ferrites enables us to use them as good catalyst supports and allow for surface functionalization for a specific catalytic activity. Thus, in the design of different ferrite supported heterogeneous catalysts, unique magnetic and structural properties such as good chemical stability of ferrites plays a pivotal role.[19]

1.1.4.2. Ferrites as heterogeneous magnetic nanocatalyst

Recent past reports have emerged suggesting that spinel nanoferrites including magnetite (Fe_3O_4) have been extensively used as efficient magnetic nanocatalysts in the field of heterogeneous catalysis for various organic transformations as shown below in **Figure 1.4**

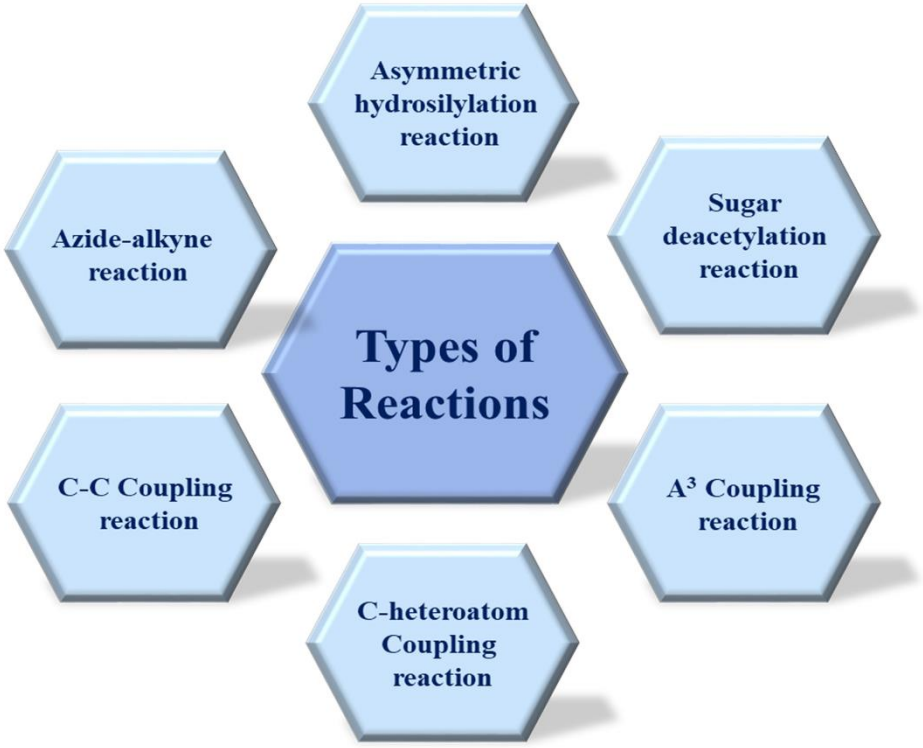

Figure 1.4 *Application of spinel ferrites in various organic transformations*

The catalytic activity of spinel ferrites in various reactions can be attributed to several factors as described below,

High surface area: Spinel ferrites often possess a high surface area due to their porous structure and fine particle size.[20] This increased surface area provides more active sites for catalytic reactions to occur.

Redox properties: Spinel ferrites can undergo redox reactions, where they can alternate between different oxidation states of the metal cations.[21] This redox behaviour is crucial for catalyzing oxidation and reduction reactions in organic transformations

Lewis acid/base sites: The metal cations in spinel ferrites can act as Lewis acid or base sites, which are important for facilitating various catalytic reactions. Following is an example where $ZnFe_2O_4$ catalyst has a dual role: Lewis acid site (activating isatin carbonyl oxygen) and Lewis base site (base proton abstraction of O^{2-} ions).[22]

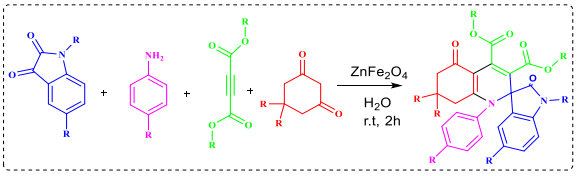

Synergistic effects: Spinel ferrites often consist of multiple metal cations in their structure. The interaction between different metal cations can create synergistic effects that enhance the catalytic activity and selectivity of the material.[23]

Magnetic properties: The magnetic nature of spinel ferrites can influence the reaction kinetics through magnetic stirring or by promoting interactions between the catalyst and reactants

Adsorption capability: The porous structure of spinel ferrites can facilitate the adsorption of reactants onto the catalyst surface, promoting their interaction and enhancing reaction rates

Stability and reusability: Spinel ferrites are generally stable under a wide range of reaction conditions, and their magnetic properties can make separation and recovery of the catalyst relatively easy, enabling their reuse in catalytic reactions

Tunable properties: Ferrites have tunable size and shape which can be achieved by adjusting the composition of the ferrite and synthesis methods. The morphology and size of ferrites will greatly influence the catalytic activity of the materials when used as catalysts. Thus enables the design of catalysts with specific activity and selectivity.[24]

1.1.4.3. Literature on unmodified ferrites and mixed ferrites for catalytic applications

Many research groups have synthesized efficient and magnetically reusable $CuFe_2O_4$ as a catalyst for various applications such as production of β, γ-unsaturated ketones from acid chloride and allyl bromide/cinnamyl chloride,[25] oxidation of alkenes to epoxide or aldehyde,[26] C-O coupling in Ullmann reaction with aryl halides and phenols. The oxidative coupling reaction with an aryl halide is said to be made easier by Cu(II) being more active than Cu(I) in

$CuFe_2O_4$.[27] It was used as a catalyst for the generation of derivatives of α-aminonitrile using condensation of different aldehydes with amines, trimethyl silyl cyanides[28]. It was also used as a ligand free magnetically reusable catalyst for the synthesis of carbonyl compounds through oxidative decarboxylation of phenyl acetic acid.[29]

$NiFe_2O_4$ as a catalyst was developed by many research groups for water gas shift reaction in industry,[30] Claisen-Schmidt condensation between acetyl ferrocene and various aldehydes,[31] synthesis of polyhydro quinoline derivatives.[32]

$CoFe_2O_4$ was synthesised as a magnetically recoverable nanocatalyst for aldol condensation of different aromatic aldehydes and acetophenone derivatives,[33] for the oxidation of primary and secondary aliphatic alcohols to produce corresponding carbonyl compounds using Oxone as oxidising agent in the presence of water.[34] It was also used for C-O bond formation from aryl halides and phenol derivatives.[35] $CoFe_2O_4$ was also developed as photocatalyst for the degradation of methylene blue (MB) and Erythrosin B.[36] There were many other unmodified ferrites used as catalysts for different organic application and photocatalytic applications.[15]

Many mixed ferrites were also used as catalysts/photocatalysts for different reactions. To name few, $CoMn_{0.2}Fe_{1.8}O_4$ for the generation of aromatic amines from nitroarenes and the reaction was studied by UV-visible spectroscopy[37] and $Co_xZn_{1-x}Fe_2O_4$,[38] $CoMn_xFe_{2-x}O_4$,[39] $Ni_xMn_{1-x}Fe_2O_4$,[40] were developed by different synthesis methods as mixed ferrite photocatalysts for the degradation of MB under different reaction conditions.

1.1.4.4. Modified ferrite based materials as heterogeneous magnetic nanocatalyst

As mentioned above, bare magnetic spinel ferrites can be used as such for numerous applications such as catalysts for organic transformations and photocatalysts for dye degradation and organic reactions. Sometimes, due to the instability and hydrophobic behaviour of bare magnetic NP's, they try to agglomerate in the absence of any surface coating. This results in decrease in surface energy with subsequent reduction in its activity for a specific application. So as to impart stability to magnetic NPs during their use or after their usage in organic transformations, surface functionalization with organic or inorganic materials is the best suggested and reported method.[41,42] Thus, surface functionalization of nanoferrites is an important step in the development of nanosystems for diverse applications. Because it reveals the intended use and enables the regulation of the physical and chemical processes at the surface due to synergistic effect of ferrite and modifier, which can be used to tune a number of magnetic, optical, and electrical properties of ferrites.

It can be done by *in situ* functionalization of synthesized ferrite NPs or post synthetic surface functionalization of obtained ferrite NPs depending on the type of synthesis method used. The presence of surface transition metal d-orbitals function as Lewis acids in the presence of donor ligands. It is a key characteristic that enables surface functionalization of the ferrite with polymers, ligands, carbonaceous materials, siliceous materials etc. and thus act as best catalytic support.[43] The advantages of surface modification of ferrites and use of surface modified ferrites in chemical catalysis and photocatalysis for various applications is shown schematically in the **Figure 1.5.**

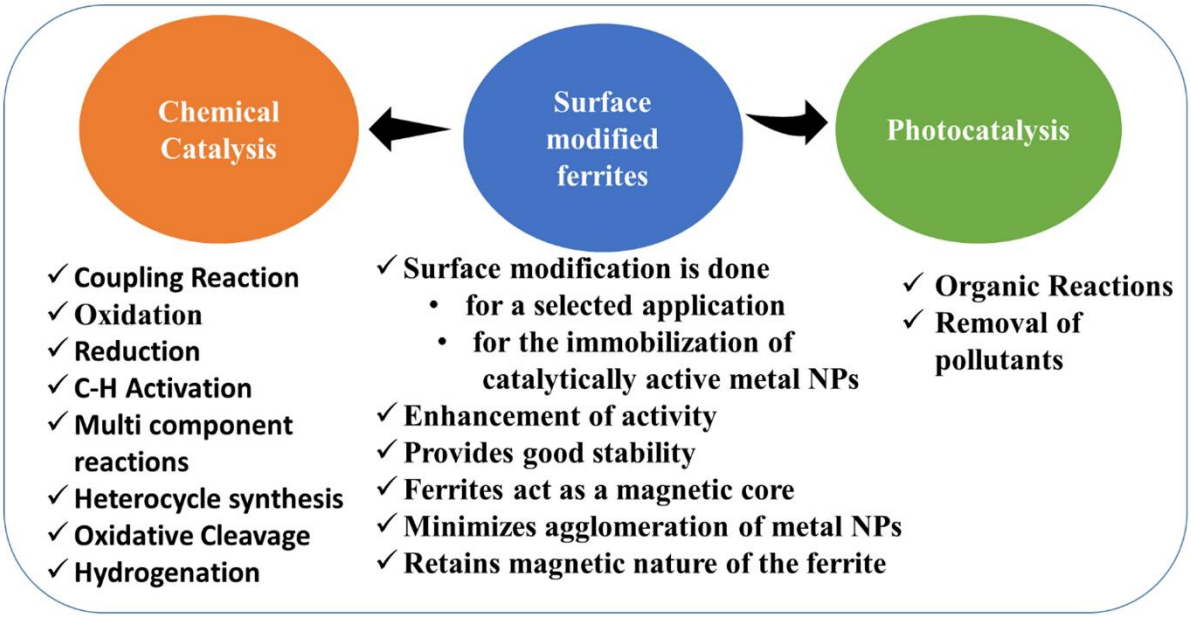

Figure 1.5 *Surface modified ferrites for chemical and photocatalysis*

Reports say that the surface modification of nanoferrites is done to immobilize catalytically active metal NPs that are usually expensive, non-separable and moreover undergo agglomeration thus decreasing the catalytic activity. In such cases, ferrites act as a best solid support and also a magnetic core of the catalyst making the recovery of the catalyst easy. In recent reports, the surface modification of the nanoferrites was performed with ligands with subsequent immobilization of metal NPs on its surface to deploy them as efficient heterogeneous magnetic nanocatalysts for organic transformations.[44,45,46]

Thus, the modification/functionalization of ferrite NPs can be achieved by following ways to attain wide range of applications and selective activity.

i. By immobilisation of various active metals

ii. Supporting various ligands on its surface to synthesize important chemical compounds

iii. Immobilization of metal NPs on surface of ferrite NPs via linkers and ligands

iv. Formation of ferrite core-shell materials using other surface modifiers

Modification of surface of spinel ferrite NPs with other active nanometals is of interest for catalysis because it enhances the catalytic activity and selectivity. This can be achieved by direct immobilization of active metal NPs on its surface.

1.1.4.5. Literature on surface functionalization of spinel ferrites

In the area of heterogeneous catalysis, ferrite-based catalysts with ferrite as a support are evolving as more and more useful materials for the establishment of sustainable procedures. This method has made it possible to perform a wide variety of organic transformations, such as C-C, C-S, and C-O coupling reactions, alkylation and oxidation processes, asymmetric synthesis, Mannich type reactions, and others.

Many research groups have developed active metal immobilized spinel nanoferrites as catalysts to enhance their activity for a specific application. To mention few reports, Pd substituted $ZnFe_2O_4$ for Heck and Suzuki cross coupling reactions under ligand free circumstances,[47] Pd-$NiFe_2O_4$ for Sonogashira cross coupling reactions,[48] Fe_3O_4-Ni for the reduction of carbonyl and nitro compounds,[49] Cu-$NiFe_2O_4$ for the preparation of aryl amines from nitroarenes mediated by $NaBH_4$.[50] For the first time, Ni-$CoFe_2O_4$ was used in the C-O coupling reaction between phenol derivatives and aromatic halides,[35] and Pd-$CoFe_2O_4$ was developed for Suzuki coupling reaction without ligand.[51] There are plenty of active metal immobilized spinel ferrites reported with enhanced activity and selectivity in organic transformations. Besides this, to make the catalyst selective and active for a specific organic transformation the alteration can be adopted in the catalyst at the selection of nanoferrite and at the selection of metal NPs. Fe_3O_4-Pd was prepared for carbonylative Sonogashira coupling reaction,[52] Fe_3O_4-Ni for reduction of nitro aromatic compounds,[49] Fe_3O_4-Co for oxidation of alcohols,[53] Fe_3O_4-CuO for Manich type of reaction,[54] Fe_3O_4-PdO for cross coupling Suzuki-Miyaura reaction,[55] Fe_3O_4-Ru_2O_3 for alkylation of aromatic amines and synthesis of aromatic imines.[56]

To enhance the effective binding, post synthetic modifications using organic ligands[57] and other materials is done which allow the effective adsorption of active metal NPs that result in enhanced reactivity compared to the corresponding homogeneous catalyst.[58] To name few such nanocatalysts, Fe_3O_4@Guanidine-Pd was reported as an efficient catalyst for Suzuki-Miyaura cross coupling reactions of aryl halides using phenyl boronic acid,[41] nanoferrite-glutathione was used for Paal-Knorr reaction for the synthesis of aryl, alkyl and heterocyclic amines.[59] Nano-FeDOPACu bimetallic catalyst was used for C-S coupling of Aryl halides

with thiophenol[60] whereas by changing the anchoring ligand from dopamine to glutathione it results to form NanoFe-GT-Cu. It was observed to show activity for the Huisgen cycloaddition (azide alkyne cycloaddition) reaction.[61] Nano-Fe_3O_4-DOPA-SnO_2 was used as heterogeneous magnetically recoverable catalyst for greener synthesis of dihydroquinazolinone derivatives using water as a solvent.[62] Fe_3O_4@SiO_2-Ru was developed for hydration of nitriles,[63] mesoporous silica supported iron oxide NPs for oxidation of alkene using H_2O_2 in aqueous medium.[64] Immobilization of Ru(II) complex was done on Fe_3O_4 support for asymmetric hydrogenation of aromatic ketones with high activity and enantioselectivity and Fe_3O_4-DOPA-Pd was used for hydrogenation reactions.[65] By changing the ferrite support to $NiFe_2O_4$ in the above catalyst with the same linker dopamine, the resulting catalyst $NiFe_2O_4$-DOPA-Pd worked very well for Suzuki and Heck C-C coupling reactions.[66] A research group have developed various catalysts by immobilization of various metals like Ni, Pd, Ru on Fe_3O_4 using dopamine as linker and explored its applications.[67] From the literature, it is also understood that activity can be changed by altering the anchoring ligand for the immobilisation of NPs over magnetic nanoferrite surface and the catalyst can be made selective for a specific organic transformation.

Further, in designing new catalytic systems, ferrites can be considered as magnetic core over which other inorganic or polymer is coated as a shell for further immobilisation of metal NPs resulting in core-shell materials as catalysts to meet the diverse applications. The choice of core and shell materials depends on the final application. Types of ferrite core@shell nanomaterials are ferrite@ferrite, ferrite@silica, ferrite@titania, perovskite@ferrite, ferrite@metal, ferrite@polymer. These different types of ferrite core@shell nano materials can be used for catalysis, biomedical applications, water purification, photocatalysis, sensors, etc. Many ferrite@core shell nanostructured materials were reported for desired applications.[68]

Based on the latest development in the field of catalysis, it is worth noting that ferrite based nanocatalysts is a growing field of research with green chemical approach in organic synthesis and transformations. It is reported and realized that the future lies in the design and development of novel magnetically recoverable, heterogeneous nanocatalyst supported on spinel ferrite/Fe_3O_4 NPs system with outstanding applications in organic synthesis.

1.1.4.6. Photocatalytic applications of nanoferrites

Another important observation from the above-mentioned literature is that spinel ferrites have low band gap and thus behave as good semiconductors. Hence, they find applications in photocatalysis as photocatalysts.[69,70] The magnetic nanoferrites show good potential in the photocatalytic degradation of pollutants and photocatalyzed organic reactions

due to their low band gap, high chemical stability, ease of preparation, surface modification, and above all strong magnetic nature for their easy recovery from the reaction mixture.

Two important reactions in photocatalysis are

i. Generation of electron-hole pair by absorption of light (photogenerated e^- -h^+ pair)

ii. Photogenerated e^- -h^+ pair separation

In the process of photocatalysis, these photogenerated e^- are responsible for reduction of organic molecules and h^+ are responsible for their oxidation. Due to the low band gap in ferrites, there is a possibility of e^- -h^+ pair recombination, thus affecting the photocatalytic activity if the ferrite is used as the only component of the catalyst. To address this fact, it is reported that integration of high band gap materials such as TiO_2, ZnO, ZnS etc with the low band gap nanoferrites will tune the band gap for visible light absorption. The resulting material can be used as magnetically retrievable, visible light active, core-shell photocatalyst (ferrite as magnetic core and other material as shell) for the degradation of many organic pollutants. To further improve the selectivity and activity for a particular organic transformation, surface of the core-shell can be functionalized by other materials and catalytically active species as described under section 1.1.4.4.

1.1.4.7. Literature on ferrite based core-shell nanophotocatalyst in dye degradation and organic transformations

Many reports are available on the application of ferrite based core-shell nanophotocatalyst for the successful degradation of toxic dyes such as methylene blue, methyl orange, rhodamine B, azo dye, congo red, etodolac, ofloxacin etc.[71,72,73] The reports on magnetic photocatalysts for various organic transformation is scarce which can be explored by ferrite based surface functionalized nanophotocatalyst.

1.2. Scope of Research Work

The modern chemical industries significantly demand the need for sustainable and affordable synthetic techniques following a greener approach in organic synthesis for synthesizing useful products. The goal of this work is to create new, effective and cost-effective reusable catalysts that may be employed for said purpose in chemical industries. Based on the aforementioned background and literature reports, the main objective of this research is to synthesize and explore potential applications of the MNCs to satisfy the needs of the chemical industry. Substantial advancement has been achieved in the development of functionalized MNCs, which offer the same or improved reactivity as comparable homogeneous catalysts. These facts motivated us to develop a few surface-modified ferrites as heterogeneous magnetic nanocatalysts and to explore their applications in chemical catalysis

under ambient conditions and photocatalysis under sunlight irradiation for a few important organic transformations that are useful in the chemical industry.

1.3. Objectives

Based on the aforementioned facts, different ferrite based heterogeneous nanocatalysts were proposed to develop for different organic transformations with the following objectives.

- To synthesize magnetically recoverable ferrite based heterogeneous nanocatalysts for their application in chemical catalysis and photocatalysis for organic transformations
- To characterize the synthesized catalysts using analytical techniques such as XRD, FTIR, SEM, FESEM, TEM, EDAX, XPS, VSM, UV-Vis DRS, ICP-OES etc.
- To study their applications in organic transformations such as
    - Coupling reactions (C-C, C-N, A^3)
        - Suzuki coupling reactions
        - Sonogashira coupling reactions
        - Chan-Lam coupling reactions
        - A^3 coupling reactions
    - Aromatic C-H activation
    - Reduction of nitroaromatic compounds
- To investigate the multifunctional behavior of the catalyst
- To investigate the magnetic recoverability of the catalyst
- To investigate the reusability and stability of the catalyst

1.4. Methods of synthesis

The properties of NPs depend on chemical composition, particle size, and morphology and can be tuned by working at their size and chemical composition. It is reported that the chemical and physical properties of spinel nanoferrites depend on the synthesis methods and conditions. Hence, the selection of a suitable method plays a vital role in tuning the properties to get spinel nanoferrites and other ferrite based materials with remarkable properties to suit a selective application.[74]

Many attempts have been made to alter the size, shape, composition, and structure of ferrites that influence their properties. This is achieved by adopting different synthesis methods with different synthesis conditions like calcination temperature, concentration of reactants, pH, stirring speed, type of dopant, duration etc.[75] A noble synthesis technique must result in NPs that are well dispersed, homogeneous in size with good crystallinity. To make the process sustainable, it should use non-toxic reagents, low temperatures and be associated with simple scalable operations. Some of the most common and important synthesis methodologies used for the synthesis of spinel nanoferrites and their associated materials are shown in the **Figure 1.6**. Outlines of the common synthesis methods are discussed below.

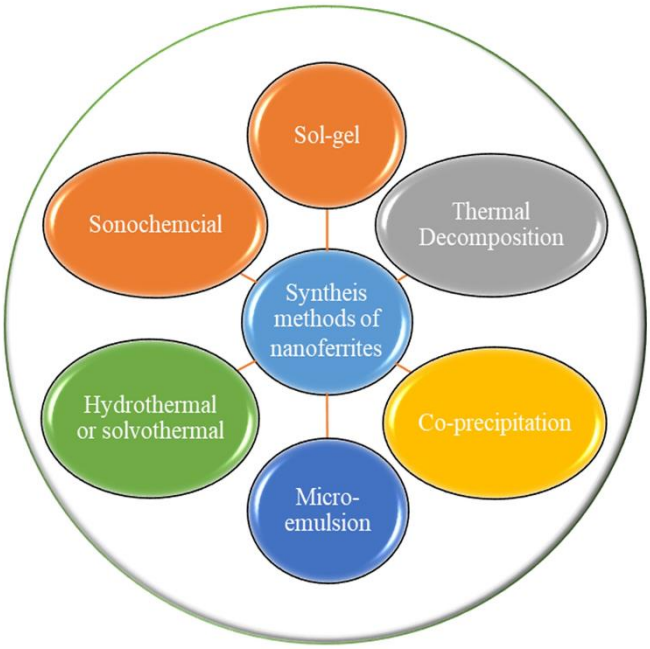

Figure.1.6 *Synthesis methods*

1.4.1. Sol-gel method

Sol-gel method is a simple, low temperature process that produce fine, highly dense, homogeneous ferrite NPs with single phase morphology. This method involves the use of metal salts or metal alkoxides as precursors which undergo hydrolysis and condensation. A standard process involves dissolving metal salts or metal alkoxides in a small amount of water, mixing them, and then adding an appropriate organic fuel (chelating/complexing reagent) such as citric acid, urea, or glycine. In order to improve the metal ion binding to citrate ions, the pH of the solution has been adjusted to ~7 by adding ammonia solution. Then the reaction mixture is heated to 70 °C to form the sol. It is further heated to 110 °C where a nitrate-fuel gel formation occurs. On further heating, initiation of autocatalytic self-combustion process of gel occurs and finally forms a loose fluffy powder which is further subjected to calcination to form

final material. The kind of organic fuel, fuel to oxidizer ratio, concentration of precursors, pH, rate of stirring, heating rate, calcination temperature, etc will affect how well ultrafine high purity powder is synthesised. Citric acid is used most frequently as organic fuel in the synthesis of large number of spinel ferrites.[18]

1.4.2. Thermal Decomposition

Another straightforward way for creating spinel ferrite NPs is thermal decomposition, which yields monodispersed particles with high crystallinity and small particle sizes. This process relies on the thermal decomposition of metallic precursors in an organic solvent with a high boiling point while stabilising it with surfactant. Surfactant act as protective coating on NPs, minimizing their agglomeration and improve the properties of material such as size, porosity, specific surface that control their magnetic properties.

Typically, an inert atmosphere is used to combine the organic solvent, surfactant, and metallic precursors on a magnetic stirrer. To create monodispersed spinel ferrites, the mixture is heated for a sufficient amount of time up to 350 °C. The mixture is cooled, the components are separated, and then it is repeatedly washed with ethanol/acetone before drying overnight. Fine particles size can be obtained, but, maintaining the temperature is difficult task.[76]

1.4.3. Co-precipitation method

Co-precipitation method is a facile, convenient, cost-effective, widely used process with less reaction time for the synthesis of ultrafine spinel nanoferrites as it produces the material with uniform particles size. The principle involved in this process is the combined precipitation of aqueous solution consisting of inorganic salts by increasing the pH of the solution. The ability to alter the reaction temperature, stirring rate, solution pH, solution concentration, and addition of alkali allows for precise control of the particle size, shape, and homogeneity. One of the limitations associated with this method is relatively broad size distribution of the particles and poor crystallinity.

The typical procedure involves the addition of stoichiometric amounts of desired inorganic salts (chlorides, sulphates, nitrates) in water with continuous stirring in an alkaline solution (NH_4OH or NaOH). pH of the solution is adjusted in the range of 7-12 with constant stirring. Mixture is heated between 60 and 100 °C with continuous stirring for an adequate amount of time to cause precipitate to form. The precipitate is collected employing an external magnet owing to the magnetic nature of the ferrite, then washed and dried. To increase the crystallinity, the resulting precipitate is subjected to calcination.[76]

1.4.4. Micro-emulsion method

This method gains attention in the synthesis of spinel ferrite NPs due to its excellent particles size, shape, uniformity and good control on dispersity. This method can provide particles with extremely small size. In the procedure, two immiscible liquids that are stabilised by surfactant molecules are dispersed. This method employs normal micellar method (oil-in-water) or reverse micellar method (water-in-oil). This technique involves mixing metal salts, a surfactant, water (a polar solvent), and a non-polar solvent in a set stoichiometric ratio to create an emulsion mixture. Surfactants that are widely used are sodium bis(2-ethylhexyl) sulfosuccinate (AOT) and tri methyl ammonium bromide (CTAB) while n-butanol or poly(oxyethylene)-4-laurylether are used as co-surfactants. The concentration of them is above critical micelle concentration (CMC). Isooctane, octanol, n-hexane are used as non-polar liquids.

In the typical procedure, all the solutions are mixed together with a reducing agent such as hydrazine, sodium borohydride, sodium hydroxide or ammonia solution and constantly stirred at 20-80 °C by increasing the pH (9-12). The precipitation occurs, which is separated, washed, dried in an oven and subjected to calcination. Then it is crushed and ground to form fine product. Major drawback of this method is the poor crystallinity of spinel ferrites, need of large amounts of solvents.[77]

1.4.5. Hydrothermal or Solvothermal method

It is one of the most environmentally friendly synthesis techniques since it uses either an aqueous or non-aqueous solvent to achieve desired particle, shape and size distribution. This process involves dissolving metal salts in the required stoichiometry in either water (hydrothermal) or an organic solvent (solvothermal), then thoroughly mixing them using magnetic stirring. The pH of the solution is raised to 9–12 by adding an appropriate reagent until a clear solution is formed. The resultant solution is subsequently introduced into an autoclave made of Teflon-coated stainless steel and heated at 140 to 200 °C for varying lengths of time to finish the reaction. Depending on the type of NPs, the temperature and reaction time vary. The generated solid particles are separated, repeatedly rinsed with ethanol and water to achieve a pH of neutral, and then dried in an oven. Then, in order to produce particles with a narrow size distribution and a high degree of crystallinity, it is ultimately subjected to calcination. The chemistry involved in the process is the initial formation of metal hydroxides which oxidise and convert into crystalline spinel ferrite due to thermal treatment under high pressures. A good control on the shape, size of the NPs can be had by adjusting the time, temperature, solvent etc.

1.4.6. Sonochemical method

It is a new, comparatively efficient, and simple process that produces spinel ferrite NPs without the usage of expensive, harmful, or dangerous substances. Sonochemistry is the study of the progress of chemical reaction under ultrasonic conditions where sound waves propagate via the liquid and results in the formation and collapse of bubbles. Particles experience in-situ calcination due to high-energy collisions among them. Effective mixing can be attained at the atomic level due to ultra-sonication so that the crystalline phase can be formed at a relatively lower temperature. The benefit of this approach is that very small amounts of NPs can be produced while maintaining good control over the reaction environment and particle size distribution. Also it is a facile, low cost, safe method with fast reaction time, good phase purity and an eco-friendly process.[77]

The advantages and disadvantages associated with various methods of above described methods are shown in the following table. Based on the mentioned features in the **Table 1.2.,** in the present work we have adopted co-precipitation method, hydrothermal method, and sonochemical method with appropriate reaction conditions for the synthesis of ferrites and different ferrite-based catalysts.

1.5. Characterization Techniques

It is understood that the spinel ferrites and surface modified ferrites can be prepared by different methods which influence the structural and physicochemical properties that enable them to use for a desired application. Hence proper characterization using modern analytical techniques is crucial for a better understanding of the properties of these materials at nano regime. Various analytical characterization techniques used in the current work are

- Powder X-ray Diffraction (PXRD)
- Fourier Transform Infrared Spectroscopy (FTIR)
- Scanning Electron Microscopy (SEM)
- Field Emission Scanning Electron Microscopy (FE-SEM)
- Transmission Electron Microscopy (TEM)
- Energy-Dispersive X-ray Analysis (EDAX)
- X-ray Photoelectron Spectroscopy (XPS)
- Vibrating Sample Magnetometer (VSM)
- UV-Visible Diffuse Reflectance Spectroscopy (UV-Vis. DRS)
- Inductively Coupled Plasma-Optical Emission Spectroscopy (ICP-OES)

Table 1.2. *Advantages and disadvantages associated with methods of synthesis of spinel ferrites*

Methods	Advantages	Disadvantages
Sol-gel method	✓ Controlled morphology ✓ Small particle size ✓ Low synthesis temperature ✓ Simple method of preparation and equipment	✓ Lower yield ✓ Release of large amount of gases ✓ Contamination with carbonaceous residues
Thermal Decomposition	✓ Better crystallinity ✓ Large scale production ✓ Small size and monodispersity	✓ High temperature ✓ Need of toxic and organic solvents
Co-precipitation method	✓ Facile synthesis ✓ Homogeneous mixing of reacting substances ✓ Good control on particle size and homogeneity	✓ Low crystallinity ✓ Long time ✓ Need good control on pH
Micro-emulsion method	✓ Cost effective ✓ Exceptional control over shape and size ✓ Short temperatures	✓ Need of more solvents, surfactants/cosurfactant ✓ Meagre crystallinity
Hydro or Solvo-thermal method	✓ Excellent control of composition and particle size ✓ Direct formation of product from solution ✓ Versatile synthesis process for numerous catalysts	✓ High pressure required ✓ Need of special reactor (autoclave) ✓ Slurry is corrosive
Sonochemical method	✓ Easy control over reaction conditions ✓ Better regulation of particle size distribution ✓ High purity and high reaction rate of the compound	

1.5.1. Powder X-ray Diffraction (PXRD)

One of the most adaptable techniques for determining material's crystal structure, crystallite size, atomic spacing, and analysis of solid phase is the PXRD method. It also provides information about the lattice constants, the presence of external atoms in the crystal lattice of the active component of the prepared material. The basis of XRD is the constructive interference of monochromatic X-rays with the crystalline substance. The XRD spectrum has

resulted from the interaction of a highly energetic incident X-ray beam with the crystalline material under test as illustrated in **Figure 1.7** by satisfying the condition of Bragg's law[78]

$$n\lambda = 2dsin\theta$$

Where n = order of reflection

λ = wavelength of incident X-rays

d = inter planar distance

θ = angle of incidence

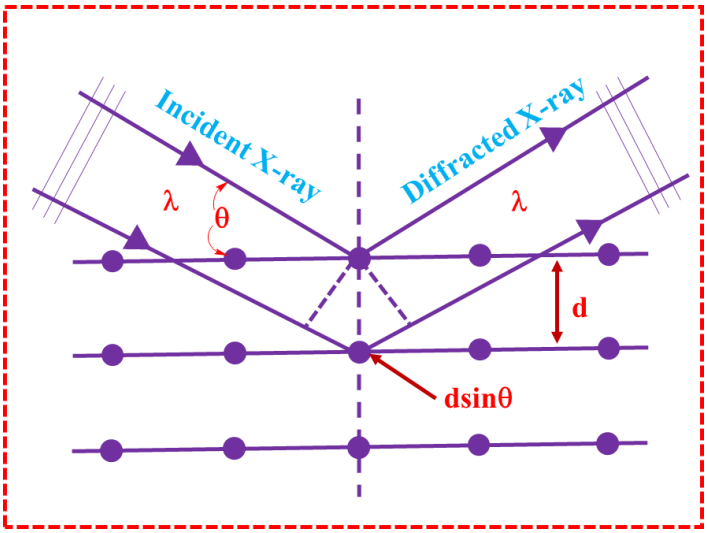

Figure 1.7 *Bragg's law for X-ray Diffraction*

The Powder Diffraction File (PDF) from the International Centre for Diffraction Data (ICDD) is the global database of experimentally determined powder diffraction patterns that includes d-spacing, which is used to determine the crystal structure of crystalline materials. The PDF contains a data set of more than a million unique materials. ICDD was earlier known as Joint Committee on Powder Diffraction Standards (JCPDS). The crystal structure and other crystallographic details of the compound under test can be obtained by comparing the observed XRD data with the standard data as per JCPDS card.

PAN Analytical Advance X-ray Diffractometer with Cu Kα radiation (λ = 1.5406 Å) in a 2θ scan range between 10 and 80° was used in the current investigation to record the PXRD patterns of our synthetic materials. The crystallite size can be obtained from the broadening of diffracted beam employing Scherer's formula[79]

$$D = \frac{0.9\,\lambda}{\beta sin\theta}$$

Where D = crystallite size

λ = wavelength of x-rays

θ = angle of diffraction

β = Full Width Half Maximum (FWHM) of the diffraction peak

1.5.2. Fourier Transform-Infrared Spectroscopy (FTIR)

FTIR spectroscopy is an important tool that has been widely used for structural and compositional analysis of materials. It deals with the variations in vibrational motion by means of the structural and bending of atoms of a molecule. Absorption spectra in IR region emerge from the transition between vibrational levels of a molecule in its ground state on irradiation with IR radiation.

The basic requirement for a vibrating molecule to interact with incident radiation and result in a transition between two vibrational energy levels is that the molecule should have a net change in dipole moment during vibration. The magnitude of the dipole moment decides the intensity of absorption. Some symmetrical molecules do not induce change in dipole moment which are called as IR inactive as they do not absorb IR radiation.[80]

In the current study, FT-IR spectra of various synthesized materials were recorded using PerkinElmer (Spectrum-100) FT-IR spectrophotometer by KBr pellet method. IR region of electromagnetic spectrum (12500-10 cm^{-1}) is divided into near-IR region (12500-4000 cm^{-1}), mid-IR (4000-400 cm^{-1}) and far IR (400-10cm^{-1}). The majority of analytical studies are limited to a portion of the middle IR region encompassing 4000 to 400 cm^{-1}.

1.5.3. Scanning Electron Microscopy (SEM)

SEM is an electron microscope that scans a sample's surface with a focused beam of electrons to create images of the material. The signals produced by the electron's interactions with the sample's atoms provide information on the sample's surface topography and chemical composition. By combining the position of the electron beam and the strength of the signal being detected while it is being scanned in a raster scan pattern, an image is produced.[81]

It provides details of the elemental composition, sample exterior morphology, and the orientation of the materials that make up the sample. Finally, a 3D image is created using the data gathered over a specific area of the complex. SEM makes it easier to analyze samples with a resolution as low as a nanometer and magnifies an image up to 2 million times. In the current study, the morphological traits and chemical composition were recorded using SEM, Carl Zeiss SMT Ltd., Zeiss EVO 18 equipped with an energy dispersive X-ray spectrometer.

1.5.4. Field Emission Scanning Electron Microscopy (FESEM)

A FESEM is used to analyze very minute topographic details on the entire surface or fractioned objects. It is widely used by researchers in biology, chemistry, and physics to observe structures that are as small as 1 nm. This technique is meant for high-resolution

imaging of different kinds of materials and the source of current used is field emission that uses a field emitter gun (FEG) to emit electrons. Thus, SEM which uses FEG as the electron source is called FESEM and is an advanced technique that offers enhanced magnification to observe very fine topographies at lower voltage than SEM.[82]

In the presentstudy, the morphological features and chemical composition are investigated by a field emission scanning electron microscope (FE-SEM; JEOL JSM-7000F instrument) integrated withan energy dispersive X-ray spectrometer (EDS). The schematic of the working of SEM is shown in **Figure 1.8.**[83]

1.5.5. Transmission Electron Microscope (TEM)

It is an electron microscope which use a broad beam of electrons that transmits through the sample and generates an image of the internal structure of the sample which details the morphology, composition, and crystal structure.[83] The sample should be very thin ~ <150 nm thick so as to allow the electrons to transmit through them. TEM is an advantageous technique over other electron microscopes as it generates high resolution images, provide crystallographic and atomic data and create a 2D image that is easy to interpret. In the current study, the high-resolution morphology of the synthesized materials is examined by using TEM; JEOL/JEM-2100 instrument operated at 200 kV. The schematic of working of TEM is shown in the **Figure 1.8.**[83]

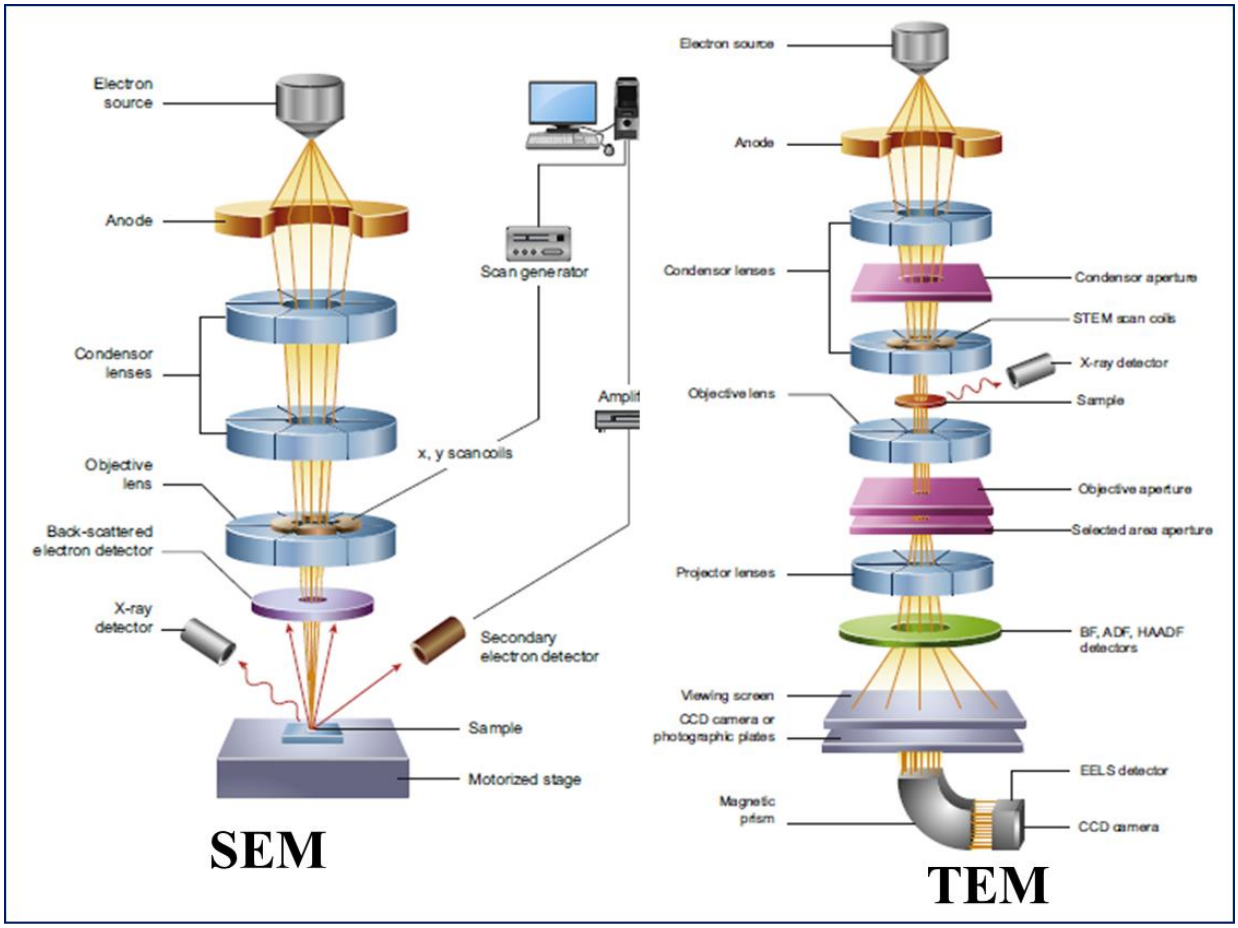

Figure 1.8 *Working of SEM and TEM*

1.5.6. Energy-Dispersive X-ray Analysis (EDAX)

It is a technique when combined with electron microscopes such as SEM, FESEM provides elemental analysis of the sample on very small areas of nm size and the overall positional mapping in it. In this technique, an electron beam with high energy ~10-20 KeV strikes an atom's inner shell, it knocks an electron out and creates an electron hole of positive charge. When one electron is displaced, the vacancy is filled by drawing another electron from an outer shell. This energy difference can be released as an X-ray as the electron moves from the outer, higher-energy shell to the inner, lower-energy shell of the atom, as shown in **Figure 1.9**. The energy of the emitted X-ray is unique to the particular element and transition and provides the elemental composition of the material or areal distribution of elements based on the scanning ability of the electron microscopes.[84]

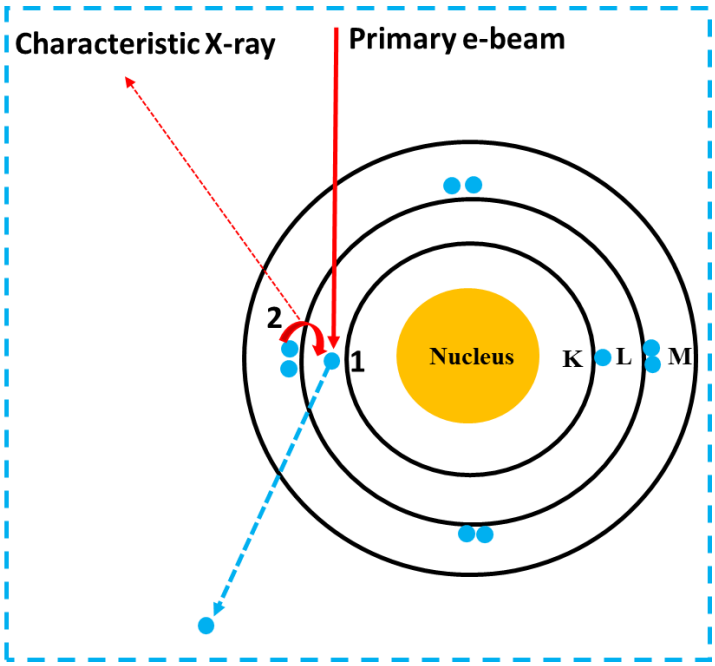

Figure 1.9 *Energy-dispersive X-ray Analysis*

1.5.7. X-ray photoelectron Spectroscopy (XPS)

The term "Electron Spectroscopy for Chemical Analysis" (ESCA) is another name for X-ray photoelectron spectroscopy (XPS). It is a method for examining the chemistry of a material's surface. Using this tool, elemental composition at the parts per thousand ranges along with the chemical and electronic state of the elements that exist within the material can be measured. Along with the information about the type of elements present, it also shows the other elements to which they are bonded. It is used to analyse inorganic compounds and catalysts etc. XPS technique is based on the photoelectric effect. In this technique, when the sample is irradiated with X-ray, the electrons are ejected from the surface and the binding energy of electrons can be given by photoelectric effect equation[85]

$$E_{binding} = E_{photons}-(E_{kinetic}+\phi)$$

Where $E_{binding}$ = electron's binding energy

E_{photon} = X-ray photon's energy

$E_{kinetic}$ = electron's kinetic energy

ϕ = a small instrumental correction factor

Atoms with higher positive oxidation states exhibit higher binding energies due to the enhanced coulombic interaction between the photo-emitted electron and the core ion. The ability of the XPS technology to distinguish between various oxidation states and chemical environments is one of its main advantages. The spectrum is obtained by plotting the emission intensity on the ordinate and electron binding energy on the abscissa. The location of XPS peaks provides information about the surface chemistry composition of the sample. Moreover,

the magnitude of the peaks correlates with the amount of the element present in the analyzed area. Thus, the technique offers a quantitative analysis of the surface composition. In the present study, the XPS spectra of synthesized materials are recorded on the Kratos/Shimadzu Amicus, Model: ESCA 3400.

1.5.8. Vibrating Sample Magnetometer (VSM)

It is an analytical technique that measures the magnetic properties of nanostructured materials. VSM data describes the size-dependent magnetic properties of the sample as a function of the applied magnetic field at ambient temperatures to describe the field dependent magnetic properties of NPs. The basis for the working of VSM is Faraday's law of electromagnetic induction, which states that a changing magnetic field produces an electric field that can be measured.[86] The sample is subjected to a steady magnetic field during the measurement. The applied magnetic field will magnetize the sample if it is magnetic because the magnetic domains will be properly aligned with the field. Larger magnetization results from a stronger constant field. By controlling and monitoring the software, the system provides information on how much the sample is magnetized and how magnetization varies depending on the strength of the magnetic field. For a specific field strength, the signal received from the probe is converted into magnetic moment of the sample. A plot of magnetization against magnetic field strength is produced when a constant magnetic field varies across a certain range, called a magnetic hysteresis loop or M-H loop as shown below in **Figure 1.10.**

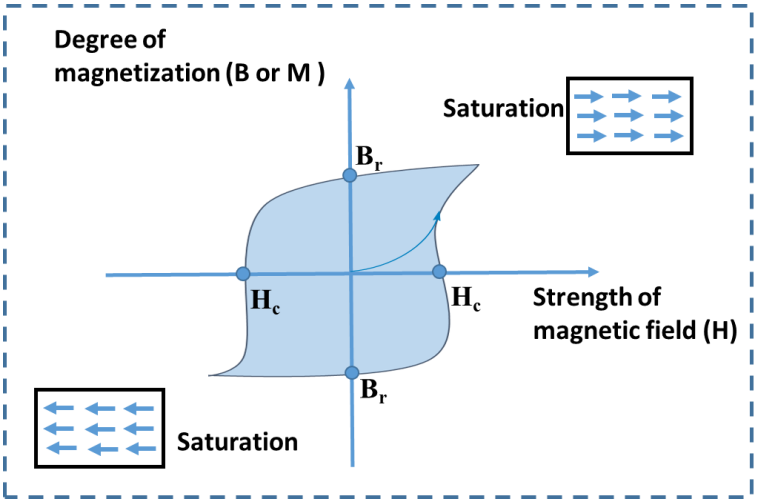

Figure 1.10 *Magnetic hysteresis loop*

Various magnetic parameters obtained from the M-H loop are coercivity (H_c), saturation magnetization (M_s), and remanent magnetization (M_r or B_r). M_s is the state where there is no further increase in magnetization with an increase in the applied field. It is a characteristic of ferromagnetic materials. M_r is the ability of the material to continue to be

magnetic when the magnetic field reaches zero. A field with the opposite direction must be applied in order to reduce M_r to zero. H_c is the magnitude of the field necessary to reduce the sample's magnetization to zero.

In the present work all the synthesized catalysts are ferrite based materials that show ferromagnetic behaviour due to which they can be magnetically recovered. To establish their magnetic nature VSM measurements were performed using VSM, Lake Shore, Model: 8600 Series.

1.5.9. UV-Visible Diffuse Reflectance Spectroscopy (UV-Vis. DRS)

It is a widely used technique to study the optical properties of the solid or powder samples such as transmission, absorption, emission, reflection, refraction, diffraction, and scattering effects by its interaction with electromagnetic radiation. In this technique, when a powdered sample is exposed to UV or visible light, the light can reflect in all directions. In diffuse reflection, a portion of the light enters the interior of a solid sample, interacts with the structure and composition, and returns to the surface. As a reference standard, barium sulphate ($BaSO_4$) must be recorded before any other powder sample.[87] In the present study, UV-Vis-DRS studies of the synthesized materials were performed using Analytik Jena, SPECORD 210 PLUS at RT.

The ferrites behave as semiconductor materials with a reasonable band gap and can be utilized for photocatalytic applications. This technique is adopted, to find the band gap of the ferrite based catalyst which is evaluated following the Tauc method using the Tauc relation

$$(\alpha h\vartheta) = A\left(h\vartheta - E_g\right)^{\eta}$$

Where A = constant

h = Planck's constant

ϑ = Frequency of light

α = absorption coefficient

E_g = Band gap energy

η is a variable that depends on the type of optical transition resulting by photon absorption.

A typical Tauc plot show the variation of $(\alpha h\vartheta)^2$ vs $h\vartheta$ as shown in **Figure.1.11**

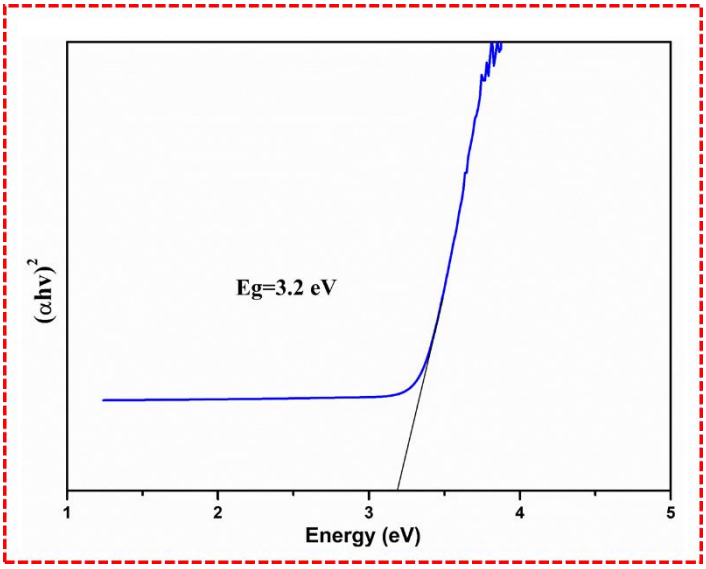

Figure 1.11 *Tauc plot*

Drawing a straight line (Tauc line) to the linear region of the optical spectrum and extrapolating will intersect the energy (hυ) axis which is termed as Band gap energy. The value of α was determined using Kubelka Munk function as shown below[88]

$$\alpha = \frac{(1-R)^2}{2R}$$

Where α is the reflection coefficient of the sample, R is the reflectance.

In the present work, the band gap energy of ferrites and ferrite based photocatalysts were determined using UV-Vis. DRS spectroscopy.

1.5.10. Inductively Coupled Plasma-Optical Emission Spectroscopy (ICP-OES)

The components of a sample are identified and quantified using this analytical approach. This method's fundamental principle is based on the observation that atoms and ions absorb energy when they move electrons from the ground state to the excited state. The source of the energy for this purpose is heat from an argon plasma which operates at 10,000 Kelvin. Those excited atoms return to their normal low energy state by releasing energy (or photon). Spectrometer measures the spectrums of these photons and it is possible to identify elements based on their individual spectrum and a value is assigned to them.[89]

ICP-OES helps to determine the real active metal content in the catalyst and also ICP-OES elemental analysis of the recovered catalyst gives information about the leaching of the metal if any. In the current study, ICP-OES analysis of the recovered catalyst was made with PerkinElmer Optima 5300 DV.

1.6. References

(1) Varma, R. S. Nano-Catalysts with Magnetic Core: Sustainable Options for Greener Synthesis. *Sustain. Chem. Process.* **2014**, *2* (1), 1–8.

(2) Irles, A.; Gonçalves, I. C.; Lopes, M. C.; Fernandes, A. C.; Ramalho, A. G.; Pertusa, J. A Biological Study on the Effects of High and Low LET Radiations Following Boron Neutron Capture Reaction at the Portuguese *Research Reactor*; **2001**; Vol. 17.

(3) Polshettiwar, V.; Varma, R. S. Aqueous Microwave Chemistry: A Clean and Green Synthetic Tool for Rapid Drug Discovery. *Chem. Soc. Rev.* **2008**, *37* (8), 1546–1557.

(4) Polshettiwar, V.; Varma, R. S. Microwave-Assisted Organic Synthesis And. **2008**, *41* (5).

(5) Singh, N. G.; Nongrum, R.; Kathing, C.; Rani, J. W. S.; Nongkhlaw, R. Bakers' Yeast: An Environment Benign Catalyst for the One-Pot Synthesis of Indolyl Chromenes and Bisindolyl Alkanes. *Green Chem. Lett. Rev.* **2014**, *7* (2), 137–144.

(6) Peng, R.; Li, S.; Sun, X.; Ren, Q.; Chen, L.; Fu, M.; Wu, J.; Ye, D. Size Effect of Pt Nanoparticles on the Catalytic Oxidation of Toluene over Pt/CeO_2 Catalysts. *Appl. Catal. B Environ.* **2018**, *220*, 462–470.

(7) Akbayrak, S.; Tonbul, Y.; Özkar, S. Nanoceria Supported Palladium(0) Nanoparticles: Superb Catalyst in Dehydrogenation of Formic Acid at Room Temperature. *Appl. Catal. B Environ.* **2017**, *206*, 384–392.

(8) Gawande, M. B.; Goswami, A.; Felpin, F. X.; Asefa, T.; Huang, X.; Silva, R.; Zou, X.; Zboril, R.; Varma, R. S. Cu and Cu-Based Nanoparticles: Synthesis and Applications in Catalysis. *Chem. Rev.* **2016**, *116* (6), 3722–3811.

(9) Miceli, M.; Frontera, P.; Macario, A.; Malara, A. Recovery/Reuse of Heterogeneous Supported Spent Catalysts. *Catalysts* **2021**, *11* (5).

(10) Yeap, S. P.; Lim, J. K.; Ooi, B. S.; Ahmad, A. L. Agglomeration, Colloidal Stability, and Magnetic Separation of Magnetic Nanoparticles: Collective Influences on Environmental Engineering Applications. *J. Nanoparticle Res.* **2017**, *19* (11).

(11) Jasrotia, R.; Puri, P.; Verma, A.; Singh, V. P. Magnetic and Electrical Traits of Sol-Gel Synthesized Ni-Cu-Zn Nanosized Spinel Ferrites for Multi-Layer Chip Inductors Application. *Journal of Solid State Chemistry* **2020**, *289* (April), 121462.

(12) Kefeni, K. K.; Msagati, T. A. M.; Mamba, B. B. Ferrite Nanoparticles: Synthesis, Characterisation and Applications in Electronic Device. *Materials Science and Engineering: B* **2017**, *215*, 37–55.

(13) Rana, G.; Dhiman, P.; Kumar, A.; Vo, D. V. N.; Sharma, G.; Sharma, S.; Naushad, M. Recent Advances on Nickel Nano-Ferrite: A Review on Processing Techniques, Properties and Diverse Applications. *Chemical Engineering Research and Design* **2021**, *175*, 182–208.

(14) Shyamaldas; Bououdina, M.; Manoharan, C. Dependence of Structure/Morphology on Electrical/Magnetic Properties of Hydrothermally Synthesised Cobalt Ferrite Nanoparticles. *Journal of Magnetism and Magnetic Materials* **2020**, *493* (August 2019), 165703.

(15) Patil, S.; Tandon, R.; Tandon, N. A Current Research on Silica Coated Ferrite Nanoparticle and Their Application: Review. *Curr. Res. Green Sustain. Chem.* **2021**, *4* (February), 100063.

(16) Pan, X.; Sun, A.; Han, Y.; Zhang, W.; Zhao, X. Structural and Magnetic Properties of Bi^{3+} Ion Doped Ni–Cu–Co Nano Ferrites Prepared by Sol–Gel Auto Combustion Method. *J. Mater. Sci. Mater. Electron.* **2019**, *30* (5), 4644–4657.

(17) Mmelesi, O. K.; Masunga, N.; Kuvarega, A.; Nkambule, T. T.; Mamba, B. B.; Kefeni, K. K. Cobalt Ferrite Nanoparticles and Nanocomposites: Photocatalytic, Antimicrobial Activity and Toxicity in Water Treatment. *Mater. Sci. Semicond. Process.* **2021**, *123* (April 2020), 105523.

(18) Soufi, A.; Hajjaoui, H.; Elmoubarki, R.; Abdennouri, M.; Qourzal, S.; Barka, N. Spinel Ferrites

Nanoparticles: Synthesis Methods and Application in Heterogeneous Fenton Oxidation of Organic Pollutants – A Review. *Appl. Surf. Sci. Adv.* **2021**, *6*, 100145.

(19) Dehghani Dastjerdi, O.; Shokrollahi, H.; Mirshekari, S. A Review of Synthesis, Characterization, and Magnetic Properties of Soft Spinel Ferrites. Inorganic Chemistry Communications 2023, 153 (March), 110797.

(20) Gao, Z.; Cui, F.; Zeng, S.; Guo, L.; Shi, J. A High Surface Area Superparamagnetic Mesoporous Spinel Ferrite Synthesized by a Template-Free Approach and Its Adsorptive Property. Microporous and Mesoporous Materials 2010, 132 (1–2), 188–195.

(21) Mekhemer, G. A. H.; Mohamed, H. A. A.; Bumajdad, A.; Zaki, M. I. Lattice-Charge Imbalance and Redox Catalysis over Perovskite-Type Ferrite- and Manganite-Based Mixed Oxides as Studied by XRD, FTIR, UV–Vis DRS, and XPS. Scientific Reports 2023, 13 (1), 1–9.

(22) Liandi, A. R.; Cahyana, A. H.; Kusumah, A. J. F.; Lupitasari, A.; Alfariza, D. N.; Nuraini, R.; Sari, R. W.; Kusumasari, F. C. Recent Trends of Spinel Ferrites (MFe2O4: Mn, Co, Ni, Cu, Zn) Applications as an Environmentally Friendly Catalyst in Multicomponent Reactions: A Review. Case Studies in Chemical and Environmental Engineering 2023, 7 (December 2022), 100303

(23) Damma, D.; Jampaiah, D.; Welton, A.; Boolchand, P.; Arvanitis, A.; Dong, J.; Smirniotis, P. G. Effect of Nb Modification on the Structural and Catalytic Property of Fe/Nb/M (M = Mn, Co, Ni, and Cu) Catalyst for High Temperature Water-Gas Shift Reaction. Catalysis Today 2020, 355 (November 2018), 921–931.

(24) SOUFI, A.; HAJJAOUI, H.; ELMOUBARKI, R.; ABDENNOURI, M.; QOURZAL, S.; BARKA, N. Spinel Ferrites Nanoparticles: Synthesis Methods and Application in Heterogeneous Fenton Oxidation of Organic Pollutants – A Review. Applied Surface Science Advances 2021, 6, 100145.

(25) Murthy, Y. L. N.; Diwakar, B. S.; Govindh, B.; Nagalakshmi, K.; Viswanath, I. V. K.; Singhc, R. Nano Copper Ferrite: A Reusable Catalyst for the Synthesis of β, γ -Unsaturated Ketones. *J. Chem. Sci.* **2012**, *124* (3), 639–645.

(26) Kooti, M.; Afshari, M. Molybdenum Schiff Base Complex Covalently Anchored to Silica-Coated Cobalt Ferrite Nanoparticles as a Novel Heterogeneous Catalyst for the Oxidation of Alkenes. *Catal. Letters* **2012**, *142* (3), 319–325.

(27) Yang, S.; Wu, C.; Zhou, H.; Yang, Y.; Zhao, Y.; Wang, C.; Yang, W.; Xu, J. An Ullmann C-O Coupling Reaction Catalyzed by Magnetic Copper Ferrite Nanoparticles. *Adv. Synth. Catal.* **2013**, *355* (1), 53–58.

(28) Gharib, A.; Pesyan, N. N.; Fard, L. V.; Roshani, M. Catalytic Synthesis of *α*-Aminonitriles Using Nano Copper Ferrite (CuFe2O4) under Green Conditions. ***2014,*** 1–9, 169803.

(29) Rahman, T.; Borah, G.; Gogoi, P. K. Spinel Structured Copper Ferrite Nano Catalyst with Magnetic Recyclability for Oxidative Decarboxylation of Phenyl Acetic Acids. *Catal. Letters* **2020**, *150* (8), 2267–2272.

(30) Kumar, P. V.; Short, M. P.; Yip, S.; Yildiz, B.; Grossman, J. C. High Surface Reactivity and Water Adsorption on $NiFe_2O_4$ (111) Surfaces. *J. Phys. Chem. C* **2013**, *117* (11), 5678–5683.

(31) Abu-Dief, A. M.; Nassar, I. F.; Elsayed, W. H. Magnetic $NiFe_2O_4$ Nanoparticles: Efficient, Heterogeneous and Reusable Catalyst for Synthesis of Acetylferrocene Chalcones and Their Anti-Tumour Activity. *Appl. Organomet. Chem.* **2016**, *30* (11), 917–923.

(32) Ahankar, H.; Ramazani, A.; Joo, S. W. Magnetic Nickel Ferrite Nanoparticles as an Efficient Catalyst for the Preparation of Polyhydroquinoline Derivatives under Microwave Irradiation in Solvent-Free Conditions. *Res. Chem. Intermed.* **2016**, *42* (3), 2487–2500.

(33) Senapati, K. K.; Phukan, P. Magnetically Separable Cobalt Ferrite Nanocatalyst for Aldol Condensations of Aldehydes and Ketones. *Society* **2011**, *9* (January 2011), 1–8.

(34) Sadri, F.; Ramazani, A.; Massoudi, A.; Khoobi, M.; Joo, S. W. Magnetic CuFe2O4

Nanoparticles as an Efficient Catalyst for the Oxidation of Alcohols to Carbonyl Compounds in the Presence of Oxone as an Oxidant. *Bulg. Chem. Commun.* **2015**, *47* (2), 539–546.

(35) Moghaddam, F. M.; Tavakoli, G.; Aliabadi, A. Application of Nickel Ferrite and Cobalt Ferrite Magnetic Nanoparticles in C–O Bond Formation: A Comparative Study between Their Catalytic Activities. *RSC Adv.* **2015**, *5* (73), 59142–59153.

(36) Naik, M. M.; Vinuth, M.; Karthik, K.; Suresha, B.; Nagaraju, G.; Sujatha, H. R. Photocatalytic Degradation of Dyes by Cobalt Ferrite Nanoparticles Synthesized by Sol-Gel Method. *AIP Conf. Proc.* **2020**, *2274* (October).

(37) Goyal, A.; Bansal, S.; Samuel, P.; Kumar, V.; Singhal, S. CoMn0.2Fe1.8O4 Ferrite Nanoparticles Engineered by Sol-Gel Technology: An Expert and Versatile Catalyst for the Reduction of Nitroaromatic Compounds. *J. Mater. Chem. A* **2014**, *2* (44), 18848–18860.

(38) Chahar, D.; Taneja, S.; Bisht, S.; Kesarwani, S.; Thakur, P.; Thakur, A.; Sharma, P. B. Photocatalytic Activity of Cobalt Substituted Zinc Ferrite for the Degradation of Methylene Blue Dye under Visible Light Irradiation. *J. Alloys Compd.* **2021**, *851*, 156878.

(39) Jauhar, S.; Singhal, S.; Dhiman, M. Manganese Substituted Cobalt Ferrites as Efficient Catalysts for H_2O_2 Assisted Degradation of Cationic and Anionic Dyes: Their Synthesis and Characterization. *Appl. Catal. A Gen.* **2014**, *486*, 210–218.

(40) Mathubala, G.; Manikandan, A.; Arul Antony, S.; Ramar, P. Photocatalytic Degradation of Methylene Blue Dye and Magneto-Optical Studies of Magnetically Recyclable Spinel NixMn1-XFe_2O_4 (x = 0.0-1.0) Nanoparticles. *J. Mol. Struct.* **2016**, *1113*, 79–87.

(41) Gawande, M. B.; Branco, P. S.; Varma, R. S. Nano-Magnetite (Fe_3O_4) as a Support for Recyclable Catalysts in the Development of Sustainable Methodologies. *Chem. Soc. Rev.* **2013**, *42* (8), 3371–3393.

(42) Shelke, S. N.; Bankar, S. R.; Mhaske, G. R.; Kadam, S. S.; Murade, D. K.; Bhorkade, S. B.; Rathi, A. K.; Bundaleski, N.; Teodoro, O. M. N. D.; Zboril, R.; Varma, R. S.; Gawande, M. B. Iron Oxide-Supported Copper Oxide Nanoparticles (Nanocat-Fe-CuO): Magnetically Recyclable Catalysts for the Synthesis of Pyrazole Derivatives, 4-Methoxyaniline, and Ullmann-Type Condensation Reactions. *ACS Sustain. Chem. Eng.* **2014**, *2* (7), 1699–1706.

(43) Odio, O. F.; Reguera, E. Nanostructured Spinel Ferrites: Synthesis, Functionalization, Nanomagnetism and Environmental Applications. *Magn. Spinels - Synth. Prop. Appl.* **2017**.

(44) Nasir Baig, R. B.; Varma, R. S. A Highly Active Magnetically Recoverable Nano Ferrite-Glutathione-Copper (Nano-FGT-Cu) Catalyst for Huisgen 1,3-Dipolar Cycloadditions. *Green Chem.* **2012**, *14* (3), 625–632.

(45) Baig, R. B. N.; Varma, R. S. A Facile One-Pot Synthesis of Ruthenium Hydroxide Nanoparticles on Magnetic Silica: Aqueous Hydration of Nitriles to Amides. *Chem. Commun.* **2012**, *48* (50), 6220–6222.

(46) Rajabi, F.; Karimi, N.; Saidi, M. R.; Primo, A.; Varma, R. S.; Luque, R. Unprecedented Selective Oxidation of Styrene Derivatives Using a Supported Iron Oxide Nanocatalyst in Aqueous Medium. *Adv. Synth. Catal.* **2012**, *354* (9), 1707–1711.

(47) Singh, A. S.; Patil, U. B.; Nagarkar, J. M. Palladium Supported on Zinc Ferrite: A Highly Active, Magnetically Separable Catalyst for Ligand Free Suzuki and Heck Coupling. *Catal. Commun.* **2013**, *35*, 11–16.

(48) Singh, A. S.; Shendage, S. S.; Nagarkar, J. M. Palladium Supported on Zinc Ferrite: An Efficient Catalyst for Ligand Free C-C and C-O Cross Coupling Reactions. *Tetrahedron Lett.* **2013**, *54* (47), 6319–6323.

(49) Gawande, M. B.; Rathi, A. K.; Branco, P. S.; Nogueira, I. D.; Velhinho, A.; Shrikhande, J. J.; Indulkar, U. U.; Jayaram, R. V.; Ghumman, C. A. A.; Bundaleski, N.; Teodoro, O. M. N. D. Regio- and Chemoselective Reduction of Nitroarenes and Carbonyl Compounds over

Recyclable Magnetic Ferrite-Nickel Nanoparticles (Fe_3O_4-Ni) by Using Glycerol as a Hydrogen Source. *Chem. - A Eur. J.* **2012**, *18* (40), 12628–12632.

(50) Zeynizadeh, B.; Mohammadzadeh, I.; Shokri, Z.; Ali Hosseini, S. Synthesis and Characterization of $NiFe_2O_4$@Cu Nanoparticles as a Magnetically Recoverable Catalyst for Reduction of Nitroarenes to Arylamines with NaBH4. *J. Colloid Interface Sci.* **2017**, *500*, 285–293.

(51) Senapati, K. K.; Roy, S.; Borgohain, C.; Phukan, P. Palladium Nanoparticle Supported on Cobalt Ferrite: An Efficient Magnetically Separable Catalyst for Ligand Free Suzuki Coupling. *J. Mol. Catal. A Chem.* **2012**, *352*, 128–134.

(52) Liu, J.; Peng, X.; Sun, W.; Zhao, Y.; Xia, C. Magnetically Separable Pd Catalyst for Carbonylative Sonogashira Coupling Reactions for the Synthesis of α,β-Alkynyl Ketones. *Org. Lett.* **2008**, *10* (18), 3933–3936.

(53) Gawande, M. B.; Rathi, A.; Nogueira, I. D.; Ghumman, C. A. A.; Bundaleski, N.; Teodoro, O. M. N. D.; Branco, P. S. A Recyclable Ferrite-Co Magnetic Nanocatalyst for the Oxidation of Alcohols to Carbonyl Compounds. *Chempluschem* **2012**, *77* (10), 865–871.

(54) Aliaga, M. J.; Ramón, D. J.; Yus, M. Impregnated Copper on Magnetite: An Efficient and Green Catalyst for the Multicomponent Preparation of Propargylamines under Solvent Free Conditions. *Org. Biomol. Chem.* **2010**, *8* (1), 43–46.

(55) Cano, R.; Ramón, D. J.; Yus, M. Impregnated Palladium on Magnetite, a New Catalyst for the Ligand-Free Cross-Coupling Suzuki-Miyaura Reaction. *Tetrahedron* **2011**, *67* (30), 5432–5436.

(56) Cano, R.; Ramón, D. J.; Yus, M. Impregnated Ruthenium on Magnetite as a Recyclable Catalyst for the N-Alkylation of Amines, Sulfonamides, Sulfinamides, and Nitroarenes Using Alcohols as Electrophiles by a Hydrogen Autotransfer Process. *J. Org. Chem.* **2011**, *76* (14), 5547–5557.

(57) Polshettiwar, V.; Baruwati, B.; Varma, R. S. Magnetic Nanoparticle-Supported Glutathione: A Conceptually Sustainable Organocatalyst. *Chem. Commun.* **2009**, *1* (14), 1837–1839.

(58) Polshettiwar, V.; Varma, R. S. Nano-Organocatalyst: Magnetically Retrievable Ferrite-Anchored Glutathione for Microwave-Assisted Paal-Knorr Reaction, Aza-Michael Addition, and Pyrazole Synthesis. *Tetrahedron* **2010**, *66* (5), 1091–1097.

(59) Somorjai, G. A.; Frei, H.; Park, J. Y. Advancing the Frontiers in Nanocatalysis, Biointerfaces, and Renewable Energy Conversion by Innovations of Surface Techniques. *J. Am. Chem. Soc.* **2009**, *131* (46), 16589–16605.

(60) Soon, G. K.; Hyeon, T. Colloidal Chemical Synthesis and Formation Kinetics of Uniformly Sized Nanocrystals of Metals, Oxides, and Chalcogenides. *Acc. Chem. Res.* **2008**, *41* (12), 1696–1709.

(61) Mackenzie, J. D.; Bescher, E. P. Chemical Routes in the Synthesis of Nanomaterials Using the Sol-Gel Process. *Acc. Chem. Res.* **2007**, *40* (9), 810–818.

(62) Dam, B.; Patil, R. A.; Ma, Y. R.; Pal, A. K. Preparation, Characterization and Catalytic Application of Nano-Fe_3O_4-DOPA-SnO_2 Having High TON and TOF for Non-Toxic and Sustainable Synthesis of Dihydroquinazolinone Derivatives. *New J. Chem.* **2017**, *41* (14), 6553–6563.

(63) Beller, M.; Fischer, H.; Kühlein, K.; Reisinger, C. P.; Herrmann, W. A. First Palladium-Catalyzed Heck Reactions with Efficient Colloidal Catalyst Systems. *J. Organomet. Chem.* **1996**, *520* (1–2), 257–259.

(64) Narayanan, R.; El-Sayed, M. A. Changing Catalytic Activity during Colloidal Platinum Nanocatalysis Due to Shape Changes: Electron-Transfer Reaction. *J. Am. Chem. Soc.* **2004**, *126* (23), 7194–7195.

(65) Guin, D.; Baruwati, B.; Manorama, S. V. Pd on Amine-Terminated Ferrite Nanoparticles: A Complete Magnetically Recoverable Facile Catalyst for Hydrogenation Reactions. *Org. Lett.*

2007, *9* (7), 1419–1421.

(66) Baruwati, B.; Guin, D.; Manorama, S. V. Pd on Surface-Modified $NiFe_2O_4$ Nanoparticles: A Magnetically Recoverable Catalyst for Suzuki and Heck Reactions. *Org. Lett.* **2007**, *9* (26), 5377–5380.

(67) Polshettiwar, V.; Varma, R. S. Green Chemistry by Nano-Catalysis. *Green Chem.* **2010**, *12* (5), 743–775.

(68) Kurian, M.; Thankachan, S. Structural Diversity and Applications of Spinel Ferrite Core - Shell Nanostructures- A Review. *Open Ceram.* **2021**, *8* (August), 100179.

(69) Ghosh, B. K.; Moitra, D.; Chandel, M.; Ghosh, N. N. Preparation of TiO_2/Cobalt Ferrite/Reduced Graphene Oxide Nanocomposite Based Magnetically Separable Catalyst with Improved Photocatalytic Activity. *J. Nanosci. Nanotechnol.* **2017**, *17* (7), 4694–4703.

(70) Huang, S.; Xu, Y.; Zhou, T.; Xie, M.; Ma, Y.; Liu, Q.; Jing, L.; Xu, H.; Li, H. Constructing Magnetic Catalysts with In-Situ Solid-Liquid Interfacial Photo-Fenton-like Reaction over Ag_3PO_4@$NiFe_2O_4$ Composites. *Appl. Catal. B Environ.* **2018**, *225*, 40–50.

(71) Shanmuganathan, R.; LewisOscar, F.; Shanmugam, S.; Thajuddin, N.; Alharbi, S. A.; Alharbi, N. S.; Brindhadevi, K.; Pugazhendhi, A. Core/Shell Nanoparticles: Synthesis, Investigation of Antimicrobial Potential and Photocatalytic Degradation of Rhodamine B. *J. Photochem. Photobiol. B Biol.* **2020**, *202* (July 2019), 111729.

(72) Thomas, B.; Alexander, L. K. Nanoreactor Based Enhancement of Photocatalysis with $Co_{0.7}Zn_{0.3}Fe_2O_4$@$SrTiO_3$ Core-Shell Nanocomposites. *J. Alloys Compd.* **2019**, *788*, 257–266.

(73) Mrotek, E.; Dudziak, S.; Malinowska, I.; Pelczarski, D.; Ryżyńska, Z.; Zielińska-Jurek, A. Improved Degradation of Etodolac in the Presence of Core-Shell $ZnFe_2O_4/SiO_2/TiO_2$ Magnetic Photocatalyst. *Sci. Total Environ.* **2020**, *724*.

(74) Dippong, T.; Levei, E. A. Recent Advances in Synthesis and Applications of MFe_2O_4 (M = Co , Cu , Mn , Ni , Zn) Nanoparticles. **2021**, *4*, 3–8.

(75) Srinivasa Rao, K.; Ranga Nayakulu, S. V.; Chaitanya Varma, M.; Choudary, G. S. V. R. K.; Rao, K. H. Controlled Phase Evolution and the Occurrence of Single Domain $CoFe_2O_4$ Nanoparticles Synthesized by PVA Assisted Sol-Gel Method. *J. Magn. Magn. Mater.* **2018**, *451*, 602–608.

(76) Dutta, S. K.; Akhter, M.; Ahmed, J.; Amin, M. K.; Dhar, P. K. Synthesis and Catalytic Activity of Spinel Ferrites: A Brief Review. *Biointerface Res. Appl. Chem.* **2022**, *12* (4), 4399–4416.

(77) Dippong, T.; Levei, E. A. Recent Advances in Synthesis and Applications of MFe_2O_4 (M = Co , Cu , Mn , Ni , Zn) Nanoparticles. **2021**, *4*, 3–8.

(78) Birks, L. S.; Friedman, H. Particle Size Determination from X-Ray Line Broadening. *J. Appl. Phys.* **1946**, *17* (8), 687–692.

(79) El Ghandoor, H.; et al. Synthesis and Some Physical Properties of Magnetite (Fe_3O_4) Nanoparticles. *Int. J. Electrochem. Sci.* **2012**, *7* (6), 5734–5745.

(80) Bacsik, Z.; Mink, J.; Keresztury, G. FTIR Spectroscopy of the Atmosphere. I. Principles and Methods. *Appl. Spectrosc. Rev.* **2004**, *39* (3), 295–363.

(81) McMullan, D. Scanning Electron Microscopy 1928–1965. *Scanning* **1995**, *17* (3), 175–185.

(82) Alyamani, A.; M., O. FE-SEM Characterization of Some Nanomaterial. *Scan. Electron Microsc.* **2012**.

(83) Inkson, B. J. *Scanning Electron Microscopy (SEM) and Transmission Electron Microscopy (TEM) for Materials Characterization*; Elsevier Ltd, **2016**.

(84) Scimeca, M.; Bischetti, S.; Lamsira, H. K.; Bonfiglio, R.; Bonanno, E. Energy Dispersive X-Ray (EDX) Microanalysis: A Powerful Tool in Biomedical Research and Diagnosis. *Eur. J. Histochem.* **2018**, *62* (1), 89–99.

(85) Materials Characterization Fundamentals, *chemistry libre texts*,

https://chem.libretexts.org/@go/page/214242

(86) Nasrollahzadeh, M.; Atarod, M.; Sajjadi, M.; Sajadi, S. M.; Issaabadi, Z. *Plant-Mediated Green Synthesis of Nanostructures: Mechanisms, Characterization, and Applications*, 1st ed.; Elsevier Ltd., **2019**; Vol. 28.

(87) George, P.; Chowdhury, P. Complex Dielectric Transformation of UV-Vis Diffuse Reflectance Spectra for Estimating Optical Band-Gap Energies and Materials Classification. *Analyst* **2019**, *144* (9), 3005–3012.

(88) Barton, D. G.; Shtein, M.; Wilson, R. D.; Soled, S. L.; Iglesia, E. Structure and Electronic Properties of Solid Acids Based on Tungsten Oxide Nanostructures. *J. Phys. Chem. B* **1999**, *103* (4), 630–640.

(89) Qamar, M. K.; Zahid, M.; Yasmeen, A.; Yasin, M. F.; Manzoor, M.; Shaukat, A.; Piracha, S.; Saleem, S. Inductively Coupled Plasma Spectroscopy as Instrumental Tool for Detection of Nanoparticles. *Sch Bull*, **2021**, *9771*, 220–224.

CHAPTER-II

Palladium-Supported Polydopamine-Coated $NiFe_2O_4$@TiO_2: A Sole Photocatalyst for Suzuki and Sonogashira Coupling Reactions under Sunlight Irradiation

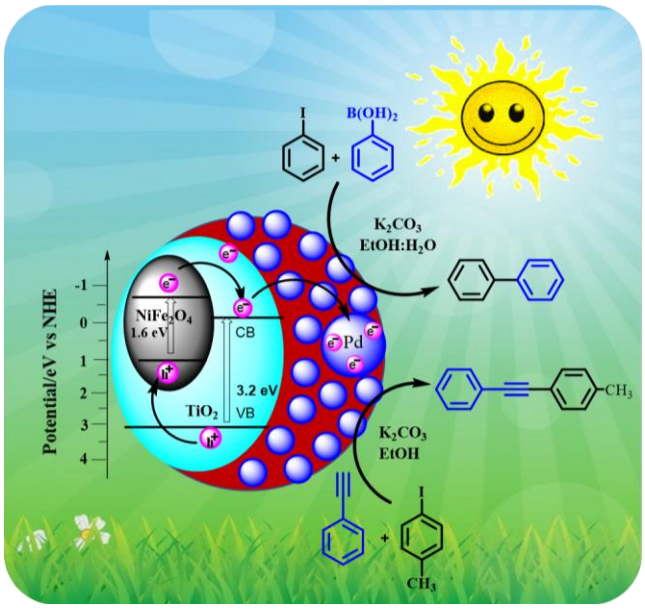

Chapter-II

Palladium-Supported Polydopamine-Coated $NiFe_2O_4$@TiO_2: A Sole Photocatalyst for Suzuki and Sonogashira Coupling Reactions under Sunlight Irradiation

2.1. Introduction

Solar energy has considerable potential as a green energy resource owing to its superabundance, cost efficiency, and non-polluting nature. The use of sunlight to carry out chemical reactions, frequently named as photo-catalysis, is a significant method to harness solar energy.[1–3] It shows good potency in a number of chemical processes such as photocatalytic degradation of pollutants, photocatalyzed organic reactions in the presence of various nanostructures, and so forth.[4–6] Two important phenomena in the photocatalysis process are efficient photogeneration of the electron−hole (e^-−h^+) pair and their separation.[7,8] The use of photo-generated holes or electrons for oxidation or reduction of organic molecules is an important aspect in light-driven chemical reactions. Regardless, the simultaneous application of both the photo-generated e^-− h^+ pairs for organic chemical reactions provides an outstanding catalytic perspective for cost-efficient and environmentally benign synthesis. Very limited reports are available on this aspect, and it has grabbed the attention of researchers to take it as a challenge in synthetic organic chemistry.[9–11]

Organic reactions involving C−C bond coupling (Suzuki and Sonogashira) are extremely significant with convenient approaches in synthetic organic chemistry in the preparation of natural products, pharmaceutical drugs, functional conjugated organic molecular materials, and so forth.[12–15] The traditional way of carrying out coupling reactions is the homogeneous catalysis using Pd/Pd complexes.[16] The notable limitations associated with the homogeneous Pd/Pd complex catalyst are its non-reusability, air and water sensitivity, and product contamination by residual Pd/ligands, thus making it inseparable.[17] These limitations accompanying the homogeneous catalysis motivated the scientific community to develop novel approaches in the form of heterogeneous catalysis with a focus on catalyst recovery and reuse.[18–21] Thus, development of eco-friendly heterogeneous photocatalysts for various organic coupling reactions with excellent stability, reusability, separability, and activity under ambient reaction conditions is crucial for synthetic organic applications.[22,23]

For the efficient harvesting of solar energy, several photocatalysts have been developed. TiO_2 is a well-known photocatalyst, but its usage is restricted due to a wide band gap (3.2 eV) that falls in the UV region. Due to environmental concerns, there is an exigency to perform the photocatalytic activity under visible light irradiation.[24–26] Consequently, the photocatalyst that

absorbs visible light and that can be easily separable from the reaction mixture is the immediate priority. Incorporating magnetic materials into solid matrices is the best choice that enables the integration of prominent methods for both photo-catalysis and magnetic separation.[27] Among the magnetic materials, spinel ferrites have extraordinary properties such as a low band gap, good stability against photo-corrosion, unique superparamagnetic nature, easy preparation, low cost, high adsorption capacity, and so forth.[28] Among the magnetic spinel ferrites, $NiFe_2O_4$, as an n-type semiconductor with a low band gap (~1.63 eV), has attracted much attention due to its effective light absorption capacity and stable physical and chemical properties. In accordance with the aforesaid facts, it is expected and reported that the integration of TiO_2 (high band gap) with $NiFe_2O_4$ (low band gap) leads to a core−shell material with a tuned band gap for visible light absorption. The resulting material thus possesses better magnetic separability for use as a good photocatalyst.[29,30]

To make this photocatalyst suitable for Suzuki and Sonogashira coupling reactions, we propose to incorporate Pd nanoparticles (NPs) onto the $NiFe_2O_4$@TiO_2 core@shell material owing to the effectiveness of Pd in catalyzing the coupling reactions. For the past few years, it has been reported that the supported Pd NPs have been explored to be a substitute for Pd complexes as a catalyst to overcome its limitations.[31−34] For good binding of Pd particles on the surface of the catalyst, it is an established fact that polydopamine (PDA) could be used as a universal surface modifying agent. It is because of the fact that PDA can form coordinate bonds with transition metal ions via its N- and O- binding sites, and metal ions can easily be reduced to metal NPs. Thus, it results in the formation of metal-supported PDA that could be used as an effective catalyst.[35−37]

Reports on the availability of a sunlight-driven sole magnetic photocatalyst under ambient conditions for both Suzuki and Sonogashira coupling reactions are scarce. Hence, in the present work, it is proposed to synthesize Pd(0) NPs supported on PDA-coated $NiFe_2O_4$@TiO_2 ($NiFe_2O_4$@TiO_2@PDA-Pd) as a nanophotocatalyst for C−C coupling reactions. Pd(0) NPs can be supported on the $NiFe_2O_4$@TiO_2@PDA material via a simple method involving mixing of Pd(II) ions with $NiFe_2O_4$@TiO_2@PDA followed by their reduction with sodium borohydride. In Suzuki and Sonogashira coupling reactions, this catalyst is expected to exhibit effective photocatalytic activity under sunlight absorption and is validated in the present work. Furthermore, the $NiFe_2O_4$@TiO_2@PDA-Pd can be easily separated with an external magnet for its reusability, without appreciable loss in catalytic efficacy.

2.2. Experimental Section

2.2.1. Materials

Ferric nitrate (Finar, 99%); nickel nitrate (Finar, 99%); titanium(IV) isopropoxide (Sigma-Aldrich,99%); dopamine hydrochloride (98%); $PdCl_2$ (Sigma-Aldrich, 99%); $NaBH_4$ (Finar, 99%); NaOH (Finar, 96%); HNO_3 (Finar, 69%); methanol (MeOH, Finar, 99%); ethanol (EtOH, Finar, 99%); ethyl acetate (EtOAc, Finar, 99%); and n-hexane (Finar, 98%); ammonium oxalate (AO); $K_2S_2O_8$ were used as starting materials, and double distilled (DD) water was used all through the experiments.

2.2.2. Synthesis of $NiFe_2O_4$ NPs

Nickel ferrite ($NiFe_2O_4$) NPs were synthesized using the hydrothermal method. In this method, $Ni(NO_3)_2{\cdot}6H_2O$ and $Fe(NO_3)_3{\cdot}9H_2O$ were taken in a 1:2 molar ratio and dissolved in 40 mL of DD water. A clear solution was obtained after 15 min of stirring at room temperature (RT). The pH of the solution was adjusted to 12 using 2 M NaOH solution with continuous stirring for 30 min. The resulting solution was placed in a stainless-steel autoclave and was heated at 180 °C for 12 h. Then, it was allowed to cool to RT. The attained product was washed three times with DD water and ethanol, followed by drying in an oven at 60 °C. Finally, it was subjected to calcination at 800 °C for 2 h. Thus, $NiFe_2O_4$ NPs were prepared.

2.2.3. Synthesis of $NiFe_2O_4$@TiO_2 (core@shell) NPs

Initially, 1 g of synthesized nickel ferrite ($NiFe_2O_4$) was dispersed in 50 ml of methanol. The mixture was magnetically stirred for 15 min. 2.5 g of titanium tetraisopropoxide [yield of TiO_2 (anatase): 1 g] was then introduced into the mixture and stirred for 10 min, followed by the addition of 10 mL of DD water. After 10 min, HNO_3 was added slowly to maintain the pH of the solution at 2. The resulting solution was continuously stirred for 90 min which then turns into a gel-like material. The gel was dried in an oven at 60 °C for 1 h, ground into a fine powder and then calcined at 500 °C for 2 h. $NiFe_2O_4$@TiO_2 NPs were thus prepared.

2.2.4. Surface Modification of $NiFe_2O_4$@TiO_2 with PDA

1 g of synthesized $NiFe_2O_4$@TiO_2 NPs was added to 500 mL of Tris buffer (10 mM, pH 8.5). 1 g of dopamine was then introduced into the resulting solution. The resulting mix was mechanically stirred at RT for 24 h. During the process, dopamine was polymerized to PDA and got coated over $NiFe_2O_4$@TiO_2, resulting in the formation of $NiFe_2O_4$@ TiO_2@PDA NPs. PDA-coated $NiFe_2O_4$@TiO_2 was separated employing an external magnet at the end of the reaction and was washed with DD water and ethanol, followed by drying in an oven at 40 °C to form the surface-modified $NiFe_2O_4$@TiO_2 with PDA.

2.2.5. Synthesis of the $NiFe_2O_4$@TiO_2@PDA-Pd Catalyst

1 g of synthesized $NiFe_2O_4$@TiO_2@PDA was dispersed in 200 mL of DD water for 20 min. Subsequently, 0.05 g of $PdCl_2$ in 20 mL of water was introduced into the reaction mixture with stirring for 24 h. Consequently, with vigorous stirring, 0.05 g of $NaBH_4$ was added to the reaction mixture. During the process, Pd(II) got reduced to Pd(0) and deposited on $NiFe_2O_4$@ TiO_2@PDA. After 1h of stirring, the resulting Pd-supported $NiFe_2O_4$@TiO_2@PDA ($NiFe_2O_4$@TiO_2@PDA-Pd) was isolated with the aid of an external magnet, washed thoroughly with DD water, and then dried at 60 °C under vacuum for 12 h.

2.2.6. Photocatalytic Suzuki Coupling Reaction

The photocatalytic activity of the prepared catalyst for a typical Suzuki coupling reaction (SCR) between aryl halides and arylboronic acid was investigated. In this process, aryl halides (1 mmol), arylboronic acid (1.5 mmol), K_2CO_3 (2.5 mmol), and the $NiFe_2O_4$@TiO_2@PDA-Pd catalyst (5 mg) were mixed in a round-bottom (RB) flask with 3 mL of EtOH and H_2O as a solvent in a 1:1 volume ratio. The reaction mixture was continuously stirred under direct sunlight from 11.00 am to 3.00 pm. The spectral distribution of natural sunlight comprise of 3-55 OF UV radiation (290-400nm), 44% of visible ration (400-700nm) and 53% of infrared radiation (700-1400nm). As the synthesized catalyst is visible light active, it works well by absorbing the visible light from the sun. The intensity of the sunlight will influence the rate of reaction. It is reported that higher light intensity will affect the recombination mechanism thus effecting utilization of electrons. The average intensity of the sunlight was measured to be 50−60 mW/cm^2 using a Newport Optical Power Meter (model 842.PE) with an average outdoor temperature of 30 °C. In the present study, moderate intensity of the sunlight was observed which will not affect the catalytic activity and the catalyst worked well. On completion of the reaction [as confirmed by thin-layer chromatography (TLC)], the catalyst was isolated by simple means with the aid of a magnet. After being extracted twice with ethyl acetate, the products were purified using column chromatography. Each reaction was performed two times and the average of the yield was reported. ^1H and ^{13}C NMR spectral analysis was performed to analyze the products.

2.2.7. Photocatalytic Sonogashira Coupling Reaction

The photocatalytic performance of the prepared catalyst for a typical Sonogashira coupling reaction between aryl halides and arylacetylene to yield diarylacetylene was investigated. In this experiment, aryl halides (1 mmol), arylacetylene (1.3 mmol), K_2CO_3 (2 mmol), and the $NiFe_2O_4$@TiO_2@PDA-Pd catalyst (10 mg) were mixed in an RB flask with 3 mL of the EtOH solvent. The reaction was continuously stirred under the irradiation of sunlight

at an average outdoor temperature of 30 °C. On completion of the reaction (as confirmed by TLC), the catalyst was set apart with the aid of a magnet. After being extracted twice with ethyl acetate, the products were purified using column chromatography. Each reaction was performed two times and the average of the yield was reported. ^{1}H and ^{13}C NMR spectral analysis was performed to analyze the products.

Catalyst recovery

The magnetic nanocatalyst was isolated from the reaction mixture for further use by holding the magnet externally to the reaction vessel. Consequently, the catalyst got stuck to the wall by external magnet and the reaction mixture was decanted into another container. The retained catalyst in the vessel was washed with DD water and ethanol for three times, dried (at 60 °C overnight) and was used in the next run. 99% of the catalyst was fully recovered with minimal loss of the catalyst. This can be understood by the fact that the recovered catalyst was reused further in the reaction where it has shown almost the same activity.

2.2.8. Characterization of the Catalyst

Powder X-ray diffraction (PXRD) analysis of the synthesized materials ($NiFe_2O_4$, $NiFe_2O_4$@TiO_2, and $NiFe_2O_4$@TiO_2@PDA-Pd) was carried out on a PAN Analytical Advance X-ray diffractometer with Ni-filtered Cu Kα (λ = 1.5406 Å) radiation in a 2θ scan range between 10 and 60° to assess the crystalline nature of the catalyst. The Fourier-transform infrared (FT-IR) spectrum for all the materials was recorded in the range of 4000−400 cm^{-1} using the PerkinElmer Spectrum by KBr pellet technique. The surface morphology of the synthesized photocatalyst was examined using scanning electron microscopy (SEM, Carl Zeiss SMT Ltd., Zeiss EVO 18), transmission electron microscopy (TEM), and selected area electron diffraction (SAED) (TEM, Jeol/JEM 2100 at 200 kV). X-ray photoelectron spectroscopy (Kratos/Shimadzu Amicus, Model: ESCA 3400) was used to determine the binding energies of elements in the catalyst. UV−vis diffuse reflectance spectra of all the materials was recorded on Analytik Jena, SPECORD 210 PLUS at RT. The magnetic hysteresis curves of the catalyst were recorded using a vibrating sample magnetometer (VSM, Lake Shore, Model: 8600 Series). Inductively coupled plasma optical emission spectroscopy (ICP-OES) analysis was aimed to ascertain the quantity of Pd in the synthesized nanocatalyst (PerkinElmer Optima 5300 DV). ^{1}H NMR and ^{13}C NMR spectra were recorded on an ADVANCED-III Bruker 400 MHz NMR spectrometer using $CDCl_3$ as the solvent and tetramethylsilane as an internal standard where chemical shifts were mentioned as parts per million (ppm).

2.3. Results and Discussion

2.3.1. Preparation of the $NiFe_2O_4$@TiO_2@PDA-Pd Catalyst

The $NiFe_2O_4$@TiO_2@PDA-Pd catalyst was synthesized by a multistep procedure (Scheme 1). In step I, the $NiFe_2O_4$ NPs were prepared by the hydrothermal method. In step II, the in situ $NiFe_2O_4$@TiO_2 core@shell structure was prepared via the sol−gel method. In step III, $NiFe_2O_4$@TiO_2 NPs were surface-modified by PDA where dopamine was polymerized in Tris buffer solution (10 mM, pH 8.5) under continuous stirring. Finally, in step IV, palladium (0) NPs were supported on $NiFe_2O_4$@TiO_2@PDA by impregnation of Pd(II) ions over the surface of the polymer (PDA) layer followed by its subsequent reduction with sodium borohydride. This led to the synthesis of the palladium-supported PDA-coated core@shell nanophotocatalyst ($NiFe_2O_4$@TiO_2@PDA-Pd). An external magnet was used to isolate the synthesized photocatalyst, which was then dried under vacuum conditions for further use. Scheme 2.1depicts the overall synthesis of the nanophotocatalyst.

Scheme 2.1. *Preparation Path of the $NiFe_2O_4$@TiO_2@PDA-Pd Nanophotocatalyst*

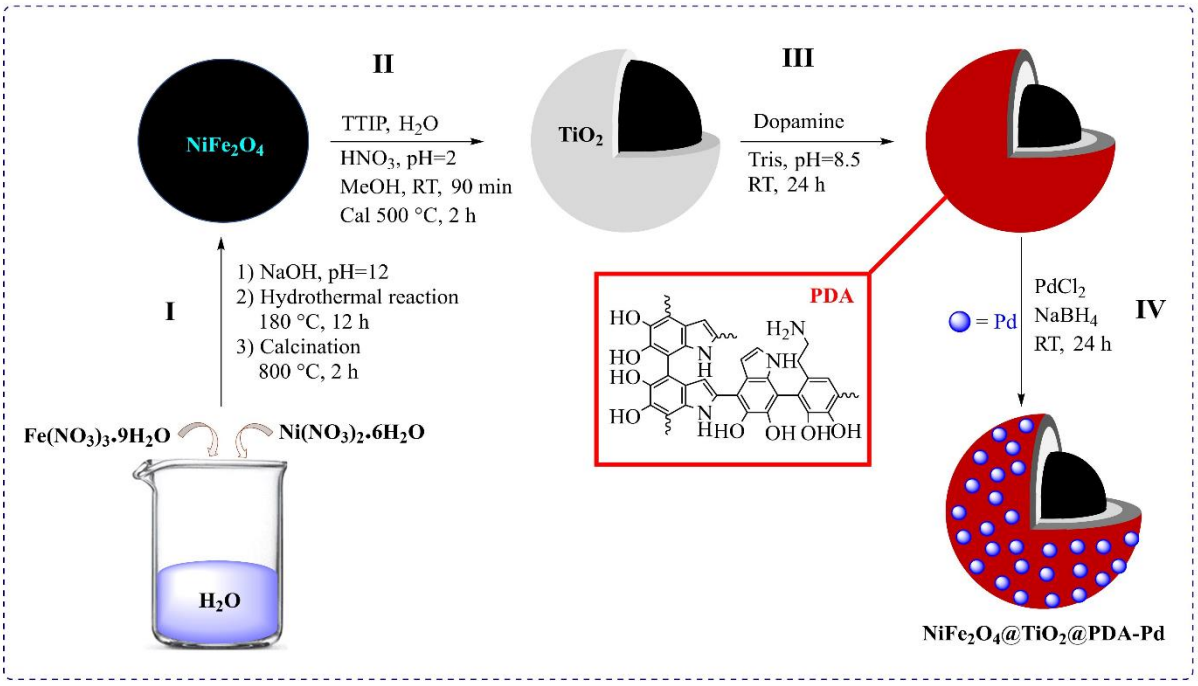

2.3.2. Characterization of the $NiFe_2O_4$@TiO_2@PDA-Pd Catalyst.

The indexed XRD patterns of the synthesized $NiFe_2O_4$, $NiFe_2O_4$@TiO_2, and $NiFe_2O_4$@TiO_2@PDA-Pd catalyst are shown in **Figure 2.1**. The broad peaks observed in the figure reveal the nanoscale range of the particles possessing a small crystallite size. The observed peaks in **Figure 2.1a(I)** at 2θ values of 18.5, 30.4, 35.8, 37.3, 43.4, 53.8, 57.4, and 63.0° were attributed to (111), (220), (311), (222), (400), (422), (511) and (440) diffractions, respectively, signifying the formation of single-phase pure crystalline spinel $NiFe_2O_4$ (ICDD

card no. 10−0325). A small peak was detected in the figure at 2θ of 33.2° for the $NiFe_2O_4$ sample calcined at 800 °C, which corresponds to a small quantity of the impure phase of α-Fe_2O_3 that occurs naturally as hematite (ICDD card 33-0664).[38] The additional peaks appeared at 2θ of 25.3 and 48.1° along with the diffraction peaks of $NiFe_2O_4$ in **Figure 1a(II)** attributed to (101), (200) diffractions of anatase (JCPDS card no. 78-2486), thus signify the formation of $NiFe_2O_4$@TiO_2 NPs.[39] The diffraction patterns of the catalyst in **Figure 2.1a(III)** depict that the crystallinity of $NiFe_2O_4$@TiO_2 NPs was intact and not altered despite the PDA coating and Pd loading as well. Also, **Figure 2.1a(III)** has no noticeable peak related to Pd NPs owing to the presence of low palladium content on the PDA surface.

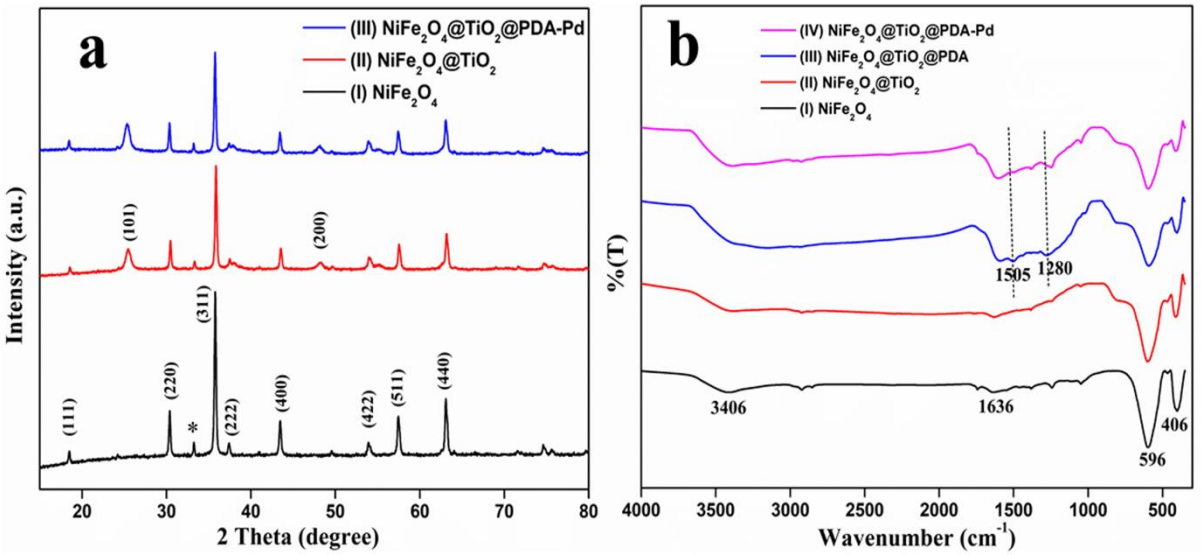

Figure 2.1. *(a) XRD spectra and (b) FTIR spectra of samples*

FT-IR spectra of the prepared samples are shown in **Figure 2.1b**. Two significant peaks were noticed in the range of 600−400 cm^{-1} for all the samples that are characteristic of the spinel structure. The peaks detected at 406 and 596 cm^{-1} correspond to the intrinsic vibrations of metal ion−oxygen complexes in octahedral and tetrahedral sites in the spinel structure, respectively, and the peaks around ∼1600 and ∼3400 cm^{-1} represent the bending and stretching mode of surface-adsorbed H_2O and also the stretching mode of OH groups **[Figure 2.1b(I)].** The peaks that appeared at 1505 and 1280 cm^{-1} in **Figure 2.1b(III),** which were not seen in **Figure 2.1b(I,III),** were attributed to C−C stretching and C−N stretching modes, respectively, that indicated the presence of −C−C−NH functional groups of PDA. The observed peak at around ∼3390 cm^{-1} indicates the presence of −OH of phenol in $NiFe_2O_4$@TiO_2@PDA. These outcomes infer that PDA has been successfully deposited on the surface of $NiFe_2O_4$@TiO_2 NPs by its adsorption. In the FTIR spectrum of the $NiFe_2O_4$@TiO_2@PDA-Pd nanocatalyst, no dramatic changes were observed as evident from **Figure 2.1b(IV).** Meanwhile, the peak

intensity observed at 1505 and 1280 cm^{-1} has shifted to a low frequency owing to the bonding interactions between the PDA functional groups and the Pd NPs.[40,41]

The surface morphology of the synthesized nanocatalyst $NiFe_2O_4@TiO_2@PDA$-Pd was observed by SEM images shown in **Figure 2.2 a,b** that represents a near spherical cluster like structure of the catalyst. Keen examination of the image depicts the presence of small particles supported on a continuous layer over a core−shell justifying the immobilization of Pd NPs on the PDA layer over the $NiFe_2O_4@TiO_2$ core−shell structure as $NiFe_2O_4@TiO_2@PDA$-Pd. Furthermore, the energy-dispersive X-ray spectroscopy (EDAX) detector attached to SEM was used to establish the existence of Pd particles over PDA on $NiFe_2O_4@TiO_2$ NPs. The SEM− EDX spectrum shown in **Figure 2.2c** describes the presence of Pd, N, Ti, Fe, Ni, C, and O elements in the catalyst. Thus, the SEM−EDAX images portray the successful coating of PDA on $NiFe_2O_4@TiO_2$ and also effective loading of Pd over the surface of $NiFe_2O_4@TiO_2@PDA$.

Deposition of Pd NPs on the surface of PDA in the catalyst was also confirmed by TEM analysis. TEM images portray a spherical shape of the NPs in the catalyst, thus the morphology observed by SEM was further confirmed. The presence of a thin continuous PDA layer around $NiFe_2O_4@TiO_2$ with a thickness of about 15.24 nm was revealed by TEM image in **Figure 2.2d**. The thick and uniform distribution of small Pd NPs throughout the PDA surface was clearly seen in the two TEM images shown in **Figure 2.2 e,f**. They depicted the magnified images at 100 and 200 nm, where Pd NPs were homogeneously decorated on the peripheral surface of $NiFe_2O_4@TiO_2@PDA$ without large agglomeration, inferring that Pd NPs were effectively immobilized on the surface of PDA. The particle size distribution histogram of the catalyst which is embedded in **Figure 2.2e,f** estimated the average size of the Pd NPs to be around 28.6 nm. It was found that the dark Pd NPs were coated over the gray PDA layer on the dark core−shell of $NiFe_2O_4@TiO_2$. These TEM images are in accordance with SEM information with respect to the morphology. The polycrystalline nature of the material was confirmed by the presence of the number of grains with different orientation of the planes as indicated in the high resolution TEM (HRTEM) image shown in **Figure 2.2g**. The lattice fringe spaces of 0.30 nm shown in the figure could possibly be ascribed to the (111) crystal plane of Pd NPs. The SAED pattern of $NiFe_2O_4@TiO_2@PDA$-Pd was depicted in **Figure 2.2h**. It revealed that diffraction rings composed of a bright spot possessing sixfold symmetry that manifested the polycrystalline nature of the material.

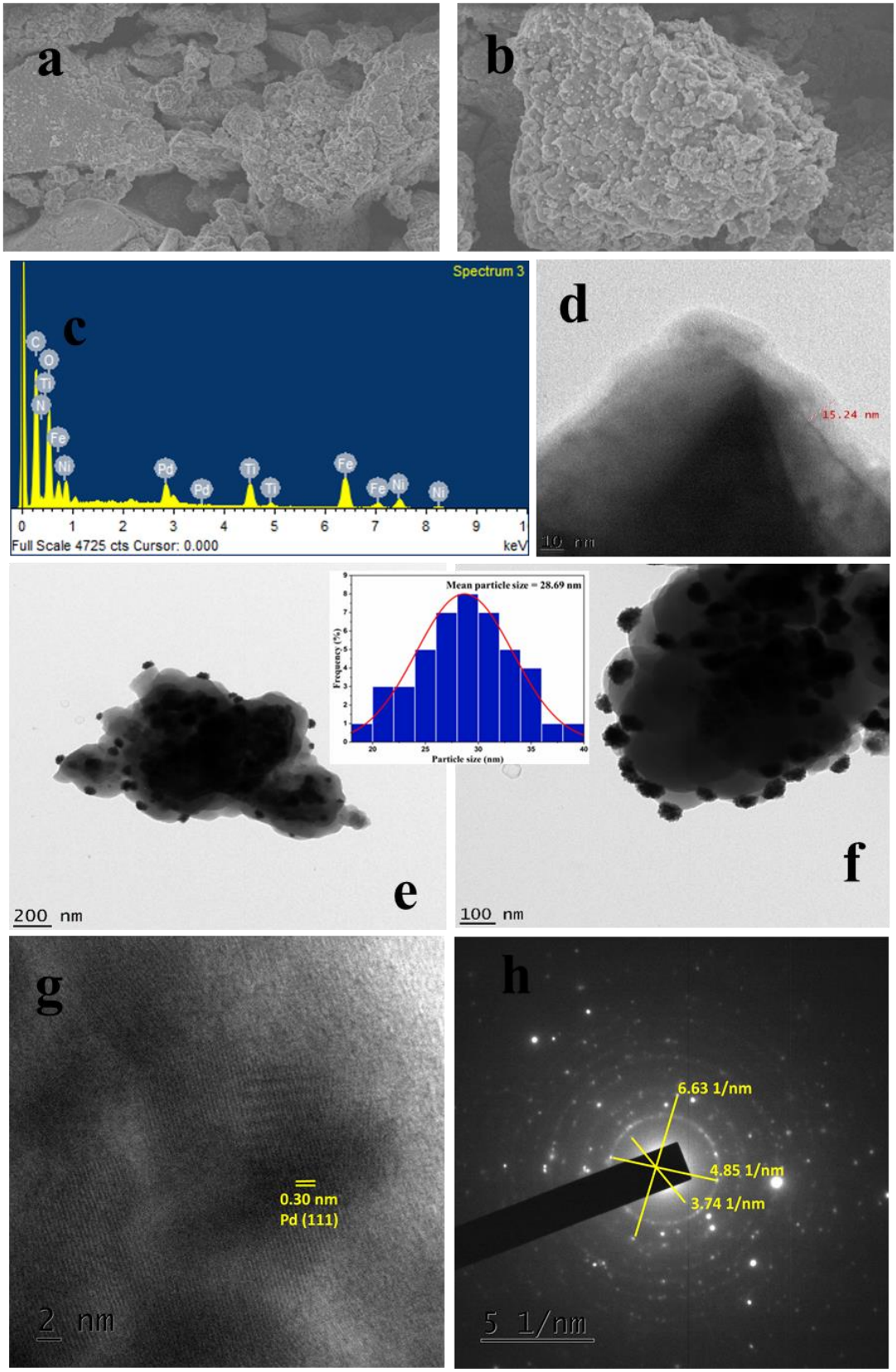

Figure 2.2. *(a,b) SEM images (c) EDAX (d) PDA layer (e,f) TEM images with a particle size histogram (g) HRTEM image and (h) SAED pattern of* $NiFe_2O_4@TiO_2@PDA\text{-}Pd$

X-ray photoelectron spectroscopy (XPS) was employed to confirm the effective coordination of Pd on the PDA layer. It is a powerful tool to understand the electronic properties of the coordinated particles on the surface such as the electron environment, binding energy, and chemical valence states of the metals. The chemical valence states of Ti, N, and Pd in the catalyst were analysed from the XPS spectra of the $NiFe_2O_4$@TiO_2@PDA-Pd nanophotocatalyst shown in **Figure 2.3.** The two noticeable bands in the figure at binding energies 458.4 and 464.9 eV were ascribed to the Ti $2p_{3/2}$ and Ti $2p_{1/2}$ photoelectrons in the Ti^{4+} chemical state, respectively. Whereas the two peaks at 455.4 and 463.4 eV were attributed to the Ti $2p_{3/2}$ and Ti $2p_{1/2}$ photoelectrons in the Ti^{3+} state in the TiO_2 chemical state, respectively (**Figure 2.3a**).[42] N1s photoelectrons of the NH group were represented by the peak at 399.7 eV in **Figure 2.3b**. It was evident from the N1s spectrum of **Figure 2.3b** that the $NiFe_2O_4$@TiO_2 core@shell NPs were successfully coated with PDA. Furthermore, the two observed bands at binding energies 335.3 and 340.6 eV in Figure 3c can be indexed as Pd(0) $3d_{5/2}$ and Pd(0) $3d_{3/2}$, respectively. These values confirm the presence of Pd(0) in the prepared catalyst which was not noticeable in XRD. These results were in accordance with the values of metallic Pd.[43]

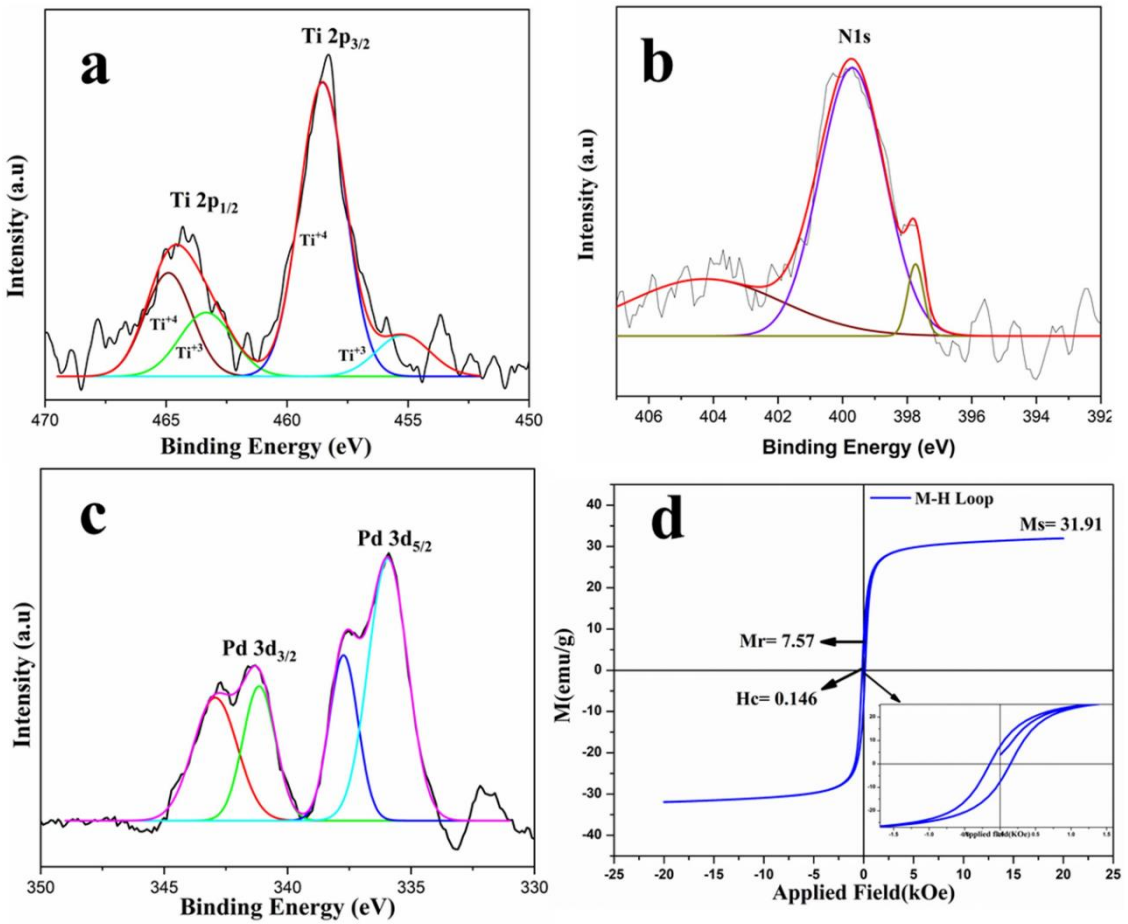

Figure 2.3. *(a) Ti 2p peaks (b) N 1s peak (c) Pd 3d peaks and (d) magnetization curve of $NiFe_2O_4$@TiO_2@PDA-Pd (inset: zoomed-in region of the area under the curve)*

The magnetic performance of the synthesized nanocatalyst was investigated with the VSM at RT. The magnetization curve of the $NiFe_2O_4@TiO_2$@PDA-Pd catalyst was depicted in **Figure 2.3d**. From the figure, the saturation magnetization (M_s), coercivity (H_c), and remanence magnetization (M_r) were found to be 31.9 emu/g, 0.146 kOe, and 7.57 emu/g respectively. The magnetization data revealed the good magnetic behavior of the synthesized catalyst, thus becoming evidential of the magnetic recovery and reusability of the catalyst.

The UV−vis diffuse reflectance spectra of the synthesized $NiFe_2O_4$, $NiFe_2O_4@TiO_2$, $NiFe_2O_4@TiO_2$@PDA, $NiFe_2O_4@TiO_2$@PDA-Pd, and pure TiO_2 were recorded, and the results were depicted in **Figure 2.4a**. It is understood from the figure that pure TiO_2 and $NiFe_2O_4$ show absorption bands with absorption edges at 400 and 700 nm, respectively, as illustrated in **Figure 2.4a(I,II).** The data confirmed that the absorption of TiO_2 was in the UV region and that of $NiFe_2O_4$ was in the visible region. However, after the surface modification of $NiFe_2O_4$ with TiO_2, the obtained core@shell ($NiFe_2O_4@TiO_2$) material exhibited absorption in the visible region as seen in **Figure 2.4a(III).** It confirmed the ability of $NiFe_2O_4@TiO_2$ to absorb visible light. Even after coating $NiFe_2O_4@TiO_2$ with PDA and also supported by the metal (Pd) on its surface, the resulting $NiFe_2O_4@TiO_2$@PDA-Pd magnetic photocatalyst still exhibited absorption in the visible region as evident from **Figure 2.4a(IV,V)**.

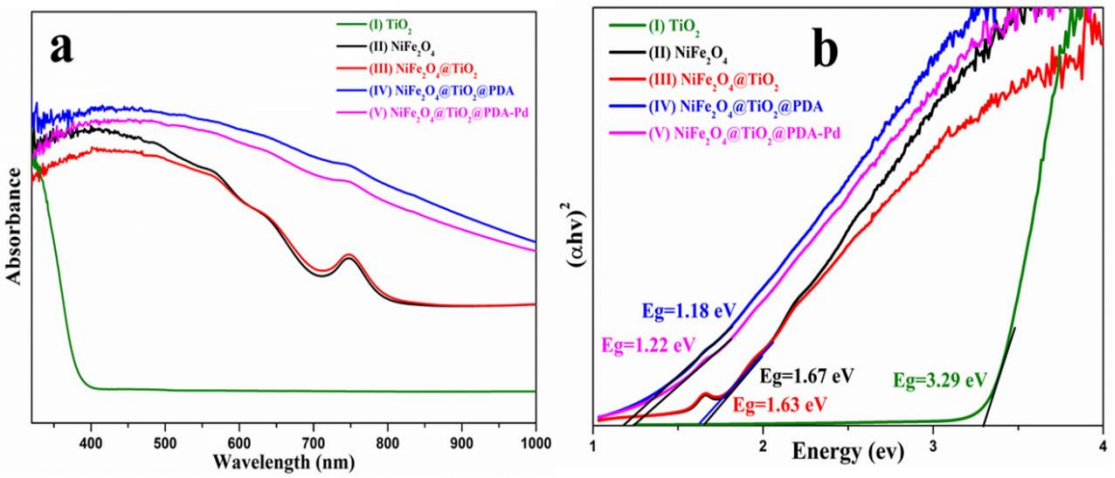

Figure 4. *(a) UV−vis absorption spectra and (b) band gap energies of the samples*

The band gap energy (E_g) of all the samples was estimated from the Tauc plot of $(\alpha h\upsilon)^2$ versus $h\upsilon$ as presented in **Figure 4b**. Extrapolation of the $h\upsilon$ value to $\alpha = 0$ resulted in absorption band gap energy (E_g). As seen from **Figure 2.4b**, E_g for pure $NiFe_2O_4$ and TiO_2 was found to be 1.67 and 3.29 eV respectively, which is in accord with the reported values.[44,45] In contrast, the band gap energy of $NiFe_2O_4@TiO_2$ was observed to be 1.63 eV which indicates the absorption in the visible region. Furthermore, the decrease in energy gap (E_g) upon core@shell formation confirms the electronic coupling between $NiFe_2O_4$ and TiO_2. After

surface modification with PDA supported by the Pd metal, an even stronger visible-region band gap energy of 1.22 eV was observed for the $NiFe_2O_4$@TiO_2@PDA-Pd nanocatalyst.

2.3.3. Application of the $NiFe_2O_4$@TiO_2@PDA-Pd Catalyst in Suzuki and Sonogashira Coupling Reactions under Sunlight

In the past few decades, Pd has been employed as an active catalyst for C−C coupling reactions. Nevertheless, most of the times, the coupling reactions with Pd as a catalyst take place under heating conditions, which consumes lot of energy. Therefore, it would be a significant improvement if the catalytic activity of Pd as a catalyst could be improved at ambient temperatures using the visible region of the sunlight (an abundant and environmentally sustainable energy source). As the synthesized catalyst shows absorption in the visible region, the validity of the catalyst was tested for the Suzuki and Sonogashira coupling reactions in natural sunlight under ambient conditions (photocatalytic coupling reactions).

2.3.3.1. Suzuki Coupling Reaction

A simple SCR involving aryl halides and arylboronic acid was performed using the synthesized $NiFe_2O_4$@TiO_2@PDA-Pd nanophotocatalyst under sunlight, at an average outdoor temperature of 30 °C. Optimization of various vital reaction conditions for the SCR, *viz*., nature of the solvent, base, light source, and Wt % of Pd, was performed. The effect of various solvents in the presence of K_2CO_3 as a base with 5% of Pd by weight on the photocatalytic SCR was observed. The obtained yield of the product was low in the presence of polar aprotic solvents, namely, dimethyl sulfoxide and dimethylformamide, and also in the presence of nonpolar solvents such as toluene (**Table 2.1, entries 1−3).** However, observed yield of the product was high in the presence of polar protic solvents such as ethanol and methanol (**Table 2.1, entries 4,5**). Furthermore, the reaction in pure H_2O resulted in moderate yield (**Table 2.1, entry 6**) of the product. It was observed that 98% yield of the product was obtained in the presence of a mixture of EtOH and H_2O as a solvent in a 1:1 ratio, indicating the significant enhancement in the photocatalytic activity (**Table 2.1, entry 7**). These results infered that photocatalyzed Suzuki reactions in the presence of the $NiFe_2O_4$@TiO_2@PDA-Pd nanophotocatalyst require protic solvents. Furthermore, the influence of other bases (Cs_2CO_3, NaOH, Et_3N) (**Table 2.1, entries 12−14**) in the solvent EtOH·H_2O (1:1) was also explored, but good yield was observed in the presence of only K_2CO_3 as a base among all (**Table 2.1, entry 7**).

To study the influence of light on the SCR, the reaction was performed in dark at RT and also at 60 °C. It was found that moderate yields (30 and 64%) (**Table 2.1, entries 15,16**) were obtained in dark at RT and at 60 °C, respectively. While performing the reaction under

visible light (Hg lamp 250W), the product yield was improved (85%) (**Table 2.1, entry 17**). To test the feasibility of environmental concerns, the reaction was initiated in natural sunlight, and an excellent yield (98%) of the product was observed. Furthermore, no product was observed in the presence of $NiFe_2O_4$, $NiFe_2O_4$@TiO_2, and $NiFe_2O_4$@TiO_2@PDA separately. Thus, this study indicates the significance of Pd presence in the synthesized nanocatalyst ($NiFe_2O_4$@TiO_2@PDA-Pd) in carrying out the SCR.

Table 2.1 *Screening of Reaction Conditions for SCR of Iodobenzene and Phenyl Boronic Acid*[a]

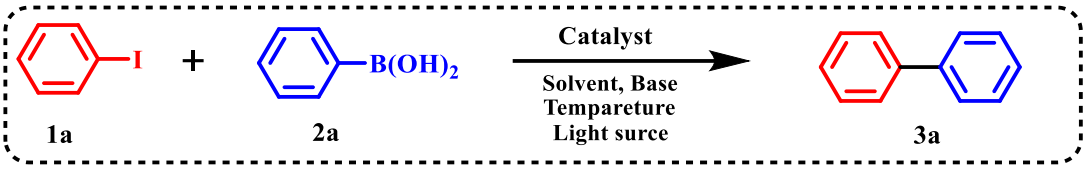

S.No	Solvent	Base	Sunlight	Yield(%)[b]
1	DMSO	K_2CO_3	+	30
2	DMF	K_2CO_3	+	36
3	Toluene	K_2CO_3	+	20
4	EtOH	K_2CO_3	+	65
5	MeOH	K_2CO_3	+	50
6	H_2O	K_2CO_3	+	42
7	**EtOH:H_2O (1:1)**	**K_2CO_3**	**+**	**98**
8	MeOH:H_2O (1:1)	K_2CO_3	+	80
9	DMSO:H_2O (1:1)	K_2CO_3	+	52
10	DMF:H_2O (1:1)	K_2CO_3	+	60
11	EtOH:H_2O (9:1)	K_2CO_3	+	70
12	EtOH:H_2O (1:1)	Cs_2CO_3	+	92
13	EtOH:H_2O (1:1)	NaOH	+	35
14	EtOH:H_2O (1:1)	Et_3N	+	14
15	EtOH:H_2O (1:1)	K_2CO_3	-	30[c]
16	EtOH:H_2O (1:1)	K_2CO_3	-	64[d]
17	EtOH:H_2O (1:1)	K_2CO_3	-	85[e]
18	EtOH:H_2O (1:1)	K_2CO_3	+	38
19	EtOH:H_2O (1:1)	K_2CO_3	+	51

[a]**Reaction conditions:** iodobenzene (1.0 mmol), phenyl boronic acid (1.5 mmol), $NiFe_2O_4$@TiO_2@PDA-Pd catalyst (5 mg) and base (2.5 mmol) in solvent (3 mL) under direct sunlight (400 to 700 nm) at 30 °C for 0.5 h. [b]Isolated yields [c]Room temperature (dark) [d]Thermal reaction at 60 °C (Dark) [e] High pressure Hg lamp (250 W) (visible range 350nm and above) at room temperature.

Active species trapping experiments were performed using scavengers to understand the role of photogenerated active species (e^- h^+ pair) in the photocatalytic mechanism of the $NiFe_2O_4$@TiO_2@PDA-Pd photocatalyst. In this experiment, $K_2S_2O_8$ was used as an e^- scavenger, and ammonium oxalate (AO) was used as a h^+ scavenger. In the presence of $K_2S_2O_8$, poor yield (38%) of the product was observed (**Table 2.1, entry 18**), whereas in the presence of AO, 51% yield of the product was observed (**Table 2.1, entry 19**). Thus, the trapping experiments indicatede that both the photogenerated active species played a significant role in the C−C coupling reaction with a major contribution from photogenerated electrons.

The reaction generality was further investigated by $NiFe_2O_4$@TiO_2@PDA-Pd under the sunlight using several aryl halides and substituted arylboronic acids to validate the scope of the synthesized catalyst (**Table 2.2**). It was observed that the presence of electron-withdrawing groups (EWGs) and electron-donating groups (EDGs) produced outstanding yields for para-substituted aryl halides. The reaction progressed effectively regardless of substrates with the EWG and EDG yielding more than 85% in most of the cases, except in case of aryl bromides and chlorides due to the stronger C−halogen bond than the C−I bond (**Table 2.2, entries 10−12**). Furthermore, it was observed that the reaction progressed faster on substrates with EDGs than on substrates with EWGs. This fact could be addressed by the inductive effects of the substituent groups on the substrates.[46]

***Table 2.2**. Substrate Scope of the SCR Catalyzed by $NiFe_2O_4$@TiO_2@PDA-Pd under Sunlight Irradiation*[a]

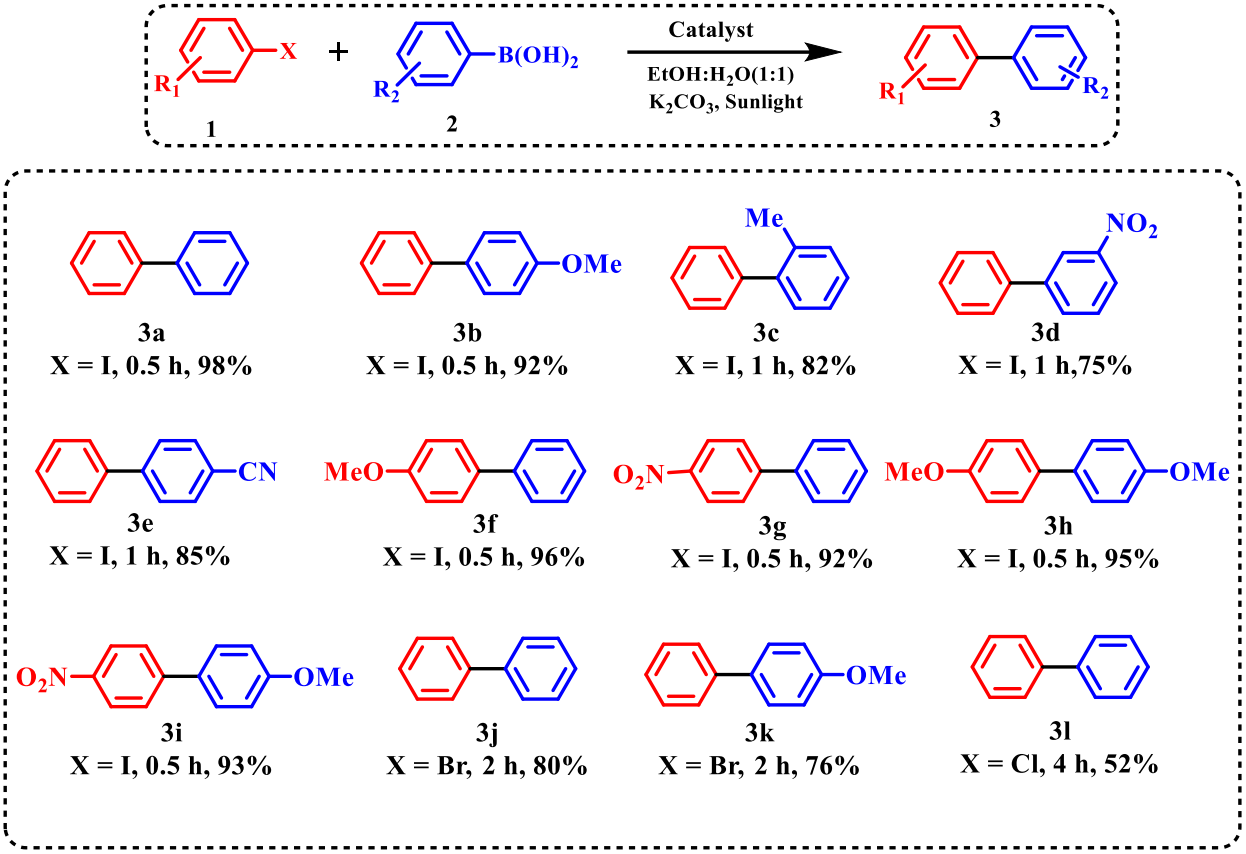

[a]**Reaction conditions:** aryl halides (1.0 mmol), phenylboronic acids (1.5 mmol), $NiFe_2O_4$@TiO_2@PDA-Pd catalyst (5 mg), and K_2CO_3 (2.5 mmol) in EtOH:H_2O (3 mL) under direct sunlight at 30 °C

2.3.3.2. Sonogashira Coupling Reaction.

The catalytic potential of the synthesized $NiFe_2O_4$@TiO_2@PDA-Pd catalyst with 5% by weight of Pd loading was further extended to test the feasibility of the Sonogashira coupling reaction involving aryl halides and arylacetylenes under sunlight, at an average outdoor temperature of 30 °C. Optimization of various vital reaction conditions, *viz.*, nature of the solvent, base, and light source for the Sonogashira reaction, was performed. In this reaction, the solvent played a significant role. EtOH was found to be an excellent solvent for this reaction out of a variety of solvents tested (**Table 2.3, entries 1−5**).

High yield of the product was obtained in the presence of K_2CO_3 as the base when compared to other bases (Cs_2CO_3, NaOH, and Et_3N) (**Table 2.3, entries 6−8**). Influence of the light source on the Sonogashira reaction was also established in the presence of the synthesized catalyst. The product yield was very low in dark at RT and moderate (59%) at 60 °C (**Table**

2.3, entries 9−10). Under vis light (Hg lamp 250W), the yield was 81%, and under sunlight, higher yield (96%) was obtained (**Table 2.3, entries 11, 2**). Thus, the fact of using sunlight in getting high yield was established.

Table 2.3*. Screening of Reaction Conditions for Sonogashira Coupling Reaction of Iodobenzene and Phenyl Acetylene*[a]

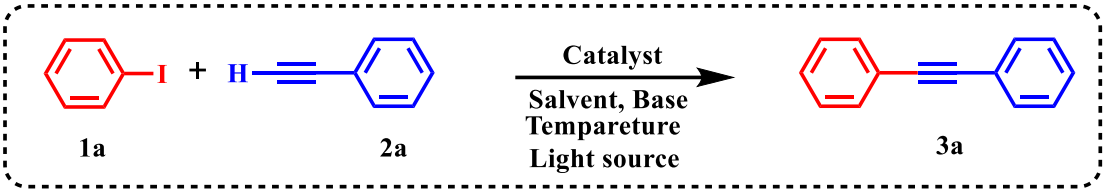

S.No	Solvent	Base	Sunlight	Yield(%)[b]
1	MeOH	K_2CO_3	+	84
2	**EtOH**	**K_2CO_3**	**+**	**96**
3	H_2O	K_2CO_3	+	32
4	EtOH:H_2O (1:1)	K_2CO_3	+	73
5	DMF	K_2CO_3	+	40
6	EtOH	Cs_2CO_3	+	82
7	EtOH	NaOH	+	27
8	EtOH	Et_3N	+	22
9	EtOH	K_2CO_3	-	26[c]
10	EtOH	K_2CO_3	-	59[d]
11	EtOH	K_2CO_3	-	81[e]

[a]**Reaction conditions:** iodobenzene (1.0 mmol), phenyl acetylene (1.3 mmol), $NiFe_2O_4$@TiO_2@PDA-Pd catalyst (10 mg) and base (2 mmol) in solvent (3 mL) under direct sunlight (400 to 700 nm) at 30 °C for 2.5 h. [b]Isolated yield [c]Room temperature (dark) [d]Thermal reaction at 60 °C (Dark) [e]High pressure Hg lamp (250 W) (visible range 350nm and above) at room temperature.

The feasibility of the Sonogashira reaction was verified with $NiFe_2O_4$, $NiFe_2O_4$@TiO_2, and $NiFe_2O_4$@TiO_2@PDA separately, and no products were observed indicating the significance of Pd in the catalyst. The substrate scope of the Sonogashira coupling reaction over the $NiFe_2O_4$@TiO_2@PDA-Pd nanophotocatalyst was also investigated using the

optimized conditions. The aryl halides with EWGs or EDGs have resulted in a higher yield of the product (**Table 2.4**).

Table 2.4 *Substrate Scope of the Sonogashira Coupling Reaction Catalyzed by $NiFe_2O_4@TiO_2@PDA$-Pd under Sunlight Irradiation*[a]

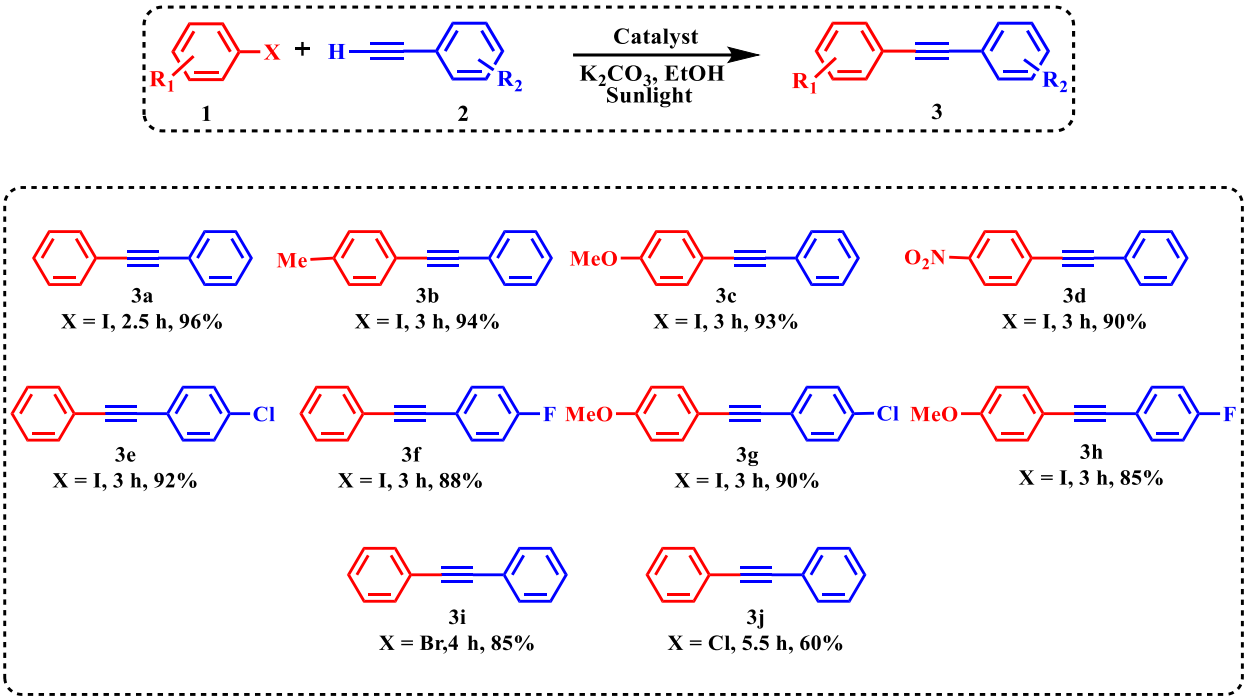

Reaction conditions: aryl halides (1.0 mmol), phenylacetylene (1.3 mmol), $NiFe_2O_4@TiO_2@PDA$-Pd catalyst (10 mg), and K_2CO_3 (2 mmol) in EtOH (3 mL) under direct sunlight at 30 °C

2.3.3.3. Stability and Recyclability of the Catalyst

Two significant parameters to be examined while evaluating a photocatalytic reaction are photo-stability and recyclability. The photo-stability and recyclability of $NiFe_2O_4@TiO_2@PDA$-Pd catalyst in photocatalytic Suzuki and Sonogashira coupling reactions were investigated in this study. Owing to the magnetic nature of the photocatalyst, it was retrieved from the reaction mixture in a simple manner with the aid of an external magnet after each cycle. The magnetically retrieved catalyst was washed with EtOH and dried, and its catalytic performance was assessed in the next run. **Figure 2.5** revealed the reuse of the recovered catalyst five times without any substantial loss of its photocatalytic activity, indicated the good stability of the catalyst.

Many heterogeneous catalysts have leaching issues. The Pd NPs of the catalyst leached into the solution lead to the decrease in the Pd content in the catalyst which was mainly responsible for its activity. To test the Pd leaching, ICP-OES analysis of the recovered catalyst was performed. It was observed that the Pd content of the nanocatalyst had decreased from (3.61) wt % to (2.26) wt % in the Suzuki reaction and to (2.45) wt % in the Sonogashira reaction after five times use. To further confirm the structural stability of the magnetic reusable catalyst, XRD analysis and FT-IR analysis on the recovered photocatalyst were performed. The XRD spectra of the $NiFe_2O_4@TiO_2@PDA$-Pd photocatalyst after five times of reused experiments was shown in Figure 2.6. No impurity peaks were detected in the XRD spectra of the reused photocatalyst, thus the stability of the catalyst was confirmed Furthermore, FT-IR analysis of the photocatalyst after five cycles of reuse was performed where it confirmed the fact that absorption peaks of the reused catalyst were intact with those of the fresh catalyst (**Figure 2.6**).

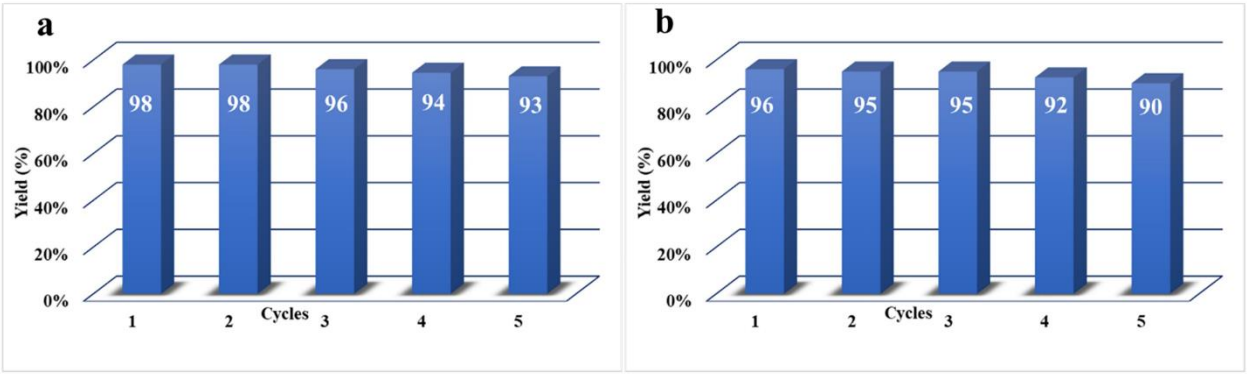

***Figure 2.5**. Recyclability of $NiFe_2O_4@TiO_2@PDA$-Pd for photocatalytic activity a) Suzuki reaction b) Sonogashira reactions.*

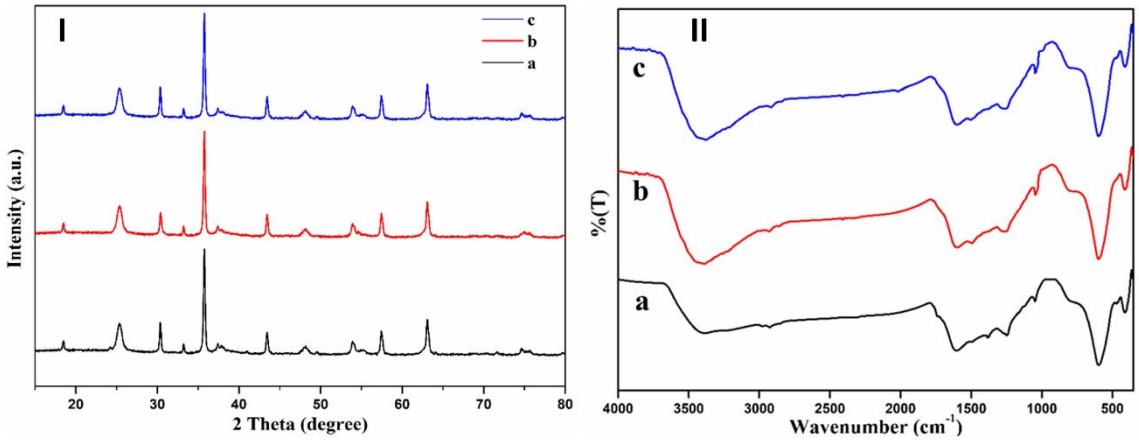

***Figure 2.6.** I) XRD spectra FTIR spectra of (a) synthesized $NiFe_2O_4@TiO_2@PDA$-Pd catalyst (b) used catalyst for Suzuki coupling reaction and (c) used catalyst for Sonogashira reaction after 5 cycles*

The efficacy of the catalyst was compared with that of already reported catalysts for Suzuki and Sonogashira coupling reactions (**Table 2.5**). It is evident from **Table 2.5** that $NiFe_2O_4$@TiO_2@PDA-Pd nanophotocatalyst was efficient in producing the desired products in both Suzuki and Sonogashira coupling reactions with an excellently good yield (98 and 96%) in short reaction time (0.5 and 2.5 h) under natural sunlight. Thus, the synthesized catalyst showed its supremacy in its activity among other reported systems.

Table 2.5. *Comparison of $NiFe_2O_4$@TiO_2@PDA-Pd with other Previously Reported Catalysts for Suzuki and Sonogashira Coupling Reactions*

S.NO	Photocatalyst	Reactions	Light source	Time (h)	Yield (%)	Cycles	Ref.
1	$NiFe_2O_4$/2D MoS_2−Pd	Suzuki	300 W Xe lamp	1	97	5	47
2	HPU/Pd@RCD	Suzuki	sunlight	0.67	97	6	46
3	PdO@WO_3	Suzuki	60 W white LED lamp,	4	99	5	48
4	Au/Pd@UIO-66-NH_2	Suzuki	300 W Xe lamp, N2	1	99	3	49
5	St-MOP@Pd	Suzuki	white LED	5	100	5	50
6	Pd_3P/CdS	Suzuki	4 X25 W LED lamp	8	99	4	51
7	Pd/SiC	Sonogashira	Xe lamp	9	97	5	31
8	Pd_3Cu1/SiC	Sonogashira	300 W Xe lamp	8	99	5	52
9	Pd@TiO_2(Nb_2O_5 or carbon)	Sonogashira	LED light source	5	99	3	12
10	Pd-B_3-Azo_4	Sonogashira	350W Xe lamp	3	94	5	53
11	BODIPY functionalized Pd(II)	Sonogashira	LED bulb, 13 W	24	92	-	54
12	**$NiFe_2O_4$@TiO_2@PDA-Pd**	**Suzuki**	**Sunlight**	**0.5**	**98**	**5**	**Present**
		Sonogashira	**Sunlight**	**2.5**	**96**	**5**	**work**

2.3.3.4. Photocatalytic Mechanism of Suzuki and Sonogashira Coupling Reactions

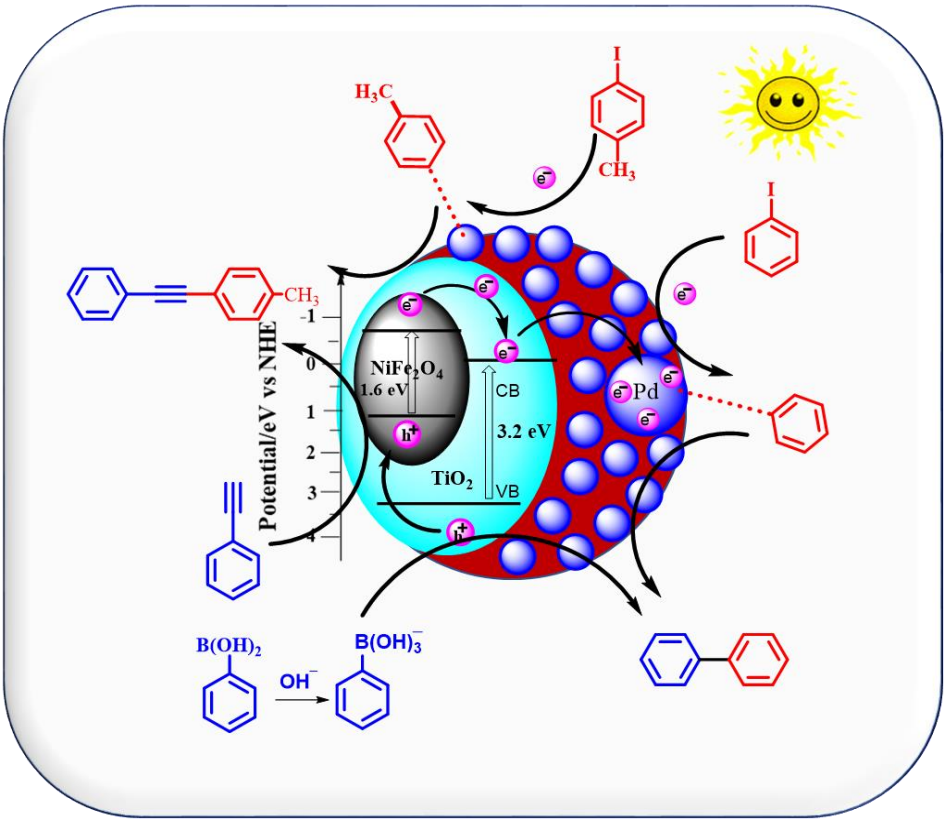

Figure 2.7. *The plausible photocatalytic mechanism over the $NiFe_2O_4$@TiO_2@PDA-Pd nano photocatalyst of Suzuki and Sonogashira coupling reactions*

A plausible photocatalytic mechanism for the Suzuki and Sonogashira coupling reactions in the presence of the $NiFe_2O_4$@TiO_2@PDA-Pd photocatalyst was proposed based on the performed experimental observations and previously reported data.[55–57] Simulated visible light irradiation of the catalyst led to the simultaneous formation of photogenerated electrons (e^-) and holes (h^+) in $NiFe_2O_4$ and TiO_2, as illustrated in **Figure 2.7**. It was because light irradiation led to the promotion of an e^- from the valence band (VB) to the conduction band (CB) leaving a h^+ in the VB. Thus, photogenerated e^-–h^+ pairs were formed simultaneously in $NiFe_2O_4$ and TiO_2. The photogenerated e^- from the CB of $NiFe_2O_4$ could be easily transferred to the CB of TiO_2 by the simultaneous transfer of photogenerated h^+ from the VB of TiO_2 to the VB of $NiFe_2O_4$. This was ascribed to the more negative CB potential of $NiFe_2O_4$ than that of TiO_2 and more positive VB potential of TiO_2 than that of $NiFe_2O_4$. Furthermore, it was also evident by the fact that the combination of $NiFe_2O_4$ and TiO_2 develops interfacial contact between them, thus creating a pathway for easy transfer of e^- from the CB of $NiFe_2O_4$ to the CB of TiO_2 and therefore the e^-–h^+ pair recombination was hindered. The photogenerated e^- available in the CB of TiO_2 would be transported through the PDA layer to

the Pd surface. Active Pd NPs would act as electron reservoirs and thus trap the electrons reaching their surface. These photogenerated electrons and Pd NPs would act as active sites and attack the C−X bond of the adsorbed aryl halides forming the aryl− Pd complex via oxidative addition. On the other hand, arylboronic acid would combine with OH^- in a basic reaction medium to produce aryl-$B(OH)_3^-$. Furthermore, C−B bond cleavage would occur to generate the biaryl−Pd complex in the presence of h^+ (transmetalation). In the final step, a biaryl product was obtained via reductive elimination.[47,58]

For the Sonogashira coupling reaction also, the photogenerated electrons and Pd NPs would act as active sites attacking the C−X bond of the adsorbed aryl halide and would result in the aryl−Pd complex. Simultaneously, photogenerated holes would attract the electronic clouds of the alkyne units in phenyl acetylene, making the terminal spC−H more acidic. Then, terminal H of the alkyne unit was deprotonated by K_2CO_3, and the resulting species combined with the aryl−Pd complex to form an alkynated Pd complex. In the final reductive elimination step, diarylacetylene was formed.[52,53] The proposed mechanism revealed the uniqueness of the synthesized photocatalyst as a sole catalyst for both Suzuki and Sonogashira coupling reactions under sunlight irradiation.

2.4. Conclusions

In summary, a magnetically recyclable Pd-supported PDA-coated core@shell $NiFe_2O_4$@TiO_2 nanocatalyst was designed and developed, with good photocatalytic activity for both Suzuki and Sonogashira coupling reactions under sunlight irradiation under ambient conditions. The activity of the catalyst was validated for both coupling reactions, and its effectiveness for reactions involving a variety of substrates under sunlight irradiation to yield biaryls and diarylacetylenes was tested. The reactions were facilitated by low Pd loading in the presence of eco-friendly polar protic solvents (ethanolic water/ethanol) in a very short reaction duration with an excellent yield (96−98%). The catalyst was validated for substituted substrates in both Suzuki and Sonogashira reactions where it gave a good yield of the product, indicating its efficacy. The plausible mechanism had been proposed for the coupling reactions where the simultaneous utilization of both the photogenerated e^-−h^+ pairs in various steps of the coupling reactions denoted an exceptional catalytic view point of the catalyst. The catalyst was retrieved with the aid of an external magnet and was reutilized for five cycles. ICP-OES analysis indicated the stability of the catalyst without considerable loss after reusing five times which was further confirmed by FTIR and XRD analysis. It was found that the $NiFe_2O_4$@TiO_2@PDA-Pd nanophotocatalyst exhibited greater activity with high yield in comparison to a number of reported catalysts.

2.5. Spectral data of synthesized products Suzuki 3a-3l & Sonogashira 3a-3j

Suzuki 3a-3l:

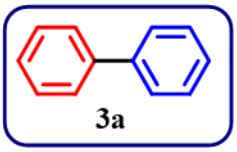

1,1'-Biphenyl (3a)

^{1}H NMR (400 MHz, $CDCl_3$): δ (ppm): 7.63 (d, J = 8.4Hz, 4H), 7.47 (t, J = 7.6 Hz, 4H), 7.37 (t, J = 7.4 Hz, 2H); ^{13}C NMR (100 MHz, $CDCl_3$): δ (ppm): 141.29, 128.79, 127.28, 127.20.

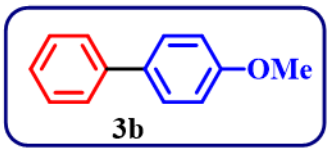

4-Methoxy-1,1'-biphenyl (3b)

^{1}H NMR (400 MHz, $CDCl_3$): δ (ppm): 7.58 (t, J = 8.4 Hz, 4H), 7.45 (t, J = 7.6 Hz, 2H), 7.34 (t, J = 7.4 Hz, 1H), 7.02 (d, J = 8.8 Hz, 2H), 3.89 (s, 3H); ^{13}C NMR (100 MHz, $CDCl_3$): δ (ppm): 159.18, 140.86, 133.81, 128.74, 128.17, 126.76, 126.68, 114.23, 55.36.

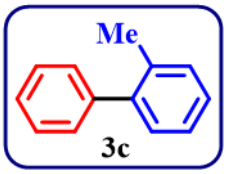

2-Methyl-1,1'-biphenyl (3c)

^{1}H NMR (400 MHz, $CDCl_3$): δ (ppm) 7.39 (t, J = 6.8 Hz, 2H), 7.36 – 7.30 (m, 3H), 7.23 (d, J = 7.2 Hz, 4H), 2.26 (s, 3H); ^{13}C NMR (100 MHz, $CDCl_3$): δ (ppm) 142.04, 135.39, 130.35, 129.85, 129.24, 128.11, 127.29, 126.81, 125.81, 20.51.

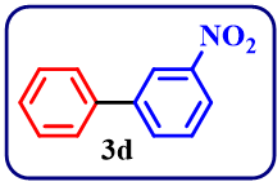

3-Nitro-1,1'-biphenyl (3d)

^{1}H NMR (400 MHz, $CDCl_3$): δ (ppm): 8.46 (t, J = 1.8 Hz, 1H), 8.21 (dd, J = 8.4, 2.4 Hz, 1H), 7.93 – 7.91 (m, 1H), 7.65 – 7.61 (m, 3H), 7.53 – 7.48 (m, 2H), 7.46 – 7.42 (m, 1H); ^{13}C NMR (100 MHz, $CDCl_3$): δ (ppm): 148.77, 142.90, 138.69, 133.05, 129.72, 129.18, 128.56, 127.17, 122.04, 121.97.

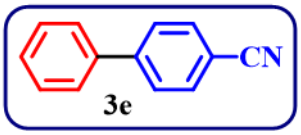

[1,1'-biphenyl]-4-carbonitrile (3e)

^{1}H NMR (400 MHz, $CDCl_3$): δ (ppm): 7.70 (q, J = 8.4 Hz, 4H), 7.59 – 7.57 (m, 2H), 7.50 – 7.45 (m, 2H), 7.44 – 7.39 (m, 1H); ^{13}C NMR (100 MHz, $CDCl_3$): δ (ppm): 145.70, 139.20, 132.61, 129.13, 128.68, 127.75, 127.25, 118.95, 110.95.

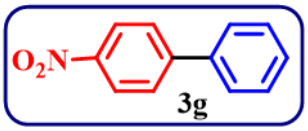

4-Nitro-1,1'-biphenyl (3g)

^{1}H NMR (400 MHz, $CDCl_3$): δ (ppm): 8.29 (d, J = 8.8 Hz, 2H), 7.73 (d, J = 8.8 Hz, 2H), 7.63 – 7.61 (m, 2H), 7.51 – 7.47 (m, 2H), 7.46 – 7.42 (m, 1H); ^{13}C NMR (100 MHz, $CDCl_3$): δ (ppm): 147.65, 147.12, 138.80, 129.17, 128.93, 127.81, 127.40, 124.12.

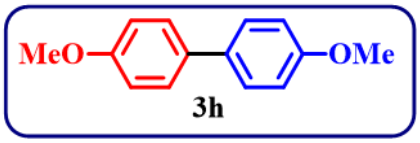

4, 4'-Dimethoxy-1,1'-biphenyl (3h)

^{1}H NMR (400 MHz, $CDCl_3$): δ (ppm): 7.47 (d, J = 8.4 Hz, 4H), 6.95 (d, J = 8.8 Hz, 4H), 3.84 (s, 6H). ^{13}C NMR (100 MHz, $CDCl_3$): δ (ppm): 158.71, 133.50, 127.73, 114.18, 55.34.

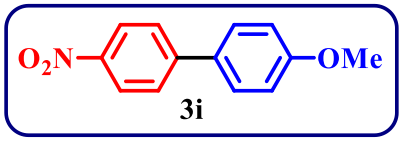

4-Methoxy-4'-Nitro-1,1'-biphenyl (3i)

^{1}H NMR (400 MHz, $CDCl_3$): δ (ppm): 8.26 (d, J = 8.8 Hz, 2H), 7.69 (d, J = 8.8 Hz, 2H), 7.58 (d, J = 8.8 Hz, 2H), 7.02 (d, J = 8.8 Hz, 2H), 3.87 (s, 3H). ^{13}C NMR (100 MHz, $CDCl_3$): δ (ppm): 160.48, 147.22, 146.58, 131.09, 128.58, 127.08, 124.15, 114.63, 55.44.

Sonogashira 3a-3j

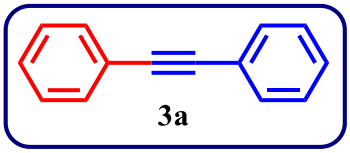

1,2-diphenylethyne (3a)

^{1}H NMR (400 MHz, $CDCl_3$): δ (ppm): 7.56 – 7.52 (m, 4H), 7.38 – 7.33 (m, 6H); ^{13}C NMR (100 MHz, $CDCl_3$): δ (ppm): 130.59, 127.32, 127.23, 122.27, 88.35.

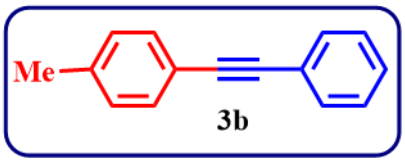

1-methyl-4-(phenylethynyl)benzene (3b)

^{1}H NMR (400 MHz, $CDCl_3$): δ (ppm): 7.54 – 7.50 (m, 2H), 7.42 (d, J = 8.4 Hz, 2H), 7.36 – 7.30 (m, 3H), 7.15 (d, J = 8 Hz, 2H), 2.37 (s, 3H). ^{13}C NMR (100 MHz, $CDCl_3$): δ (ppm): 138.39, 131.56, 131.51, 129.12, 128.32, 128.07, 123.50, 120.21, 89.56, 88.72, 21.51.

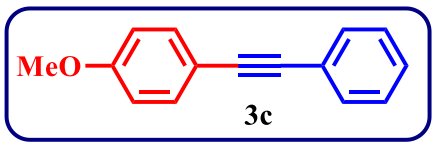

1-methoxy-4-(phenylethynyl)benzene (3c)

^{1}H NMR (400 MHz, $CDCl_3$): δ (ppm): 7.46 – 7.37 (m, 4H), 7.29 – 7.22 (m, 3H), 6.80 (d, J = 8.8 Hz, 2H), 3.75 (s, 3H). ^{13}C NMR (100 MHz, $CDCl_3$): δ (ppm): 159.64, 133.06, 131.46, 128.32, 127.94, 123.62, 115.42, 114.02, 89.38, 88.08, 55.31.

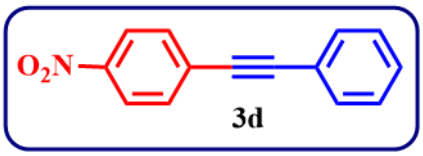

1-nitro-4-(phenylethynyl)benzene (3d)

^{1}H NMR (400 MHz, $CDCl_3$): δ (ppm): 8.15 (d, J = 8.8 Hz, 2H), 7.59 (d, J = 8.8 Hz, 2H), 7.51–7.47 (m, 2H), 7.34 – 7.29 (m, 3H); ^{13}C NMR (100 MHz, $CDCl_3$): δ (ppm): 145.99, 131.25, 130.83, 129.26, 128.26, 127.52, 122.62, 121.10, 93.69, 86.53.

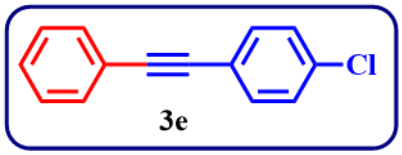

1-chloro-4-(phenylethynyl)benzene (3e)

^{1}H NMR (400 MHz, $CDCl_3$): δ (ppm): 7.56 – 7.49 (m, 2H), 7.48 – 7.43 (m, 2H), 7.37 – 7.32 (m, 4H), 7.31 (q, J = 2 Hz, 1H); ^{13}C NMR (100 MHz, $CDCl_3$): δ (ppm): 134.27, 132.82, 131.61, 128.70, 128.49, 128. 40, 122.94, 121.80, 90.32, 88.24.

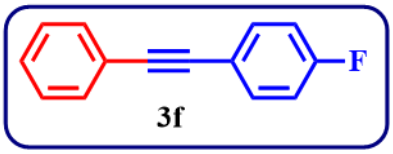

1-fluoro-4-(phenylethynyl)benzene (3f)

^{1}H NMR (400 MHz, $CDCl_3$): δ (ppm): 7.55 – 7.48 (m, 4H), 7.38 – 7.31 (m, 3H), 7.07 – 7.02 (m, 2H); ^{13}C NMR (100 MHz, $CDCl_3$): δ (ppm): 161.27, 133.52, 133.48, 131.56, 128.38, 128.34, 123.10, 115.64, 89.62, 88.28.

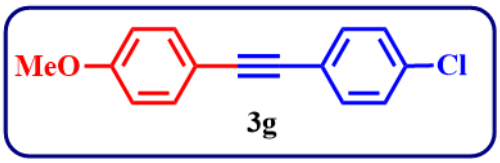

1-chloro-4-((4-methoxyphenyl)ethynyl)benzene (3g)

^{1}H NMR (400 MHz, $CDCl_3$): δ (ppm): 7.44 (dd, J = 10.4, 8.4 Hz, 4H), 7.31 (d, J = 8 Hz, 2H), 6.88 (d, J = 8.4 Hz, 2H), 3.83 (s, 3H); ^{13}C NMR (100 MHz, $CDCl_3$): δ (ppm): 159.80, 133.88, 133.07, 132.64, 128.64, 122.14, 115.03, 114.06, 90.36, 86.99, 55.32.

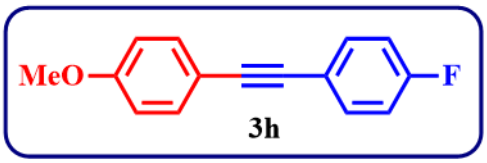

1-fluoro-4-((4-methoxyphenyl)ethynyl)benzene (3h)

^{1}H NMR (400 MHz, $CDCl_3$): δ (ppm): 7.54 – 7.45 (m, 4H), 7.07 – 7.03 (m, 2H), 6.92 – 6.88 (m, 2H), 3.85 (s, 3H); ^{13}C NMR (100 MHz, $CDCl_3$): δ (ppm): 161.45, 159.69, 133.32, 133.24, 133.01, 115.69, 115.47, 114.04, 89.02, 55.32.

2.6. References

(1) Ong, W. J. Learning from Natural Leaves: Going Green with Artificial Photosynthesis Forum. *ACS Appl. Mater. Interfaces* **2019**, *11* (6), 5579–5580.

(2) Linic, S.; Christopher, P.; Ingram, D. B. Plasmonic-Metal Nanostructures for Efficient Conversion of Solar to Chemical Energy. *Nat. Mater.* **2011**, *10* (12), 911–921.

(3) Wang, F.; Li, C.; Chen, H.; Jiang, R.; Sun, L. D.; Li, Q.; Wang, J.; Yu, J. C.; Yan, C. H. Plasmonic Harvesting of Light Energy for Suzuki Coupling Reactions. *J. Am. Chem. Soc.* **2013**, *135* (15), 5588–5601.

(4) Yu, C.; Li, G.; Kumar, S.; Yang, K.; Jin, R. Phase Transformation Synthesis of Novel Ag_2O/Ag_2CO_3 Heterostructures with High Visible Light Efficiency in Photocatalytic Degradation of Pollutants. *Adv. Mater.* **2014**, *26* (6), 892–898.

(5) Li, X. H.; Antonietti, M. Metal Nanoparticles at Mesoporous N-Doped Carbons and Carbon Nitrides: Functional Mott–Schottky Heterojunctions for Catalysis. *Chem. Soc. Rev.* **2013**, *42* (16), 6593–6604.

(6) Long, R.; Rao, Z.; Mao, K.; Li, Y.; Zhang, C.; Liu, Q.; Wang, C.; Li, Z. Y.; Wu, X.; Xiong, Y. Efficient Coupling of Solar Energy to Catalytic Hydrogenation by Using Well-Designed Palladium Nanostructures. *Angew. Chemie - Int. Ed.* **2015**, *54* (8), 2425–2430.

(7) Yang, X.; Zhang, S.; Li, P.; Gao, S.; Cao, R. Visible-Light-Driven Photocatalytic Selective Organic Oxidation Reactions. *J. Mater. Chem. A* **2020**, *8* (40), 20897–20924.

(8) Kim, J. H.; Lee, M.; Lee, J. S.; Park, C. B. Self-Assembled Light-Harvesting Peptide Nanotubes for Mimicking Natural Photosynthesis. *Angew. Chemie - Int. Ed.* **2012**, *51* (2), 517–520.

(9) Li, X. H.; Chen, J. S.; Wang, X.; Sun, J.; Antonietti, M. Metal-Free Activation of Dioxygen by Graphene/g-C_3N_4 Nanocomposites: Functional Dyads for Selective Oxidation of Saturated Hydrocarbons. *J. Am. Chem. Soc.* **2011**, *133* (21), 8074–8077.

(10) Nguyen, C. C.; Vu, N. N.; Do, T. O. Recent Advances in the Development of Sunlight-Driven Hollow Structure Photocatalysts and Their Applications. *J. Mater. Chem. A* **2015**, *3* (36), 18345–18359.

(11) Kou, J.; Lu, C.; Wang, J.; Chen, Y.; Xu, Z.; Varma, R. S. Selectivity Enhancement in Heterogeneous Photocatalytic Transformations. *Chem. Rev.* **2017**, *117* (3), 1445–1514.

(12) Elhage, A.; Lanterna, A. E.; Scaiano, J. C. Light-Induced Sonogashira C-C Coupling under Mild Conditions Using Supported Palladium Nanoparticles. *ACS Sustain. Chem. Eng.* **2018**, *6* (2), 1717–1722.

(13) Shafiei, N.; Nasrollahzadeh, M.; Baran, T.; Baran, N. Y.; Shokouhimehr, M. Pd Nanoparticles Loaded on Modified Chitosan-Unye Bentonite Microcapsules: A Reusable Nanocatalyst for Sonogashira Coupling Reaction. *Carbohydr. Polym.* **2021**, *262* (January), 117920.

(14) Baran, T.; Akay, S.; Kayan, B. Fabrication of Palladium Nanoparticles Supported on Natural Volcanic Tuff/Fe_3O_4 and Its Catalytic Role in Microwave-Assisted Suzuki–Miyaura Coupling Reactions. *Catal. Letters* **2021**, *151* (4), 1102–1110.

(15) Nasrollahzadeh, M.; Motahharifar, N.; Ghorbannezhad, F.; Soheili Bidgoli, N. S.; Baran, T.; Varma, R. S. Recent Advances in Polymer Supported Palladium Complexes as (Nano)Catalysts for Sonogashira Coupling Reaction. *Mol. Catal.* **2020**, *480* (September 2019), 110645.

(16) D'Alterio, M. C.; Casals-Cruañas, È.; Tzouras, N. V.; Talarico, G.; Nolan, S. P.; Poater, A. Mechanistic Aspects of the Palladium-Catalyzed Suzuki-Miyaura Cross-Coupling Reaction. *Chem. - A Eur. J.* **2021**, *27* (54), 13481–13493.

(17) Fusini, G.; Rizzo, F.; Angelici, G.; Pitzalis, E.; Evangelisti, C.; Carpita, A. Polyvinylpyridine-Supported Palladium Nanoparticles: An Efficient Catalyst for Suzuki–Miyaura Coupling Reactions. *Catalysts* **2020**, *10* (3),330.

(18) Çalışkan, M.; Baran, T. Facile Synthesis of Biaryls by Palladium Nanoparticles Adorned on Kaolin/$NiFe_2O_4$ Composite as a Magnetically Retrievable Nanocatalyst. *Colloids Interface Sci. Commun.* **2021**, *43* (March),100445.

(19) Orooji, Y.; Pakzad, K.; Nasrollahzadeh, M.; Tajbakhsh, M. Novel Magnetic Lignosulfonate-Supported Pd Complex as an Efficient Nanocatalyst for N-Arylation of 4-Methylbenzenesulfonamide. *Int. J. Biol. Macromol.* **2021**, *182*, 564–573.

(20) Nasrollahzadeh, M.; Bidgoli, N. S. S.; Issaabadi, Z.; Ghavamifar, Z.; Baran, T.; Luque, R. Hibiscus Rosasinensis L. Aqueous Extract-Assisted Valorization of Lignin: Preparation of Magnetically Reusable Pd NPs@Fe_3O_4-Lignin for Cr(VI) Reduction and Suzuki-Miyaura Reaction in Eco-Friendly Media. *Int. J. Biol. Macromol.* **2020**, *148*, 265–275.

(21) Baran, T.; Nasrollahzadeh, M. Cyanation of Aryl Halides and Suzuki-Miyaura Coupling Reaction Using Palladium Nanoparticles Anchored on Developed Biodegradable Microbeads. *Int. J. Biol. Macromol.* **2020**, *148*, 565–573.

(22) Zhang, S.; Chang, C.; Huang, Z.; Ma, Y.; Gao, W.; Li, J.; Qu, Y. Visible-Light-Activated Suzuki-Miyaura Coupling Reactions of Aryl Chlorides over the Multifunctional Pd/Au/Porous Nanorods of CeO_2 Catalysts. *ACS Catal.* **2015**, *5* (11), 6481–6488.

(23) Parasram, M.; Gevorgyan, V. Visible Light-Induced Transition Metal-Catalyzed Transformations: Beyond Conventional Photosensitizers. *Chem. Soc. Rev.* **2017**, *46* (20), 6227–6240.

(24) Schneider, J.; Matsuoka, M.; Takeuchi, M.; Zhang, J.; Horiuchi, Y.; Anpo, M.; Bahnemann, D. W. Understanding TiO 2 Photocatalysis : Mechanisms and Materials. *Chem. rev.* **2014**, *114*,9919-9986.

(25) Ghosh, B. K.; Moitra, D.; Chandel, M.; Ghosh, N. N. Preparation of TiO_2/Cobalt Ferrite/Reduced Graphene Oxide Nanocomposite Based Magnetically Separable Catalyst with Improved Photocatalytic Activity. *J. Nanosci. Nanotechnol.* **2017**, *17* (7), 4694–4703.

(26) Ghosh, B. K.; Moitra, D.; Chandel, M.; Lulla, H.; Ghosh, N. N. Ag Nanoparticle Immobilized Mesoporous TiO_2-Cobalt Ferrite Nanocatalyst: A Highly Active, Versatile, Magnetically Separable and Reusable Catalyst. *Mater. Res. Bull.* **2017**, *94*, 361–370.

(27) Liu, H.; Jia, Z.; Ji, S.; Zheng, Y.; Li, M.; Yang, H. Synthesis of TiO_2/SiO_2@Fe_3O_4 Magnetic Microspheres and Their Properties of Photocatalytic Degradation Dyestuff. *Catal. Today* **2011**, *175* (1), 293–298.

(28) Gao, X.; Liu, X.; Zhu, Z.; Wang, X.; Xie, Z. Enhanced Photoelectrochemical and Photocatalytic Behaviors of MFe_2O_4 (M = Ni, Co, Zn and Sr) Modified TiO_2 Nanorod Arrays. *Sci. Rep.* **2016**, *6* (April), 1–11.

(29) Huang, S.; Xu, Y.; Zhou, T.; Xie, M.; Ma, Y.; Liu, Q.; Jing, L.; Xu, H.; Li, H. Constructing Magnetic Catalysts with In-Situ Solid-Liquid Interfacial Photo-Fenton-like Reaction over Ag_3PO_4@$NiFe_2O_4$ Composites. *Appl. Catal. B Environ.* **2018**, *225*, 40–50.

(30) Zhu, H. Y.; Jiang, R.; Fu, Y. Q.; Li, R. R.; Yao, J.; Jiang, S. T. Novel Multifunctional $NiFe_2O_4$/ZnO Hybrids for Dye Removal by Adsorption, Photocatalysis and Magnetic Separation. *Appl. Surf. Sci.* **2016**, *369*, 1–10.

(31) Wang, B.; Guo, X.; Jin, G.; Guo, X. Visible-Light-Enhanced Photocatalytic Sonogashira Reaction over Silicon Carbide Supported Pd Nanoparticles. *Catal. Commun.* **2017**, *98*, 81–84.

(32) Elhage, A.; Lanterna, A. E.; Scaiano, J. C. Tunable Photocatalytic Activity of Palladium-Decorated TiO_2: Non-Hydrogen-Mediated Hydrogenation or Isomerization of Benzyl-Substituted Alkenes. *ACS Catal.* **2017**, *7* (1), 250–255.

(33) Feizi Mohazzab, B.; Jaleh, B.; Issaabadi, Z.; Nasrollahzadeh, M.; Varma, R. S. Stainless Steel Mesh-GO/Pd NPs: Catalytic Applications of Suzuki-Miyaura and Stille Coupling Reactions in Eco-Friendly Media. *Green Chem.* **2019**, *21* (12), 3319–3327.

(34) Khazaei, A.; Khazaei, M.; Nasrollahzadeh, M. Nano-Fe_3O_4@SiO_2 Supported Pd(0) as a Magnetically Recoverable Nanocatalyst for Suzuki Coupling Reaction in the Presence of Waste Eggshell as Low-Cost Natural Base. *Tetrahedron* **2017**, *73* (38), 5624–5633.

(35) Liu, R.; Guo, Y.; Odusote, G.; Qu, F.; Priestley, R. D. Core-Shell Fe_3O_4 Polydopamine Nanoparticles Serve Multipurpose as Drug Carrier, Catalyst Support and Carbon Adsorbent. *ACS Appl. Mater. Interfaces* **2013**, *5* (18), 9167–9171.

(36) Li, H.; Xi, J.; Donaghue, A. G.; Keum, J.; Zhao, Y.; An, K.; McKenzie, E. R.; Ren, F. Synthesis and Catalytic Performance of Polydopamine Supported Metal Nanoparticles. *Sci. Rep.* **2020**, *10* (1), 1–7.

(37) Ju, P.; Wu, S.; Su, Q.; Li, X.; Liu, Z.; Li, G.; Wu, Q. Salen-Porphyrin-Based Conjugated Microporous Polymer Supported Pd Nanoparticles: Highly Efficient Heterogeneous Catalysts for Aqueous C-C Coupling Reactions. *J. Mater. Chem. A* **2019**, *7* (6), 2660–2666.

(38) Laokul, P.; Amornkitbamrung, V.; Seraphin, S.; Maensiri, S. Characterization and Magnetic Properties of Nanocrystalline $CuFe_2O_4$, $NiFe_2O_4$, $ZnFe_2O_4$ Powders Prepared by the Aloe Vera Extract Solution. *Curr. Appl. Phys.* **2011**, *11* (1), 101–108.

(39) Liu, Y.; Cherkasov, N.; Gao, P.; Fernández, J.; Lees, M. R.; Rebrov, E. V. The Enhancement of Direct Amide Synthesis Reaction Rate over TiO_2@SiO_2@$NiFe_2O_4$ Magnetic Catalysts in the Continuous Flow under Radiofrequency Heating. *J. Catal.* **2017**, *355*, 120–130.

(40) Farzad, E.; Veisi, H. Fe_3O_4/SiO_2 Nanoparticles Coated with Polydopamine as a Novel Magnetite Reductant and Stabilizer Sorbent for Palladium Ions: Synthetic Application of Fe_3O_4/SiO_2@PDA/Pd for Reduction of 4-Nitrophenol and Suzuki Reactions. *J. Ind. Eng. Chem.* **2018**, *60*, 114–124.

(41) Veisi, H.; Sarachegol, P.; Hemmati, S. Palladium(II) Anchored on Polydopamine Coated-Magnetic Nanoparticles (Fe_3O_4@PDA@Pd(II)): A Heterogeneous and Core–Shell Nanocatalyst in Buchwald–Hartwig C–N Cross Coupling Reactions. *Polyhedron* **2018**, *156*, 64–71.

(42) Rohani, S.; Ziarati, A.; Ziarani, G. M.; Badiei, A.; Burgi, T. Engineering of Highly Active Au/Pd Supported on Hydrogenated Urchin-like Yolk@shell TiO_2 for Visible Light Photocatalytic Suzuki Coupling. *Catal. Sci. Technol.* **2019**, *9* (14), 3820–3827.

(43) Manna, J.; Akbayrak, S.; Özkar, S. Palladium(0) Nanoparticles Supported on Polydopamine Coated Fe_3O_4 as Magnetically Isolable, Highly Active and Reusable Catalysts for Hydrolytic Dehydrogenation of Ammonia Borane. *RSC Adv.* **2016**, *6* (104), 102035–102042.

(44) Babu, B.; Koutavarapu, R.; Shim, J.; Kim, J.; Yoo, K. Improved Sunlight-Driven Photocatalytic Abatement of Tetracycline and Photoelectrocatalytic Water Oxidation by Tin Oxide Quantum Dots Anchored on Nickel Ferrite Nanoplates. *J. Electroanal. Chem.* **2021**, *900* (July 2020), 115699.

(45) Tran, C. Van; La, D. D.; Thi Hoai, P. N.; Ninh, H. D.; Thi Hong, P. N.; Vu, T. H. T.; Nadda, A. K.; Nguyen, X. C.; Nguyen, D. D.; Ngo, H. H. New TiO_2-Doped Cu–Mg Spinel-Ferrite-Based Photocatalyst for Degrading Highly Toxic Rhodamine B Dye in Wastewater. *J. Hazard. Mater.* **2021**, *420* (April), 126636.

(46) Duarah, R.; Karak, N. Hyperbranched Polyurethane/Palladium-Reduced Carbon Dot Nanocomposite: An Efficient and Reusable Mesoporous Catalyst for Visible-Light-Driven C-C Coupling Reactions. *Ind. Eng. Chem. Res.* **2019**, *58* (36), 16307–16319.

(47) Fu, W.; Xu, X.; Wang, W.; Shen, J.; Ye, M. In-Situ Growth of $NiFe_2O_4$/2D MoS_2 p-n Heterojunction Immobilizing Palladium Nanoparticles for Enhanced Visible-Light Photocatalytic Activities. *ACS Sustain. Chem. Eng.* **2018**, *6* (7), 8935–8944.

(48) Yim, D.; Raza, F.; Park, J. H.; Lee, J. H.; Kim, H. I.; Yang, J. K.; Hwang, I. J.; Kim, J. H. Ultrathin WO_3 Nanosheets Converted from Metallic WS_2 Sheets by Spontaneous Formation and Deposition of PdO Nanoclusters for Visible Light-Driven C-C Coupling Reactions. *ACS Appl.*

Mater. Interfaces **2019**, *11* (40), 36960–36969.

(49) Subudhi, S.; Mansingh, S.; Tripathy, S. P.; Mohanty, A.; Mohapatra, P.; Rath, D.; Parida, K. The Fabrication of Au/Pd Plasmonic Alloys on UiO-66-NH_2: An Efficient Visible Light-Induced Photocatalyst towards the Suzuki Miyaura Coupling Reaction under Ambient Conditions. *Catal. Sci. Technol.* **2019**, *9* (23), 6585–6597.

(50) Ryu, S. H.; Choi, S. J.; Seon, J. H.; Jo, B.; Lee, S. M.; Kim, H. J.; Ko, Y. J.; Ko, K. C.; Ahn, T. K.; Son, S. U. Visible Light-Driven Suzuki-Miyaura Reaction by Self-Supported Pd Nanocatalysts in the Formation of Stille Coupling-Based Photoactive Microporous Organic Polymers. *Catal. Sci. Technol.* **2020**, *10* (16), 5535–5543.

(51) Yang, H. Q.; Chen, Q. Q.; Liu, F.; Shi, R.; Chen, Y. Highly Efficient Photocatalytic Suzuki Coupling Reaction by Pd_3P/CdS Catalyst under Visible-Light Irradiation. *Chinese Chem. Lett.* **2021**, *32* (2), 676–680.

(52) Wang, B.; Wang, Y.; Li, J.; Guo, X.; Bai, G.; Tong, X.; Jin, G.; Guo, X. Photocatalytic Sonogashira Reaction over Silicon Carbide Supported Pd-Cu Alloy Nanoparticles under Visible Light Irradiation. *Catal. Sci. Technol.* **2018**, *8* (13), 3357–3362.

(53) Nath, I.; Chakraborty, J.; Khan, A.; Arshad, M. N.; Azum, N.; Rab, M. A.; Asiri, A. M.; Alamry, K. A.; Verpoort, F. Conjugated Mesoporous Polyazobenzene–Pd(II) Composite: A Potential Catalyst for Visible-Light-Induced Sonogashira Coupling. *J. Catal.* **2019**, *377*, 183–189.

(54) Dissanayake, K. C.; Ebukuyo, P. O.; Dhahir, Y. J.; Wheeler, K.; He, H. A BODIPY-Functionalized PdII Photoredox Catalyst for Sonogashira C-C Cross-Coupling Reactions. *Chem. Commun.* **2019**, *55* (34), 4973–4976.

(55) Li, Y.; Zhang, Z.; Pei, L.; Li, X.; Fan, T.; Ji, J.; Shen, J.; Ye, M. Multifunctional Photocatalytic Performances of Recyclable Pd-$NiFe_2O_4$/Reduced Graphene Oxide Nanocomposites via Different Co-Catalyst Strategy. *Appl. Catal. B Environ.* **2016**, *190*, 1–11.

(56) He, Z.; Xia, Y.; Tang, B.; Su, J. Fabrication and Photocatalytic Property of Magnetic $NiFe_2O_4$/Cu_2O Composites. *Mater. Res. Express* **2017**, *4* (9), 095501.

(57) Jiang, J.; Chen, Z.; Wang, P.; Gu, P. Y.; Liu, J.; Zhang, Z.; Xu, Q. Preparation of Black Hollow TiO_2 Nanotube-Coated PDA@Ag_2S Heterostructures for Efficient Photocatalytic Reduction of Cr(VI). *J. Solid State Chem.* **2022**, *307* (September 2021), 122865.

(58) Xiao, Q.; Sarina, S.; Jaatinen, E.; Jia, J.; Arnold, D. P.; Liu, H.; Zhu, H. Efficient Photocatalytic Suzuki Cross-Coupling Reactions on Au-Pd Alloy Nanoparticles under Visible Light Irradiation. *Green Chem.* **2014**, *16* (9), 4272–4285.

2.7. Selected NMR (^{1}H & ^{13}C) spectra of the products in

2.7.1. Suzuki Coupling Reaction

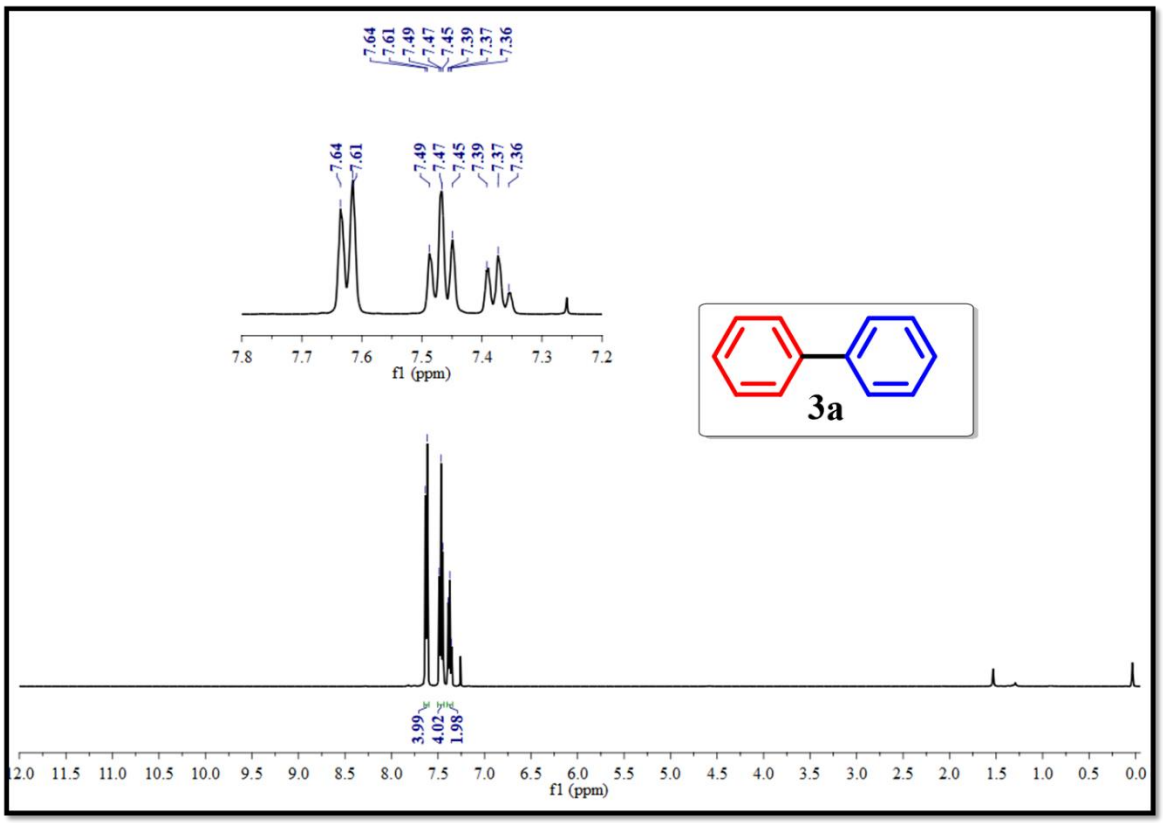

^{1}H NMR spectrum of the compound 1,1'-Biphenyl (3a)

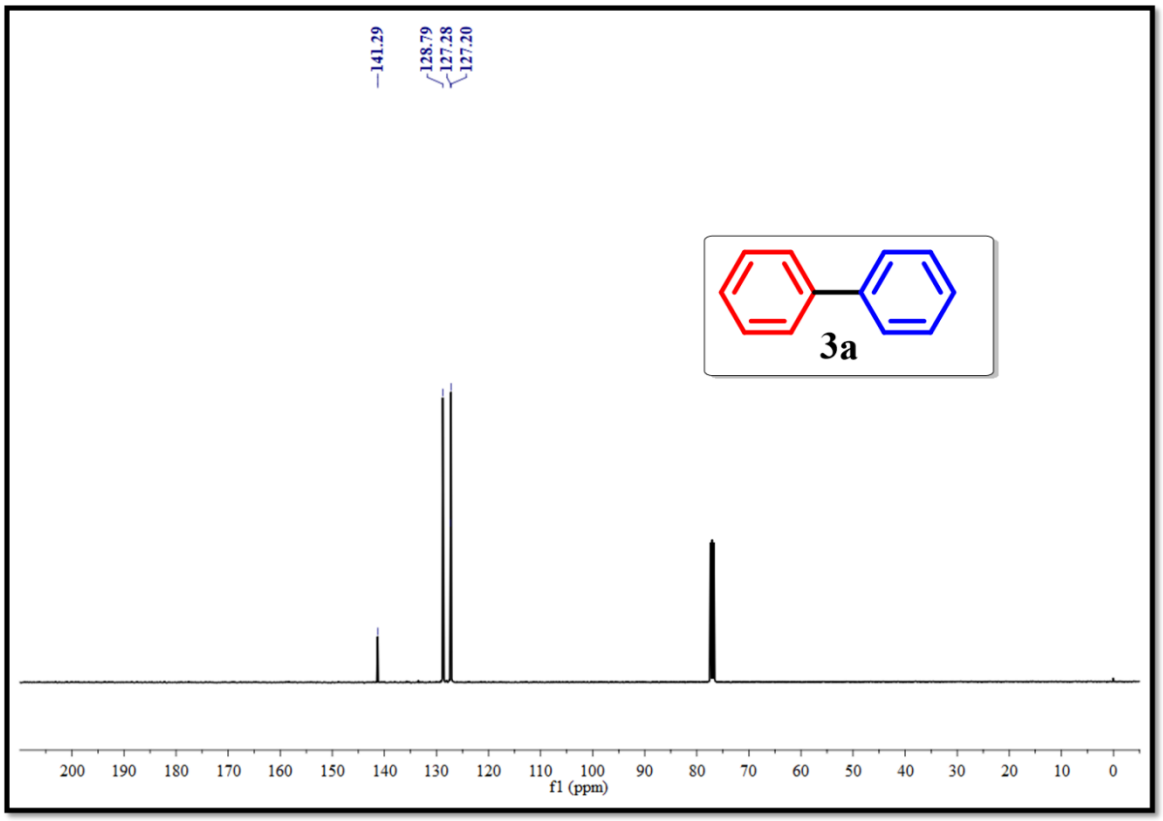

^{13}C NMR spectrum of the compound 1,1'-Biphenyl (3a)

2.7.2. Sonogashira Coupling Reaction:

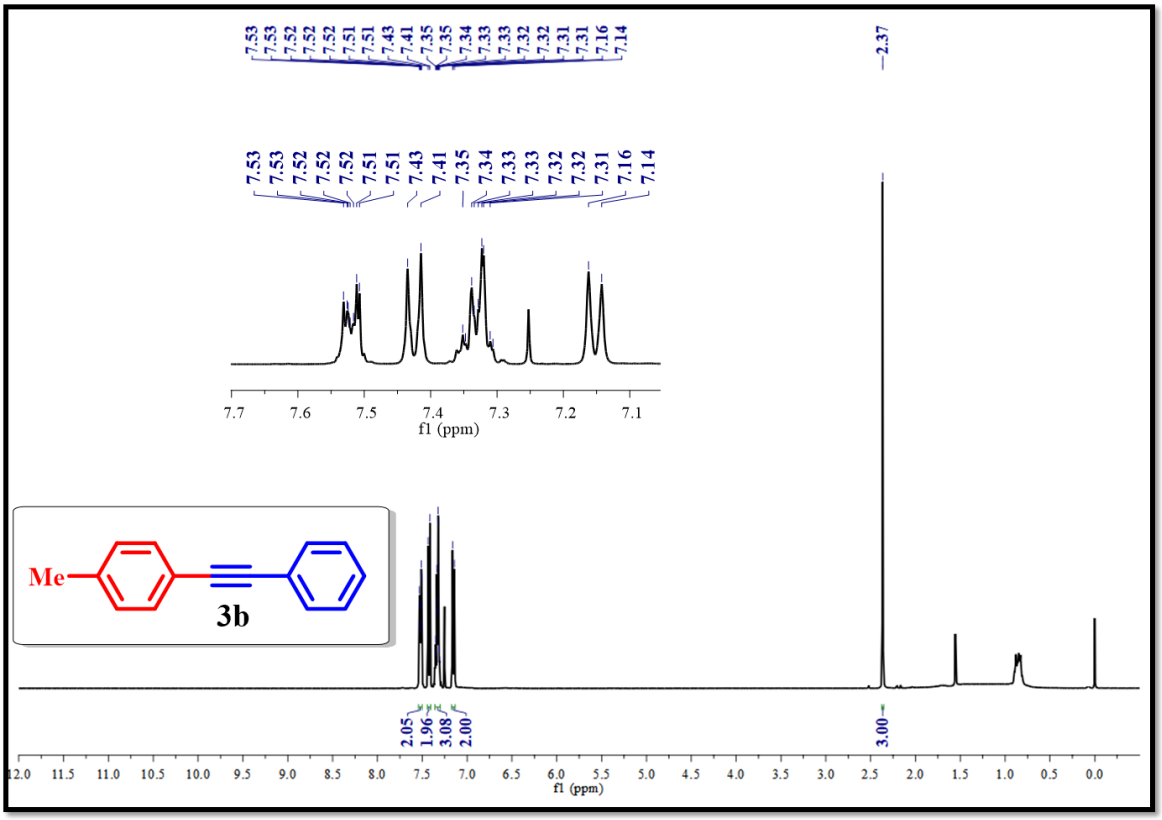

^{1}H NMR spectrum of the compound 1-methyl-4-(phenylethynyl)benzene (3b)

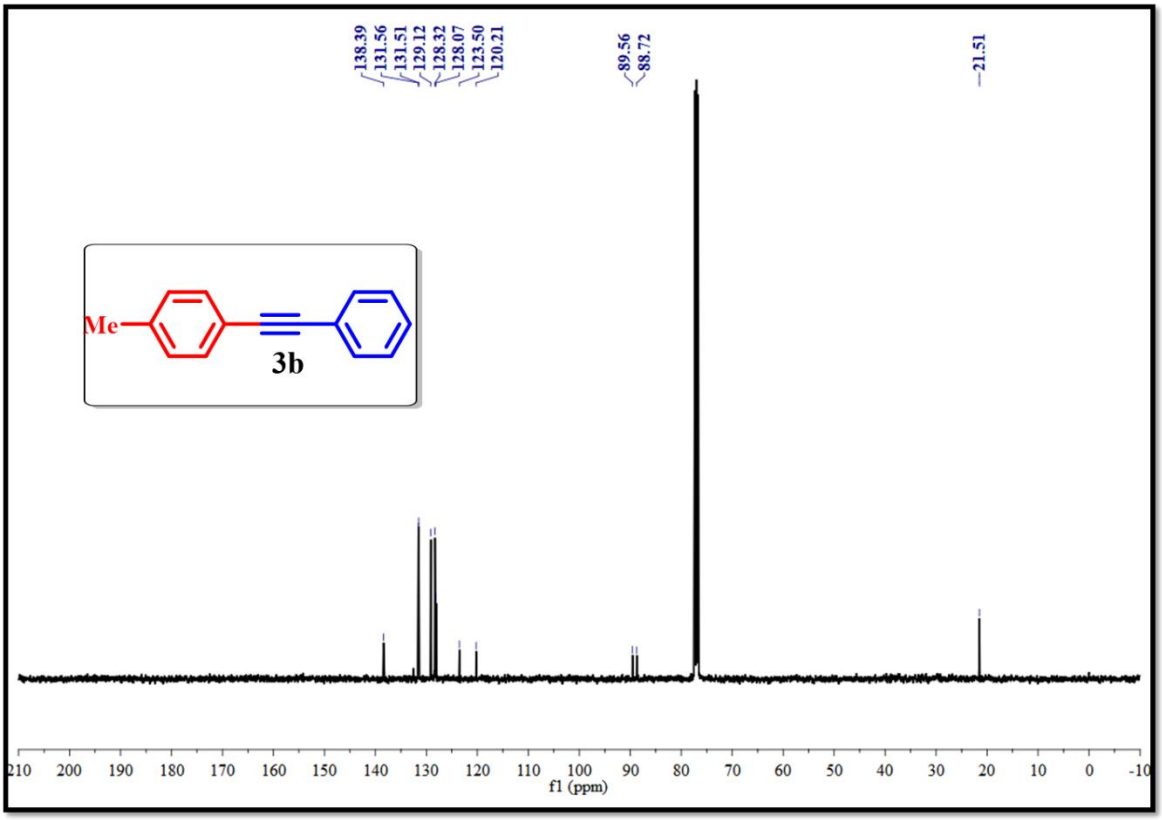

^{13}C NMR spectrum of the compound 1-methyl-4-(phenylethynyl)benzene (3b)

CHAPTER-III

Direct Ortho-C-H Arylation of Benzamides/Benzoic Acids with Aryl Halides Catalyzed by Pyridine-2-carboimine Pd-complex Immobilized on Amine Functionalized Magnetic Nanoparticles

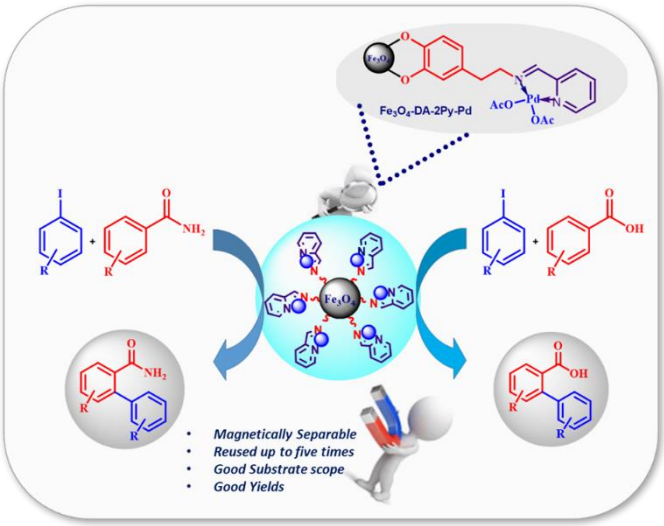

Chapter-III

Direct Ortho-C-H Arylation of Benzamides/Benzoic Acids with Aryl Halides Catalyzed by Pyridine-2-carboimine Pd-complex Immobilized on Amine Functionalized Magnetic Nanoparticles

3.1. Introduction

One of the main challenges in the field of organic synthesis is the development of novel approaches for the synthesis of compounds that are biologically and industrially significant while maintaining atom-economy.[1,2] Biaryl subunit is an important structural motif that can be seen in wide range of industrially significant compounds such as natural products, organic functional materials, polymers, liquid crystals and biologically important compounds in pharmaceuticals etc.[3,4,5] For the past few decades, most effective synthetic methods that have emerged to form aryl-aryl bonds are traditional cross-coupling reactions such as Suzuki,[6] Sonogashira,[7] Heck,[8] Kumada,[9] Negishi,[10] and Stille[11] reactions. These techniques typically need prefunctionalized starting materials which are either expensive or challenging to produce.

Compared to standard protocols, C-H arylation, which entails mixing an aryl halide (C_{Ar-X}) and an arene (C_{Ar-H}) to cause the cleavage of the sp2 C-H bond in order to create C-C bonds, is emerging as a more environmentally friendly, productive, and cost-effective methodology to make biaryls.[12,13,14,15] In the recent past, pyridyl,[16,17] acylamino,[18,19] oxazolyl,[20,21] carboxyl,[22,23] hydroxyl,[24,25] and oxime [26,27] were commonly employed as directing groups in the arene to facilitate C–H activation through intermolecular arylation in the formation of C–C bonds.

Hitherto, plethora of transition metal complexes as homogeneous catalysts ($Pd(OAc)_2$,[13] $Pd(OTf)_2 \cdot 2H_2O$,[28] $Pd(PPh_3)_4$,[29] and $[PdCl(-C_3H_5)]_2$),[4] $Pd_2(dba)_3$,[30] have been reported for C-H activation which are associated with difficulty in catalyst separation, regeneration and reuse. Besides it, large amount of these expensive catalysts needs to be used for effective activity which is of great concern on economic point of view and also they are meant for on time use. Consequently, it leads to the loss of large amount of expensive metal thus limiting the practical application of the catalyst on large scale in industry. Hence, there is an immediate need to develop alternate recyclable catalysts by heterogenization of these homogeneous catalysts for the generation of a library of biaryls via C-H activation by overcoming the associated difficulties.

An interesting strategy that has been adopted for the hetrogenization is the immobilisation of the existing homogenous complexes onto a variety of solid supports. In addition to the advantages of product separation and catalyst recovery by filtration or centrifugation, these

solid supported heterogeneous catalysts also exhibit improved efficiency as a result of the stable active site, which makes them a compelling alternative to the traditional homogeneous catalysts. However, the selection of a support material is crucial for regulating the catalytic activity since it can assist to hold the active sites on its surface through effective coordination during catalysis.[31] In this regard, magnetic nanoparticles (MNPs) established themselves as outstanding and prospective solid support materials due to their durability, inertness, availability, non-toxicity, and chemical stability. Due to their enormous surface area to volume ratio, these nanoparticles provide a large number of possible active sites for further functionalization of the surface. In addition, their magnetic nature makes it possible to rapidly extract them from the reaction mixture using an external magnet, which reduces the need for laborious filtration and centrifugation techniques in heterogeneous catalysis. The magnetic separation can speed up catalyst recovery by cutting down on energy consumption and catalyst loss. Most of the magnetic supported catalysts can be reused many times by retaining their initial activity.[32,33]

However, despite the numerous benefits that MNPs as supports provide, they have a significant tendency to agglomerate that reduces their effectiveness and stability. Based on recent studies, this issue can be resolved by surface-functionalizing MNPs with different materials, like precious metals,[34] silica,[6] polymers,[35] and carbon.[36] When polymers are coated on solid supports (MNPs), they acquire a number of advantageous characteristics, including superior chemical inertness, outstanding thermal stability, and ease of subsequent functionalization.[37] Among polymers, dopamine (DA) with functional catechol and amine groups is good compared to other supports because of its significant properties such as availability, safety, non-toxicity, biocompatibility, biodegradability, capability. These properties are helpful for further functionalization and chemical modification of the resulting structure thus found extensive applications in the field of catalysis.[38,39]

It is reported that magnetite (Fe_3O_4) is an ideal magnetic support which is simple to prepare and provides active surface for its surface functionalization by adsorption/immobilization of ligands or metal resulting in a sustainable catalyst. Thus, Fe_3O_4 can be surface functionalized by DA to result in Fe_3O_4-DA where in amine functionality is introduced on the support which facilitates for further chemical modifications of the catalyst for a specific and selective application in catalysis. In many cases, schiff base condensation strategy is adopted to anchor the catalytically active Pd on supports wherein the amine functionality is allowed to interact with a carbonyl source and get converted into an imine. Thus, allow effective metal binding enhancing the activity and reducing the leaching of the active expensive metal. This reflects

the greener approach in the development of heterogeneous catalyst. Recently, there has been a lot of interest in the directing group assisted one-step synthesis of biaryls from aromatic compounds towards the goal of heterogenization with the emergence of more sustainable chemistry.

Based on aforementioned different strategies, and in continuation with the objective of development of new heterogeneous catalysts, it is proposed to synthesize pyridine-2-carboimine Pd-complex immobilized on amine functionalized Fe_3O_4 MNPs (Fe_3O_4-DA-2Py-Pd) as heterogeneous magnetically recoverable catalyst by Schiff base condensation strategy for ortho C-H arylation in producing biaryls. Based on the literature, Fe_3O_4-DA-2Py-Pd would become the first magnetically reusable heterogeneous nanocatalyst for the ortho-arylation of benzamides and bezoic acids using aryl iodides containing -$CONH_2$ and -COOH as pointing groups. This catalyst would be advantageous due to low loading of expensive metal, effective binding by Schiff base strategy, magnetic separability and expected to work excellently well for dual applications thus establishing the sustainable approach.

3.2. Experimental Section

3.2.1. Materials

The starting materials used in the present work were Ferric nitrate (99%, Finar); Ferric chloride (99%, Finar); Palladium acetate (Sigma Aldrich); Ammonia solution (Sigma Aldrich); Dopamine hydrochloride (SRL, 98%); 2-pyridine carboxaldehyde (Avra, 98%); Acetone (99%, Finar); Ethanol (EtOH), (99%, Finar); Ethyl acetate (EtOAc) (99%, Finar); n-hexane (98%, Finar). Water that had been double-distilled (DD) was utilised throughout the experimental process.

3.2.2. Synthesis of Fe_3O_4 nanoparticles

The magnetic Fe_3O_4 nanocatalyst was synthesized using the co-precipitation method. In this method, $Fe(NO_3)_3.9H_2O$ and $FeCl_2.4H_2O$ were dissolved in 50 mL of DD water in 1:2 molar ratio and the mixture was agitated for 30 minutes at room temperature (RT) to obtain a clear solution. Ammonia solution was added to the mixture and constantly agitated until the pH of the mixture was around 10. The resulting mixture was constantly agitated for two hours at RT, and then the resultant product was dried in an oven at 60 °C after being washed three times using DD water and ethanol.

3.2.3. Surface modification of Fe_3O_4 with DA

Fe_3O_4 nanoparticles (1 g) were sonicated for 30 minutes to disperse them in 25 mL of water. To this solution, 1 g of dopamine hydrochloride mixed in 5 mL of water was added, and it was further sonicated for two hours. After that, acetone was used to precipitate the amine-

functionalized magnetic nanomaterial (Fe_3O_4-DA), which was subsequently separated using an external magnet and vacuum-dried for two hours at 50 °C.

3.2.4. Synthesis of Fe_3O_4-DA-2Py

Fe_3O_4-DA nanoparticles (1g) and 2-pyridine carboxyaldehyde (2.0 mmol) was stirred in 100 mL ethanol solution at RT for 24 h. The obtained pyridine-2-carboimine immobilized on amine functionalized Fe_3O_4 magnetic support (Fe_3O_4-DA-2Py) was washed three times with ethanol, and vacuum dried for 12 h at 50 °C after being separated using an external magnet.

3.2.5. Synthesis of Fe_3O_4-DA-2Py-Pd nanocatalyst

$Pd(OAc)_2$ (25 mg) and Fe_3O_4-DA-2Py (500 mg) were agitated in 20 mL of acetone solution at RT for 12 h. The resulting nanocatalyst was separated using an external magnet and vacuum-dried for 12 h at 50 °C.

3.2.6. Ortho C-H arylation of Benzamides

In ortho C-H arylation of Benzamides, the reactants *viz*., benzamides (1 mmol), aryl halides (1.5 mmol) and silver acetate (2 mmol) along with prepared nanocatalyst (20 mg) were mixed in 3 mL of AcOH. The reaction was constantly swirled for 12 hours at 120 °C. Upon completion of the reaction (as monitored by TLC), the catalyst was quickly separated employing an external magnet. Ethyl acetate was used twice to extract the products. Each reaction was performed two times and the average of the yield was reported. The products were examined using ^1H & ^{13}C NMR spectral analysis after purification on a microcolumn loaded with silica gel.

3.2.7. Ortho C-H arylation of Benzoic acids

In ortho C-H arylation of Benzoic acids, the reactants *viz.*, benzoic acids (1 mmol), aryl halides (1.5 mmol) and silver acetate (2 mmol) along with nanocatalyst (20 mg) were mixed in 3 mL of AcOH. The reaction was constantly swirled for 12 h at 120 °C. Upon completion of the reaction (as monitored by TLC), the catalyst was quickly separated employing an external magnet. Ethyl acetate was used twice to extract the products. Each reaction was performed two times and the average of the yield was reported. The products were examined using ^1H & ^{13}C NMR spectral analysis after purification on a microcolumn loaded with silica gel.

Catalyst recovery

The magnetic nanocatalyst was isolated from the reaction mixture for further use by holding the magnet externally to the reaction vessel. Consequently, the catalyst got stuck to the wall by external magnet and the reaction mixture was decanted into another container. The retained catalyst in the vessel was washed with DD water and ethanol for three times, dried (at 60 °C overnight) and was used in the next run. 99% of the catalyst was fully recovered with

minimal loss of the catalyst. This can be understood by the fact that the recovered catalyst was reused further in the reaction where it has shown almost the same activity.

3.2.8. Characterization of Catalyst:

Several analytical techniques were used to carry out the structural characterization of the synthesised materials. Utilising Ni-filtered Cu K (λ= 1.5406 Å) radiation, powder X-ray diffraction (PXRD) investigations were conducted with a PAN Analytical Advance X-ray diffractometer in a 2θ scan range between 10° and 80°. FT-IR spectra of the synthesised compounds were obtained using KBr pellet method with the PerkinElmer Spectrum between 4000 and 400 cm^{-1}. To comprehend the surface morphology, grain size, particle size distribution, and crystallinity of the Fe_3O_4-DA-2Py-Pd nanocatalyst, studies were conducted using Field Emission Scanning Electron Microscope (FESEM, Quanta FEG 250), Transmission Electron Microscopy (TEM), and Selected Area Electron Diffraction (SAED) (TEM, JEOL/JEM-2100). Using Kratos/Shimadzu Amicus, ESCA 3400, X-ray photoelectron spectroscopy, the binding energies of the elements in the Fe_3O_4-DA-2Py-Pd catalyst were ascertained. To further understand the catalyst's magnetic behaviour, the magnetic hysteresis curves were obtained using a vibrating sample magnetometer (VSM, Lake Shore, 8600 Series). On an advanced-III Bruker 400 MHz NMR spectrometer, ^1H and ^{13}C NMR spectra were recorded using $CDCl_3$ as a solvent and TMS as an internal standard. The units used to express chemical shifts were parts per million (ppm).

3.3. Results and Discussions

Scheme 3.1. *The preparation of the Fe_3O_4-DA-2Py-Pd nanocatalyst*

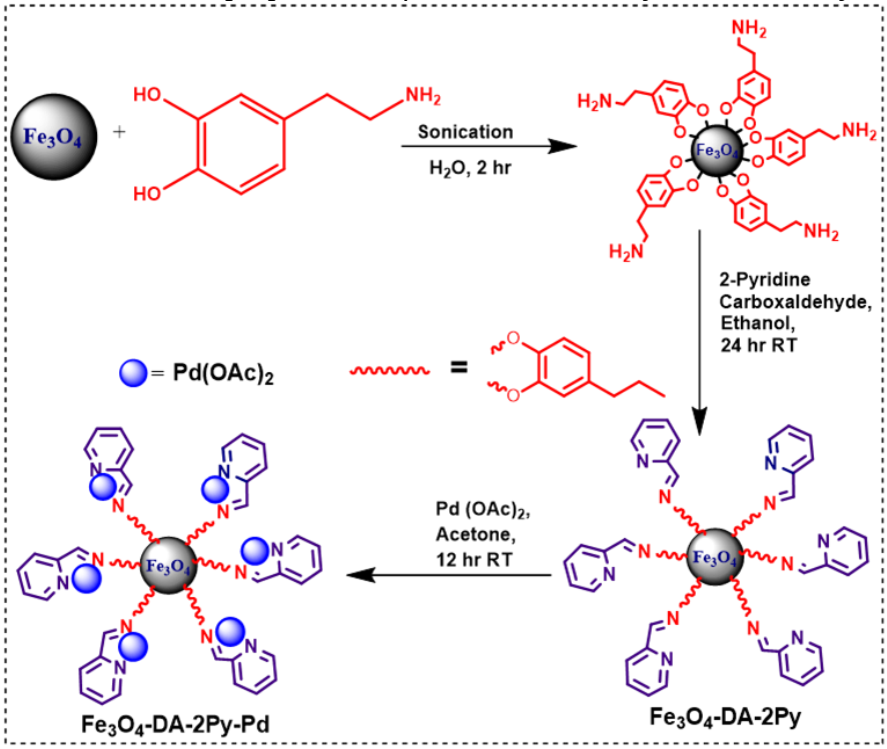

3.3.1. Preparation of Fe_3O_4-DA-2Py-Pd nanocatalyst

A four-step (IV) methodology was used to make the Fe_3O_4-DA-2Py-Pd catalyst (**Scheme 3.1**). The co-precipitation approach was used in step I to create the Fe_3O_4 NPs. Surface functionalization of Fe_3O_4 NPs was done with DA in step II, to form amine functionalized Fe_3O_4 MNPs (Fe_3O_4-DA) via sonication method. In step III, 2-pyridinecarboxaldehyde and Fe_3O_4-DA were continuously stirred to create a Schiff base material (Fe_3O_4-DA-2Py). At last, in step IV, palladium acetate was loaded on the Schiff base material to led to the synthesis of pyridine-2-carboimine Pd-complex immobilized on amine functionalized Fe_3O_4 MNPs (Fe_3O_4-DA-2Py-Pd) as heterogeneous catalyst. To make use of the synthesised nanocatalyst further, it was separated using an external magnet and then vacuum-dried.

3.3.2. Characterization of Fe_3O_4-DA-2Py-Pd catalyst:

The indexed X-ray diffraction patterns of synthesized Fe_3O_4, Fe_3O_4-DA-Py, and Fe_3O_4-DA-Py-Pd catalyst were illustrated in **Figure 3.1a**. The broad peaks in the Figure established the formation of particles in the nano-regime. The observed peaks in **Figure 3.1a(I)** at 2θ values of 30.1°, 35.4°, 43.1°, 53.9°, 56.9°, and 63.9° correspond to the diffractions of (220), (311), (400), (422), (511), and (440), respectively. These peaks indicated the formation of single phased perfect crystalline spinel Fe_3O_4 (JCPDS card No. 19-0629).[40] The catalyst's diffraction patterns in **Figure 1a(II)** demonstrated that, despite the surface being changed with DA and Schiff base as well, the crystallinity of Fe_3O_4 NPs remained unaltered. **Figure 3.1a(III)** did not show any identifiable peaks associated with Pd NPs owing to the low palladium content on the Schiff base material surface in the catalyst.

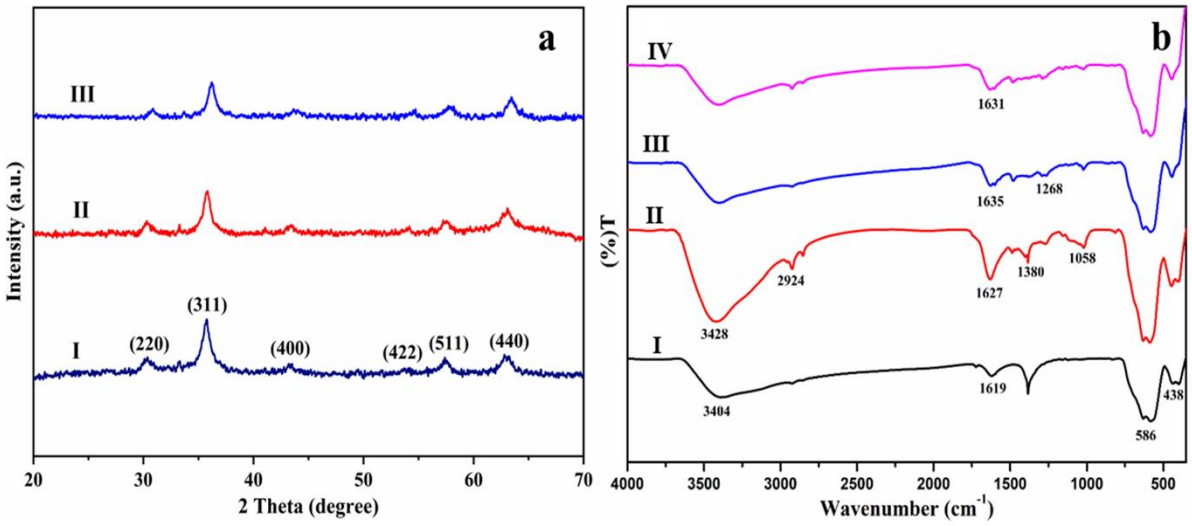

Figure 3.1 *a) XRD patterns b) FTIR spectra*

FT-IR spectra of synthesized Fe_3O_4, Fe_3O_4-DA, Fe_3O_4-DA-Py, and Fe_3O_4-DA-Py-Pd catalyst were shown in **Figure 3.1b**. Two noticeable peaks observed between 600 - 400 cm^{-1} were characteristic of spinel structure. The intrinsic vibrations of the M^{n+}-O bond at the octahedral and tetrahedral regions of the spinel structure were responsible for the prominent peaks seen at 438 and 586 cm^{-1} in **Figure 1b(I)**. The absorption peaks at 3404 and 1619 cm^{-1} were attributed to bending and stretching vibration of surface OH groups. The peaks observed at 3428 and 1627 cm^{-1} in **Figure 1b(II)** were ascribed to the bending and stretching vibration of NH_2. The absorption peaks at 2924 and 1380 cm^{-1} indicated the stretching and bending vibration of C-H and those observed at 1058 cm^{-1} indicated C-O stretching vibration. This data revealed the successful surface functionalization of Fe_3O_4 with DA. In **Figure 1b(III)** the absorption peak at 1635 and 1268 cm^{-1} indicated the C=N and C-N stretching vibration signifying the formation of Schiff base. As shown in **Figure 1b(IV)**, there were no notable changes in the FTIR spectrum of the Fe_3O_4-DA-Py-Pd nanocatalyst. Through bonding interactions between the Schiff base functional groups and the Pd NPs, the peak intensity measured at 1635 cm^{-1} had slightly moved to a lower value of 1631 cm^{-1}.[41,42]

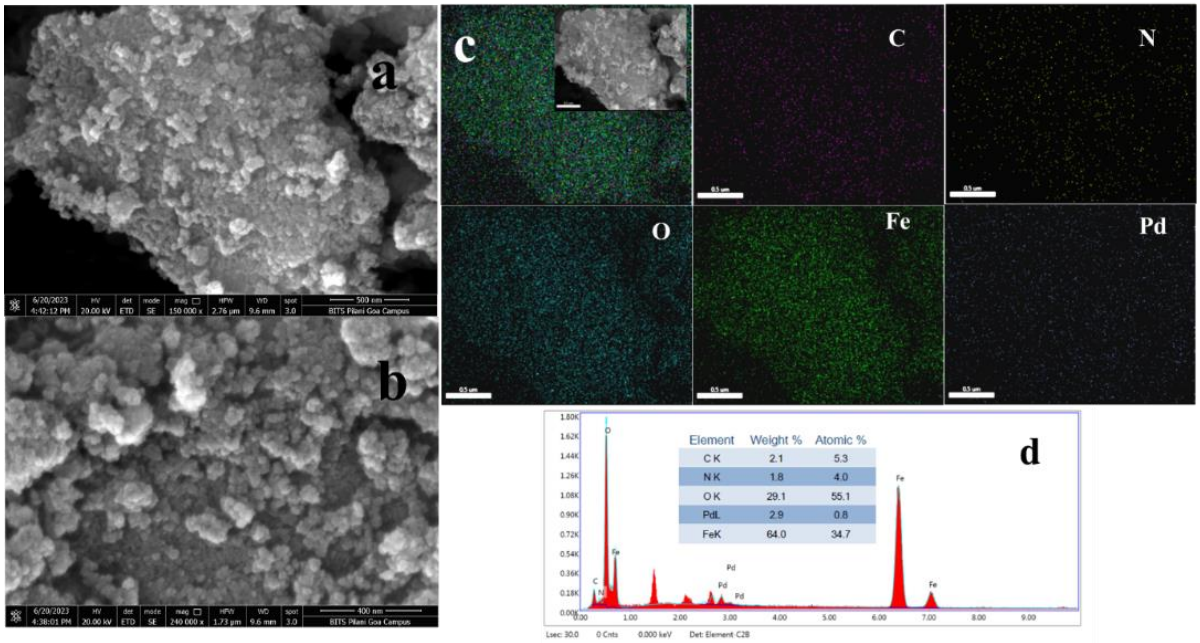

Figure 3.2. *(a, b) FE-SEM images (c) EDAX mapping (d) EDAX data of Fe_3O_4-DA-2Py-Pd*

The surface morphology of the synthesized Fe_3O_4-DA-Py-Pd nanocatalyst was depicted in FE-SEM images in **Figure 3.2(a, b)** which revealed uniform spherical morphology of the nanocatalyst. The elemental mapping spectra and energy dispersive X-ray elemental composition (EDAX) were captured during FE-SEM recording. The catalyst's elemental mapping (**Figure 3.2c**) confirmed that all of the elements (Pd, Fe, N, C, and O) were uniformly

distributed across the surface of Fe_3O_4. Furthermore, the subsequent figures displayed the mapping spectra of each of the elements C, N, O, Fe, and Pd. These images clearly revealed that the magnetic Fe_3O_4 support was functionalized with DA and the surface of Fe_3O_4-DA was further modified to form Schiff base whose surface was immobilized with Pd to result in the formation of the expected Fe_3O_4-DA-Py-Pd nanocatalyst. The EDAX elemental composition of Fe_3O_4-DA-Py-Pd from **Figure 3.2d** revealed the presence of C, N, O, Pd, and Fe elements which confirmed the successive surface modification, Schiff base formation and effective loading of Pd on the Fe_3O_4 support.

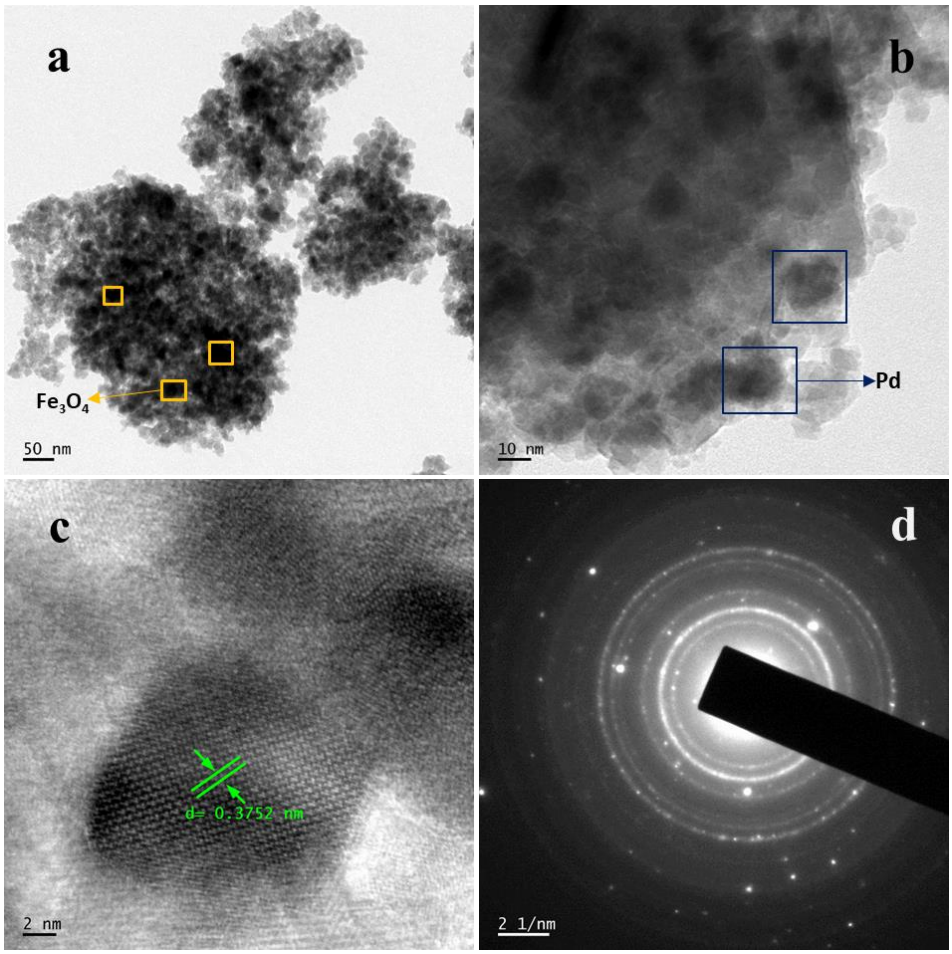

Figure 3.3*. (a, b) TEM images (c) Lattice Fringe Spaces (d) SAED Pattern of Fe_3O_4-DA-2Py-Pd*

The TEM was used to describe the catalyst's morphological properties, including size, crystallinity, and surface morphology. The presence of large black spots with high amount of Fe in the TEM image in **Figure 3.3a** could represent magnetic nanoparticles. As seen in **Figure 3.3b**, there was a light grey halo surrounding these huge black dots, over which little dark grey spots were visible. Thus, presence of palladium NPs was confirmed. The high resolution TEM (HRTEM) image shown in **Figure 3.3c** was indicative of the number of grains with different

orientation of the planes, thus the polycrystalline nature of the material was confirmed. The lattice fringe spaces of 0.37 nm shown in the figure could possibly be ascribed to the (111) crystal plane of Pd NPs. The SAED pattern of Fe_3O_4-DA-2Py-Pd was depicted in **Figure 3.3d.** The diffraction rings composed of a bright spot in the figure possessing sixfold symmetry manifested the polycrystalline nature of the material.

X-ray photoelectron spectroscopy (XPS) was employed to verify that Pd was effectively coordinated in the catalyst. It was an effective instrument for comprehending the electronic characteristics of the metals in the catalyst, including their chemical valence states, electron environment, and binding energy. The chemical valence states of the Fe and Pd metals in the catalyst were analysed using the XPS spectra displayed in **Figure 3.4.** The two bands that are apparent at binding energies of 711.9 and 725.2 eV were attributed to the Fe 2p3/2 and Fe 2p1/2 photoelectrons in the Fe^{2+} chemical state, as shown in **Figure 3.4a.** On the other hand, the two peaks observed at 714.3 and 726.9 eV were ascribed to the Fe 2p3/2 and Fe 2p1/2 photoelectrons in the Fe^{3+} chemical state of Fe_3O_4. Furthermore, in the Pd^{2+} chemical state, the two identified bands in **Figure 3.4b** at binding energies of 339.0 eV and 345.1 eV were labelled as Pd 3d5/2 and Pd 3d3/2 photoelectrons, respectively.

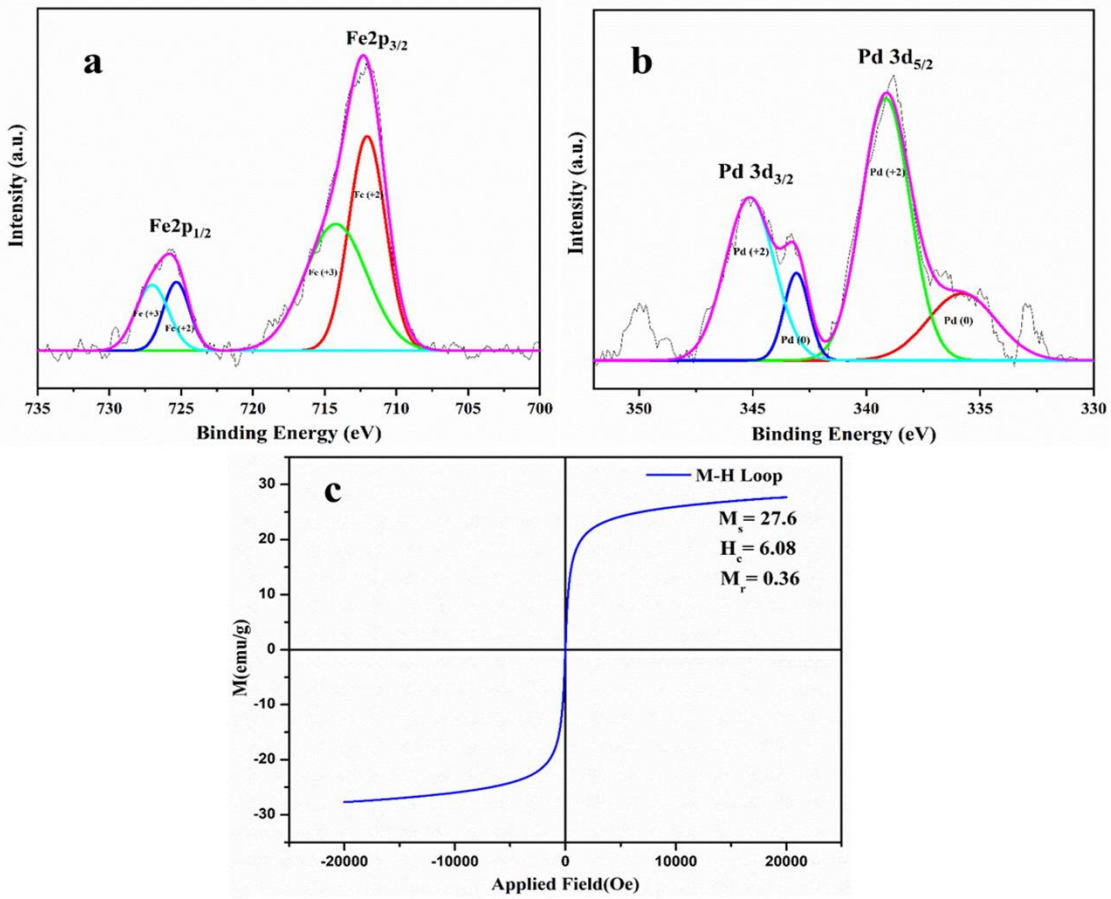

Figure 3.4*. (a) Fe XPS (b) Pd XPS (c) VSM of Fe_3O_4-DA-2Py-Pd*

These results substantiated the existence of Pd^{2+} content in the produced catalyst, which was not detected by XRD. The two low intensity bands seen in **Figure 3.4b** at binding energies of 335.1 eV and 342.8 eV could be labelled as Pd 3d5/2 and Pd 3d3/2 photoelectrons, respectively, in the Pd (0) chemical state.[43,6,44]

The RT magnetization studies were carried out using VSM in order to ascertain the magnetic behaviour of the Fe_3O_4-DA-2Py-Pd catalyst. The results were displayed as a hysteresis curve in **Figure 3.4c.** The saturation magnetization (Ms), remanence magnetization (Mr) and coercivity (Hc) were found to be 27.6 emu/g, 0.36 emu/g, and 6.08 Oe respectively. The catalyst's magnetic retrievability and reusability was demonstrated by the evaluated magnetic parameters from Figure.

3.3.3. Application of Fe_3O_4-DA-2Py-Pd catalyst in ortho-arylation of Benzamide and Benzoic Acid

Over the last few decades, $Pd(OAc)_2$ has been deployed as an active homogenous catalyst for the majority of aromatic C-H activation reactions, both in the presence of ligands and in ligand free conditions.[15,45] This was associated with difficulty in catalyst separation, regeneration and reuse. It was necessary to significantly improve the catalyst in order to heterogenize it for simple separation and also to minimise the loss of expensive Pd catalyst. The synthesized catalyst (Fe_3O_4-DA-2Py-Pd)**,** a magnetically separable catalyst under ligand free conditions would address this issue. The catalyst's ability to activate the aromatic C-H bond of benzoic acids and benzamides was studied.

3.3.3.1. Ortho-arylation of benzamide

Bezamide (1 mmol) and iodobenzene (2 mmol) were taken as model substrates under reflux condition with different additives, and acetic acid (AcOH) as solvent at 120 °C in the ortho-arylation of benzamides to yield biaryls. The catalytic activity of the Fe_3O_4-DA-2Py-Pd nanocatalyst (20 mg) was investigated for the aforementioned typical reaction by optimizing the reaction conditions. The optimized reaction conditions were summarized in **Table 3.1**. In the presence of Ag_2CO_3 as an additive, a considerable product yield was obtained (**Table 3.1 entry 1**) and the reaction had not at all occurred in the presence of other additives such as Ag_2O, $AgNO_3$, $Cu(OAc)_2$, Cu_2O, K_2CO_3, CS_2CO_3, $Cu(OAc)_2$ (**Table 3.1, entry 2 to 7**). On the other hand, reasonable yield of the product was observed in the presence of Ag_2CO_3:K_2CO_3 (1:1) as additive (**Table 3.1 entry 8**). The reaction was also tried with AgOAc added, and almost same product yield was obtained (**Table 3.1 entry 9**). From the tabulated data, AgOAc was found to be a good additive among all which gave the highest yield (74%) of the targeted

product (**Table 3.1 entry 9**) in the presence of Fe_3O_4-DA-2Py-Pd nanocatalyst. Thus, AgOAc was used as an additive for further optimization of reaction conditions.

Table 3.1. *Optimization of Reaction Conditions for the reaction of benzamide and iodo benzene by Fe_3O_4-DA-2Py-Pd*[a]

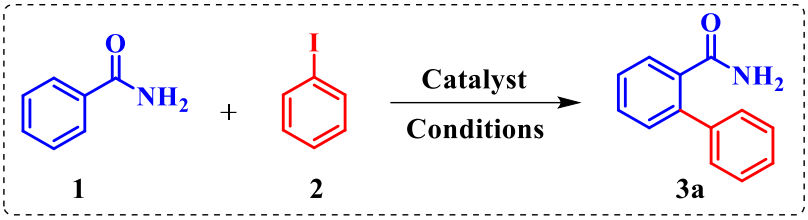

1 2 3a

S.NO	Additive	Solvent	Yield(%)[b]
1	Ag_2CO_3	AcOH	70
2	Ag_2O	AcOH	NR
3	$AgNO_3$	AcOH	NR
4	Cu_2O	AcOH	NR
5	K_2CO_3	AcOH	NR
6	CS_2CO_3	AcOH	NR
7	$Cu(OAc)_2$	AcOH	NR
8	Ag_2CO_3:K_2CO_3(1:1)	AcOH	73
9	**AgOAc**	**AcOH**	**74**
10	AgOAc	DMF	NR
11	AgOAc	1,4-Dioxane	NR
12	AgOAc	Toulene	NR
13	AgOAc	AcOH	NR[c]
14	AgOAc	AcOH	40[d]
15	AgOAc	AcOH	65[e]
16	AgOAc	AcOH	74[f]

[a]**Reaction conditions:** Benzamide (1.0 mmol), Iodobenzene (2 mmol), Fe_3O_4-DA-2Py-Pd catalyst (20 mg) and additive (2 mmol) in solvent (3 mL). [b]Isolated yields, [c]Without catalyst reaction, [d]10 mg catalyst, [e]15 mg catalyst, [f]25 mg catalyst.

To optimize the type of solvent, different solvents such as DMF, 1,4-dioxane, and toluene were used. In these solvents, the reaction did not progress (**Table 3.1, entries 10,11,12**). Hence, it was evident that among different additives and solvents used, AgOAc and AcOH were found to be a good choice which gave the highest product yield (74%) (**Table 3.1 entry 9**). In order to realize the catalyst's impact, the reaction was also examined without the catalyst. Since no product was produced, it is likely that the catalyst was essential to the

reaction. (**Table 3.1, entry 13**). The aforementioned findings revealed that Fe_3O_4-DA-2Py-Pd functions as a highly effective catalyst for the ortho-arylation of benzamides when AgOAc was used as additive and AcOH as a solvent. The amount of catalyst was optimised by carrying out the reaction at 120 °C with varying amounts of Fe_3O_4-DA-2Py-Pd nanocatalyst, in the presence of AgOAc as an additive and AcOH as a solvent. The yields of the products observed using different amounts of catalyst (10 mg, 15 mg, and 20 mg) were 40%, 65%, and 74% respectively (**Table 3.1, entries 14, 15, 9**). The product yield (74%) didn't increase further when 25 mg of catalyst was employed. (**Table 3.1, entry16**). Thus, the optimized amount of the catalyst was 20 mg.

Table 3.2. *Substrate Scope of the ortho arylation of Benzamide catalysed by Fe_3O_4-DA-2Py-Pd*

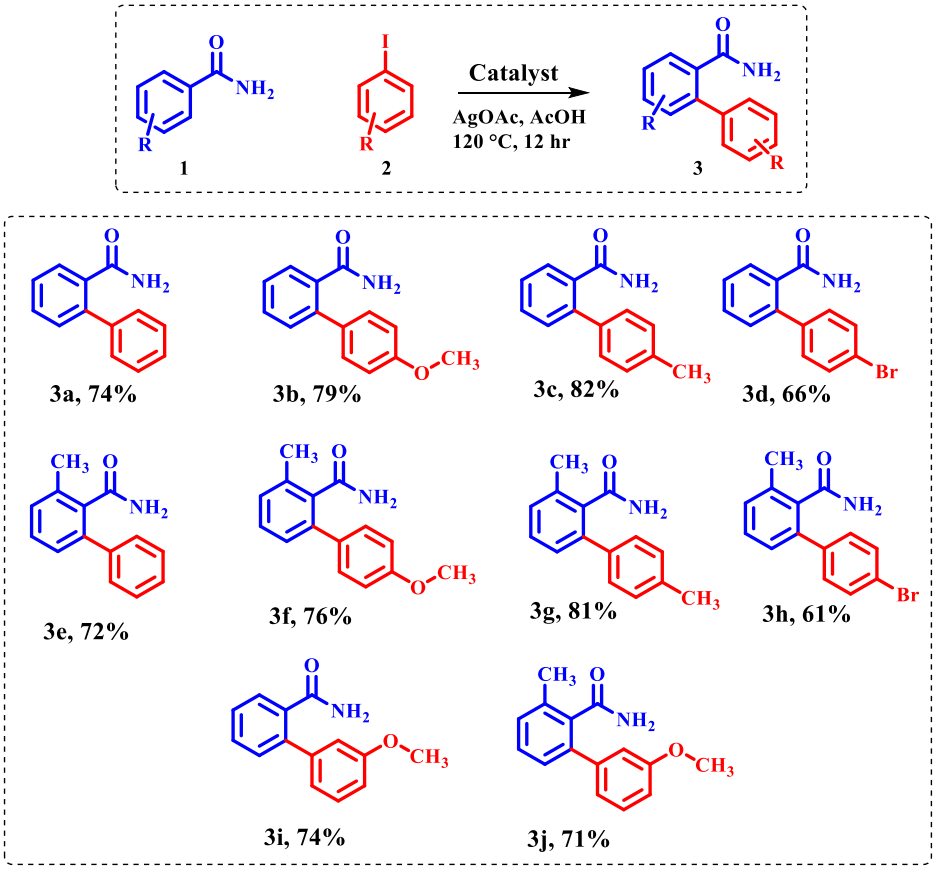

Employing the Fe_3O_4-DA-2Py-Pd catalytic system and optimised reaction conditions, substituted benzamides and substituted aryl iodides were chosen as coupling partners for the synthesis of biaryls, to investigate the substrate scope of ortho arylation of benzamide. The model reaction along with the optimized reaction conditions was shown in **Table 3.2.** It was evident that the intended products 3a-j (**Table 3.2**) could be obtained by the reaction of benzamides and aryl iodides with either electron-donating (EDG) or electron withdrawing groups (EWG). It has been found that para-substituted aryl iodides gave good yield in the presence of EDG groups. **Table 3.2** (3e-3h) demonstrated that O-methyl substitution on the

benzamide phenyl ring lowered the product yield a little, indicating that the "ortho-substituent" effect was not noticeable.

3.3.3.2. Ortho arylation of benzoic acid

Employing acetic acid as a solvent, AgOAc as an additive, and benzoic acid and aryl iodides as coupling partners, the synthesised Fe_3O_4-DA-2Py-Pd catalyst's catalytic potential was further extended to test the viability of ortho arylation of benzoic acid at 120 °C. The same optimization conditions were extended to the ortho-arylation of benzoic acid as in the ortho-arylation of benzamide. The substrate scope of the ortho arylation of benzoic acid over the Fe_3O_4-DA-2Py-Pd nanocatalyst was also investigated by choosing substituted benzoic acids and substituted aryl iodide as coupling partners for the synthesis of biaryls under the same optimized conditions and was shown in **Table 3.3.** The reaction yields were influenced by the substituent's position in the substrate, as demonstrated by the positional isomers of methyl-substituted benzoic acid (**Table 3.3, entries 3c, 3g; 3d, 3h**). The steric hindrance caused by the ortho substituents may have contributed to the decreased yields of the ortho-substituted benzoic acids in these positional isomers when compared to their para isomers. From **Table 3.3**, it was also evident that benzoic acids with EDG gave more yield than those with EWG. The inductive effects of the substituent groups on the substrates would address this phenomenon.[46]

Table 3.3*. Substrate Scope of ortho arylation of benzoic acids catalysed by Fe_3O_4-DA-2Py-Pd*

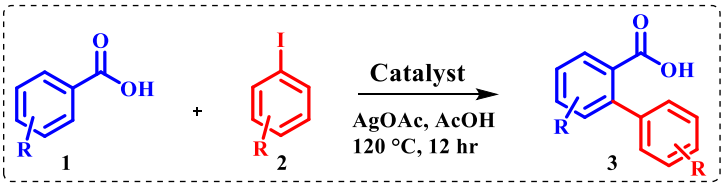

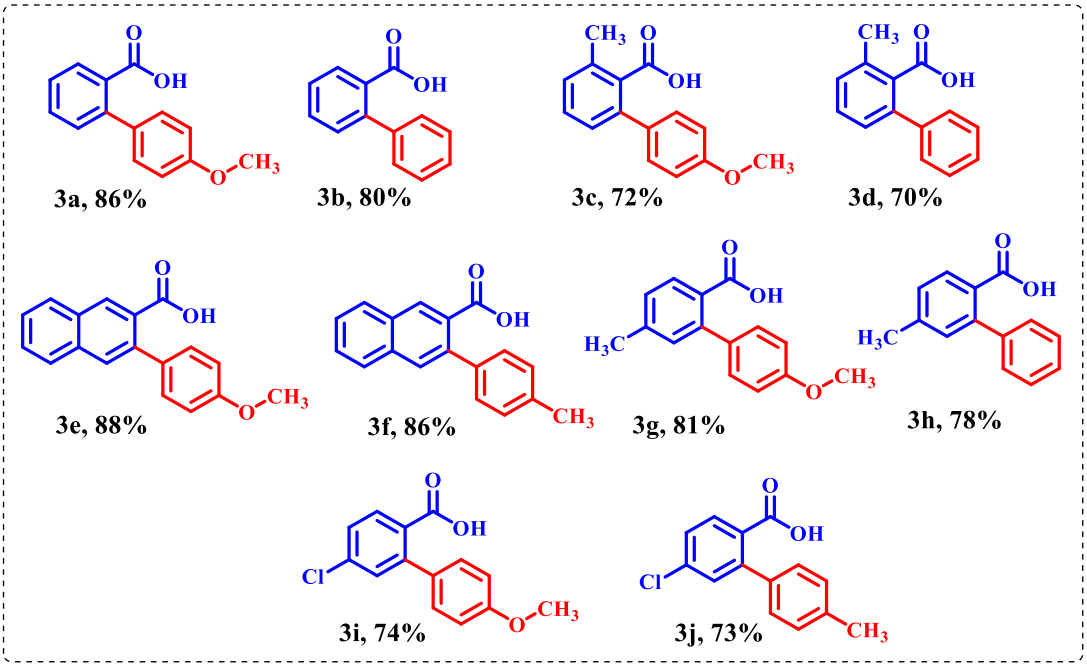

3.3.3.3. Recyclability of the catalyst

Recycling the catalyst in organic synthesis is a crucial issue from an industrial, economic, and environmental standpoint. The recyclability of Fe_3O_4-DA-2Py-Pd nanocatalyst for ortho arylation of benzamide and benzoic acid was examined. Once the reaction was finished in each cycle, the catalyst was extracted from the reaction mixture by means of an external magnet. After being dried and washed with ethanol, the magnetically recovered catalyst was examined for its activity in the next cycle. As depicted in **Figure 3.5**, the catalyst was retrieved and used for at least 5 successive runs without noticeable loss in activity. In the fifth run, the product yields for the benzamide C-H activation and benzoic acid C-H activation reaction were 70% and 81%, respectively.

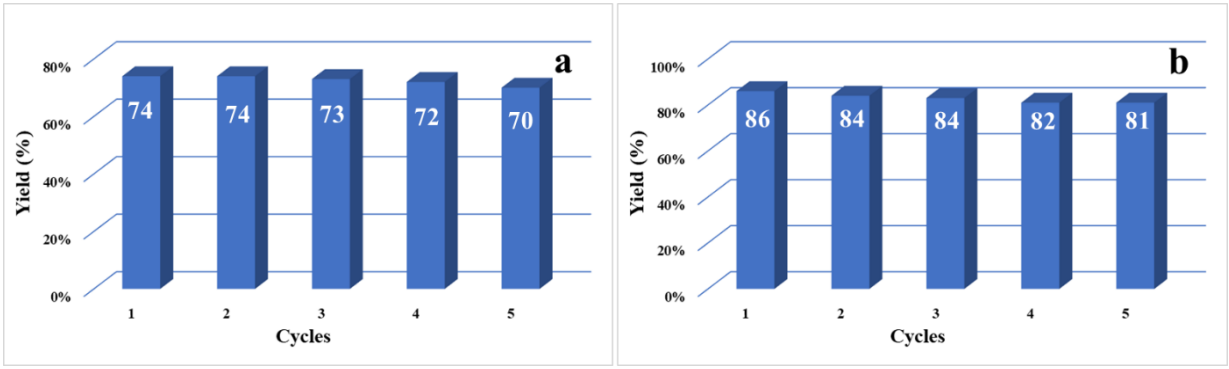

Figure 3.5: *Recyclability test of catalyst for a) ortho arylation of benzamide reaction b) ortho arylation of benzoic acid reaction*

Subsequently, the reused catalyst was examined for its structural stability after five cycles by employing XRD and FT-IR analysis. The recycled catalyst's XRD spectra in **Figure 3.6(I)** showed no impurity peak and its FT-IR spectra revealed that their absorption peaks matched with those of the fresh catalyst in **Figure 3.6(II)**, indicating a similarity between the two. Consequently, the catalyst's structural stability was verified.

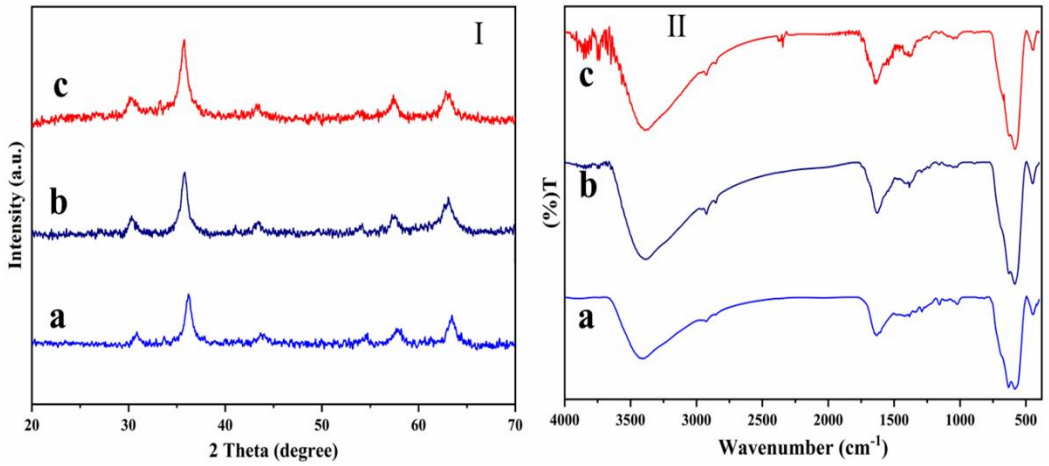

Figure 3.6*. I) XRD spectra II) FTIR spectra of (a) synthesized nanocatalyst (b) used catalyst for ortho-arylation of benzamide and (c) used catalyst for ortho-arylation benzoic acid after 5 cycles*

. The efficiency of the Fe_3O_4-DA-2Py-Pd nanocatalyst was compared with the previously reported catalysts for ortho arylation of benzamides and benzoic acids (**Table 3.4**). The catalysts shown in the **entry 1 to 4** are non-reusable homogeneous catalysts that were meant for ortho arylation of benzoic acid with more reaction time. The catalyst shown in **entry 5 and 6** were meant for ortho arylation of benzamide. Out of these two, catalyst in the **entry 5** was homogeneous non-reusable catalyst and **entry 6** was heterogeneous reusable catalyst with low product yield and used for only benzamide C-H activation. Whereas synthesized Fe_3O_4-DA-2Py-Pd nanocatalyst in the present work was found to work excellently well as a magnetically reusable catalyst. It was able to produce the desired biaryl products in orthoarylation of both benzamide and benzoic acid with satisfactory yield of 88 and 82% respectively as evident from **Table 3.4.** Thus, synthesized catalyst demonstrated its superiority over previously reported catalysts in terms of sustainability.

Table 3.4 *Comparison of Fe_3O_4-DA-2Py-Pd with other previously reported catalysts for Benzamide/Benzoic acid C-H activation reaction:*

S.NO	Catalyst	Reaction	Additive	Solvent	Temp (°C)	Time (h)	Yield (%)	Reuse	Ref.
1	$Pd(OAc)_2$	Benzoic acid	Ag_2CO_3/K_2CO_3	AcOH	120	24	81	0	[13]
2	$Pd(OAc)_2$ /Ligand	Benzoic acid	KOAc, NMe_4Cl,	AcOH	120	43	87	0	[12]
3	$Pd(OAc)_2$	Benzoic acid	Ag_2CO_3/Cs_2CO_3	HFIP	30	12	95	0	[15]
4	$(Ru(p\text{-}cym)Cl_2)_2$/ PCy_3	Benzoic acid	K_2CO_3	NMP	100	24	97	0	[47]
5	$Pd(OAc)_2$	Benzamide	Ag_2O	AcOH	120	5	82	0	[45]
6	Pd/Mesoporous Silica	Benzamide	AgOAc	AcOH	120	15	76	5	[1]
7	**Fe_3O_4-DA-2Py-Pd**	**Benzoic acid**	**AgOAc**	**AcOH**	**120**	**12**	**88**	**5**	**This work**
		Benzamide	**AgOAc**	**AcOH**	**120**	**12**	**82**	**5**	

3.3.3.4. Plausible Mechanism of ortho-arylation of benzamide/benzoic acid over Fe_3O_4-DA-2Py-Pd

A plausible reaction mechanism was proposed for ortho-arylation of benzamide/benzoic acid and iodobenzene as shown in **Figure 3.7** based on the previous studies and the aforementioned experimental findings.[6,1,12,14] This mechanism would mainly involve three major steps, *viz.*, aromatic C-H activation, oxidative addition, and reductive elimination. Step-1 involved cyclopalladation of benzamide/benzoic acid via aromatic C-H activation of benzamide/benzoic acid to form aryl Pd (II) intermediate-1. In step-2, intermediate-1 would undergo oxidative addition to give Pd (IV) Complex intermediate-2. Finally, in step-3, reductive elimination of Pd (IV) Complex intermediate-2 would give the final product regenerating the catalyst.

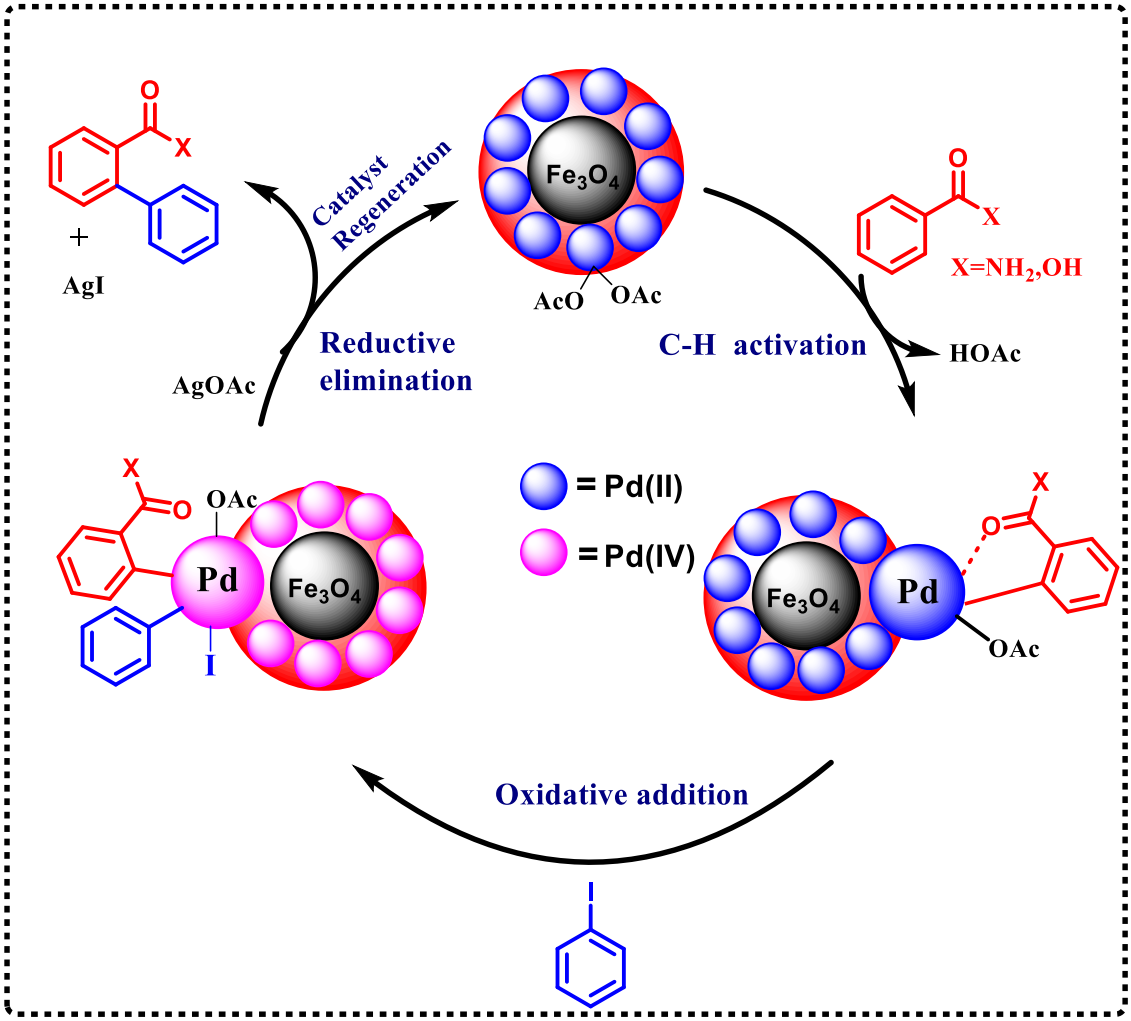

Figure 3.7*. Plausible reaction mechanism for Fe_3O_4–DA-2Py-Pd catalyzed Benzamide/Benzoic Acid C-H activation reaction*

3.4. Conclusions

In summary, Fe_3O_4-DA-2Py-Pd nanocatalyst was successfully synthesized for ortho arylation of both benzamide and benzoic acid by aryl iodide. Catalyst was magnetically recoverable and worked exceptionally well for the said application under ligand free conditions with an excellent yield of the product (88% & 82%) respectively. The efficacy of the catalyst was validated for substituted benzamides/benzoic acids and substituted aryl iodide (coupling partners) for the synthesis of biaryls which gave good yield of the products. It was found that the catalyst may be reused for at least five cycles with no appreciable reduction in activity. After 5 cycles, the structural stability of the reused catalyst was established by XRD and FT-IR study. This catalyst is the first magnetically reusable catalyst for aforementioned applications. On comparison of this catalyst with reported catalysts, it was understood that current catalyst is superior to the reported ones due to its unique features such as i) presence of low amount of expensive active metal ii) effective binding of active metal by Schiff base strategy iii) Magnetic separability of the catalyst iv) Use of catalyst for dual applications. Thus, the sustainable application of the synthesized catalyst (Fe_3O_4-DA-2Py-Pd) was established.

3.5. Spectral data of synthesized products Benzamide C-H activation 3a-3j & Benzoic acid C-H activation 3a-3j

Benzamide C-H activation:

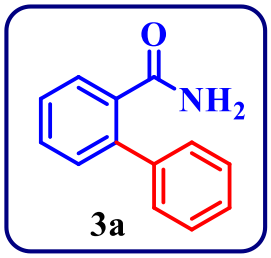

[1,1'-biphenyl]-2-carboxamide

^{1}H NMR (400 MHz, $CDCl_3$): δ (ppm): 7.78 (d, J = 8.0 Hz, 1H), 7.50 (t, J = 7.6 Hz, 1H), 7.46 – 7.35 (m, 7H), 5.67 (brs, 1H), 5.27 (brs, 1H); ^{13}C NMR (100 MHz, $CDCl_3$): δ (ppm): 171.41, 140.20, 139.87, 134.39, 130.55, 130.43, 129.07, 128.80, 128.71, 127.95, 127.63.

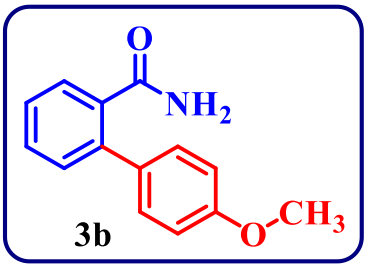

4'-methoxy-[1,1'-biphenyl]-2-carboxamide

^{1}H NMR (400 MHz, $CDCl_3$): δ (ppm): 7.77 (dd, J = 7.6, 1.2 Hz, 1H), 7.50 – 7.46 (m, 1H), 7.40 (t, J = 7.6 Hz, 1H), 7.37 – 7.30 (m, 3H), 6.87 (d, J = 7.8 Hz, 2H), 5.87 (s, 1H), 5.32 (s, 1H), 3.85 (s, 3H).; ^{13}C NMR (100 MHz, $CDCl_3$): δ (ppm): 171.51, 159.34, 139.88, 134.25, 130.52, 130.42, 129.42, 129.10, 128.67, 127.40, 114.09, 55.28.

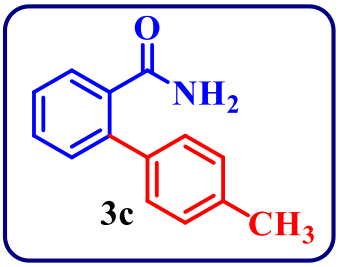

4'-methyl-[1,1'-biphenyl]-2-carboxamide

^{1}H NMR (400 MHz, $CDCl_3$): δ (ppm): 7.77 (d, J = 7.6 Hz, 1H), 7.48 (t, J = 7.6 Hz, 1H), 7.40 (t, J = 7.6 Hz, 1H), 7.36 – 7.31 (m, 3H), 7.23 (d, J = 7.8 Hz, 2H), 5.86 (brs, 1H), 5.32 (brs, 1H), 2.39 (s, 3H); ^{13}C NMR (100 MHz, $CDCl_3$): δ (ppm): 171.53, 139.89, 137.82, 137.26, 134.27, 130.53, 130.44, 129.44, 129.11, 128.69, 127.41, 21.21.

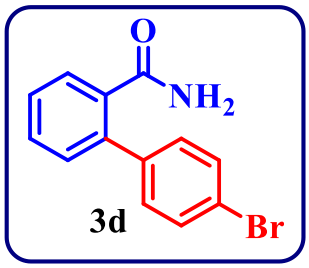

4'-bromo-[1,1'-biphenyl]-2-carboxamide

^{1}H NMR (400 MHz, $CDCl_3$): δ (ppm): 7.71 (d, J = 7.6 Hz, 1H), 7.58 – 7.47 (m, 3H), 7.43 (t, J = 7.6 Hz, 1H), 7.33 (t, J = 8.4 Hz, 3H), 5.85 (brs, 1H), 5.37 (brs, 1H); ^{13}C NMR (100 MHz, $CDCl_3$): δ (ppm): 171.29, 139.07, 138.61, 134.56, 131.82, 130.64, 130.38, 130.25, 128.84, 127.94, 122.32.

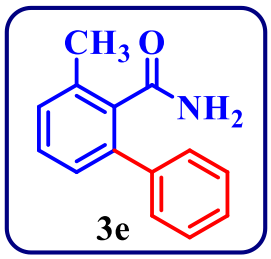

3-methyl-[1,1'-biphenyl]-2-carboxamide

^{1}H NMR (400 MHz, $CDCl_3$): δ (ppm): 7.45 (d, J = 7.6 Hz, 2H), 7.39 – 7.29 (m, 4H), 7.20 (t, J = 8 Hz, 2H), 5.80 (brs, 1H), 5.33 (brs, 1H), 2.43 (s, 3H); ^{13}C NMR (100 MHz, $CDCl_3$): δ (ppm): 172.12, 140.44, 138.97, 135.67, 135.34, 129.37, 129.03, 128.65, 128.43, 127.54, 127.39, 19.57.

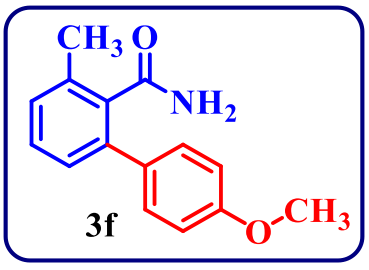

4'-methoxy-3-methyl-[1,1'-biphenyl]-2-carboxamide

^{1}H NMR (400 MHz, $CDCl_3$): δ (ppm): 7.39 (d, J = 8.8 Hz, 2H), 7.30 (d, J = 7.6 Hz, 1H), 7.19 (d, J = 6.4 Hz, 2H), 6.92 (d, J = 8.8 Hz, 2H), 5.89 (brs, 1H), 5.32 (brs, 1H), 3.83 (s, 3H), 2.44 (s, 3H); ^{13}C NMR (100 MHz, $CDCl_3$): δ (ppm): 172.59, 159.21, 138.61, 135.47, 135.35, 132.77, 129.76, 129.06, 129.00, 127.34, 113.90, 55.27, 19.57.

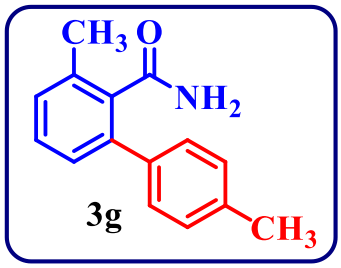

3,4'-dimethyl-[1,1'-biphenyl]-2-carboxamide

^{1}H NMR (400 MHz, $CDCl_3$): δ (ppm): 7.36 (d, J = 8 Hz, 2H), 7.31 (t, J = 8 Hz, 1H), 7.22 – 7.16 (m, 4H), 5.70 (brs, 1H), 5.30 (brs, 1H), 2.44 (s, 3H), 2.38 (s, 3H); ^{13}C NMR (100 MHz, $CDCl_3$): δ (ppm): 172.20, 138.93, 137.52, 137.34, 135.58, 135.34, 129.18, 129.03, 128.52, 127.38, 21.18, 19.58.

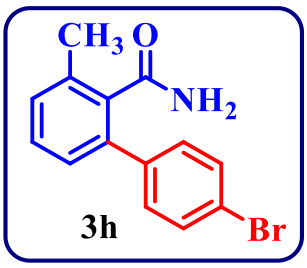

4'-bromo-3-methyl-[1,1'-biphenyl]-2-carboxamide

^{1}H NMR (400 MHz, $CDCl_3$): δ (ppm): 7.51 (d, J = 8.4 Hz, 2H), 7.35 – 7.31 (m, 3H), 7.23 (d, J = 7.6 Hz, 1H), 7.16 (d, J = 7.6 Hz, 1H), 5.86 (brs, 1H), 5.36 (brs, 1H), 2.44 (s, 3H); ^{13}C NMR (100 MHz, $CDCl_3$): δ (ppm): 171.93, 139.28, 137.69, 135.53, 135.43, 131.59, 130.30, 129.72, 129.20, 127.15, 122.00, 19.50.

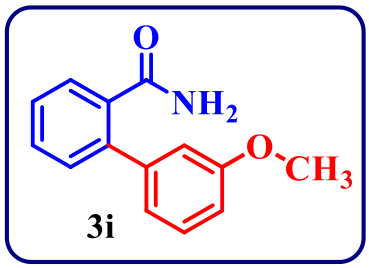

3'-methoxy-[1,1'-biphenyl]-2-carboxamide

^{1}H NMR (400 MHz, $CDCl_3$): δ (ppm): 7.83 – 7.79 (m, 1H), 7.54 – 7.45 (m, 2H), 7.38 – 7.33 (m, 2H), 7.04 – 6.97 (m, 2H), 6.94 (d, J = 8 Hz, 1H), 5.61 (s, 1H), 5.32 (s, 1H), 3.83 (s, 3H).; ^{13}C NMR (100 MHz, $CDCl_3$): δ (ppm): 172.18, 159.54, 141.94, 138.96, 135.71, 135.46, 131.04, 129.57, 129.12, 127.34, 121.16, 114.17, 113.52, 55.35.

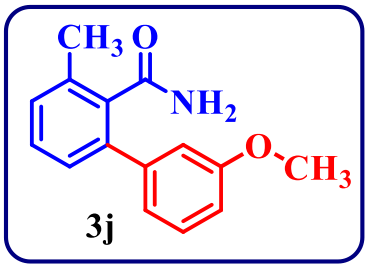

3'-methoxy-3-methyl-[1,1'-biphenyl]-2-carboxamide

^{1}H NMR (400 MHz, $CDCl_3$): δ (ppm): 7.34 – 7.26 (m, 2H), 7.21 (t, J = 7.2 Hz, 2H), 7.04 – 7.01 (m, 2H), 6.89 (d, J = 8.2 Hz, 1H), 5.78 (brs, 1H), 5.36 (brs, 1H), 3.80 (s, 3H), 2.44 (s, 3H); ^{13}C NMR (100 MHz, $CDCl_3$): δ (ppm): 172.08, 159.45, 141.84, 138.86, 135.62, 135.36, 129.47, 129.02, 127.24, 121.06, 114.07, 113.42, 55.25, 19.55.

Benzoic acid C-H activation:

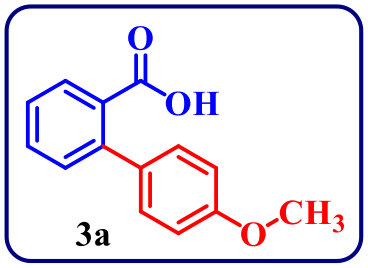

4'-methoxy-[1,1'-biphenyl]-2-carboxylic acid

^{1}H NMR (400 MHz, $CDCl_3$): δ (ppm): 7.91 (d, J = 8.0 Hz, 1H), 7.53 (t, J = 7.2 Hz, 1H), 7.40 – 7.34 (m, 2H), 7.27 (d, J = 8.0 Hz, 2H), 6.91 (d, J = 8.8 Hz, 2H), 3.83 (s, 3H).; ^{13}C NMR (100 MHz, $CDCl_3$): δ (ppm): 172.85, 159.10, 142.81, 133.36, 131.93, 131.17, 130.62, 130.44, 129.66, 126.84, 113.62, 55.25.

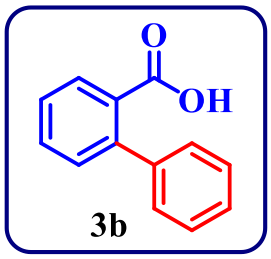

[1,1'-biphenyl]-2-carboxylic acid

^{1}H NMR (400 MHz, $CDCl_3$): δ (ppm): 7.93 (d, J = 7.8 Hz, 1H), 7.55 (t, J = 7.4 Hz, 1H), 7.42 (d, J = 7.6 Hz, 1H), 7.38– 7.32 (m, 6H); ^{13}C NMR (100 MHz, $CDCl_3$): δ (ppm): 172.94, 143.30, 141.08, 131.98, 131.18, 130.63, 129.52, 128.49, 128.07, 127.34, 127.19.

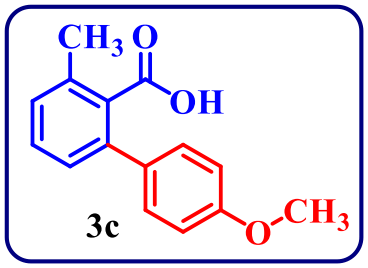

4'-methoxy-3-methyl-[1,1'-biphenyl]-2-carboxylic acid

^{1}H NMR (400 MHz, $CDCl_3$): δ (ppm): 7.37 – 7.33 (m, 3H), 7.20 (d, J = 7.6 Hz, 2H), 6.92 (d, J = 8.8 Hz, 2H), 3.83 (s, 3H), 2.45 (s, 3H); ^{13}C NMR (100 MHz, $CDCl_3$): δ (ppm): 173.61, 159.18, 139.70, 135.35, 133.09, 130.45, 129.64, 129.52, 128.84, 127.45, 113.86, 55.27, 19.91.

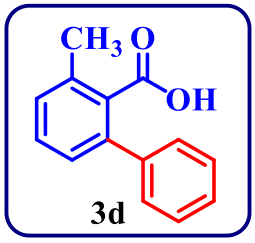

3-methyl-[1,1'-biphenyl]-2-carboxylic acid

^{1}H NMR (400 MHz, $CDCl_3$): δ (ppm): 7.41 – 7.34 (m, 6H), 7.23 – 7.20 (m, 2H), 2.45 (s, 3H); ^{13}C NMR (100 MHz, $CDCl_3$): δ (ppm): 174.24, 140.68, 140.17, 135.45, 132.21, 129.70, 129.22, 128.79, 128.38, 127.52, 127.47, 19.93.

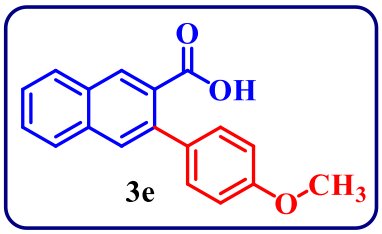

3-(4-methoxyphenyl)-2-naphthoic acid

^{1}H NMR (400 MHz, $CDCl_3$): δ (ppm): 8.52 (s, 1H), 7.94 (d, J = 8.0 Hz, 1H), 7.85 (d, J = 8.4 Hz, 1H), 7.79 (s, 1H), 7.60 (t, J = 7.8 Hz, 1H), 7.54 (t, J = 7.8 Hz, 1H), 7.37 (d, J = 8.8 Hz, 2H), 6.96 (d, J = 8.8 Hz, 2H), 3.86 (s, 3H); ^{13}C NMR (100 MHz, $CDCl_3$): δ (ppm): 172.68, 159.01, 138.69, 134.82, 133.55, 132.27, 131.33, 130.46, 130.06, 129.84, 128.78, 128.62, 127.71, 126.68, 113.63, 55.29.

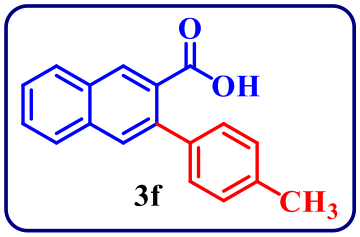

3f

3-(p-tolyl)-2-naphthoic acid

^{1}H NMR (400 MHz, $CDCl_3$): δ (ppm): 8.53 (s, 1H), 7.95 (d, J = 8.0 Hz, 1H), 7.86 (d, J = 8.4 Hz, 1H), 7.79 (s, 1H), 7.63 – 7.53 (m, 2H), 7.37 (d, J = 8.8 Hz, 2H), 7.23 (d, J = 8.4 Hz, 2H), 2.44 (s, 3H); ^{13}C NMR (100 MHz, $CDCl_3$): δ (ppm): 172.77, 138.71, 137.10, 134.84, 133.57, 132.29, 131.35, 130.48, 130.08, 129.86, 129.55, 128.80, 128.64, 127.73, 126.70, 21.39.

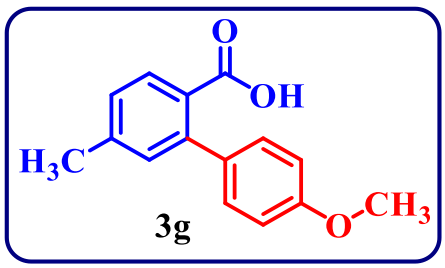

3g

4'-methoxy-5-methyl-[1,1'-biphenyl]-2-carboxylic acid

^{1}H NMR (400 MHz, $CDCl_3$): δ (ppm): 7.85 (d, J = 8.0 Hz, 1H), 7.25 (d, J = 6.4 Hz, 3H), 7.19 (d, J = 7.6 Hz, 1H), 7.15 (s, 1H), 6.91 (d, J = 8.8 Hz, 2H), 3.84 (s, 3H), 2.41 (s, 3H); ^{13}C NMR (100 MHz, $CDCl_3$): δ (ppm): 172.14, 159.01, 143.13, 142.65, 133.59, 132.09, 131.04, 129.65, 127.62, 126.26, 113.52, 55.26, 21.50.

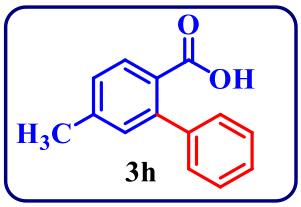

3h

5-methyl-[1,1'-biphenyl]-2-carboxylic acid

^{1}H NMR (400 MHz, $CDCl_3$): δ (ppm): 7.87 (d, J = 8.0 Hz, 1H), 7.38 – 7.30 (m, 5H), 7.22 (d, J = 8.0 Hz, 1H), 7.16 (s, 1H), 2.42 (s, 3H); ^{13}C NMR (100 MHz, $CDCl_3$): δ (ppm): 172.25, 143.62, 142.72, 141.33, 132.08, 131.04, 129.19, 128.48, 128.32, 127.97, 127.93, 127.22, 21.50.

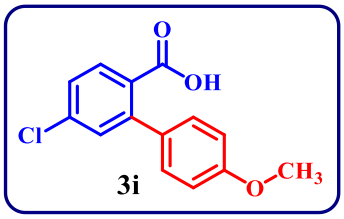

3i

5-chloro-4'-methoxy-[1,1'-biphenyl]-2-carboxylic acid

^{1}H NMR (400 MHz, $CDCl_3$): δ (ppm): 7.86 (d, J = 8.8 Hz, 1H), 7.37– 7.34 (m, 2H), 7.24 (d, J = 8.8 Hz, 1H), 6.91 (d, J = 8.8 Hz, 2H), 3.84 (s, 3H); ^{13}C NMR (100 MHz, $CDCl_3$): δ (ppm): 172.14, 159.01, 143.13, 142.65, 133.59, 132.09, 131.04, 129.65, 127.62, 126.26, 113.52, 55.26,

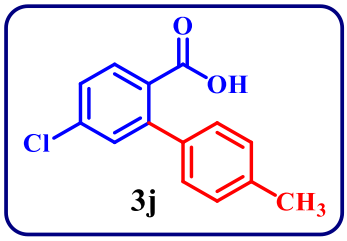

3j

5-chloro-4'-methyl-[1,1'-biphenyl]-2-carboxylic acid

^{1}H NMR (400 MHz, $CDCl_3$): δ (ppm): 7.87 (d, J = 8.8 Hz, 9H), 7.39 – 7.36 (m, 2H), 7.25 (d, J = 8.6 Hz, 20H), 7.21 (d, J = 6.8 Hz, 3H), 2.38 (s, 3H); ^{13}C NMR (100 MHz, $CDCl_3$): δ (ppm): 171.23, 144.75, 138.06, 137.43, 132.14, 131.23, 130.91, 129.61, 128.83, 128.50, 127.01, 21.36.

3.6. References

(1) Parsharamulu, T.; Venkanna, D.; Lakshmi Kantam, M.; Bhargava, S. K.; Srinivasu, P. The First Example of Ortho -Arylation of Benzamides over Pd/Mesoporous Silica: A Novel Approach for Direct Sp2 C-H Bond Activation. *Ind. Eng. Chem. Res.* **2014**, *53* (52), 20075–20084.

(2) Srinivas, M.; Srinivasu, P.; Bhargava, S. K.; Kantam, M. L. Direct Synthesis of Two-Dimensional Mesoporous Copper Silicate as an Efficient Catalyst for Synthesis of Propargylamines. *Catal. Today* **2013**, *208*, 66–71.

(3) Bringmann, G.; Walter, R.; Weirich, R. The Directed Synthesis of Biaryl Compounds: Modern Concepts and Strategies. *Angew. Chemie Int. Ed. English* **1990**, *29* (9), 977–991.

(4) Hassan, J.; Sévignon, M.; Gozzi, C.; Schulz, E.; Lemaire, M. Aryl-Aryl Bond Formation One Century after the Discovery of the Ullmann Reaction. *Chem. Rev.* **2002**, *102* (5), 1359–1469.

(5) Lloyd-Williams, P.; Giralt, E. Atropisomerism, Biphenyls and the Suzuki Coupling: Peptide Antibiotics. *Chem. Soc. Rev.* **2001**, *30* (3), 145–157.

(6) Aghahosseini, H.; Saadati, M. R.; Rezaei, S. J. T.; Ramazani, A.; Asadi, N.; Yahiro, H.; Mori, M.; Shajari, N.; Kazemizadeh, A. R. A Robust Polyfunctional Pd(II)-Based Magnetic Amphiphilic Nanocatalyst for the Suzuki–Miyaura Coupling Reaction. *Sci. Rep.* **2021**, *11* (1), 1–11.

(7) Ciriminna, R.; Pandarus, V.; Gingras, G.; Béland, F.; Carà, P. D.; Pagliaro, M. Heterogeneous Sonogashira Coupling over Nanostructured SiliaCat Pd(0). *ACS Sustain. Chem. Eng.* **2013**, *1* (1), 57–61.

(8) Khalafi-Nezhad, A.; Panahi, F. Size-Controlled Synthesis of Palladium Nanoparticles on a Silica-Cyclodextrin Substrate: A Novel Palladium Catalyst System for the Heck Reaction in Water. *ACS Sustain. Chem. Eng.* **2014**, *2* (5), 1177–1186.

(9) Tsai, F. Y.; Lin, B. N.; Chen, M. J.; Mou, C. Y.; Liu, S. T. Anchored Palladium Bipyridyl Complex in Nanosized MCM-41: A Recyclable and Efficient Catalyst for the Kumada-Corriu Reaction. *Tetrahedron* **2007**, *63* (20), 4304–4309.

(10) Liu, J.; Deng, Y.; Wang, H.; Zhang, H.; Yu, G.; Wu, B.; Zhang, H.; Li, Q.; Marder, T. B.; Yang, Z.; Lei, A. Effective Pd-Nanoparticle (PdNP)-Catalyzed Negishi Coupling Involving Alkylzinc Reagents at Room Temperature. *Org. Lett.* **2008**, *10* (13), 2661–2664.

(11) Pacardo, D. B.; Sethi, M.; Jones, S. E.; Naik, R. R.; Knecht, M. R. Biomimetic Synthesis of Pd Nanocatalysts for the Stille Coupling Reaction. *ACS Nano* **2009**, *3* (5), 1288–1296.

(12) Arroniz, C.; Denis, J. G.; Ironmonger, A.; Rassias, G.; Larrosa, I. An Organic Cation as a Silver(I) Analogue for the Arylation of Sp2 and Sp3 C-H Bonds with Iodoarenes. *Chem. Sci.* **2014**, *5* (9), 3509–3514.

(13) Arroniz, C.; Ironmonger, A.; Rassias, G.; Larrosa, I. Direct Ortho -Arylation of Ortho -Substituted Benzoic Acids : Overriding Pd-Catalyzed Protodecarboxylation. *Org. Lett.* **2013**, 4, 910–913.

(14) Chen, X.; Engle, K. M.; Wang, D. H.; Jin-Quan, Y. Palladium(II)-CataIyzed C-H Aetivation/C-C Cross-Coupling Reactions: Versatility and Practicality. *Angew. Chemie - Int. Ed.* **2009**, *48* (28), 5094–5115.

(15) Zhu, C.; Zhang, Y.; Kan, J.; Zhao, H.; Su, W. Ambient-Temperature Ortho C-H Arylation of Benzoic Acids with Aryl Iodides with Ligand-Supported Palladium Catalyst. *Org. Lett.* **2015**, *17* (14), 3418–3421.

(16) Chen, X.; Goodhue, C. E.; Yu, J. Q. Palladium-Catalyzed Alkylation of Sp2 and Sp3 C-H Bonds with Methylboroxine and Alkylboronic Acids: Two Distinct C-H Activation Pathways. *J. Am. Chem. Soc.* **2006**, *128* (39), 12634–12635.

(17) Kim, J.; Chang, S. A New Combined Source of "CN" from N, N -Dimethylformamide and Ammonia in the Palladium-Catalyzed Cyanation of Aryl C-H Bonds. *J. Am. Chem. Soc.* **2010**,

132 (30), 10272–10274.

(18) Yang, S.; Li, B.; Wan, X.; Shi, Z. Ortho Arylation of Acetanilides via Pd(II)-Catalyzed C-H Functionalization. *J. Am. Chem. Soc.* **2007**, *129* (19), 6066–6067.

(19) Li, B. J.; Tian, S. L.; Fang, Z.; Shi, Z. J. Multiple C-H Activations to Construct Biologically Active Molecules in a Process Completely Free of Organohalogen and Organometallic Components. *Angew. Chemie - Int. Ed.* **2008**, *47* (6), 1115–1118.

(20) Chen, X.; Li, J. J.; Hao, X. S.; Goodhue, C. E.; Yu, J. Q. Palladium-Catalyzed Alkylation of Aryl C-H Bonds with Sp3 Organotin Reagents Using Benzoquinone as a Crucial Promoter. *J. Am. Chem. Soc.* **2006**, *128* (1), 78–79.

(21) Giri, R.; Chen, X.; Yu, J. Q. Palladium-Catalyzed Asymmetric Iodination of Unactivated C-H Bonds under Mild Conditions. *Angew. Chemie - Int. Ed.* **2005**, *44* (14), 2112–2115.

(22) Engle, K. M.; Wang, D. H.; Yu, J. Q. Constructing Multiply Substituted Arenes Using Sequential Palladium(II)-Catalyzed C-H Olefination. *Angew. Chemie - Int. Ed.* **2010**, *49* (35), 6169–6173.

(23) Zhang, Y.-H.; Yu, J.-Q. ChemInform Abstract: Pd(II)-Catalyzed Hydroxylation of Arenes with 1 Atm of O_2 or Air. . *ChemInform* **2010**, *41* (10), 14654–14655.

(24) Lu, Y.; Leow, D.; Wang, X.; Engle, K. M.; Yu, J. Q. Hydroxyl-Directed C-H Carbonylation Enabled by Mono-N-Protected Amino Acid Ligands: An Expedient Route to 1-Isochromanones. *Chem. Sci.* **2011**, *2* (5), 967–971.

(25) Lu, Y.; Wang, D. H.; Engle, K. M.; Yu, J. Q. Pd(II)-Catalyzed Hydroxyl-Directed C-H Olefination Enabled by Monoprotected Amino Acid Ligands. *J. Am. Chem. Soc.* **2010**, *132* (16), 5916–5921.

(26) Thirunavukkarasu, V. S.; Parthasarathy, K.; Cheng, C. H. Synthesis of Fluorenones from Aromatic Aldoxime Ethers and Aryl Halides by Palladium-Catalyzed Dual C-H Activation and Heck Cyclization. *Angew. Chemie - Int. Ed.* **2008**, *47* (49), 9462–9465.

(27) Sun, C. L.; Liu, N.; Li, B. J.; Yu, D. G.; Wang, Y.; Shi, Z. J. Pd-Catalyzed C-H Functionalizations of O-Methyl Oximes with Arylboronic Acids. *Org. Lett.* **2010**, *12* (1), 184–187.

(28) Jeon, W. H.; Lee, T. S.; Kim, E. J.; Moon, B.; Kang, J. Palladium(II)-Catalyzed Ortho-Arylation via Phosphate-Group-Directed C-H Activation. *Tetrahedron* **2013**, *69* (25), 5152–5159.

(29) Shen, X.; Jones, G. O.; Watson, D. A.; Bhayana, B.; Buchwald, S. L. Enantioselective Synthesis of Axially Chiral Biaryls by the Pd-Catalyzed Suzuki-Miyaura Reaction: Substrate Scope and Quantum Mechanical Investigations. *J. Am. Chem. Soc.* **2010**, *132* (32), 11278–11287.

(30) Zhou, Y.; Zhang, X.; Liang, H.; Cao, Z.; Zhao, X.; He, Y.; Wang, S.; Pang, J.; Zhou, Z.; Ke, Z.; Qiu, L. Enantioselective Synthesis of Axially Chiral Biaryl Monophosphine Oxides via Direct Asymmetric Suzuki Coupling and DFT Investigations of the Enantioselectivity. *ACS Catal.* **2014**, *4* (5), 1390–1397.

(31) Pharande, P. S.; Rashinkar, G. S.; Pore, D. M. Cellulose Schiff Base-Supported Pd(II): An Efficient Heterogeneous Catalyst for Suzuki Miyaura Cross-Coupling. *Res. Chem. Intermed.* **2021**, *47* (11), 4457–4476.

(32) Sharma, S.; Kaur, M.; Sharma, C.; Choudhary, A.; Paul, S. Biomass-Derived Activated Carbon-Supported Copper Catalyst : An E Ffi Cient Heterogeneous Magnetic Catalyst for Base-Free Chan−Lam Coupling and Oxidations. *ACS Omega* **2021,** 6, 19529-19545**.**

(33) Tandon, R.; Tandon, N.; Patil, S. M. RSC Advances Overview on Magnetically Recyclable Ferrite Nanoparticles : Synthesis and Their Applications in Coupling and Multicomponent Reactions. *RSC Advances*, **2021**, 11, 29333–29353.

(34) Lee, Y.; Garcia, M. A.; Frey Huls, N. A.; Sun, S. Synthetic Tuning of the Catalytic Properties of Au-Fe_3O_4 Nanoparticles. *Angew. Chemie* **2010**, *122* (7), 1293–1296.

(35) Zheng, K.; Shen, C.; Qiao, J.; Tong, J.; Jin, J.; Zhang, P. Novel Magnetically-Recyclable, Nitrogen-Doped Fe_3O_4@Pd NPs for Suzuki–Miyaura Coupling and Their Application in the Synthesis of Crizotinib. *Catalysts* **2018**, *8* (10).

(36) Manna, J.; Akbayrak, S.; Özkar, S. Palladium(0) Nanoparticles Supported on Polydopamine Coated Fe_3O_4 as Magnetically Isolable, Highly Active and Reusable Catalysts for Hydrolytic Dehydrogenation of Ammonia Borane. *RSC Adv.* **2016**, *6* (104), 102035–102042.

(37) Naghipour, A.; Fakhri, A. Heterogeneous Fe_3O_4@chitosan-Schiff Base Pd Nanocatalyst: Fabrication, Characterization and Application as Highly Efficient and Magnetically-Recoverable Catalyst for Suzuki-Miyaura and Heck-Mizoroki C-C Coupling Reactions. *Catal. Commun.* **2016**, *73*, 39–45.

(38) Baig, R. B. N.; Varma, R. S. A Highly Active and Magnetically Retrievable Nanoferrite-DOPA-Copper Catalyst for the Coupling of Thiophenols with Aryl Halides. *Chem. Commun.* **2012**, *48* (20), 2582–2584.

(39) Nasir Baig, R. B.; Varma, R. S. Organic Synthesis via Magnetic Attraction: Benign and Sustainable Protocols Using Magnetic Nanoferrites. *Green Chem.* **2013**, *15* (2), 398–417.

(40) Iyengar, S. J.; Joy, M.; Ghosh, C. K.; Dey, S.; Kotnala, R. K.; Ghosh, S. Magnetic, X-Ray and Mössbauer Studies on Magnetite/Maghemite Core-Shell Nanostructures Fabricated through an Aqueous Route. *RSC Adv.* **2014**, *4* (110), 64919–64929.

(41) Sharma, R. K.; Dutta, S.; Sharma, S. Quinoline-2-Carboimine Copper Complex Immobilized on Amine Functionalized Silica Coated Magnetite Nanoparticles: A Novel and Magnetically Retrievable Catalyst for the Synthesis of Carbamates via C-H Activation of Formamides. *Dalt. Trans.* **2014**, *44* (3), 1303–1316.

(42) Alazemi, A. M.; Dawood, K. M.; Al-Matar, H. M.; Tohamy, W. M. Efficient and Recyclable Solid-Supported Pd(II) Catalyst for Microwave-Assisted Suzuki Cross-Coupling in Aqueous Medium. *ACS Omega* **2022**, *7* (33), 28831–28848.

(43) Gogoi, R.; Saikia, R.; Borah, G. Agro Waste Derived Nanosilica Supported Pd(Ll) Complex: A Protocol for Copper Free Sonogashira Reaction in Water. *J. Organomet. Chem.* **2019**, *897*, 80–88.

(44) Banda, P. G.; Mucherla, R. Palladium-Supported Polydopamine-Coated $NiFe_2O_4$@TiO_2: A Sole Photocatalyst for Suzuki and Sonogashira Coupling Reactions under Sunlight Irradiation. *ACS Omega* **2022**, *7* (33), 29356–29368.

(45) Li, D. D.; Yuan, T. T.; Wang, G. W. Palladium-Catalyzed Ortho-Arylation of Benzamides via Direct Sp_2C-H Bond Activation. *J. Org. Chem.* **2012**, *77* (7), 3341–3347.

(46) Duarah, R.; Karak, N. Hyperbranched Polyurethane/Palladium-Reduced Carbon Dot Nanocomposite: An Efficient and Reusable Mesoporous Catalyst for Visible-Light-Driven C-C Coupling Reactions. *Ind. Eng. Chem. Res.* **2019**, *58* (36), 16307–16319.

(47) Huang, L.; Weix, D. J. Ruthenium-Catalyzed C-H Arylation of Diverse Aryl Carboxylic Acids with Aryl and Heteroaryl Halides. *Org. Lett.* **2016**, *18* (20), 5432–5435.

3.7. Selected NMR (^{1}H & ^{13}C) spectra of the products in

3.7.1. Benzamide C-H activation

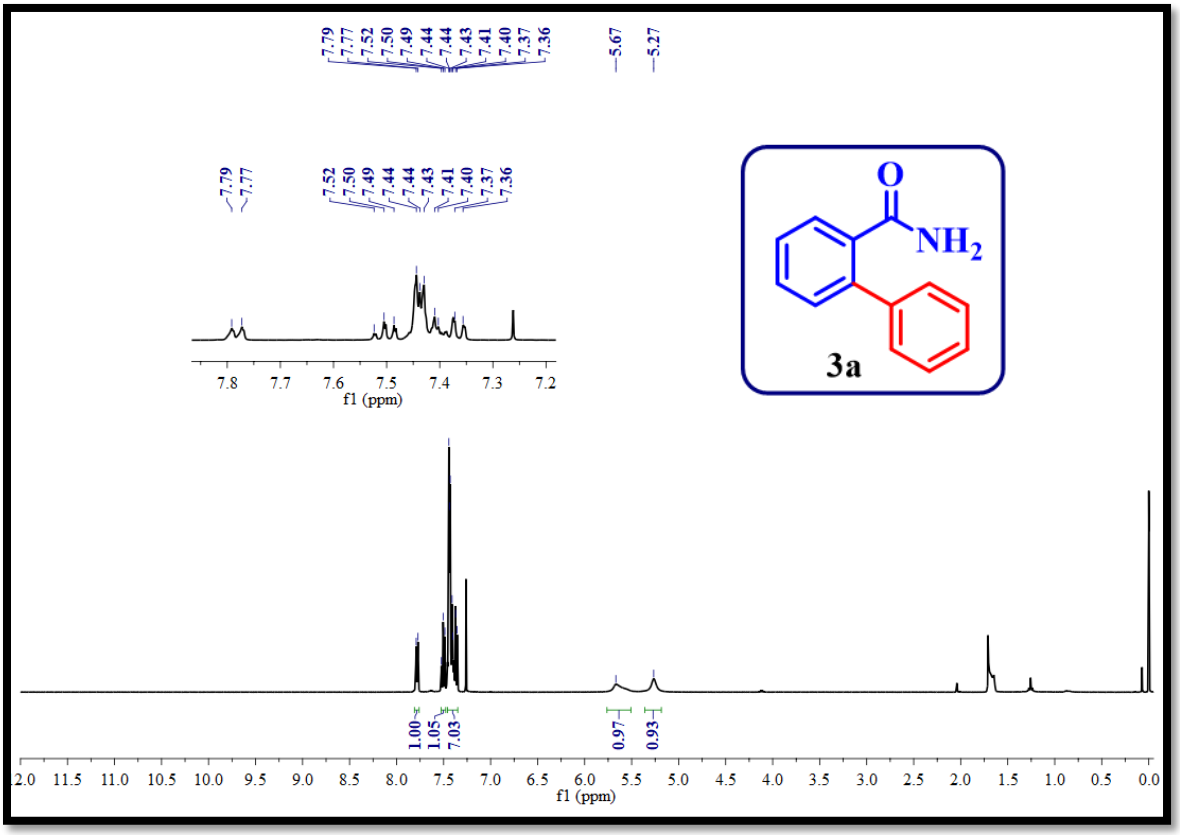

^{1}H NMR spectrum of the compound 3-methyl-[1,1'-biphenyl]-2-carboxamide(3a)

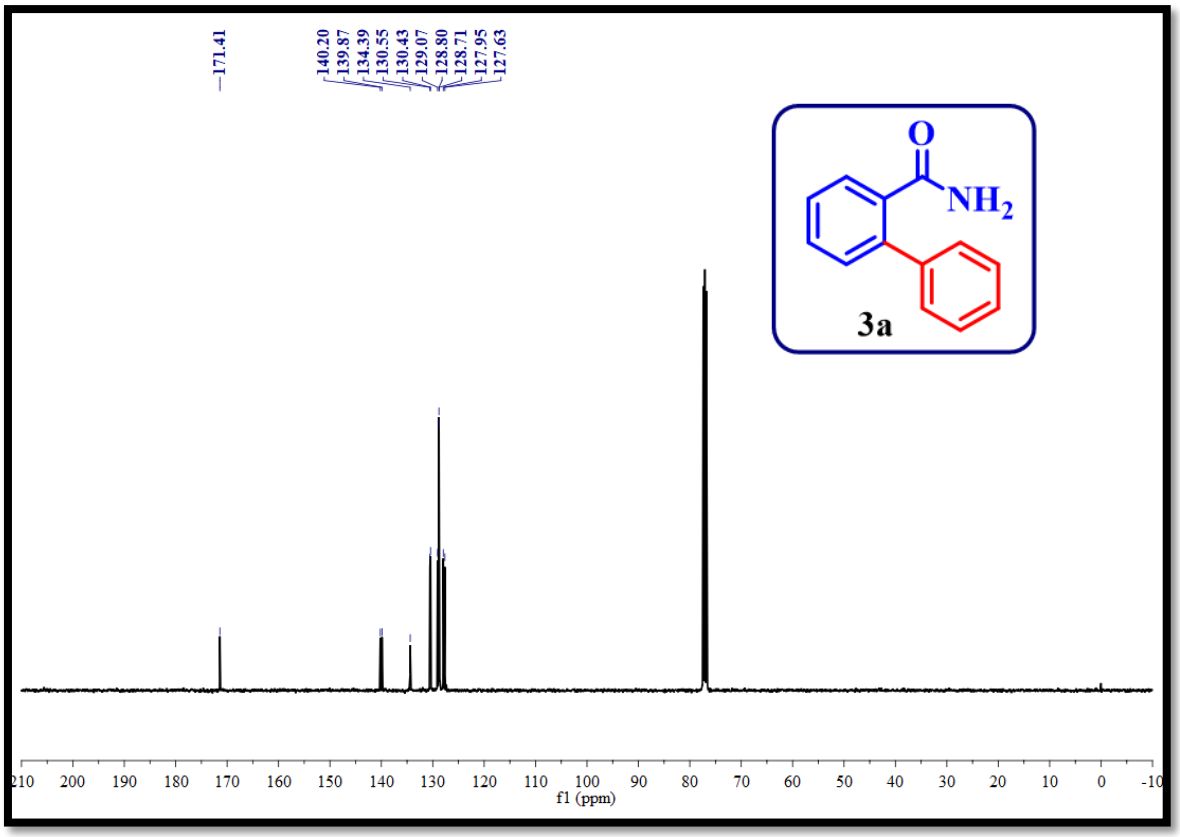

^{13}C NMR spectrum of the compound 3-methyl-[1,1'-biphenyl]-2-carboxamide(3a)

3.7.2. Benzoic acid C-H activation:

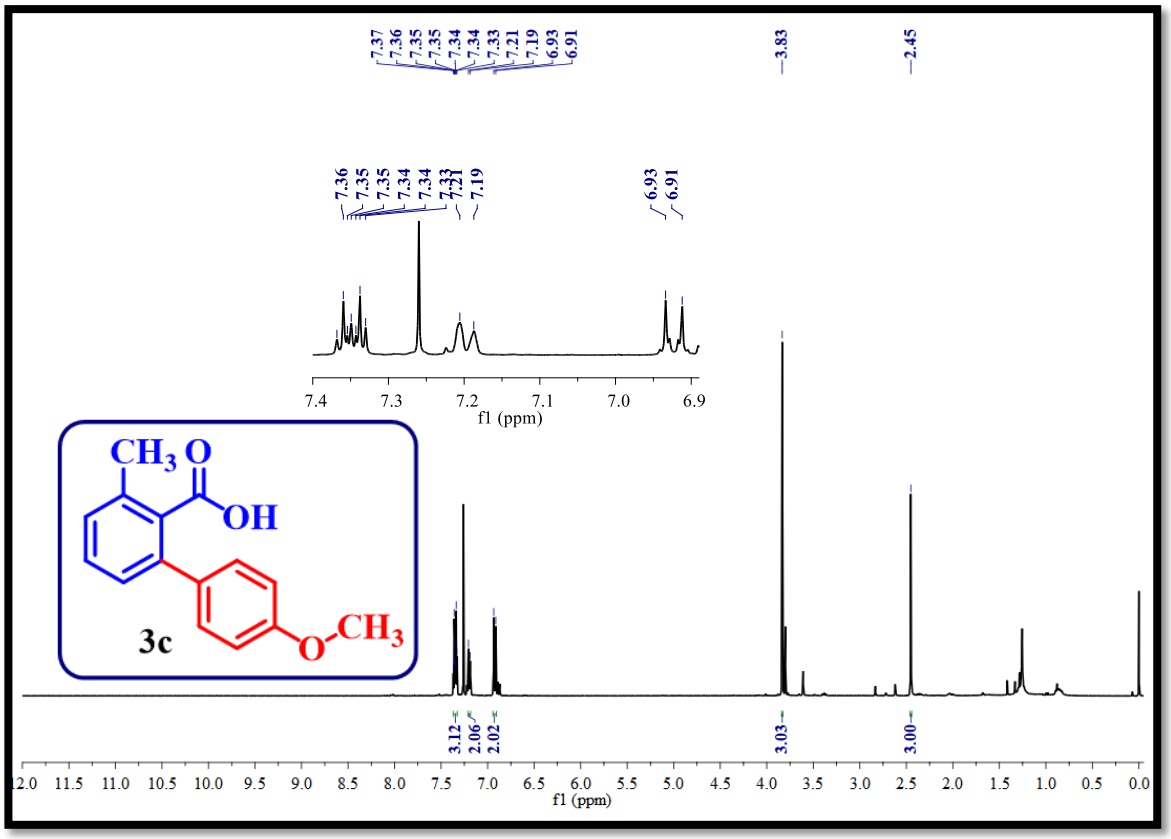

[1]H NMR spectrum of the compound 4'-methoxy-3-methyl-[1,1'-biphenyl]-2-carboxylic acid (3c)

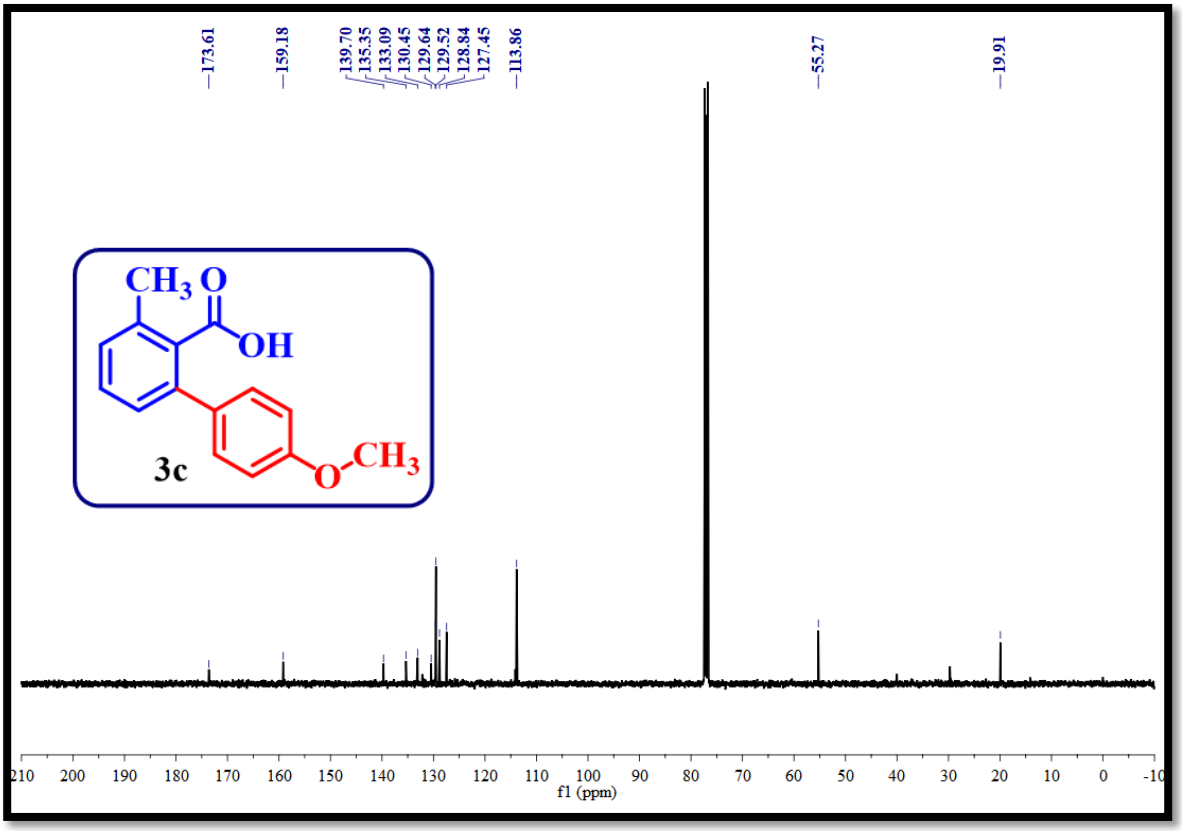

[13]C NMR spectrum of the compound 4'-methoxy-3-methyl-[1,1'-biphenyl]-2-carboxylic acid(3c)

CHAPTER-IV

Magnetically Reusable $CuFe_2O_4$ Nanocatalyst for its Dual Catalytic Action in Sonogashira and Chan-Lam Coupling Reactions

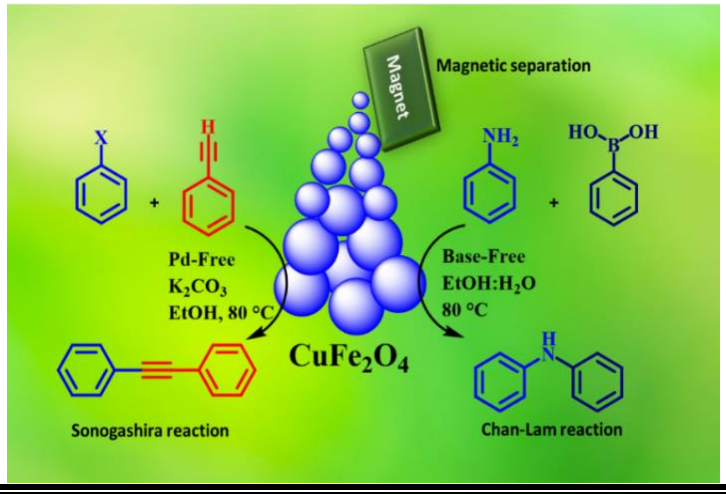

Chapter-IV

Magnetically Reusable $CuFe_2O_4$ Nanocatalyst for its Dual Catalytic Action in Sonogashira and Chan-Lam Coupling Reactions

4.1. Introduction

Study on coupling reactions is invariably a significant area in organic synthesis. One of the areas of organic chemistry that has received the attention of researchers is the development of carbon-carbon (C-C) bonds and carbon-nitrogen (C-N) bonds via coupling reactions. The deployment of catalysts in performing coupling reactions is an emerging topic in organic synthesis. In recent times, the use of magnetically recoverable nanocatalysts in performing cross-coupling processes to develop C-C and C-N bonds in the reactions has been explored as a greener and simple strategy in the generation of a wide range of drugs, bioactive molecules, natural products and so forth to satisfy the demand of industry and society.[1,2,3,4] Among magnetically recoverable nanocatalysts, magnetic nanoparticles (MNPs) have attained great interest nowadays, because of their unique features such as large surface-to-volume ratio, enhanced activity, good thermal stability, less toxicity, good potential for surface modification to make them suitable for a specific application. Besides these features, the significant greatness of these MNPs is their simple way of separation from the reaction mixture with the aid of an external magnet for further use. It is a proven fact that the magnetically separable catalyst is the best favorable strategy to overcome the limitations associated with homogeneous catalysis, and tedious methods of separation of catalyst from the reaction mixture in heterogeneous catalysis such as filtration and centrifugation.[5,6,7]

In recent days, magnetic spinel ferrite NPs (MFe_2O_4, M=Mn, Fe, Co, Ni, Cu, Zn) were explored to be efficient materials as catalysts in synthetic organic chemistry, owing to their remarkable electronic and magnetic properties which enables the separation of the catalyst using an external magnet.[8,9,10,11,12] Among them, copper spinel ferrites ($CuFe_2O_4$) gained attention because of their noteworthy properties such as low-cost, ease of synthesis, moderate saturation magnetization, good coercivity with outstanding chemical and thermal stability under high temperatures. An added advantage of these ferrites is their magnetic recovery and easy surface functionalization for a specific application. During the past decade, $CuFe_2O_4$ and their surface-functionalized materials were extensively used as catalysts in the field of catalysis for organic synthesis.[13,14]

Reactions comprising of C-C and C-N bond development gained much attention owing to their significance in the synthetic organic chemistry for the development of complex molecules from simpler units. Most important and well-known C-C coupling reactions are Heck, Negishi, Suzuki and Sonogashira reactions.[15,16,17,18] Among these, Sonogashira coupling reactions are notable that involves the formation of aryl alkynes from terminal alkynes and aryl halides. It is because, aryl alkynes are used as important intermediates in synthesizing numerous agrochemicals, polymers and pharmaceuticals.[19] Usually, the Sonogashira coupling reaction is conventionally mediated by Pd in the presence of metal co-catalyst, ligands and a base.[20] Commonly used co-catalysts are copper salts, Zn, Sn, Al etc and ligands are pyridines, pyrimidines etc. Currently, research community prefer to use Pd-free and ligand free catalytic system because of expensive nature of Pd and ligands. Instead of Pd, cheaper metals such as Fe, Ni would be used as catalysts but they need complex ligands, copper as a co-catalyst, and harsh reaction conditions.[21] Thus, numerous methods have been developed for the Pd-free Sonogashira coupling reactions using other low-cost transition metals such as Cu, Rh, Zn, Co. Despite having good progress, many of the reported Pd-free procedures are associated with harsh reaction conditions, lower yields of the product, more reaction time, tedious workup procedure etc.[22,23] On the other hand, many copper-based homogeneous catalysts were reported as a substitute for the Pd-based catalysts for the Sonogashira reaction because of their inexpensive nature, good selectivity and catalytic activity.[24,25] In spite of great achievements as homogeneous catalysts, they are also associated with limitations such as non-recoverability of the metal and ligand, non-recyclability and single-use nature of the catalyst (non-reusability). Hence, it is intended to prepare a simple copper catalyst that should be heterogeneous and magnetic in nature to favour its easy recovery. It is proposed to synthesise simple magnetic nano $CuFe_2O_4$ as a catalyst for Songashira-coupling reaction with Pd-free conditions. Simultaneously its usefulness for the development of C-N bond in base-free reaction conditions was also tried to explore.

C-N bond is an integral part of many useful compounds such as agrochemicals, natural products, pharmaceuticals, dyes etc. C-N coupling reaction involving arylamine synthesis by amination (N-arylation) is a significant research area in synthetic organic chemistry owing to their numerous uses in the generation of bioactive compounds, HIV-protease inhibitors, heterocycles, medicinally important compounds, and natural products, etc. Three important strategies reported so far for development of C-N bond are the Ullmann coupling, Buchward-Hart Wig amination and Chan-Lam coupling. Ullman coupling reaction involving coupling of aryl halides with amines mediated by Cu(I) was reported to be associated with a few

limitations.[26] To overcome these, Buchward-Hart Wig reactions have emerged that comprise of aryl halide coupling with amines mediated by Pd (II). But those reported catalysts were not suitable for the coupling reaction of aryl halides with excess electrons or ortho-substituted aryl halides with aromatic amines. But, they were successful by small Pd loading thus making the process expensive.[26] Consequently, Chan-Lam proposed a new strategy for C-N bond development by arylation of amines using aryl boronic acid mediated by Cu(II) source which uses mild reaction conditions and weak base. Overall among all the strategies, the Chan- Lam coupling methodology seems to be advantageous in view of low toxicity, good stability, ligand free and mild reaction conditions, good structural diversity of aryl boronic acid.[26,27] Until now, many catalysts were reported but they were homogeneous in nature.[28] To overcome the limitations associated with homogeneous catalysts, and to favor easy separation of the catalyst, a magnetic heterogeneous catalyst is the need for the Chan-Lam coupling reaction. Thus, it is intended to explore the catalytic activity of simple magnetic $CuFe_2O_4$ for Chan-Lam coupling reaction under base-free mild conditions.

Based on the available literature it is understood that many Pd-free, Cu-based complex catalytic systems were reported[29] for the said applications. But, simple, reusable, magnetically recoverable catalyst via facile synthesis method for both C-C and C-N coupling reaction was not reported. Thus, current work reports the synthesis of reusable, magnetic $CuFe_2O_4$ nanocatalyst via a simple co-precipitation method for the Sonogashira coupling reaction (C-C) under Pd-free, ligand free conditions and Chan-Lam coupling reaction (C-N) under base free conditions.

4.2. Experimental Section

4.2.1. Materials

Ferric nitrate (99%, Finar,); Copper acetate (99%, Finar); Ammonia solution; Methanol (MeOH) (99%, Finar); Ethanol (EtOH), (99%, Finar); Ethyl acetate (EtOAc) (99%, Finar); n-hexane (98%, Finar) were used as starting materials. Throughout the investigation, Double Distilled (DD) water was used.

4.2.2. Synthesis of $CuFe_2O_4$ nanocatalyst

The magnetic $CuFe_2O_4$ nanocatalyst was synthesized using the facile Co-precipitation method. In this process, a clear solution was produced by dissolving $Cu(OAc)_2.H_2O$ (1 mmol), $Fe(NO_3)_3.9H_2O$ (2 mmol) in 50 mL of DD water and the mixture was stirred continuously for 30 minutes at room temperature (RT). The pH of the solution was adjusted to ~10 with the addition of ammonia solution while being stirred continuously. The resulting mixture was constantly agitated for two hours at RT, and then the obtained product was washed three times

with DD water and ethanol before being dried in an oven at 60 °C. It was then calcined for 2 h at 550 °C.

4.2.3. Sonogashira coupling reaction

In a typical Sonogashira coupling reaction experiment, the reactants *viz.*, aryl halides (1 mmol), phenyl acetylenes (1.5 mmol) along with K_2CO_3 (2 mmol), $CuFe_2O_4$ catalyst (20 mg) were mixed in 3 mL of EtOH. The reaction mixture was constantly stirred at 80 °C for 12 h. Soon after the reaction was completed (as tracked by TLC), the catalyst was readily separated using an external magnet. Ethyl acetate was used twice to extract the products and purified on a microcolumn loaded with silica gel. Then, the products were examined using ^{1}H and ^{13}C NMR spectral analysis.

4.2.4. Chan-Lam coupling reaction

In the Chan-Lam reaction, aryl amines (1 mmol), phenylboronic acid (1.5 mmol), and $CuFe_2O_4$ catalyst (20 mg) were mixed in 3 mL of EtOH:H_2O (1:1). The reaction mixture was constantly stirred at 80 °C for 10 h. After the completion of the reaction (as tracked by TLC), the catalyst was readily isolated using a magnet. Ethyl acetate was used twice to extract the products and purified on a microcolumn loaded with silica gel. Then, the products were examined using ^{1}H and ^{13}C NMR spectral analysis.

Catalyst recovery

The magnetic nanocatalyst was isolated from the reaction mixture for further use by holding the magnet externally to the reaction vessel. Consequently, the catalyst got stuck to the wall by external magnet and the reaction mixture was decanted into another container. The retained catalyst in the vessel was washed with DD water and ethanol for three times, dried (at 60 °C overnight) and was used in the next run. 99% of the catalyst was fully recovered with minimal loss of the catalyst. This can be understood by the fact that the recovered catalyst was reused further for the reaction where it has shown almost the same activity.

4.2.5. Characterization of Catalyst

The structural characteristics of the synthesized $CuFe_2O_4$ were carried out using various techniques. Powder X-ray diffraction (PXRD) studies were performed using a PAN Analytical Advance X-ray diffractometer in a 2θ scan range between 10° and 80° utilizing Ni-filtered Cu K (λ= 1.5406Å) radiation. FT-IR spectra for $CuFe_2O_4$ were recorded between 4000 and 400 cm^{-1} using the PerkinElmer Spectrum by KBr pellet technique. Scanning Electron Microscope (SEM, Make: TESCAN, Model: VEGA3 LMU) was used to understand the surface morphology of the $CuFe_2O_4$ catalyst. The magnetic hysteresis curve of the catalyst was obtained using a vibrating sample magnetometer (VSM, Lake Shore, Model: 8600 Series) to

understand the magnetic behavior of the catalyst. Using $CDCl_3$ as a solvent and TMS as an internal standard, ^{1}H and ^{13}C NMR spectra were recorded on an advanced-III Bruker 400 MHz NMR spectrometer. Chemical shifts were expressed as parts per million (ppm).

4.3. Results and Discussion

4.3.1. Preparation of the $CuFe_2O_4$ Catalyst

$CuFe_2O_4$ catalyst was synthesized by a simple one step (I) procedure (**Scheme 1**). $CuFe_2O_4$ NPs were prepared by using Co-precipitation method in 2 h. An external magnet was used to isolate the synthesized nanocatalyst, which was then dried under vacuum conditions for its further use. The overall synthesis of nanocatalyst was shown in **Scheme 1**.

Scheme 4.1. *Preparation Path of the $CuFe_2O_4$ Nanocatalyst*

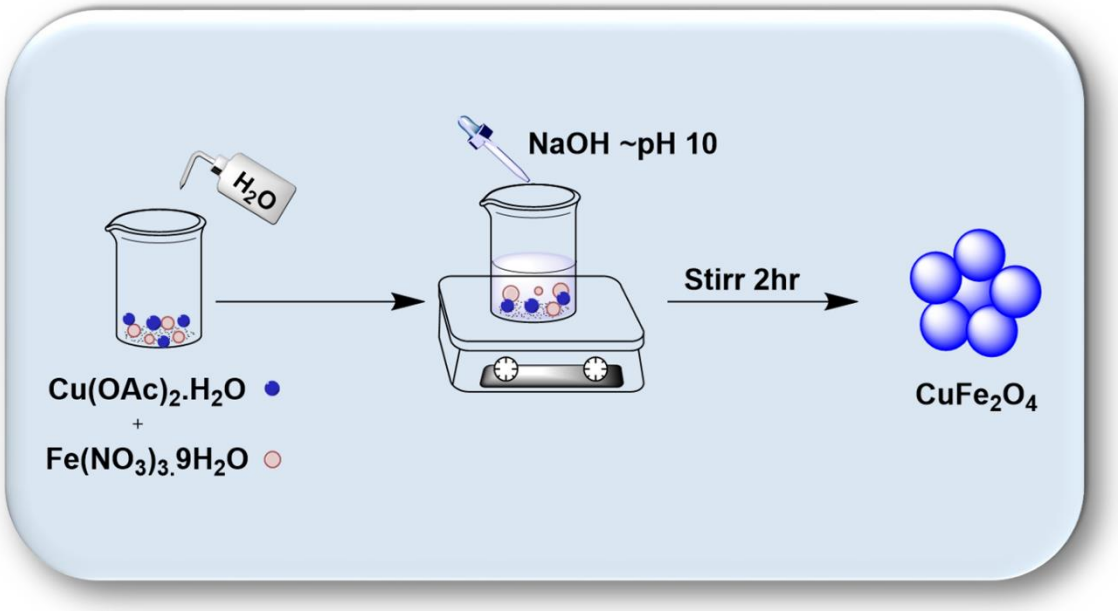

4.3.2. Characterization of the $CuFe_2O_4$ Catalyst

The XRD patterns of synthesized $CuFe_2O_4$ catalyst were depicted in Fig4.1a. The XRD patterns revealed the existence of clear distinctive peaks at 2θ=18.5°, 30.4°, 35.8°, 37.4°, 43.4°, 53.8°, 57.4°, 62.5° of the spinel ferrite structure that were indexed to (111), (220), (311), (222), (400), (422), (511) and (440) reflection planes. These planes were identical with the distinctive peaks of $CuFe_2O_4$, standard JCPDS data card no. 77-0010. Thus, the formation of single phased cubic spinel structure of the catalyst with fd3m space group was confirmed without any impurity peak.[30,31] The formation of particles in the nano-regime was confirmed by the broad peaks and the average crystallite size of $CuFe_2O_4$ was cculated to be around 19.16 nm using the Debye-Scherrer's formula.[32] The most intense peak (311) from the figure at 35.8° was the representative peak of the spinel phase.

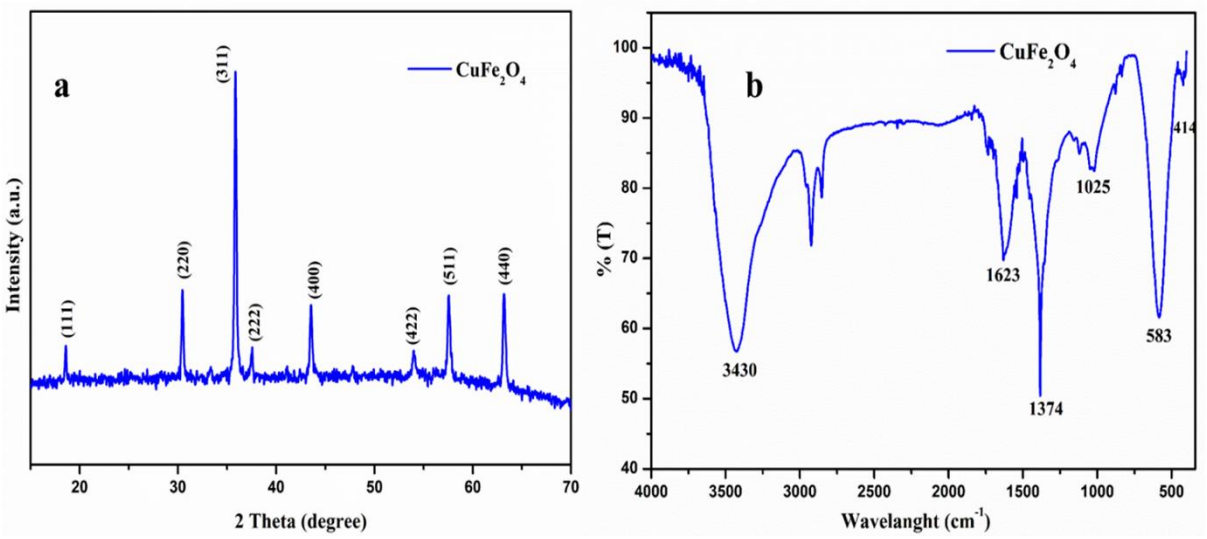

Figure 4.1 *(a) XRD spectra and (b) FTIR spectra of sample*

FT-IR spectra of the synthesized $CuFe_2O_4$ catalyst's was depicted in **Figure 4.1b.** The appearance of two prominent peaks between 600 and 400 cm^{-1} were representative of spinel structure in consistent with Waldrons report.[33] These were the result of M-O band stretching vibrations i.e. they were due to Fe-O and Cu-O vibtrations at both A (tetrahedral sites) and B (octahedral sites). It was reported that Cu prefer to occupy octahedral B site while Fe ions can be distributed between A & B sites resulting in the formation of inverse spinel structure of the ferrites.[34] The substantial peaks observed at 414 cm^{-1} and 583 cm^{-1} were because of the intrinsic stretching vibrations of the M^{n+}-O bond in the octahedral and tetrahedral locations of the spinel structure respectively.[35] The absorption peak at 3430 cm^{-1} and 1623 cm^{-1} signifies stretching and bending vibration of surface OH groups. The observed peaks at 1374 cm^{-1} and 1025 cm^{-1} denote the overtone O-H stretching vibrations of hydroxyl group of water on catalyst.[36]

SEM images in **Figure 4.2 (a,b)** established that agglomeration of sub micrometric range particles has resulted in micrometric clusters with irregular shape. This means that small particles have been synthesized during the synthesis process but during the calcination, they coalesced with each other resulting in bigger agglomerates. From the obtained SEM results, it was difficult to estimate the size of individual particles but it was evident that they were below 1µ. It was also evident that in spite of the irregular shape of the aggregates, shape of individual nanoparticles looked like spherical.

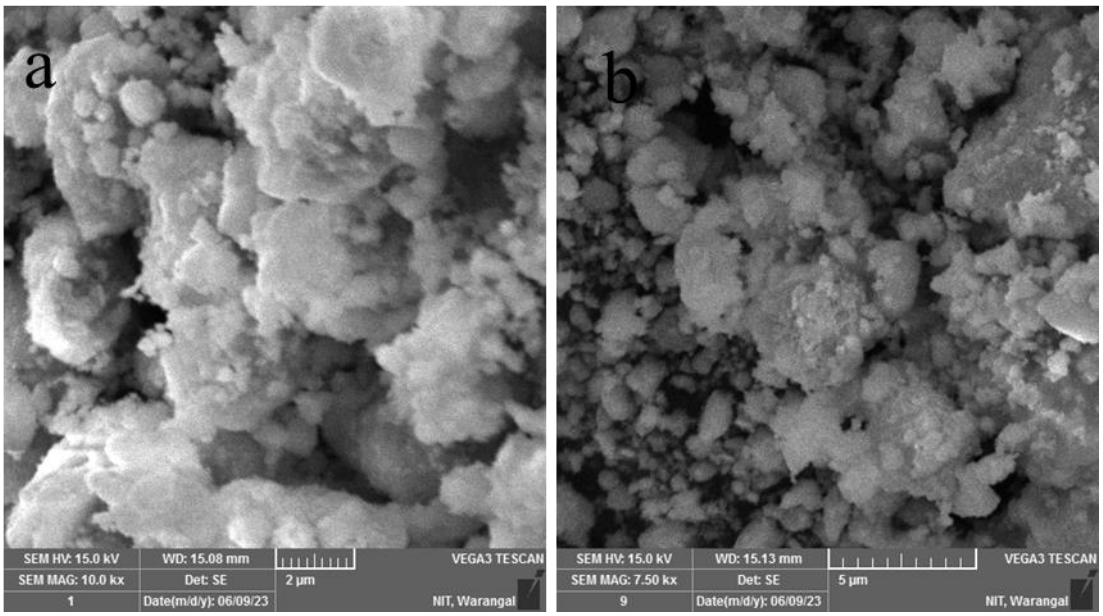

Figure 4.2. *a,b SEM images of the $CuFe_2O_4$ nanocatalyst*

To establish the magnetic behaviour of the $CuFe_2O_4$ catalyst, the RT magnetization measurements were performed using VSM and the results were shown in the form of magnetization curve (magnetic hysteresis curve) in **Figure 4.3.** As the applied magnetic field is dropped to zero, the $CuFe_2O_4$ nanocatalyst had still 4.71 emu/g remanence (M_r) value with coercivity (H_c) of 147 Oe. The saturation magnetization (M_s) was found to be 18.67 emu/g. This behaviour of synthesized catalyst explicitly supported the presence of ferromagnetic component in it. Thus, the magnetic retrievability and reusability of the catalyst was supported by the evaluated magnetic parameters from **Figure 4.3** which the notable magnetic performance of the synthesized catalyst was manifested.

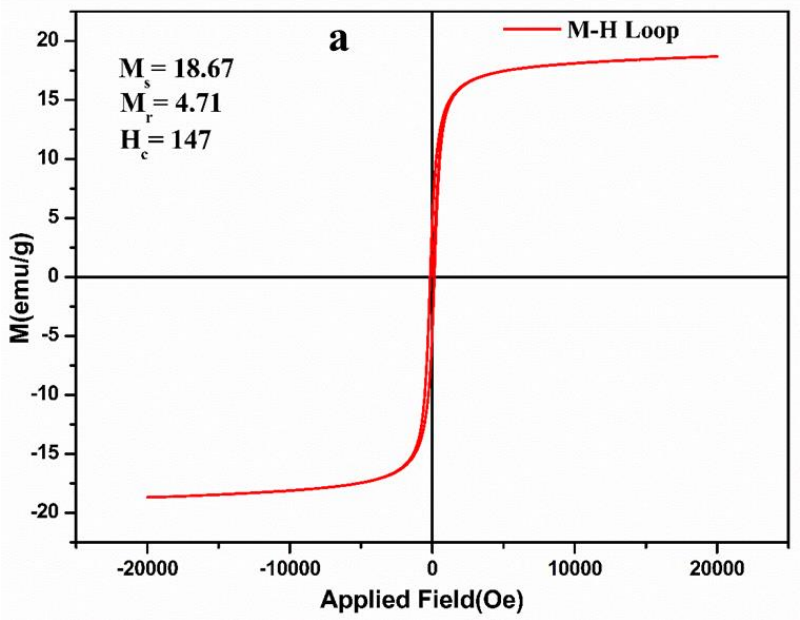

Figure 4.3*. a) VSM of $CuFe_2O_4$ nanocatalyst*

4.3.3. Application of $CuFe_2O_4$ catalyst in Sonogashira and Chan-Lam coupling reactions

4.3.3.1. Sonogashira coupling reactions

A simple Sonogashira coupling reaction combining aryl halide and phenyl acetylene was performed using the synthesized $CuFe_2O_4$ nanocatalyst. Several important reaction conditions for the Sonogashira reaction *viz.*, type of the solvent, base, temperature and amount of the catalyst (mg) were optimized systematically. The effect of different solvents on the reaction using K_2CO_3 as a base and 20 mg of the catalyst at 80 °C was studied. The product's yield was low in the presence of polar aprotic solvents like DMF, DMSO and nonpolar solvents like toluene (**Table 4.1, entry 1-3**). Furthermore, it was observed that poor yield of the product was obtained in presence of pure H_2O as solvent (**Table 4.1, entry 4**). But, when polar protic solvents like ethanol and methanol were used, a significant yield of the product (96% and 90 % respectively) was obtained (**Table 4.1, entry 5, 6**). Hence, it confirmed that EtOH as a solvent gave a higher yield (**Table 4.1, entry 5**). Further, the effect of mixture of polar protic solvents on the product yield was also investigated. However, no significant yield was seen. (**Table 4.1, entry 7-8**). These findings implied that EtOH, a protic solvent was an optimized solvent for Sonogashira reactions in the presence of $CuFe_2O_4$ nanocatalyst.

To identify the right base for the reaction, the effect of other bases (Cs_2CO_3, NaOH, Et_3N) on the reaction, other than K_2CO_3 (**Table 4.1, entries 9–11**) in EtOH as solvent was also investigated. However, the use of just K_2CO_3 as a base produced the best yield of all the bases used (**Table 4.1, entry 5**) at 80 °C with 20 mg of the catalyst. Thus, K_2CO_3 was the optimized base for Sonogashira reactions in the presence of $CuFe_2O_4$ nanocatalyst.

In general, the yield of the reaction is significantly influenced by temperature. To understand the effect of temperature, the reaction was carried out in the presence of $CuFe_2O_4$ nanocatalyst (20 mg) using EtOH as solvent and K_2CO_3 as base at various other temperatures (RT, 60 °C, and 100 °C). At RT, a very low yield was noted (**Table 4.1, entry 12**), and the reaction moved forward more quickly at 60 °C compared to RT. The yield of the product, increased noticeably at temperatures greater than RT (60 °C, 80 °C, and 100 °C) (**Table 4.1, entries 13, 5, 14**). These findings from **Table 4.1** implied that the optimum temperature was 80 °C. In order to optimize the amount of catalyst, the reaction was conducted with various quantities of $CuFe_2O_4$ nanocatalyst at 80 °C in the presence of EtOH as solvent and K_2CO_3 as base. The yields of the products observed using different amounts of catalyst (10 mg, 15 mg, and 20 mg) were 58%, 81%, and 96% respectively (**Table 4.1, entries 15, 16, 5**). In the presence of 25 mg of catalyst, the yield of the product was 95% (**Table 4.1, entry 17**). From these findings, it may be concluded that the optimum dosage of the catalyst was 20 mg.

Table 4.1. *Optimization of Reaction Conditions for the reaction of Iodobenzene and Phenyl Acetylene by $CuFe_2O_4$*[a]

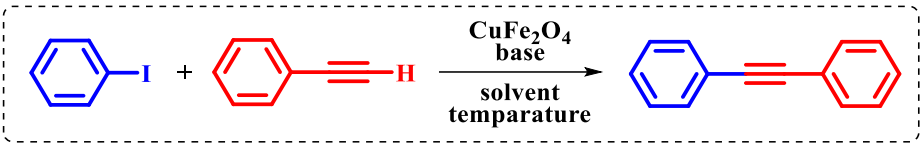

S.No	Solvent	Base	Temperature	Time (hr)	Yeild(%)[b]
1	DMF	K_2CO_3	100	12	58
2	DMSO	K_2CO_3	100	12	30
3	Toluene	K_2CO_3	100	12	20
4	H_2O	K_2CO_3	100	12	42
5	**EtOH**	**K_2CO_3**	**80**	**12**	**96**
6	MeOH	K_2CO_3	80	12	90
7	EtOH:H_2O (1:1)	K_2CO_3	80	12	78
8	MeOH:H_2O (1:1)	K_2CO_3	80	12	62
9	EtOH	Cs_2CO_3	80	12	80
10	EtOH	NaOH	80	12	76
11	EtOH	Et_3N	80	12	14
12	EtOH	K_2CO_3	RT	12	Trace
13	EtOH	K_2CO_3	60	12	64
14	EtOH	K_2CO_3	100	12	95
15	EtOH	K_2CO_3	80	12	58[c]
16	EtOH	K_2CO_3	80	12	81[d]
17	EtOH	K_2CO_3	80	12	96[e]

[a]**Reaction conditions:** iodobenzene (1.0 mmol), phenyl acetylene (1.5 mmol), $CuFe_2O_4$ catalyst (20 mg) and base (2 mmol) in solvent (3 mL). [b]Isolated yields, [c]10 mg catalyst, [d]15 mg catalyst, [e]25 mg catalyst.

With these optimized conditions, the catalyst was further used to validate the substrate scope of Sonogashira coupling reaction by considering different aryl halides (X= Cl, Br, I), substituted aryl halides and substituted phenyl acetylenes (**Table 4.2**).

It was found that para-substituted aryl iodides yield exceptionally well in the presence of both EWG and EDG groups giving more than 85% yield of the product in most cases. This inferred that the reaction progressed successfully regardless of the substrates with EWG and

EDG. The reaction was also feasible with aryl bromide and chlorides (**Table 4.2, compounds 7, 8**) but with low yield of the product because the C-X (X= Cl, Br) bond is stronger than the C-I bond. Further, it was also observed that the reaction proceeded rapidly in case of substrates with EDG than those with EWG. The inductive effects of the substituent groups on the substrates could address this phenomenon.

Table 4.2 *Substrate Scope of the Sonogashira coupling reaction catalyzed by* $CuFe_2O_4$

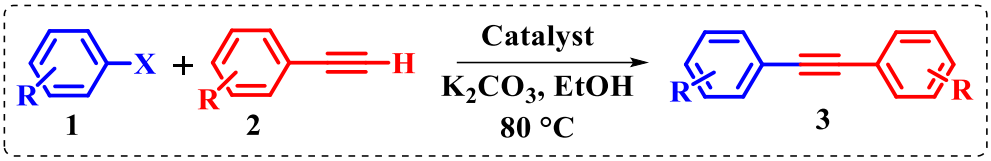

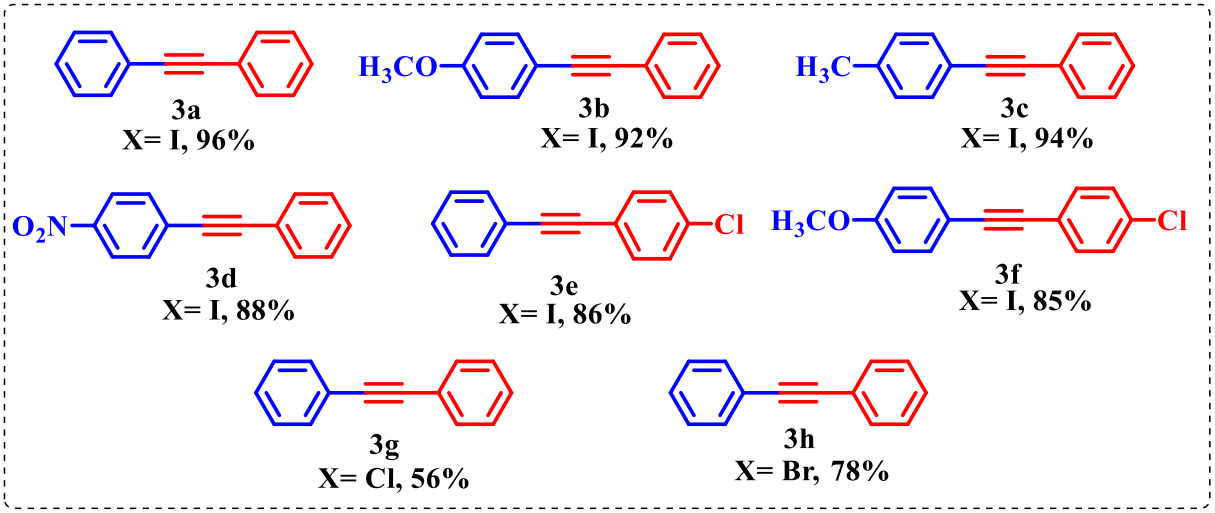

For Sonogashira coupling reactions, the effectiveness of the $CuFe_2O_4$ nanocatalyst was compared with previously reported Pd-free catalysts (**Table 4.3**).

Catalysts mentioned in entries 1-3 were complex in nature and used DMF as a solvent which was reported as toxic and certainly generate obnoxious environment for workers which is not safe.[37] Catalyst shown in the entry 4 in spite of being simple, also used DMF as a solvent and used high temperature, larger time (130 °C and 48 h). The catalyst in **entry 5** was complex in nature and used high temperature 140 °C but still resulted in low yield (72%). Catalyst in **entry 6** was also simple, magnetic in nature but took 18 h with low yield (84%). It was clear from **Table 4.3** that our $CuFe_2O_4$ nanocatalyst worked effectively in the Sonogashira coupling reaction in green solvent EtOH with K_2CO_3 as a base at low temperature (80 °C) in 12 h with a good yield of 96% when compared to all the catalysts in the **Table 4.3**. Thus, catalyst in the present work demonstrated its superiority over previously reported systems in terms of its activity.

Table 4.3 *Comparison of $CuFe_2O_4$ with other previously reported Pd-free catalysts for Sonogashira coupling reactions*

S.NO	Catalyst	Base	Solvent	Temperature (°C)	Time (h)	Yield (%)	Ref.
1	Cu_2O/RGO	KOH	DMF	150	12	95	38
2	Cu/Cu_2O NPs	K_2CO_3	DMF	90	12	90	39
3	BNPs-DETA-CuI (I)	Et_3N	DMF	70	10	95	40
4	Cu NPs	K_2CO_3	DMF	130	48	96	22
5	Co-MS@MNPs/CS	KOH	DMSO	140	10	72	41
6	α-Fe_2O_3 NPs	K_2CO_3	EG	80	18	84	42
7	**$CuFe_2O_4$**	**K_2CO_3**	**EtOH**	**80**	**12**	**96**	**This work**

We propose a plausible mechanism for the Sonogashira coupling reaction of aryl halide and phenyl acetylene in the presence of $CuFe_2O_4$ catalyst based on prior findings and experimental observations.[38,24] Based on the structural characterization, it is understood that Cu(II) occupies octahedral site and Fe occupies both the tetrahedral and octahedral sites. It was an established fact that octahedral site of the spinel ferrite exhibits higher catalytic activity compared to tetrahedral site because of its larger size which allows for better accommodation of reactant species. Thus, as mentioned above, Cu and Fe present in octahedral site were responsible for their activity in Sonogashira coupling reaction which is in line with the reported fact.[43]

Hence, based on the observations and earlier reports, the reaction would proceed via two steps *viz.*, oxidative addition and reductive elimination. Spinel ferrite acting as Lewis acid increased the electrophilicity of specific groups of reactants by accepting the electron to form bonds. The synergistic effect of both the ions was responsible for the oxidative addition reaction. The reaction initiated with the formation of an intermediate 1 between phenylacetylene and active sites in the catalyst in the presence of base. The intermediate was then processed via oxidative addition with an aryl halide to produce intermediate 2, which then undergone reductive elimination to generate the desired product.

4.3.3.2. Chan-Lam coupling reaction

A simple Chan-Lam coupling reaction with aryl amines and phenylboronic acid as coupling partners was achieved in the presence of synthesized $CuFe_2O_4$ nanocatalyst under base-free conditions. To optimize reaction conditions, aniline and phenylboronic acid were initially used as model substrates. Important reaction conditions such as type of the solvent, time, temperature, and amount of catalyst (mg) for the Chan-Lam reaction were optimized.

The influence of different solvents using 25 mg of the catalyst on Chan-Lam coupling reaction at 80 °C was investigated and the outcomes were depicted in **Table 4.4**. The results showed that a very low yield of the product was produced when the reaction mixture was agitated for 12 h in H_2O, Toluene, CH_3CN, DMF, DMSO (**Table 4.4, entries 1 to 5**). However, an increase in the yield was observed when the reaction was carried out in EtOH or MeOH **(Table 4.4, entries 6, 7**). The reaction was also tried in mixture of polar protic solvents and it was found that combination of solvents such as EtOH:H_2O (1:1) (**Entry 8**) and MeOH:H_2O (1:1) (**Entry 9**) produced better yields than their individual solvent components (**Entries 1,6,7**). Among these, it was discovered that a 95% yield of the product was achieved when the reaction was run for 12 h at 80 °C with EtOH:H_2O (1:1) as a solvent (**Entry 8**). When the reaction was further investigated under the same conditions for 10 h, the yield of the product was still 95% (**Entry 10**), showing that EtOH:H_2O (1:1) (**Table 4.4, entry 10**) was the optimized solvent with 10 h of reaction time as it has significantly increased the catalytic activity.

In general, the yield of the reaction will be significantly influenced by temperature. To realize the effect of temperature, the model reaction was also carried out at various temperatures (RT, 60 °C, 80 °C and 100 °C) in EtOH:H_2O using $CuFe_2O_4$ nanocatalyst . At RT, a relatively low product yield was noted (**Table 4.4, entry 11**). The yield of the product in the Chan-Lam reaction, however, significantly increased at temperatures greater than RT (60 °C, 80 °C, and 100 °C) (**Table 4.4, entries 12,10,13**). These results implied that the optimum temperature was 80 °C.

To optimize the amount of catalyst, the reaction was run with different amounts of $CuFe_2O_4$ (10 mg, 15 mg, 20 mg and 25 mg) nanocatalyst at 80 °C in EtOH:H_2O (1:1) as solvent for 10 h. The yields of the products were found to be 49%, 73%, 95%, 95% respectively for the corresponding amount of the catalyst (**Table 4.4, entries 14,15,16,10**). Thus, it may be concluded that the optimum dosage of the catalyst is 20 mg.

In order to achieve the best possible product yield, the Chan-Lam reaction was optimized to employ 20 mg of $CuFe_2O_4$ as a catalyst in EtOH:H_2O (1:1) as a solvent in the absence of base at 80 °C for 10 h.

Table 4.4 *Optimization of Reaction Conditions for the reaction of aniline and phenyl boronic acid by $CuFe_2O_4$*[a]

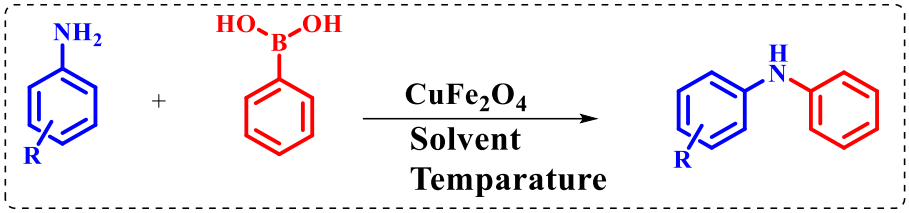

S.No	Solvent	Temperature	Time (hr)	Yeild(%)[b]
1	H_2O	100	12	38
2	Toluene	100	12	Trace
3	CH_3CN	100	12	Trace
4	DMF	100	12	Trace
5	DMSO	100	12	Trace
6	EtOH	80	12	85
7	MeOH	80	12	80
8	EtOH:H_2O (1:1)	80	12	95
9	MeOH:H_2O (1:1)	80	12	92
10	EtOH:H_2O (1:1)	80	10	95
11	EtOH:H_2O (1:1)	RT	10	Trace
12	EtOH:H_2O (1:1)	60	10	60
13	EtOH:H_2O (1:1)	100	10	92
14	EtOH:H_2O (1:1)	80	10	49[c]
15	EtOH:H_2O (1:1)	80	10	73[d]
16	**EtOH:H_2O (1:1)**	**80**	**10**	**95[e]**

[a]**Reaction conditions**: aniline (1.0 mmol), phenyl boronic acid (1.5 mmol), $CuFe_2O_4$ catalyst (25 mg) in solvent (3 mL). [b]Isolated yields, [c]10 mg catalyst, [d]15 mg catalyst, [e]20 mg catalyst

With these optimized conditions, the catalyst $CuFe_2O_4$ was further used to validate the substrate scope of the Chan-Lam coupling reaction by considering several aryl amines and phenylboronic acid as coupling partners and the data was depicted in **Table 4.5**. It was observed that the presence of EWG as well as EDG produced exceptional yields for para-substituted aryl amines. Regardless of the substrates with EWG and EDG, the reaction efficiently progressed, giving more than 80% yield.

Table 4.5 *Substrate Scope of the Chan-lam coupling reaction catalyzed by* $CuFe_2O_4$

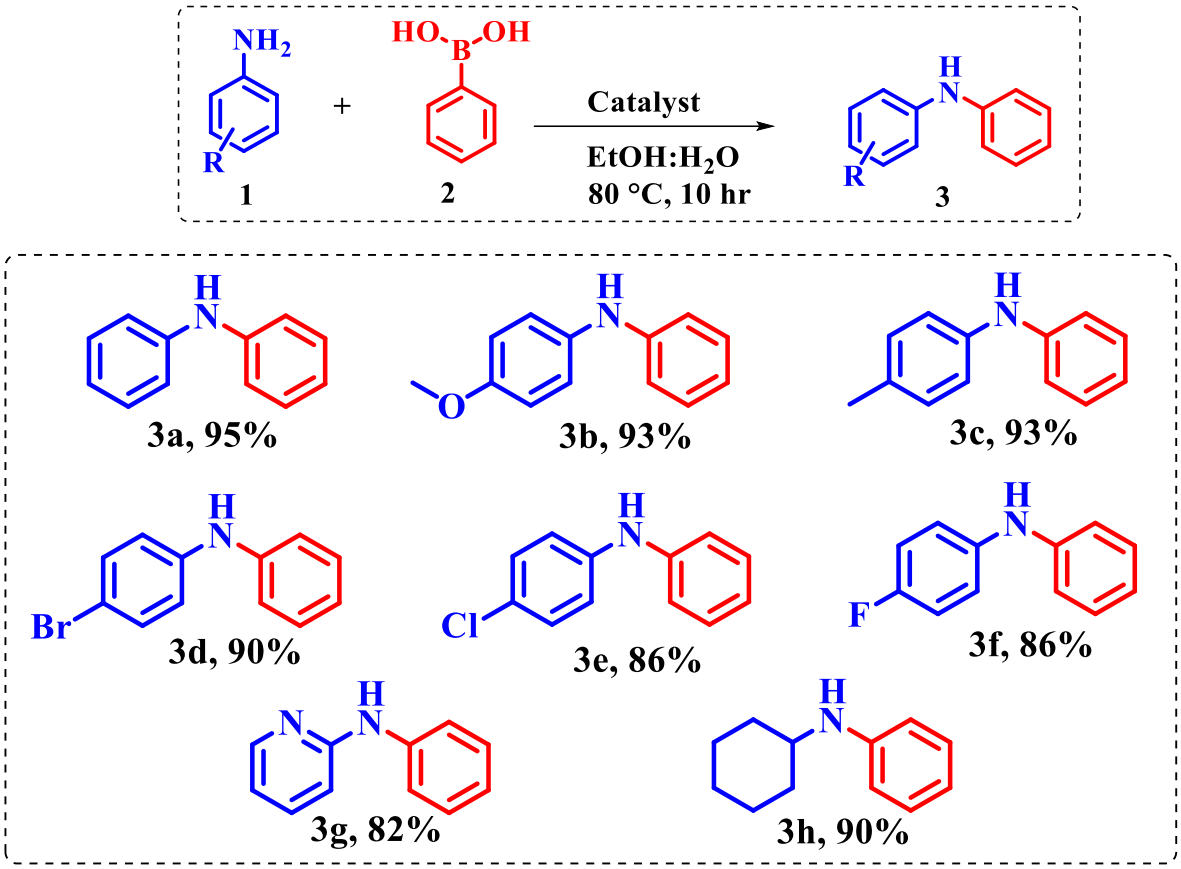

The efficiency of the $CuFe_2O_4$ nanocatalyst was compared with previously reported catalysts for the Chan-Lam coupling reaction (**Table 4.6**). The catalysts in the **entry 1 and 2** were complex in nature, used base and gave 88% yield employing different solvents under different reaction conditions. The catalyst shown in **entry 3** was simple but used base and the yield of the product was also low. The complex catalyst in the **entry 4** also used base and took long time for the reaction with a yield of 90%. The catalyst in the **entry 5** also used base, it was complex in nature and took less time with a product yield of 85%. The catalyst shown in **entry 6** worked in base-free conditions at RT with a yield of 91% in 8 h but it was complex in nature. According to **Table 4.6**, $CuFe_2O_4$ nanocatalyst in the current work functioned excellently well to produce the necessary products in the Chan-Lam coupling reaction utilizing the green solvent EtOH:H_2O (1:1) under base-free conditions at low temperature (80 °C) in 10 h with a satisfactory yield of 95%. Thus, the current catalyst demonstrated its superiority over previously reported systems in terms of its activity.

Table 4.6 *Comparison of $CuFe_2O_4$ with other previously reported catalysts for Chan-Lam coupling reactions*

S.NO	Catalyst	Base	Solvent	Temperature (°C)	Time (h)	Yield (%)	Ref.
1	GO@AF-SB-Cu	K_2CO_3	CH_3CN	80	12	88	29
2	POVCF 1	K_2CO_3	CH_3OH	RT	16	88	44
3	$Cu(OAc)_2$	K_2CO_3	$CH_3CN:H_2O$	RT	12	80	45
4	Copper(II) NHC complex	K_2CO_3	MeOH	RT	24	90	46
5	Chitosan anchored copper(II) SB complexes	K_2CO_3	CH_3CN	reflux	9	85	26
6	Cu/PI-COF	-	$MeOH:H_2O$	RT	8	91	47
7	**$CuFe_2O_4$**	**-**	**$EtOH:H_2O$**	**80**	**10**	**95**	**This work**

4.3.3.3. Recyclability of the catalyst

Recycling of the catalyst in organic synthesis would be an important issue of concern from environmental, economic, and industrial viewpoint. The recyclability of $CuFe_2O_4$ nanocatalyst for Sonogashira coupling reaction and Chan-Lam coupling reaction was examined here. In each cycle, the catalyst was isolated from the reaction mixture soon after the completion of reaction using an external magnet. The separated catalyst was dried, washed with ethanol and reused for the subsequent run where the activity of the magnetically recovered catalyst was examined. As depicted in **Figure 4.4**, the catalyst was retrieved and used for at least 5 successive runs without noticeable loss in activity as evident from the yield of the product in the figure. In the fifth run, the product yields for the Sonogashira and Chan-Lam reactions were 90% and 88%, respectively.

Furthermore, the structural stability of the reused catalyst in both C-C and C-N coupling reactions were confirmed by XRD, FT-IR after five cycles. The XRD spectra of the recycled catalyst in **Figure 4.5** revealed that there were no impurity peaks and it was similar to that of unused catalyst. The FT-IR spectra of the recycled catalyst revealed that its absorption peaks matched with those of the fresh catalyst as evident from **Figure 4.5** These facts confirmed that the catalyst was structurally stable after 5 cycles of its use.

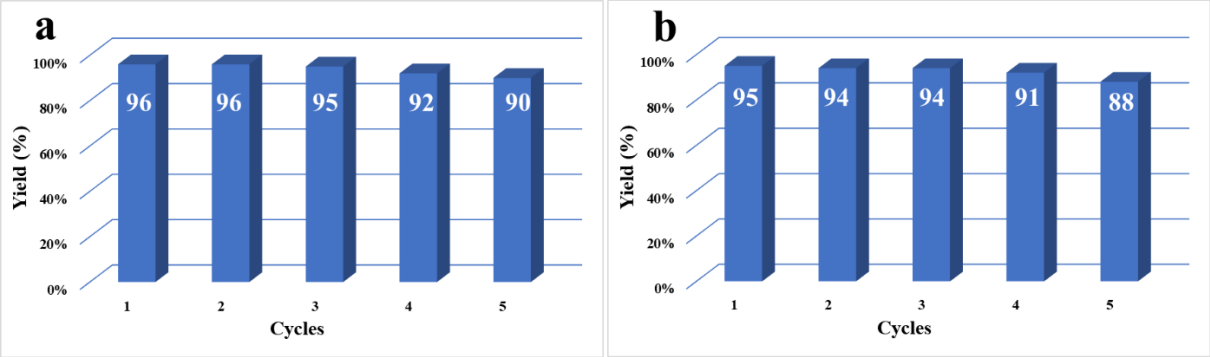

Figure 4.4: *Recyclability test of $CuFe_2O_4$ nanocatalyst for a) Sonogashira coupling reaction b) Chan-Lam coupling reaction*

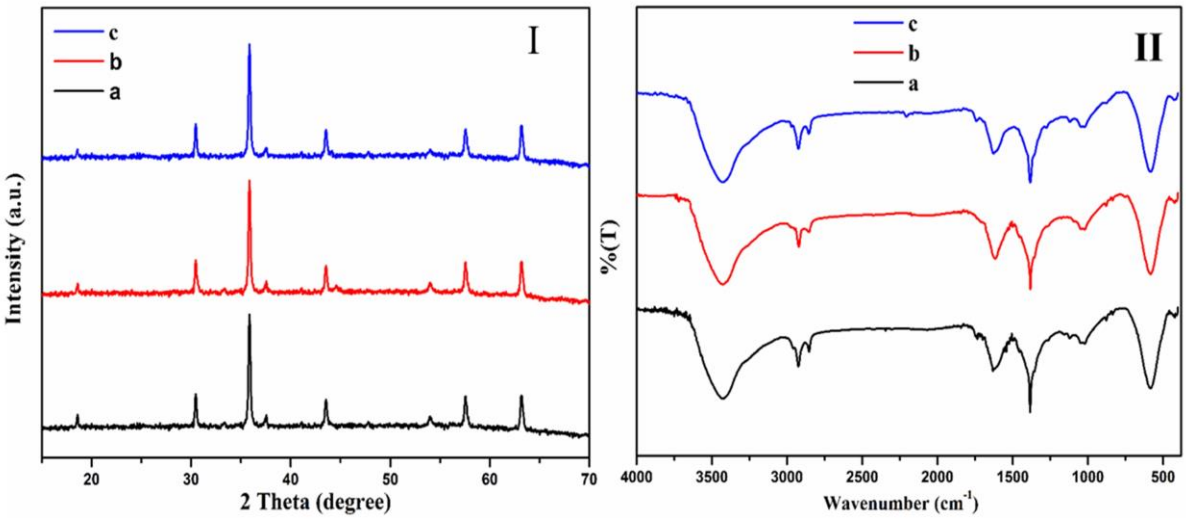

Figure 4.5*. I) XRD spectra II) FTIR spectra of (a) synthesized $CuFe_2O_4$ nanocatalyst (b) used catalyst for Sonogashira coupling reaction and (c) used catalyst for Chan-Lam reaction after 5 cycles*

4.3.3.4. Plausible Mechanism of Chan-Lam Coupling Reaction

We proposed a reasonable reaction mechanism for the Chan-Lam coupling reaction between aniline and phenylboronic acid as shown in **Figure 4.6** based on the prior studies and the aforementioned experimental findings.[48,6] Spinel ferrite acting as Lewis acid increased the electrophilicity of specific groups of reactants by accepting the electron to form bonds. In this mechanism Cu(II) was the active species responsible for the reaction and Fe do not involve in the activity but was only responsible for magnetic recovery.[48] This mechanism would mainly involve three major steps, *viz.*, oxidative addition, transmetalation, and reductive elimination. Step-1 involved the oxidative addition of aniline to the active site of the catalyst surface (Cu) to generate intermediate-1. In step-2, intermadiate-1 undergone transmetalation to give intermediate-2, where both the aniline and phenylboronic acid moieties were attached to the

active sites on the surface of the catalyst. Finally, reductive elimination of intermediate-2 in step-3 would give the final product while regenerating the catalyst.

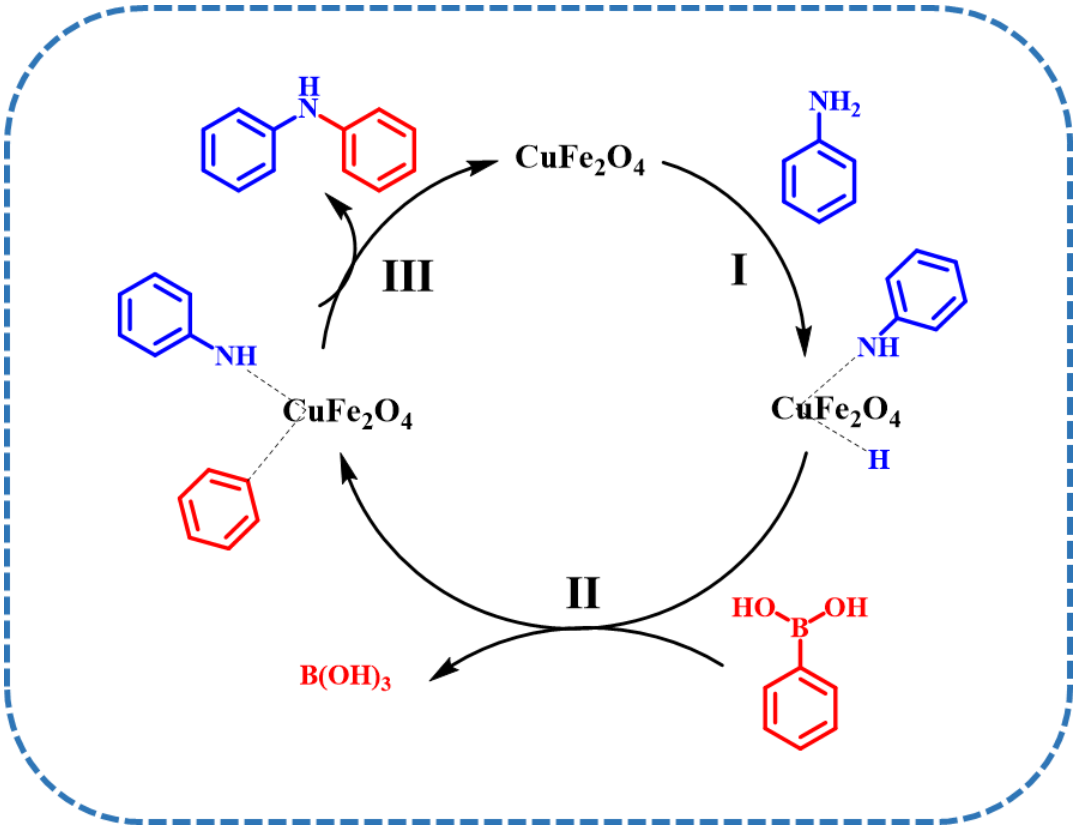

Figure 4.6. *Plausible reaction mechanism for $CuFe_2O_4$ catalyzed Cha-lam coupling reaction*

4.4. Conclusions

In summary, magnetically reusable $CuFe_2O_4$ nanocatalyst was synthesized via simple Co-precipitation method for both Sonogashira and Chan-Lam coupling reactions under ambient reaction conditions. Catalyst worked excellently well for Sonogashira reaction under Pd-free conditions and for Chan-Lam reaction under base free conditions in the presence of eco-friendly solvents (EtOH and EtOH:H_2O) with an excellent yield of the product (96% & 95%) respectively. The efficacy of the catalyst was validated for substituted coupling partners in both Sonogashira and Chan-Lam reactions which gave good yield of the products. The catalyst was found to have excellent reusability for a minimum of five cycles without significant loss in the activity. After 5 cycles, the structural stability and surface morphology of the reused catalyst was investigated by XRD, FT-IR and SEM analysis. The findings of the current study would provide a sustainable approach to synthesize magnetically recoverable and reusable $CuFe_2O_4$ nanocatalyst for dual applications in Pd-free C-C coupling and base free C-N coupling reactions with broad substrate scope thus making the catalyst inexpensive.

4.5. Spectral data of synthesized products Sonogashira 3a-3f & Chan-Lam 3a-3h

Sonogashira 3a-3f:

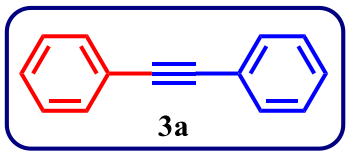

1,2-diphenylethyne (3a)

^{1}H NMR (400 MHz, $CDCl_3$): δ (ppm): 7.56 – 7.52 (m, 4H), 7.38 – 7.33 (m, 6H); ^{13}C NMR (100 MHz, $CDCl_3$): δ (ppm): 130.50, 127.23, 127.14, 122.18, 88.26.

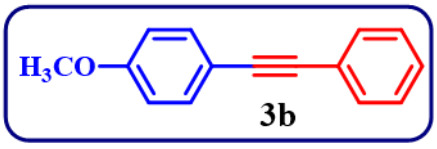

1-methoxy-4-(phenylethynyl)benzene (3b)

^{1}H NMR (400 MHz, $CDCl_3$): δ (ppm): 7.48 – 7.40 (m, 4H), 7.30 – 7.24 (m, 3H), 6.82 (d, J = 8.8 Hz, 2H), 3.77 (s, 3H). ^{13}C NMR (100 MHz, $CDCl_3$): δ (ppm): 159.75, 133.17, 131.57, 128.43, 128.05, 123.73, 115.53, 114.13, 89.49, 88.19, 55.42.

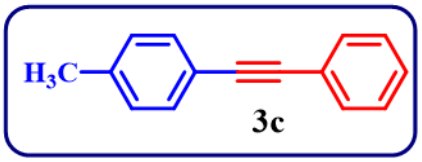

1-methyl-4-(phenylethynyl)benzene (3c)

^{1}H NMR (400 MHz, $CDCl_3$): δ (ppm): 7.55 – 7.51 (m, 2H), 7.43 (d, J = 8.4 Hz, 2H), 7.37 – 7.31 (m, 3H), 7.16 (d, J = 8 Hz, 2H), 2.38 (s, 3H). ^{13}C NMR (100 MHz, $CDCl_3$): δ (ppm): 138.51, 131.68, 131.63, 129.24, 128.44, 128.19, 123.62, 120.33, 89.68, 88.84, 21.63.

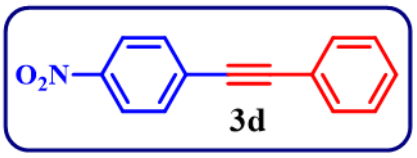

1-nitro-4-(phenylethynyl)benzene (3d)

^{1}H NMR (400 MHz, $CDCl_3$): δ (ppm): 8.16 (d, J = 8.8 Hz, 2H), 7.60 (d, J = 8.8 Hz, 2H), 7.52–7.48 (m, 2H), 7.35 – 7.31 (m, 3H); ^{13}C NMR (100 MHz, $CDCl_3$): δ (ppm): 145.94, 131.21, 130.79, 129.21, 128.2, 127.58, 122.58, 121.06, 93.65, 86.49.

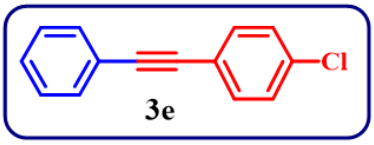

1-chloro-4-(phenylethynyl)benzene (3e)

^{1}H NMR (400 MHz, $CDCl_3$): δ (ppm): 7.52 – 7.47 (m, 2H), 7.46 – 7.41 (m, 2H), 7.35 – 7.31 (m, 4H), 7.39 (t, J = 2 Hz, 1H); ^{13}C NMR (100 MHz, $CDCl_3$): δ (ppm): 134.58, 133.13, 131.92, 129.01, 128.80, 128. 71, 123.25, 90.63, 88.55.

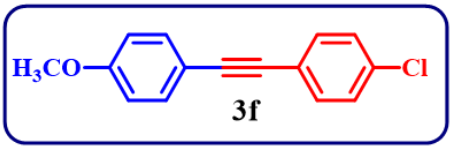

1-chloro-4-((4-methoxyphenyl)ethynyl)benzene (3f)

^{1}H NMR (400 MHz, $CDCl_3$): δ (ppm): 7.44 (dd, J = 10.5, 8.4 Hz, 4H), 7.30 (d, J = 8 Hz, 2H), 6.88 (d, J = 8.4 Hz, 2H), 3.83 (s, 3H); ^{13}C NMR (100 MHz, $CDCl_3$): δ (ppm): 159.91, 133.99, 133.18, 132.75, 128.75, 122.25, 115.14, 114.17, 90.47, 87.10, 55.43.

Chan-Lam Coupling 3a-3h:

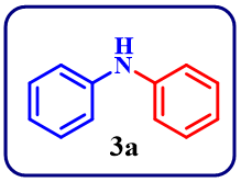

Diphenylamine (3a)

^{1}H NMR (400 MHz, $CDCl_3$): δ (ppm): 7.33 – 7.27 (m, 4H), 7.11 (d, J = 7.6 Hz, 4H), 6.96 (t, J = 7.4 Hz, 2H), 5.73 (brs, 1H); ^{13}C NMR (100 MHz, $CDCl_3$): δ (ppm): 143.14, 129.35, 121.01, 117.85.

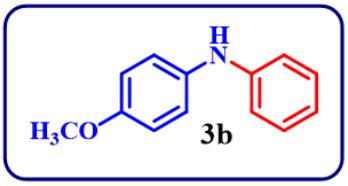

4-methoxy-N-phenylaniline (3b)

^{1}H NMR (400 MHz, $CDCl_3$): δ (ppm): 7.23 – 7.18 (m, 2H), 7.07 (d, J = 8.8 Hz, 2H), 6.91 (d, J = 7.6 Hz, 2H), 6.87 – 6.81 (m, 3H), 5.49 (brs, 1H), 3.80 (s, 3H); ^{13}C NMR (100 MHz, $CDCl_3$): δ (ppm): 155.29, 145.18, 135.74,129.31, 122.22, 119.57, 115.65, 114.68, 55.60.

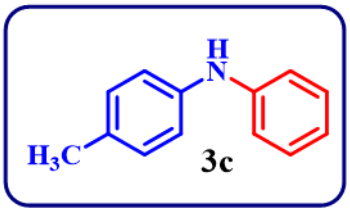

4-Methyl-N-phenylaniline (3c)

^{1}H NMR (400 MHz, $CDCl_3$): δ (ppm): 7.25 – 7.21 (m, 2H), 7.08 (d, J = 8.0 Hz, 2H), 7.03–6.98 (m, 4H), 6.87 (t, J = 7.2 Hz, 1H), 5.60 (brs, 1H), 2.30 (s, 3H); ^{13}C NMR (100 MHz, $CDCl_3$): δ (ppm): 143.96, 140.29, 130.95, 129.86, 129.31, 122.73, 120.31, 118.92, 116.87, 20.69.

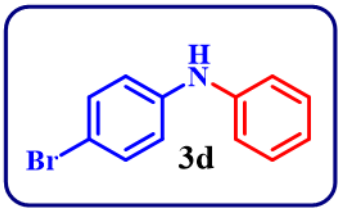

4-bromo-N-phenylaniline (3d)

^{1}H NMR (400 MHz, $CDCl_3$): δ (ppm): 7.34 (d, J = 9.2 Hz, 2H), 7.30 – 7.26 (m, 2H), 7.05 (d, J = 7.2 Hz, 2H), 6.98– 6.91 (m, 3H), 5.67 (brs, 1H); ^{13}C NMR (100 MHz, $CDCl_3$): δ (ppm): 142.45, 142.42, 132.19, 129.47, 121.67, 119.03, 118.31, 112.63.

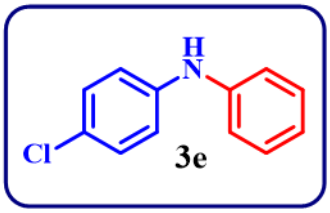

4-chloro-N-phenylaniline (3e)

^{1}H NMR (400 MHz, $CDCl_3$): δ (ppm): 7.30–7.26 (m, 2H), 7.20 (d, J = 8.8 Hz, 2H), 7.05 (d, J = 7.4 Hz, 2H), 7.00– 6.93 (m, 3H), 5.60 (brs, 1H); ^{13}C NMR (100 MHz, $CDCl_3$): δ (ppm): 142.65, 141.87, 129.46, 129.29, 125.53, 121.54, 118.83, 118.13.

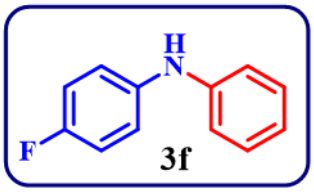

4-floro-N-phenylaniline (3f)

^{1}H NMR (400 MHz, $CDCl_3$): δ (ppm): 7.26–7.22 (m, 2H), 7.07–7.03 (m, 2H), 7.00–6.95 (m, 4H), 7.20 (t, J = 7.2 Hz, 1H), 5.61 (brs, 1H); ^{13}C NMR (100 MHz, $CDCl_3$): δ (ppm): 158.1 (d, J_{CF}=158.1 Hz), 143.84, 138.84, 129.43, 120.75, 120.66, (d, J_{CF}=7.9 Hz), 116.91, 115.95 (d, J_{CF}=22.4 Hz)

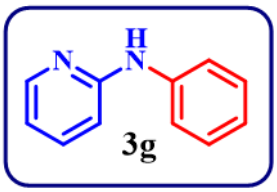

N-phenylpyridin-2-amine (3g)

^{1}H NMR (400 MHz, $CDCl_3$): δ (ppm): 8.19 (brs, 1H), 7.52–7.47 (m, 1H), 7.34–7.31 (m, 4H), 7.08–7.04 (m, 1H), 6.59 (d, J = 8.4 Hz, 1H), 6.78– 6.70 (m, 2H); ^{13}C NMR (100 MHz, $CDCl_3$): δ (ppm): 156.14, 148.27, 140.52, 138.09, 129.53, 123.17, 120.68, 115.20, 108.49.

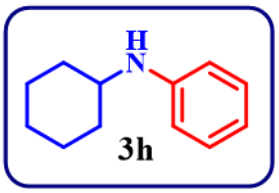

N-cyclohexylaniline (3h)

^{1}H NMR (400 MHz, $CDCl_3$): δ (ppm): 7.17–7.12 (m, 2H), 6.65 (t, J = 7.2 Hz, 1H), 6.58 (d, J = 7.6 Hz, 2H), 5.62 (brs, 1H), 3.28– 3.21 (m, 1H), 2.08– 2.03 (m, 2H), 1.79– 1.61 (m, 4H), 1.43– 1.24 (m, 4H); ^{13}C NMR (100 MHz, $CDCl_3$): δ (ppm): 147.55, 129.45, 117.05, 113.37, 51.91, 33.67, 26.13, 25.22.

4.6. References

(1) Kazemi, M. Based on $CuFe_2O_4$ MNPs: Magnetically Recoverable Nanocatalysts in Coupling Reactions. *Synth. Commun.* **2020**, *50* (14), 2114–2131.

(2) Tarahomi, M.; Alinezhad, H.; Maleki, B. Immobilizing Pd Nanoparticles on the Ternary Hybrid System of Graphene Oxide, Fe_3O_4 Nanoparticles, and PAMAM Dendrimer as an Efficient Support for Catalyzing Sonogashira Coupling Reaction. *Appl. Organomet. Chem.* **2019**, *33* (11), 1–13.

(3) Taghavi, R.; Rostamnia, S. Schiff-Base Post-Synthetic Modification of IRMOF-3 to Encapsulate Pd Nanoparticles : It's Application in C-C Bond Formation Cross- Coupling Suzuki Reaction. *Chem. Methodol.* **2022**, *6* (8), 629–638.

(4) Maleki, A.; Taheri-Ledari, R.; Ghalavand, R.; Firouzi-Haji, R. Palladium-Decorated o-Phenylenediamine-Functionalized Fe_3O_4/SiO_2 Magnetic Nanoparticles: A Promising Solid-State Catalytic System Used for Suzuki–Miyaura Coupling Reactions. *J. Phys. Chem. Solids* **2020**, *136* (July 2019), 109200.

(5) Sharma, C.; Sharma, N.; Sharma, S.; Sharma, S.; Paul, S. Nano-Rod like Morphology of Ni@Fe_3O_4-NDCs on Interaction of NDC-Supported Fe_3O_4 with Nickel NPs: An Efficient Catalyst for Ligand Free Chan-Lam Coupling Reaction in Aqueous Medium. *Curr. Res. Green Sustain. Chem.* **2021**, *4* (May), 100133.

(6) Sharma, S.; Kaur, M.; Sharma, C.; Choudhary, A.; Paul, S. Biomass-Derived Activated Carbon-Supported Copper Catalyst : An E Ffi Cient Heterogeneous Magnetic Catalyst for Base-Free Chan − Lam Coupling and Oxidations. *ACS Omega*. **2021**, 6, (2021), 19529.

(7) Iraqui, S.; Rashid, H. As Stable and Efficient Catalysts for the Synthesis of Aryl Thioethers via C – S Coupling Reactions. *New J. Chem.* **2022**, 46, (2022),22766–22777.

(8) Kharisov, B. I.; Dias, H. V. R.; Kharissova, O. V. Mini-Review : Ferrite Nanoparticles in the Catalysis. *Arab. J. Chem.* **2019**, *12* (7), 1234–1246.

(9) Maleki, A.; Azadegan, S. Amine-Functionalized Silica-Supported Magnetic Nanoparticles: Preparation, Characterization and Catalytic Performance in the Chromene Synthesis. *J. Inorg. Organomet. Polym. Mater.* **2017**, *27* (3), 714–719.

(10) Saadati-Moshtaghin, H. R.; Maleki, B.; Tayebee, R.; Kahrobaei, S.; Abbasinohoji, F. 6-Methylguanamine-Supported $CoFe_2O_4$: An Efficient Catalyst for One-Pot Three-Component Synthesis of Isoxazol-5(4H)-One Derivatives. *Polycycl. Aromat. Compd.* **2022**, *42* (3), 885–896.

(11) Maleki, A.; Kamalzare, M. An Efficient Synthesis of Benzodiazepine Derivatives via a One-Pot, Three-Component Reaction Accelerated by a Chitosan-Supported Superparamagnetic Iron Oxide Nanocomposite. *Tetrahedron Lett.* **2014**, *55* (50), 6931–6934.

(12) Maleki, A.; Ravaghi, P.; Aghaei, M.; Movahed, H. A Novel Magnetically Recyclable Silver-Loaded Cellulose-Based Bionanocomposite Catalyst for Green Synthesis of Tetrazolo[1,5-a]Pyrimidines. *Res. Chem. Intermed.* **2017**, *43* (10), 5485–5494.

(13) Rahman, T.; Borah, G.; Gogoi, P. K. Spinel Structured Copper Ferrite Nano Catalyst with Magnetic Recyclability for Oxidative Decarboxylation of Phenyl Acetic Acids. *Catal. Letters* **2020**, *150* (8), 2267–2272.

(14) Shaabani, A.; Hezarkhani, Z.; Nejad, M. K. Cr- and Zn-Substituted Cobalt Ferrite Nanoparticles Supported on Guanidine – Modified Graphene Oxide as Efficient and Recyclable Catalysts. *J. Mater. Sci.* **2017**, *52* (1), 96–112.

(15) Mitrofanov, A. Y.; Murashkina, A. V; Martín-garcía, I.; Alonso, F.; Beletskaya, I. P. Catalysis Science & Technology by Supported Copper Nanoparticles. *Catal. Sci. Technol.* **2017**, **7,** 4401–4412.

(16) Arundhathi, R.; Damodara, D.; Mohan, V. Aluminium Hydrotalcite : Importance in C À C Couplings of Deactivated Aryl Chlorides. *Adv. Synth. Catal*. **2013**, 355, 751–756.

(17) Budarin, V. L.; Shuttleworth, P. S.; Clark, J. H.; Luque, R. Industrial Applications of C-C Coupling Reactions. *Adv. Synth. Catal*., **2010**, 7, 614–627.

(18) Sheikh, S.; Nasseri, M. A.; Allahresani, A.; Varma, R. S. Copper Adorned Magnetic Nanoparticles as a Heterogeneous Catalyst for Sonogashira Coupling Reaction in Aqueous Media. *Sci. Rep.* **2022**, 12, 1–14.

(19) Can, H. Reduced Graphene Oxide-Supported CuPd Alloy Nanoparticles as E Ffi Cient Catalysts for the Sonogashira Cross-Coupling Reactions. *ACS Appl. Mater. Interfaces.* **2015**, 7, 3199.

(20) Mino, T.; Suzuki, S.; Hirai, K.; Sakamoto, M.; Fujita, T. Hydrazone-Promoted Sonogashira Coupling Reaction with Aryl Bromides at Low Palladium Loadings. *Synlett* **2011**, No. 9, 1277–1280.

(21) Ghabdian, M. Heterogenized Cu(II) Salen Complex Grafted on Graphene Oxide Nanosheets as a Precursing Catalyst for the Pd - Free Sonogashira Coupling. *Appl Organometal Chem*. **2018**, 1,4545**.**

(22) Hagihara, S. N,N-Dimethylformamide-Stabilized Copper Nanoparticles as a Catalyst Precursor for Sonogashira–Hagihara Cross Coupling. *RSC Adv*. **2017**, 7, 22869–22874.

(23) Hajipour, A. R.; Hadi, S.; Mohammadsaleh, F. Choline Chloride / CuCl as an Effective Homogeneous Catalyst for Palladium-Free Sonogashira Cross-Coupling Reactions. *Tetrahedron Lett.* **2014**, *55* (3), 654–656.

(24) Ali, M.; Zinat, N.; Milad, R.; Ali, K. Magnetic Cu – Schiff Base Complex with an Ionic Tail as a Recyclable Bifunctional Catalyst for Base / Pd - Free Sonogashira Coupling Reaction. *J. Iran. Chem. Soc.* **2019**, *16* (12), 2693–2705.

(25) Hajipour, A. R.; Hosseini, S. M.; Mohammadsaleh, F. DABCO-Functionalized Silica–Copper(i)Complex: A Novel and Recyclable Heterogeneous Nanocatalyst for Palladium-Free Sonogashira Cross-Coupling Reactions. *NewJ.Chem***. 2016**, 40, 6939–6945.

(26) Kumari, S.; Pathak, D. D. Synthesis and Development of Chitosan Anchored Copper (II) Schiff Base Complexes as Heterogeneous Catalysts for N-Arylation of Amines. *Tetrahedron Lett.* **2015**, *56* (27), 4135–4142.

(27) Sanjeeva, K.; Wu, T. Chan e Lam Coupling Reactions : Synthesis of Heterocycles. *Tetrahedron* **2012**, *68* (38), 7735–7754.

(28) J. Q. Chen, J. H. Li, and Z. B. Dong, *Advanced Synthesis and Catalysis.* **2020**, **362**, 3311.

(29) Kumar, A.; Layek, S.; Agrahari, B.; Kujur, S.; Deo, D. Graphene Oxide Immobilized Copper (II) Schiff Base Complex [GO@AF-SB-Cu]: A Versatile Catalyst for Chan-Lam Coupling Reaction. *ChemistrySelect.* **2019**, 4, 1337–1345.

(30) Haija, M. A.; Basina, G.; Banat, F.; Ayesh, A. I. Adsorption and Gas Sensing Properties of $CuFe_2O_4$ Nanoparticles. *Mater. Sci. Pol.* **2019**, *37* (2), 289–295.

(31) Manuscript, A. Dalton Transactions. *J. Chem. Soc. Dalt. Trans.* **1972**, 1772.

(32) Kanagaraj, M.; Sathishkumar, P.; Selvan, G. K.; Kokila, I. P.; Arumugam, S. Structural and Magnetic Properties of $CuFe_2O_4$ As-Prepared and Thermally Treated Spinel Nanoferrites. **2014**, *52* , 124–130.

(33) N. S. Al-Kadhi, G. M. Al-Senani, R. S. Almufarij, O. H. Abd-Elkader, N. M. Deraz, *Crystals*, **2023**, 13, 758.

(34) Deraz, N. M. Size and Crystallinity-Dependent Magnetic Properties of Copper Ferrite Nano-Particles. *J. Alloys Compd.* **2010**, *501* (2), 317–325.

(35) Sagayaraj, R.; Leonard, H. J.; Xavier, H. S.; Praveen, P.; Elayakumar, K.; Yogambal, C. Structural, Vibrational, Morphological and Magnetic Properties of Copper Ferrite NanoParticles ($Cu_{0.4}MFe_{2.96}MO_4$) by Co-Precipitation Method. *Joseph's J. Humanit. Sci.* **2019**, *6*, 58–62.

(36) Sathyaseelan, B.; Killivalavan, G.; Senthilnathan, K.; Elayaperumal, M. Photocatalytic Dye Degradation Properties of Zinc Copper Ferrites Photocatalytic Dye Degradation Properties of

Zinc Copper Ferrites Nanoparticles. *J Nanostruct*, 9, 694, **2019**, 9, 694.

(37) Yu, S.; Sharma, R.; Morose, G.; Nagarajan, R. Identifying Sustainable Alternatives to Dimethyl Formamide for Coating Applications Using Hansen Solubility Parameters. *J. Clean. Prod.* **2021**, *322*, 129011.

(38) Wang, B.; Wang, Y.; Guo, X.; Jiao, Z.; Jin, G.; Guo, X. Reduced Graphene Oxide Supported Cu_2O Nanoparticles as an e Ffi Cient Catalyst for Sonogashira Coupling Reaction. *Catal. Commun.* **2017**, *101* (April), 36–39.

(39) Sarmah, M.; Sarmah, D.; Dewan, A.; Bora, P.; Boruah, P. K.; Das, M. R. Dual Responsive Sustainable - Cu_2O/Cu Nanocatalyst for Sonogashira and Chan - Lam Cross - Coupling Reactions. *Catal. Letters* **2023**, *153* (5), 1423–1437.

(40) Bakherad, M.; Doosti, R.; Mirzaee, M. Catalyzed by Boehmite Nanoparticle-Anchored. *Res. Chem. Intermed.* **2017**, *43* (12), 7347–7363.

(41) Hajipour, A. R.; Rezaei, F.; Khorsandi, Z. Magnetic Chitosan as Reusable Catalyst. *Green Chem*. **2017**, 19, 1353–1361.

(42) Kataria, M.; Pramanik, S.; Kaur, N.; Kumar, M.; Bhalla, V. Ferromagnetic α-Fe_2O_3 NPs: A Potential Catalyst in Sonogashira–Hagihara Cross Coupling and Hetero-Diels–Alder Reactions. *Green Chem.* **2016**, 18, 1495–1505.

(43) Rao Volla, C. M.; Vogel, P. Iron/Copper-Catalyzed C-C Cross-Coupling of Aryl Iodides with Terminal Alkynes. *Tetrahedron Lett.* **2008**, *49* (41), 5961–5964.

(44) Huang, X.; Qi, Y.; Gu, Y.; Gong, S. Polyoxovanadate-Based Copper Frameworks As. *Dalton Trans.* **2020**, 49, 10970–10976.

(45) Saikia, R.; Das, S.; Almin, A.; Mahanta, A.; Sarma, B.; Thakur, A. J.; Bora, U. Biomolecular Chemistry Synthesis of Pharma-Relevant Motifs Through. *Org. Biomol. Chem.* **2023**, 21, 3143–3155.

(46) Cope, J. D.; Sheridan, P. E.; Galloway, C. J.; Awoyemi, R. F.; Stokes, S. L.; Emerson, J. P. Synthesis and Characterization of a Tetradentate, N - Heterocyclic Carbene Copper(II) Complex and Its Use as a Chan−Evans− Lam Coupling Catalyst. *Organometallics.* **2020**, 39, 4457.

(47) Han, Y.; Zhang, M.; Zhang, Y.; Zhang, Z. Framework : An e Ffi Cient and Recyclable Coupling Reaction of Aryl Boronic Acids And. *Green Chem*. **2018**, 20 4891–4900.

(48) Sharma, C.; Sharma, N.; Sharma, S.; Sharma, S.; Paul, S. Current Research in Green and Sustainable Chemistry Nano-Rod like Morphology of Ni@Fe_3O_4-NDCs on Interaction of NDC-Supported Fe_3O_4 with Nickel NPs : An Ef Fi Cient Catalyst for Ligand Free Chan-Lam Coupling Reaction in Aqueous Medium. *Curr. Res. Green Sustain. Chem.* **2021**, *4* (May), 100133.

4.7. Selected NMR (^{1}H & ^{13}C) spectra of products in

4.7.1. Sonogashira Coupling Reaction

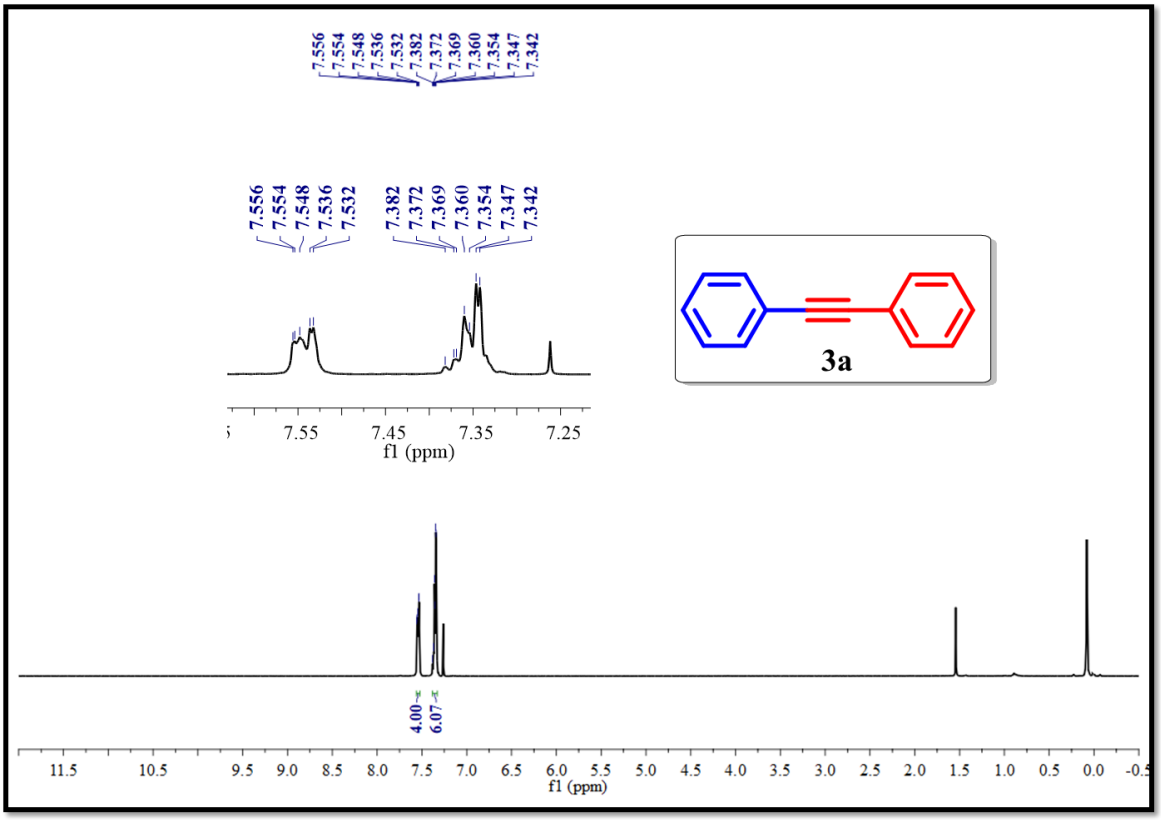

^{1}H NMR spectrum of the compound 1,2-diphenylethyne (3a).

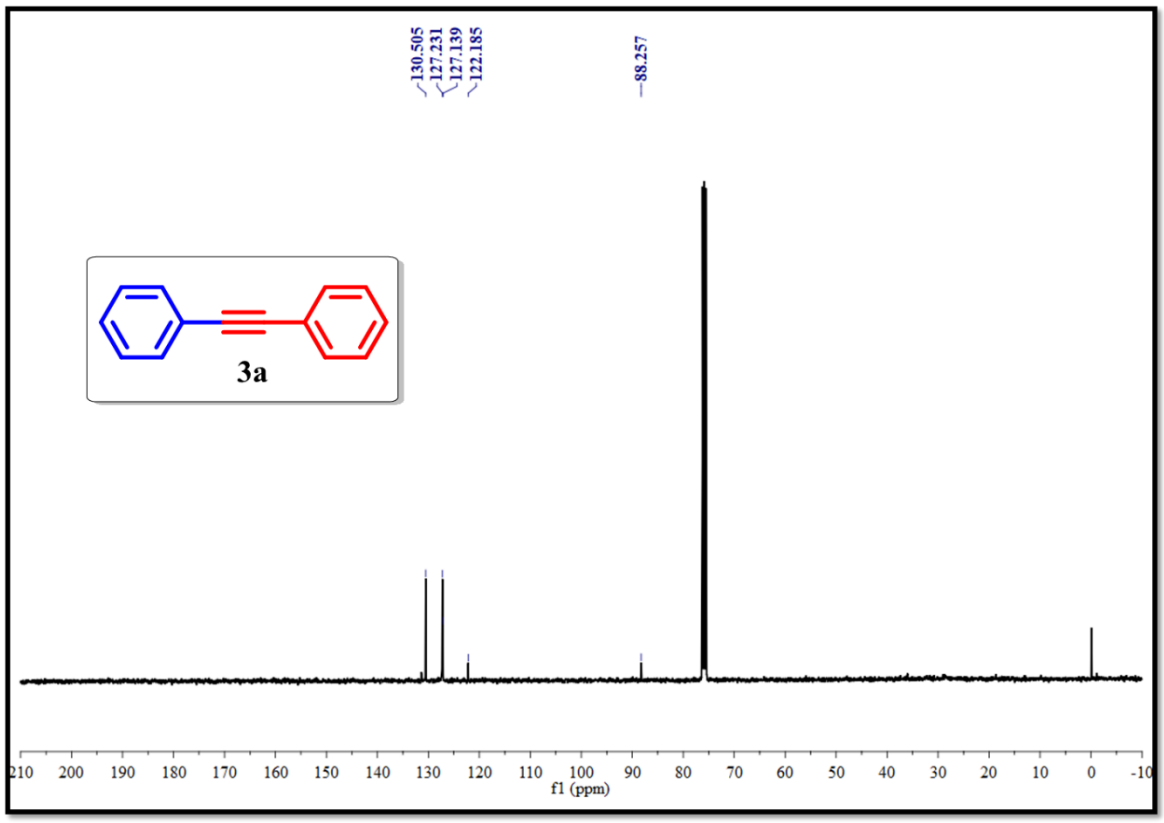

^{13}C NMR spectrum of the compound 1,2-diphenylethyne (3a)

4.7.2. Chan-Lam Coupling Reaction

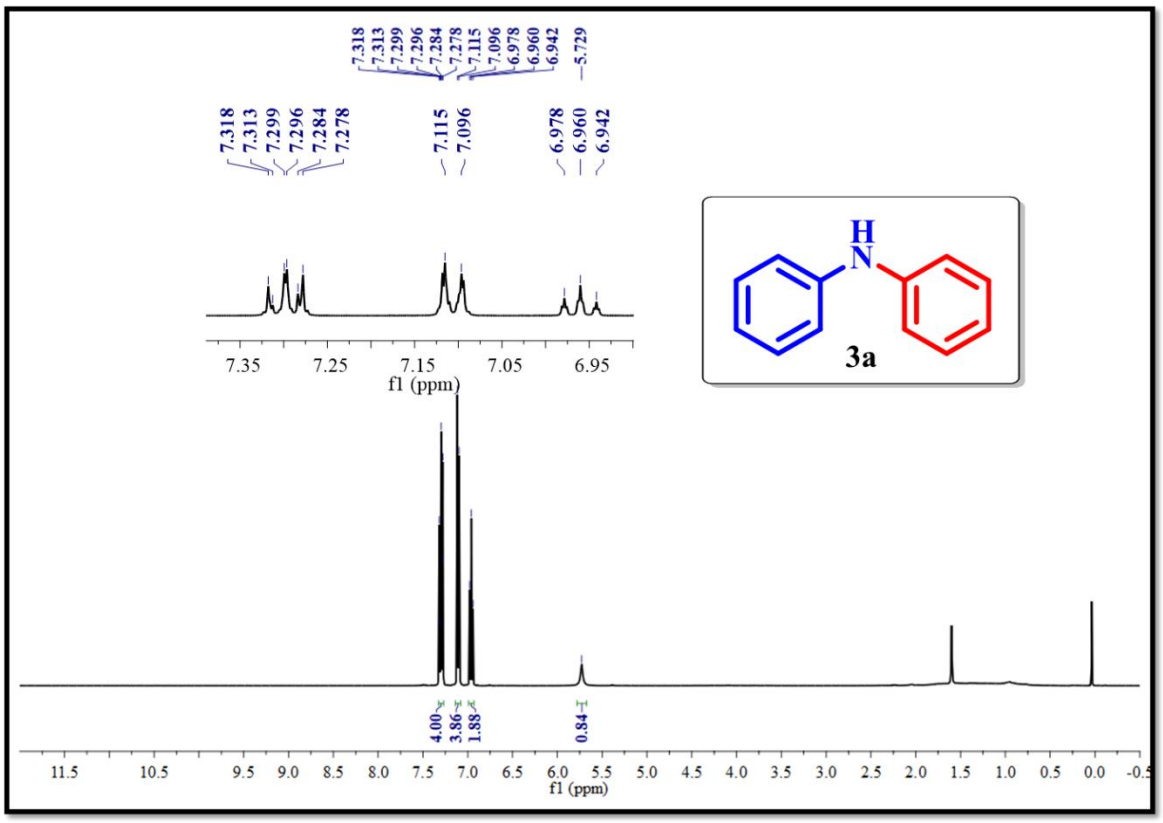

^{1}H NMR spectrum of the compound Diphenylamine (3a)

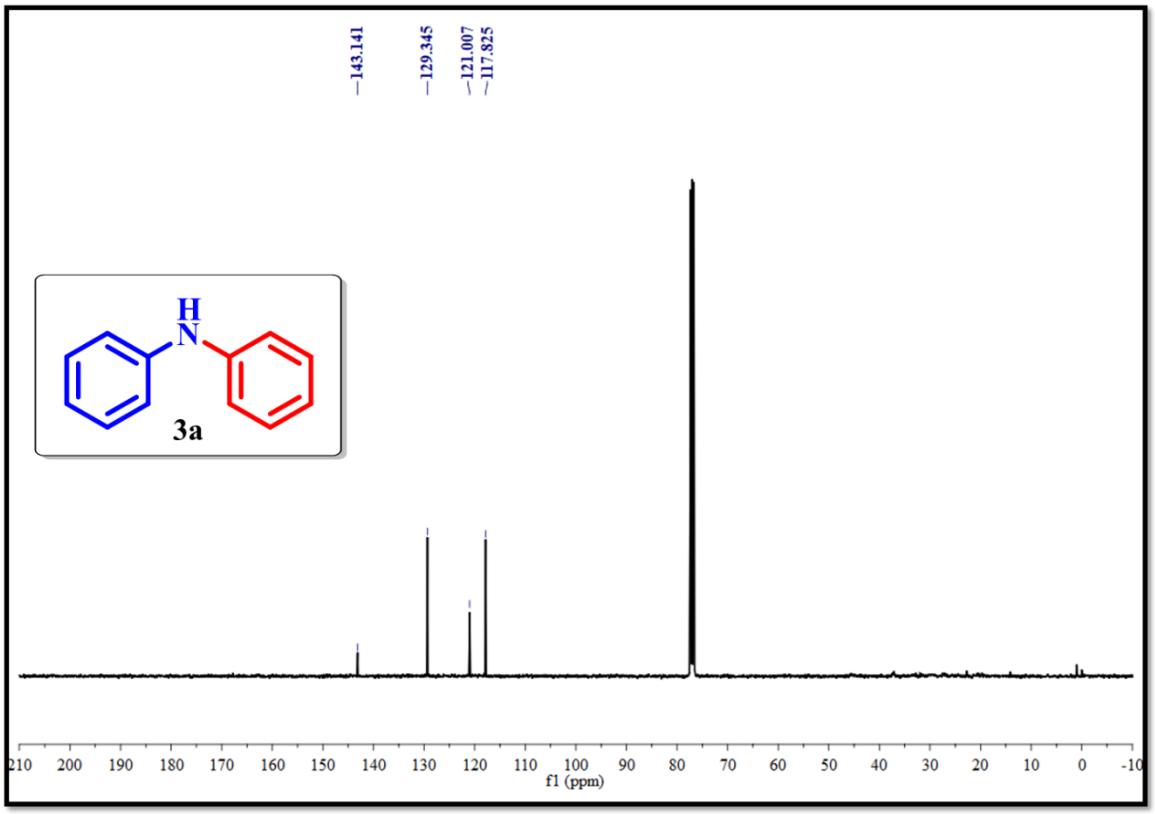

^{13}C NMR spectrum of the compound Diphenylamine (3a)

CHAPTER-V

Synthesis of Cu Supported Fe_3O_4-NH_2 Nanocatalyst for One Pot Three-Component (A^3) Coupling Reaction

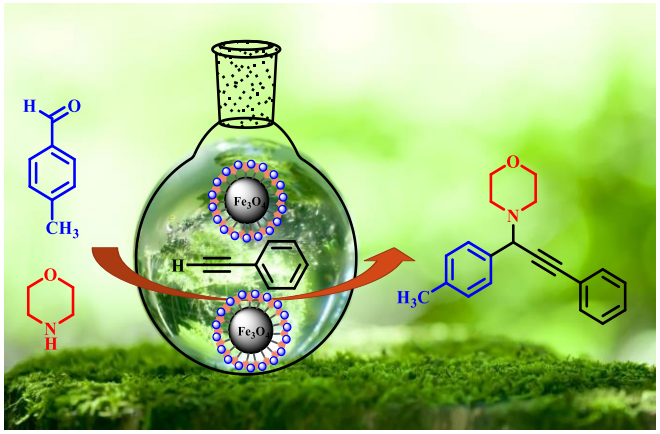

Chapter-V

Synthesis of Cu Supported Fe_3O_4-NH_2 Nanocatalyst for One Pot Three-Component (A^3) Coupling Reaction

5.1. Introduction

In recent history, 3 component coupling reaction (A^3 coupling reaction or aldehyde-alkene-amine coupling) catalysed by transition metals is a reaction of prominent interest and important tool in organic synthesis. It is a one-pot three-component condensation (Mannich type reaction) between an amine, an aldehyde and alkyne to produce Propargylamines with atom economy. Propargylamines are diverse substances that are widely used as intermediates for developing heterocycles with nitrogen encompassing natural products, drugs and molecules with biological activity in pharmaceuticals.[1,2,3] In the process of formation of the product, activation of alkyne C-H bond is an important step for which the selection of an appropriate catalyst is crucial.[4]

Since the 2000s, this reaction has been widely studied in the perspective of homogeneous catalysis with the use of inorganic salts of different metals along with active Au,[3] Ag,[5] and Cu metals.[6] Later, transition metal complexes as homogeneous catalysts were developed to enhance the process.[7,8] It was reported that a wide variety of transition metal based catalysts containing Cu,[9] Ag,[10] Au,[11] Zn,[12] Fe,[13] In,[14] Ni,[15] Hg,[16] Ru,[17] Co,[18] and Nb,[19] were used for C–H bond activation in 1-alkynes for the A^3 coupling. The most often used salts among them are those that contain Cu^+/Cu^{2+}, Ag^+ and Au^+/Au^{3+}.[20] Even though, the reaction in the presence of homogeneous catalyst had a high efficiency, the complications associated with separation, reusability and product purification led to the development of heterogeneous catalysts.[21] Copper systems were of particular focus because of its abundance and inexpensive nature.[22]

Previously, many methods have been explored for the immobilization of catalytically active copper NPs on different types of solid supports which include polymers,[23] silica,[24] carbon nano tubes,[25] activated carbon [26] to facilitate the catalyst to be easily separated from the reaction mixture. However, there was no significant increase of catalytic activity which was reported to be due to mass transfer constraint. To enhance the activity, great attention has been paid towards small and non-porous supports which are expected to increase the diffusion process. In recent past, magnetic NPs have been evolved as possible substitutes to regular materials as supports. It is because they are strong, easily available and possess large surface area to act as best heterogeneous catalyst supports.[27,28] Further, amine functionalization of

these magnetic NPs is a well-established methodology for the immobilization of metal NPs because, amines are best known for stabilization of metal NPs to reduce agglomeration with the retention of their required properties. It is also reported that amine functionalization will enhance the catalytic activity. Magnetite (Fe_3O_4) is the simple, easily available best magnetic material to be used as support which can be amine functionalised by simple method to form Fe_3O_4-NH_2.[29,30]

Based on aforementioned different strategies, and in continuation of the research interest in developing new heterogeneous catalyst, Cu supported amine functionalized magnetic nanocatalyst (Fe_3O_4-NH_2-Cu) was proposed in the current work. It was synthesized via simple twostep process for its use in A^3 coupling reaction. Furthermore, the Fe_3O_4-NH_2-Cu was easily isolated for reuse by an external magnet, without significant reduction in its efficacy.

5.2. Experimental Section

5.2.1. Materials

The starting materials used in the present work were Ferric nitrate (99%, Finar,); Ferric chloride (99%, Finar); Ethylene glycol (EG) (99%, Finar); CH_3COONa (SRL, 98% purity), ethanolamine (98%, Merck), Hydrazine monohydrate (99%, Finar); Sodium borohydride (98.5%, Finar); Ethyl alcohol (EtOH-99%, Finar); Ethyl ethanoate (EtOAc-99%, Finar); n-hexane (98%, Finar). Water that had been double-distilled (DD) was utilised throughout the experiment.

5.2.2. Synthesis of amine factionalized ferrite (Fe_3O_4–NH_2)

By employing the Co-precipitation technique, amine-functionalized ferrite (Fe_3O_4−NH_2) was synthesized. Initially, in this process, 10.0 mL of EG was used to dissolve 15 mmol of CH_3COONa. The mixture was then heated to 100 °C while being stirred magnetically, and refluxed for 15 minutes. To the preheated solution, a solution containing ferric chloride and ferric nitrate in 1:2 mmol ratio dissolved in 5.0 mL of EG was added. After stirring the mixture for half an hour, 3.5 mL of ethanolamine was added. After being heated to 200 °C for 12 hours, the mixture was cooled. Once the reaction was finished the system was cooled to room temperature (RT). The resultant product was recovered using an external magnet and washed with DD water and ethanol for three times. The final product (Fe_3O_4−NH_2) was then dried for 12 h at 70 °C in an oven.

5.2.3. Synthesis of Fe_3O_4–NH_2-Cu nanocatalyst

$Cu(OAc)_2 \cdot 2H_2O$ (50 mg) was added to a suspension of amine-functionalized Fe_3O_4 (500 mg) in 50 mL DD water. To bring the pH of this mixture to 9, hydrazine monohydrate solution in water was added drop wise. Subsequently 50 mg of $NaBH_4$ was added. At RT, the

reaction mixture was then agitated for 24 h. The final product was separated using an external magnet and washed three times in DD water and acetone. The resulting product (Fe_3O_4–NH_2-Cu) was dried for 12 h at 70 °C.

5.2.4. General procedure of Propargylamines

In a conventional A^3 coupling reaction, the reactants, 1 mmol each of amines and aldehydes, 1.5 mmol of phenyl acetylenes, 15 mg of Fe_3O_4–NH_2-Cu catalyst were added under solvent-free conditions at 80 °C for 5 h. After the completion of the reaction (as determined by TLC), the catalyst was separated using a magnet. The required compounds were extracted twice with ethyl acetate and purified on a microcolumn filled with silica gel. Then, the products were examined using ^1H and ^{13}C NMR spectral analysis.

5.2.5. Characterization of Catalyst

The structural characterisation of the synthesized Fe_3O_4–NH_2-Cu catalyst was carried out using various techniques. A PAN Analytical Advance X-ray diffractometer was used to conduct powder X-ray diffraction (PXRD) experiments using a 2θ scan range between 10° and 80° and Ni-filtered Cu K (λ = 1.5406 Å) radiation. FT-IR spectra for Fe_3O_4–NH_2-Cu were recorded between 4000 and 400 cm^{-1} using the PerkinElmer Spectrum by KBr pellet method. A field emission scanning electron microscope (FESEM, Model: Quanta FEG 250) was employed to comprehend the surface morphology. The binding energies of the various elements in the Fe_3O_4–NH_2-Cu catalyst were ascertained using X-ray photoelectron spectroscopy (Kratos/Shimadzu Amicus, Model: ESCA 3400). In order to gain insight into the magnetic behaviour of the catalyst, the magnetic hysteresis curves of the catalyst were recorded using a vibrating sample magnetometer (VSM, Lake Shore, Model: 8600 Series). On an advanced-III Bruker 400 MHz NMR spectrometer, ^1H and ^{13}C NMR spectra were recorded using $CDCl_3$ as a solvent and TMS as an internal standard. Parts per million (ppm) were used to represent chemical shifts.

5.3. Results and Discussions

5.3.1. Preparation scheme of Fe_3O_4-NH_2-Cu nanocatalyst

A two-step process was used to make the Fe_3O_4-NH_2-Cu catalyst (**Scheme 5.1**). In step I, Co-precipitation process was used to create the amine functionalized Fe_3O_4 NPs (Fe_3O_4-NH_2). In step II, Copper NPs were loaded on the amine functionalized Fe_3O_4 surface to form a Cu supported amine functionalized Fe_3O_4 nanocatalyst (Fe_3O_4-NH_2-Cu). The synthesised nanocatalyst was separated using an external magnet, and it was then vacuum-dried for further usage.

Scheme 5.1. *The preparation of the Fe_3O_4-NH_2-Cu nanocatalyst*

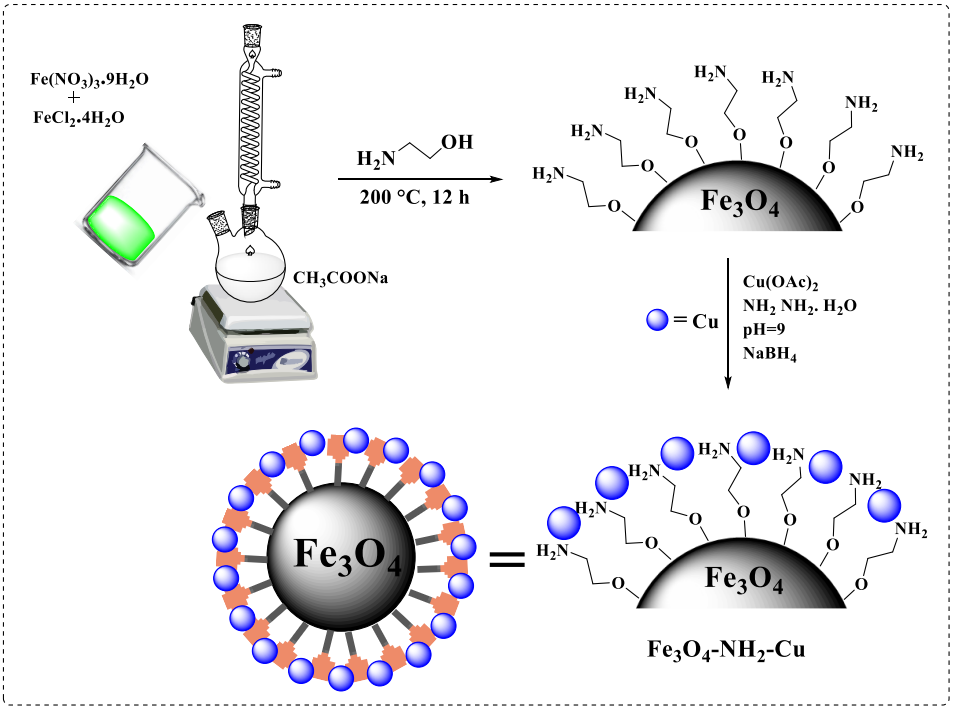

5.3.2. Characterization of Fe_3O_4-NH_2-Cu catalyst:

The labelled XRD patterns of prepared materials (I. Fe_3O_4-NH_2 and II. Fe_3O_4-NH_2-Cu) were depicted in **Figure 5.1a**. The broad peaks in the image confirmed that particles were formed in the nano-regime. The observed peaks in **Figure 5.1a(I)** at 2θ values of 18.5°, 30.2°, 35.6°, 43.2°, 53.5°, 57.1°, and 62.9° were attribute to (111), (220), (311), (400), (422), (511) and (440) diffractions, respectively. This confirmed the development of single phased pure crystalline spinel Fe_3O_4. (JCPDS card No. 88-0315).[31] There was no change in the XRD spectrum even after Cu loading as evident from **Figure 5.Ia(II)** that was due to low loading of Cu metal. The broad peaks represent the formation of NPs and the most intense peak (311) as evident from the figure at 35.6° was the representative peak of the spinel phase.

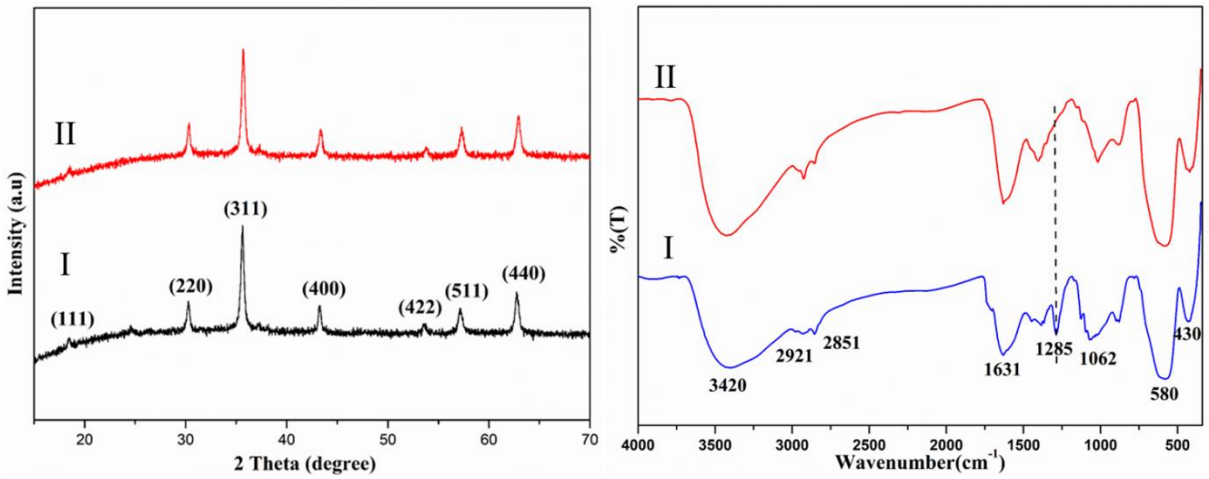

Figure 5.1. *a) XRD spectra b) FT-IR spectra of the Fe_3O_4-NH_2-Cu catalyst*

FT-IR spectra of synthesized Fe_3O_4-NH_2 and Fe_3O_4-NH_2-Cu catalyst was depicted **Figure 5.1b** depicts the. The two pronounced peaks between 600 and 400 cm^{-1} in **Figure 5.1b(I)** indicative of spinel structure. The significant peaks at 430 and 580 cm^{-1} were caused by the intrinsic vibrations Mn^{+}-O bond in the octahedral and tetrahedral locations of the spinel structure accordingly. The absorption peak at 3420 and 1631 cm^{-1} would specifiy stretching and bending vibration of surface NH_2 groups. The observed peaks at 2921 and 2851 cm^{-1} signified stretching vibrations of C-H groups. The observed peak at 1062 cm^{-1} indicated stretching vibrations of C-O group and at 1285 cm^{-1} showed stretching vibrations of C-N group. FTIR spectrum in **Figure 5.1b(II)** showed a shift in the C-N stretching vibration peak observed at 1285cm^{-1} to higher frequency range. This would be due to the bonding interaction between Cu and NH_2 group. This confirmed the Cu immobilization on Fe_3O_4-NH_2.[32,33]

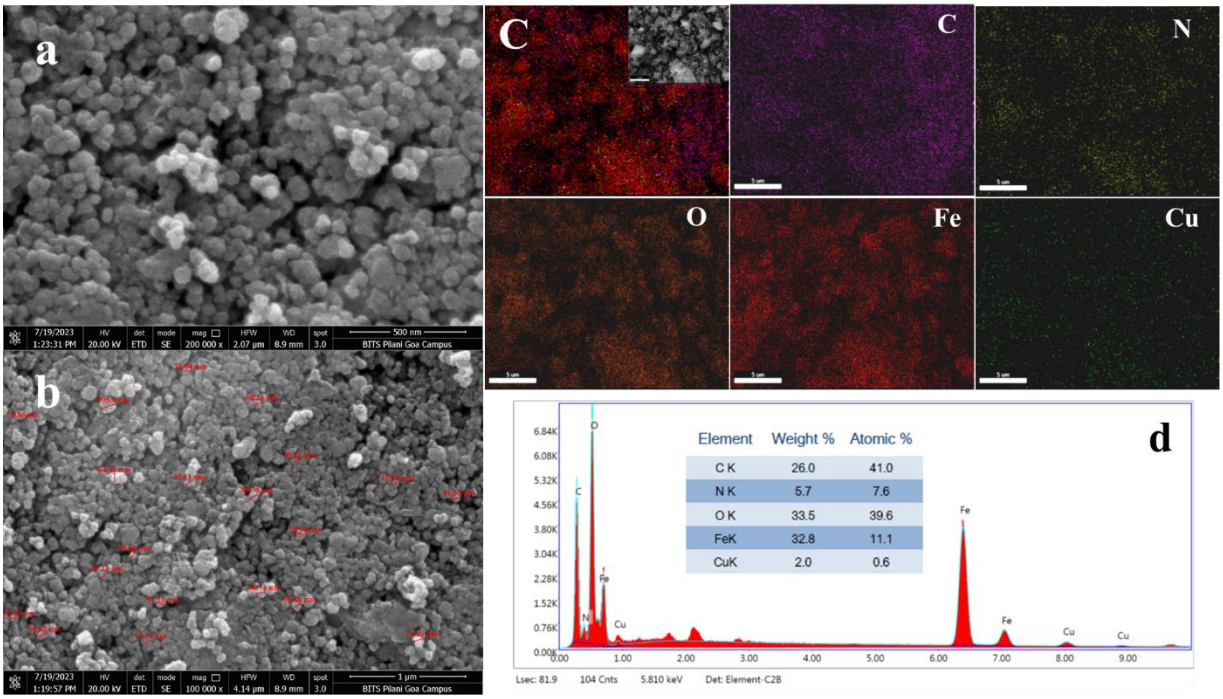

Figure 5.2. *(a, b) FESEM images, (c) EDAX Mapping (d) EDAX data of Fe_3O_4-NH_2-Cu nanocatalyst.*

The synthesised Fe_3O_4-NH_2-Cu nanocatalyst was found to have a spherical surface morphology as evident from **Figure 5.2(a, b)** of the FESEM images. The elemental mapping spectra and energy dispersive X-ray elemental composition (EDAX) were recorded during FESEM recording. The catalyst's elemental mapping (**Figure 5.2c**) indicated that all elements, including Cu, Fe, N, C, and O were uniformly distributed across the surface of Fe_3O_4. The subsequent figures contained mapping spectra for the specific elements C, N, O, Fe, and Cu. These images revealed that Fe_3O_4 was functionalized with amine and Cu was successfully

loaded on the Surface to result in the formation of the expected Fe_3O_4-NH_2-Cu nanocatalyst. The EDAX elemental composition of Fe_3O_4-NH_2-Cu from **Figure 5.2d** revealed the existence of Cu, Fe, N, C, and O elements which confirmed the successive surface modification, and effective loading of Cu on the Fe_3O_4 support.

The effective coordination of Cu on the surface was verified using X-ray photoelectron spectroscopy (XPS). It was an effective instrument for comprehending the electronic characteristics of the metals in the catalyst, including the chemical valence states, binding energy, and electron environment. The chemical valence states of Fe and Cu in the catalyst were analysed using the XPS spectra of the Fe_3O_4-NH_2-Cu nanocatalyst displayed in **Figure 5.3**. The two noticeable bands in **Figure 5.3a** at binding energies 711.7 and 724.0 eV were ascribed to the Fe $2p_{3/2}$ and Fe $2p_{1/2}$ photoelectrons in the Fe^{2+} chemical state whereas the two peaks at 714.2 and 726.2 eV were attributed to the Fe $2p_{3/2}$ and Fe $2p_{1/2}$ photoelectrons in the Fe^{3+} state in the Fe_3O_4 chemical state respectively**.** The two detected bands in **Figure 3b** with binding energies of 933.9 eV and 953.6 eV could be sequentially indexed as Cu(I)2p3/2 and Cu(I)2p1/2. These results demonstrated the presence of Cu(I), which was undetected in XRD pattern of the catalyst. Two weak bands observed in **Figure 5.3b** were categorised as Cu(0)2p3/2 and Cu(0)2p1/2 at binding energies of 932.7 eV and 950.4 eV, respectively. These results were in consistent with the values of copper (I) and copper (0).[34,35]

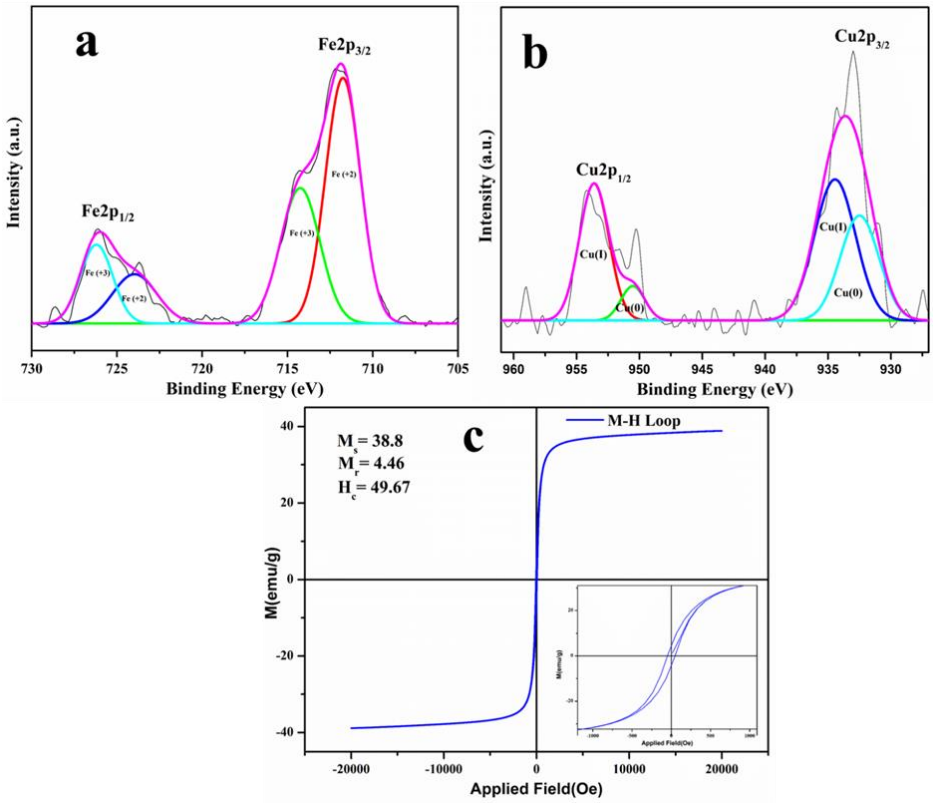

Figure 5.3*. (a) Fe XPS, (b) Cu XPS, (c) VSM of Fe_3O_4-NH_2-Cu.*

The results of the RT magnetization measurements (magnetic hysteresis curve) that were carried out using VSM in order to determine the magnetic behaviour of the Fe_3O_4-NH_2-Cu catalyst were displayed **Figure 5.3c**. The nanocatalyst exhibited a coercivity (H_c) of 49.6 Oe and a remanence (M_r) value of 4.46 emu/g even after the applied magnetic field was removed completely. It was found that the saturation magnetization (M_s) was 38.8 emu/g. This response of synthesized catalyst explicitly supported the presence of ferromagnetic component in it. The assessed magnetic parameters from **Figure 5.3c** revealed the considerable magnetic performance of the synthesised catalyst, thus established the magnetic retrievability and reusability of the catalyst.

5.3.3. Application of Fe_3O_4–NH_2-Cu catalyst in A^3 coupling reactions

A simple A^3 coupling reaction combining amines, aryl aldehyde and phenyl acetylene was performed using the synthesized Fe_3O_4–NH_2-Cu nanocatalyst. Initially, the model reaction was performed with morpholine (1a), 4-methyl benzaldehyde (2a), and phenyl acetylene (3a) using 15 mg of Fe_3O_4–NH_2-Cu nanocatalyst in the presence various solvents at different temperatures for 5 h as shown in **Table 5.1**.

In the presence of solvents such toluene, 1,4-dioxane, DMSO, and DMF, the reaction continued to produce the intended product at 100 °C with a low to moderate yield (**Table 5.1**, **entries 1-4**). At 100 °C with water as the solvent and 60 °C with EtOH as the solvent, the reaction did not progress (**Table 5.1**, **entry 5,6**). The reaction was performed without solvent (neat condition) also at 100 °C and an excellent yield 97% of the product was obtained (**Table 5.1**, **entry 7**). Thus, proved that the solvent was not needed for the reaction. The reaction was carried out under neat condition at various temperatures ranging from RT to 100 °C to understand the impact of temperature (**Table 5.1**, **entries 7−10**). At RT, a very low yield of the product was observed (**Table 5.1**, **entry 8**) and the yield was however increased noticeably at temperatures greater than RT (60 °C, 80 °C, and 100 °C) (**Table 5.1**, **entries 9, 10, 7**). Based on the findings from **Table 5.1**, the optimum temperature was declared as 80 °C. The reaction was examined without a catalyst in order to understand its effect. Since no product was generated, it was established that the catalyst was essential to the progress of the reaction. (**Table 5.1, entry 11**). The reaction was carried out with various amounts of Fe_3O_4–NH_2-Cu nanocatalyst at 80 °C under neat conditions in order to optimise the catalyst quantity. The yields of the product observed with different quantities of catalyst (5 mg, 10 mg, 15 mg,) were 47%, 83%, and 97% respectively. No increase in the yield of the product was observed (97%) when 20 mg of catalyst was used (**Table 5.1**, **entries 12, 13, 10 and 14**). Therefore, it may be concluded that 15 mg of catalyst was the ideal dosage for the reaction.

***Table 5.1**. Optimization of Reaction Conditions for the reaction of morpholine, aldehyde and phenyl acetylene by Fe_3O_4–NH_2-Cu* [a]

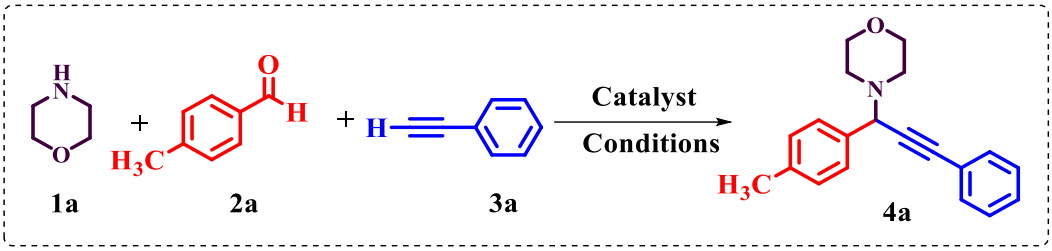

S.No	Solvent	Temperature (°C)	Yield(%)[b]
1	Toluene	100	80
2	1,4-Dioxane	100	75
3	DMF	100	40
4	DMSO	100	65
5	H_2O	100	Trace
6	EtOH	60	Trace
7	Neat	100	97
8	Neat	RT	40
9	Neat	60	82
10	Neat	80	97
11	Neat	80	n.r[c]
12	Neat	80	48[d]
13	Neat	80	83[e]
14	Neat	80	97[f]

[a]**Reaction conditions:** morpholine (1 mmol), 4-methyl benzaldehyde (1 mmol), phenyl acetylene (1.5 mmol), Fe_3O_4–NH_2-Cu catalyst (15 mg) and in solvent (3 mL), time-5h. [b]Isolated yields, [c]Without catalyst reaction, [d]5 mg catalyst, [e]10 mg catalyst, [f]20 mg catalyst.

The Fe_3O_4–NH_2-Cu catalytic system was employed to study the substrate range of A^3 coupling reaction of substituted benzaldehydes with different amines and phenyl acetylene as coupling partners for the synthesis of Propargylamines by following the optimized reaction conditions. The model reaction along with the reaction conditions was shown in **Table 5.2**. When numerous cyclic secondary amines, including piperidine, morpholine, and even noncyclic secondary amines, like Et_2NH, were used to investigate the substrate range, a very good yield of the desired product was discovered, as shown in **Table 5.2.** Substrate scope was also validated with phenyl acetylene and different aldehydes which gave good product yield.

Table 5.2 *Substrate Scope of the A^3 coupling reaction catalysed by Fe_3O_4–NH_2-Cu:*

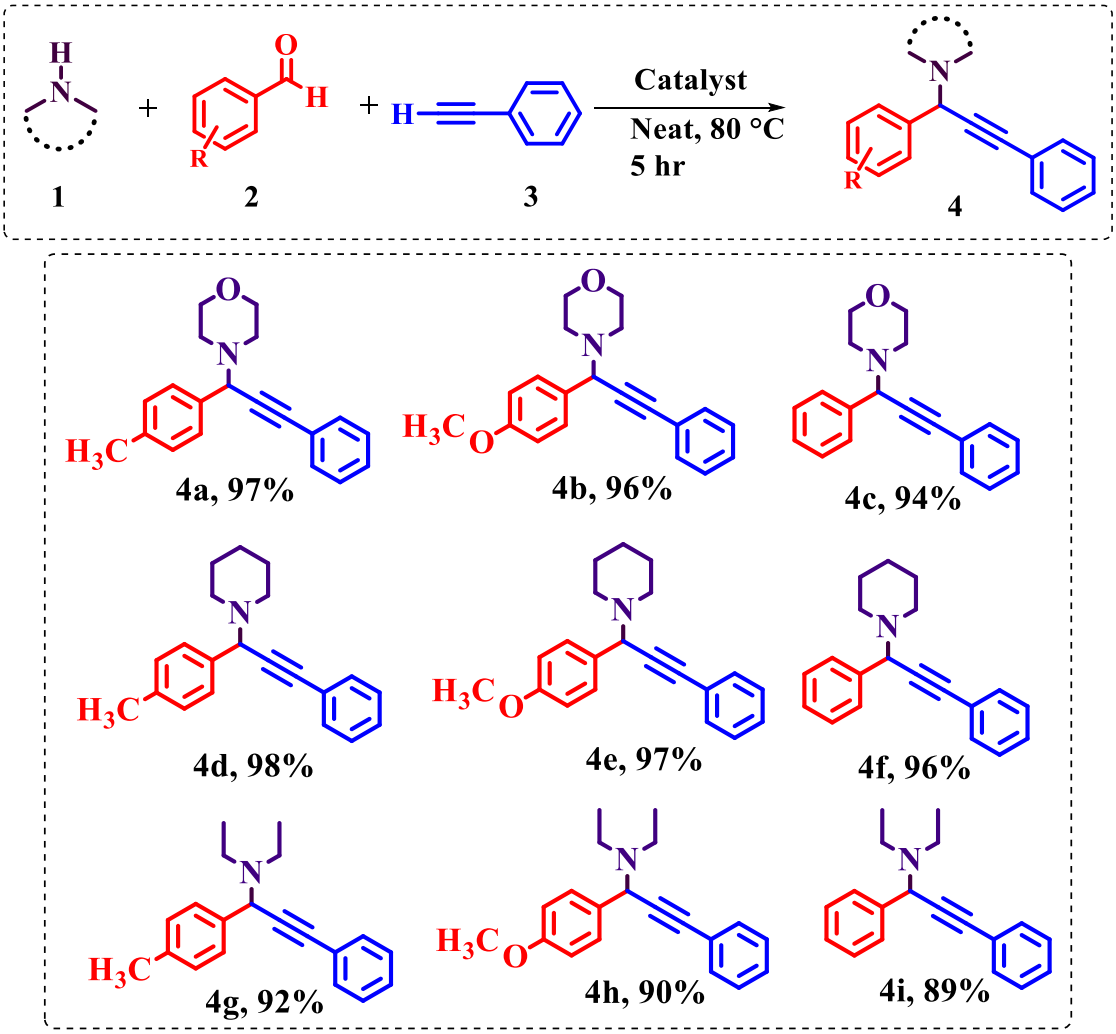

The efficacy of the Fe_3O_4–NH_2-Cu nanocatalyst was compared with previously reported catalysts for A^3 coupling reactions and presented in **Table 5.4.** Catalysts mentioned in **entries 1-4** were complex Cu based materials, consumed more reaction time, and produced less yield in presence of solvent. Catalyst shown in the **entry 5** was also complex Cu based structure, worked under solvent free condition with less reaction time but in microwave condition. The catalysts in **entry 6,7** were expensive Ag and Au based materials and consumed more reaction time. The catalyst in **entry 8** needed less reaction time and used solvent free condition but was expensive Ag based catalyst. **Table 5.4** revealed that in comparison to other catalysts (**entries 1-8**), Fe_3O_4–NH_2-Cu nanocatalyst in the present work functioned effectively in the A^3 coupling reaction in solvent free condition at low temperature (80 °C) in 5 hours with a good yield (97%) of the product. The catalyst could be easily isolated from the reaction mixture by employing an external magnet and could be reused. Catalyst in the current work

thus demonstrated its superiority over previously reported systems by its activity and reusability.

Table 5.4 *Comparison of Fe_3O_4–NH_2-Cu with other previously reported catalysts for A^3 coupling reactions*

S.NO	Catalyst	Solvent	Temperature(°C)	Time (h)	Yield (%)	Ref.
1	Cu Based LMOF 1, MON 1	1,4-Dioxne	90	12	84	[36]
2	Cu@dwCNT	THF	reflux	16	100	[37]
3	Cu/BNNS	H_2O	50	16	96	[38]
4	CTD-GO	H_2O	100	6	92	[39]
5	Cu/NH_2/MCM-41	neat	120 (MW)	2	68	[34]
6	Ag Co/Hi-ZSM-5	H_2O	70	16	86	[40]
7	UiO-66-biguanidine/Au	H_2O	80	10	95	[41]
8	PIm/Fe⌒Zn⌒Ag	neat	90	6	90	[42]
9	**Fe_3O_4–NH_2-Cu**	**neat**	**80**	**5**	**97**	**This work**

5.3.4. Recyclability of the catalyst

Recycling of the catalyst in organic synthesis is an issue of great concern from environmental, economic, and industrial viewpoint. The recyclability of Fe_3O_4–NH_2-Cu nanocatalyst for A^3 coupling reaction was examined here. Using an external magnet, the catalyst was separated from the reaction mixture at the end of each cycle. The magnetically recovered catalyst's activity was assessed in the following run after it had been dried and washed with EtOH. As depicted in **Figure 5.4**, the catalyst was retrieved and used for at least 5 successive runs without noticeable loss in activity as evident from the **Figure 5.4.**

After five cycles, XRD studies have verified the structural stability of the recycled catalyst. There were no impurity peaks in the regenerated catalyst's XRD spectra as evident from **Figure 5.4(b)**. The catalyst's structural stability was thus validated.

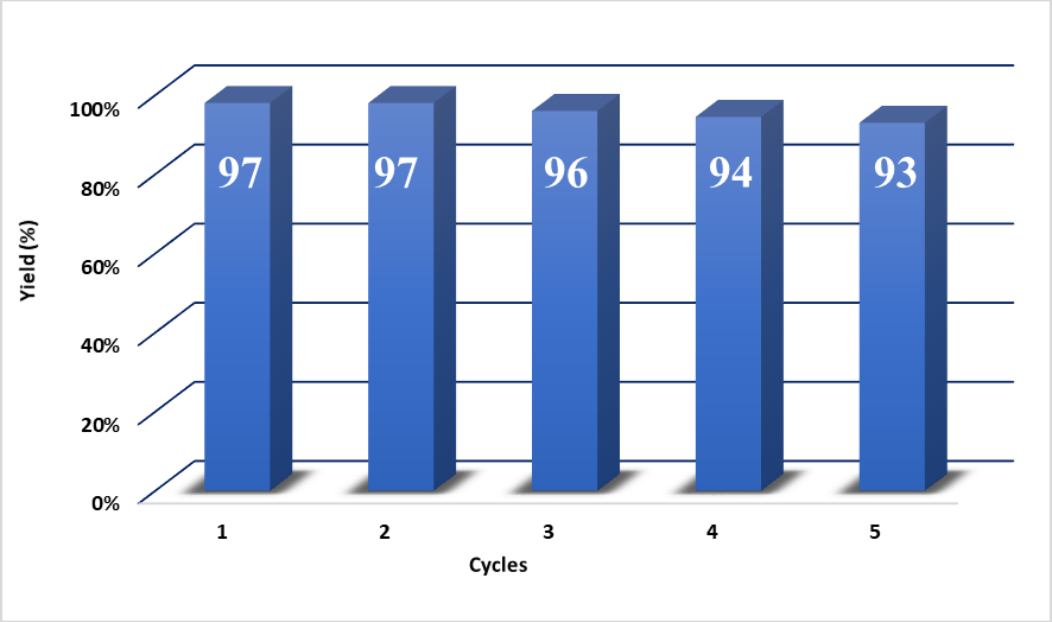

Figure 5.4: *Recyclability test of Fe_3O_4–NH_2-Cu nanocatalyst for A^3 coupling reaction*

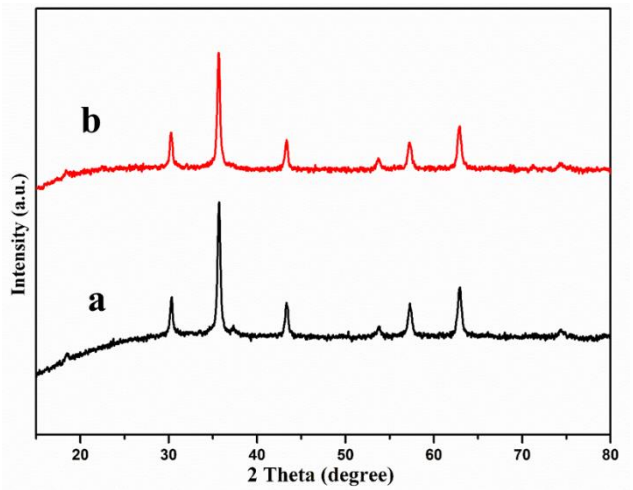

Figure 5.5: *XRD spectra of (a) synthesized Fe_3O_4-NH_2-Cu nanocatalyst (b) used catalyst after 5 cycles*

5.3.5. Plausible Mechanism of A^3 Coupling Reaction

An appropriate reaction mechanism was proposed for the A^3 coupling reaction between amine, aldehyde and phenyl acetylene as shown in **Figure 5.5** based on the prior studies and the aforementioned experimental findings.[43,44,45] This mechanism mainly involved two major steps. The C-H bond was activated in Step 1 by the coordination of a terminal alkyne to Cu supported on amine functionalized Fe_3O_4. The consequence was the formation of intermediate I of the appropriate copper-alkylidine complex. The fact that Cu metal was known to exhibit strong alkynophilicity for terminal alkynes made this a very beneficial step. On the other hand, the iminium ion intermediate II was generated when the aldehyde combines in-situ with

secondary amine. In step 2, the intermediates of the copper-alkylidine complex and the iminium ion interacted to form the appropriate products and regenerated the catalyst.

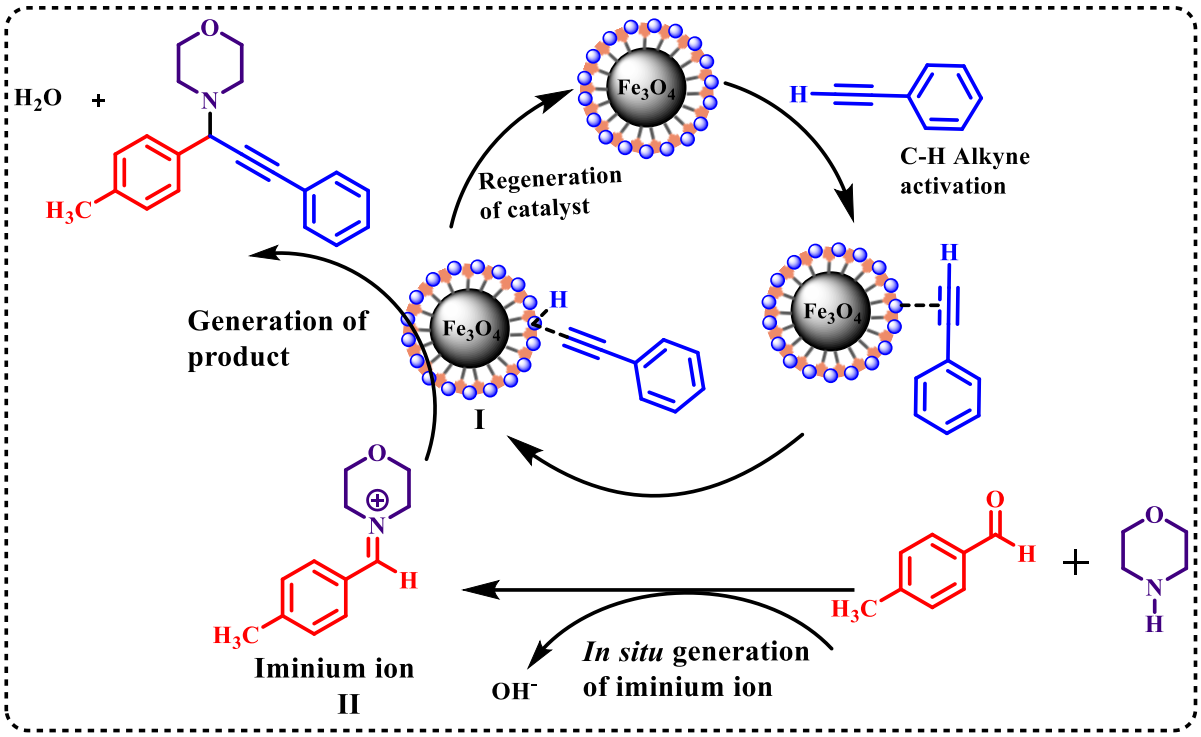

Figure 5.5: *Plausible reaction mechanism for Fe_3O_4–NH_2-Cu catalyzed A^3 coupling reaction*

5.3. Conclusions

In summary, magnetically reusable Fe_3O_4–NH_2-Cu nanocatalyst was synthesized via simple two-step procedure for A^3 coupling reactions under ambient reaction conditions. Catalyst worked excellently well for A^3 coupling reaction under solvent free condition, at low temperature and in less time with good yield of the product (97%). The effectiveness of the catalyst was demonstrated for substituted substrates in A^3 coupling reactions that produced excellent product yields. Without experiencing a significant reduction in activity, the catalyst was discovered to exhibit high reusability for at least five cycles. After 5 cycles, the structural stability of the reused catalyst was confirmed by XRD. The findings of the current study provided a sustainable approach to synthesize magnetically reusable Fe_3O_4–NH_2-Cu nanocatalyst for A^3 coupling reaction with broad substrate scope.

5.4. Spectral data of synthesized products of A^3 coupling reaction 3a-3i

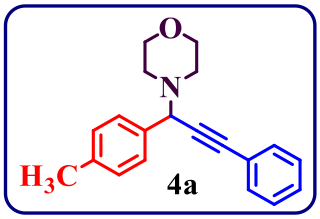

4-(3-phenyl-1-(p-tolyl)prop-2-yn-1-yl)morpholine

^{1}H NMR (400 MHz, $CDCl_3$): δ (ppm): 7.52−7.48 (m, 4H), 7.33−7.31 (m, 3H), 7.17 (d, *J* = 7.8 Hz, 2H), 4.74 (s, 1H), 3.74−3.71 (m, 4H), 2.64 – 2.61 (m, 4H), 2.36 (s, 3H); ^{13}C NMR (100 MHz, $CDCl_3$): δ (ppm): 137.50, 134.80, 131.81, 128.93, 128.54, 128.30, 128.21, 123.07, 88.26, 85.35, 67.18, 61.81, 49.92, 21.12.

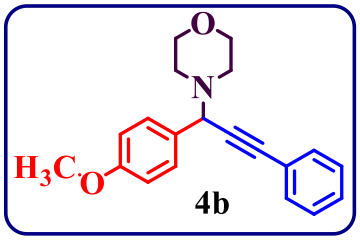

4-(1-(4-methoxyphenyl)-3-phenylprop-2-yn-1-yl)morpholine

^{1}H NMR (400 MHz, $CDCl_3$): δ (ppm): 7.54−7.49 (m, 4H), 7.35−7.31 (m, 3H), 6.90 (d, *J* = 8.8 Hz, 2H), 4.73 (s, 1H), 3.81 (s, 3H), 3.76−3.68 (m, 4H), 2.67 – 2.57 (m, 4H); ^{13}C NMR (100 MHz, $CDCl_3$): δ (ppm): 159.22, 131.81, 129.90, 129.74, 128.32, 128.24, 123.04, 113.57, 88.26, 85.39, 67.19, 61.46, 55.31, 49.82.

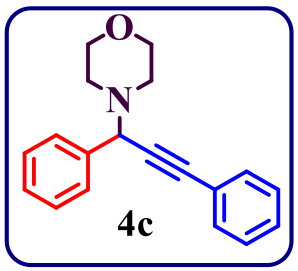

4-(1,3-diphenylprop-2-yn-1-yl)morpholine

^{1}H NMR (400 MHz, $CDCl_3$): δ (ppm): 7.63 (d, *J* = 7.0 Hz, 2H), 7.53−7.50 (m, 2H), 7.39−7.31 (m, 6H), 4.79 (s, 1H), 3.78−3.70 (m, 4H), 2.67 – 2.60 (m, 4H); ^{13}C NMR (100 MHz, $CDCl_3$): δ (ppm): 137.79, 131.82, 128.62, 128.33, 128.27, 128.25, 127.80, 122.99, 88.52, 85.05, 67.16, 62.06, 49.89.

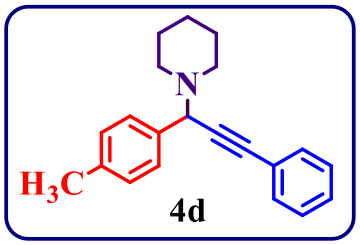

1-(3-phenyl-1-(p-tolyl)prop-2-yn-1-yl)piperidine

^{1}H NMR (400 MHz, $CDCl_3$): δ (ppm): 7.52−7.48 (m, 4H), 7.32−7.28 (m, 3H), 7.15 (d, *J* = 7.8 Hz, 2H), 4.76 (s, 1H), 2.60−2.53 (m, 4H), 2.34 (s, 3H), 1.63 – 1.54 (m, 4H), 1.45– 1.41 (m, 2H); ^{13}C NMR (100 MHz, $CDCl_3$): δ (ppm): 137.17, 135.51, 131.85, 128.82, 128.57, 128.31, 128.06, 123.45, 87.70, 86.38, 62.16, 50.69, 26.19, 24.50, 21.18.

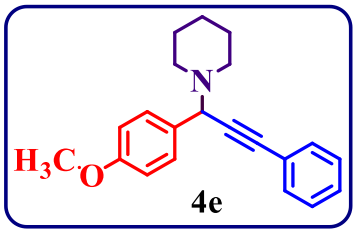

1-(1-(4-methoxyphenyl)-3-phenylprop-2-yn-1-yl)piperidine

^{1}H NMR (400 MHz, $CDCl_3$): δ (ppm): 7.54−7.49 (m, 4H), 7.33−7.29 (m, 3H), 6.88 (d, *J* = 8.8 Hz, 2H), 4.75 (s, 1H), 3.80 (s, 3H), 2.57−2.52 (m, 4H), 1.63 – 1.54 (m, 4H), 1.44– 1.41 (m, 2H); ^{13}C NMR (100 MHz, $CDCl_3$): δ (ppm): 159.02, 131.82, 130.63, 129.72, 128.29, 128.04, 123.40, 113.42, 87.66, 86.40, 61.79, 55.29, 50.61, 26.16, 24.49.

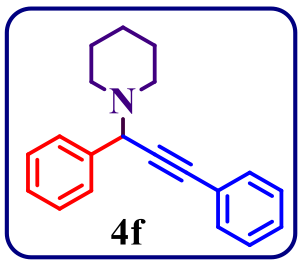

1-(1,3-diphenylprop-2-yn-1-yl)piperidine

^{1}H NMR (400 MHz, $CDCl_3$): δ (ppm): 7.63 (d, *J* = 6.8 Hz, 2H), 7.53−7.50 (m, 2H), 7.38−7.30 (m, 6H), 4.85 (s, 1H), 2.60 (t, *J* = 5.2 Hz, 4H), 1.64 – 1.57 (m, 4H), 1.47– 1.42 (m, 2H); ^{13}C NMR (100 MHz, $CDCl_3$): δ (ppm): 138.18, 131.83, 129.80, 128.70, 128.30, 128.10, 127.59, 123.27, 87.96, 85.87, 62.29, 50.62, 25.99, 24.35.

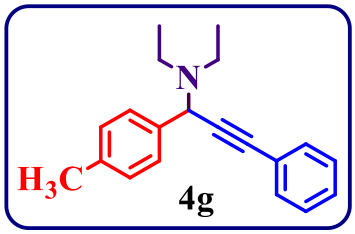

N,N-diethyl-3-phenyl-1-(p-tolyl)prop-2-yn-1-amine

^{1}H NMR (400 MHz, $CDCl_3$): δ (ppm): 7.56 (d, *J* = 7.8 Hz, 2H), 7.51−7.48 (m, 2H), 7.33−7.28 (m, 3H), 7.16 (d, *J* = 7.8 Hz, 2H), 5.03 (s, 1H), 2.68 – 2.52 (m, 4H), 2.35 (s, 3H), 1.08 (t, *J* = 7.2 Hz, 6H); ^{13}C NMR (100 MHz, $CDCl_3$): δ (ppm): 136.95, 136.62, 131.80, 128.78, 128.37, 128.30, 128.01, 123.46, 87.34, 86.33, 56.79, 44.52, 21.13, 13.45.

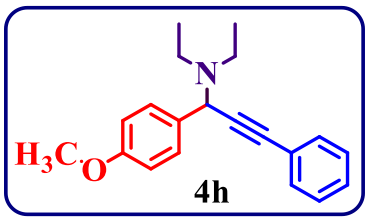

N,N-diethyl-1-(4-methoxyphenyl)-3-phenylprop-2-yn-1-amine

^{1}H NMR (400 MHz, $CDCl_3$): δ (ppm): 7.59 (d, *J* = 8.6 Hz, 2H), 7.52−7.47 (m, 2H), 7.34−7.29 (m, 3H), 6.89 (d, *J* = 8.8 Hz, 2H), 5.01 (s, 1H), 3.81 (s, 3H), 2.67 – 2.51 (m, 4H), 1.08 (t, *J* = 7.2 Hz, 6H); ^{13}C NMR (100 MHz, $CDCl_3$): δ (ppm): 158.90, 131.79, 129.52, 129.36, 128.30, 128.02, 123.43, 113.41, 87.35, 86.38, 56.48, 55.29, 44.48, 13.51.

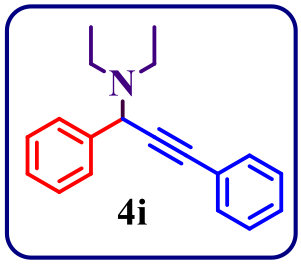

N,N-diethyl-1,3-diphenylprop-2-yn-1-amine

^{1}H NMR (400 MHz, $CDCl_3$): δ (ppm): 7.68 (d, *J* = 8.0 Hz, 2H), 7.53−7.49 (m, 2H), 7.38−7.27 (m, 6H), 5.05 (s, 1H), 2.70 – 2.50 (m, 4H), 1.08 (t, *J* = 7.2 Hz, 6H); ^{13}C NMR (100 MHz, $CDCl_3$): δ (ppm): 139.85, 131.80, 128.39, 128.30, 128.04, 127.27, 123.42, 87.47, 86.12, 57.03, 44.58, 13.56.

5.5. References

(1) Querard, P.; Girard, S. A.; Uhlig, N.; Li, C. J. Gold-Catalyzed Tandem Reactions of Amide-Aldehyde-Alkyne Coupling and Cyclization-Synthesis of 2,4,5-Trisubstituted Oxazoles. *Chem. Sci.* **2015**, *6* (12), 7332–7335..

(2) Wei, C.; Li, Z.; Li, C. J. The Development of A^3-Coupling (Aldehyde-Alkyne-Amine) and AA^3-Coupling (Asymmetric Aldehyde-Alkyne-Amine). *Synlett* **2004**, 9, 1472–1483.

(3) Wei, C.; Li, C. J. A Highly Efficient Three-Component Coupling of Aldehyde, Alkyne, and Amines via C-H Activation Catalyzed by Gold in Water. *J. Am. Chem. Soc.* **2003**, *125* (32), 9584–9585.

(4) Peshkov, V. A.; Pereshivko, O. P.; Van der Eycken, E. V. A Walk around the A^3-Coupling. *Chem. Soc. Rev.* **2012**, *41* (10), 3790–3807.

(5) Wei, C.; Li, Z.; Li, C. J. The First Silver-Catalyzed Three-Component Coupling of Aldehyde, Alkyne, and Amine. *Org. Lett.* **2003**, *5* (23), 4473–4475.

(6) Shi, L.; Tu, Y. Q.; Wang, M.; Zhang, F. M.; Fan, C. A. Microwave-Promoted Three-Component Coupling of Aldehyde, Alkyne, and Amine via C-H Activation Catalyzed by Copper in Water. *Org. Lett.* **2004**, *6* (6), 1001–1003.

(7) Rasheed, O. K.; Bawn, C.; Davies, D.; Raftery, J.; Vitorica-Yrzebal, I.; Pritchard, R.; Zhou, H.; Quayle, P. The Synthesis of Group 10 and 11 Metal Complexes of 3,6,9-Trithia-1-(2,6)-Pyridinacyclodecaphane and Their Use in A^3-Coupling Reactions. *European J. Org. Chem.* 2017, ***2017*** (35), 5252–5261.

(8) Beillard, A.; Métro, T. X.; Bantreil, X.; Martinez, J.; Lamaty, F. A^3-Coupling Reaction and [Ag(IPr)2]PF6: A Successful Couple. *European J. Org. Chem.* **2017**, *2017* (31), 4642–4647.

(9) Frindy, S.; El Kadib, A.; Lahcini, M.; Primo, A.; García, H. Copper Nanoparticles Supported on Graphene as an Efficient Catalyst for A^3 Coupling of Benzaldehydes. *Catal. Sci. Technol.* **2016**, *6* (12), 4306–4317.

(10) Trose, M.; Dell'Acqua, M.; Pedrazzini, T.; Pirovano, V.; Gallo, E.; Rossi, E.; Caselli, A.; Abbiati, G. [Silver(I)(Pyridine-Containing Ligand)] Complexes as Unusual Catalysts for A^3-Coupling Reactions. *J. Org. Chem.* **2014**, *79* (16), 7311–7320.

(11) Jiang, Y.; Zhang, X.; Dai, X.; Zhang, W.; Sheng, Q.; Zhuo, H.; Xiao, Y.; Wang, H. Microwave-Assisted Synthesis of Ultrafine Au Nanoparticles Immobilized on MOF-199 in High Loading as Efficient Catalysts for a Three-Component Coupling Reaction. *Nano Res.* **2017**, *10* (3), 876–889.

(12) Mandlimath, T. R.; Sathiyanarayanan, K. I. Facile Synthesis of $ZnAl_2O_4$ Nanoparticles: Efficient and Reusable Porous Nano $ZnAl_2O_4$ and Copper Supported on $ZnAl_2O_4$ Catalysts for One Pot Green Synthesis of Propargylamines and Imidazo[1,2-a]Pyridines by A^3 Coupling Reactions. *RSC Adv.* **2016**, *6* (4), 3117–3125.

(13) Tan, Y. J.; Wang, F. J.; Asirib, A. M.; Marwanib, H. M.; Zhang, Z. $FeCl_3$-Mediated One-Pot Cyclization–Aromatization of Anilines, Benzaldehydes, and Phenylacetylenes under Ball Milling: A New Alternative for the Synthesis of 2,4-Diphenylquinolines. *J. Chinese Chem. Soc.* **2018**, *65* (1), 65–73.

(14) Zhang, Y.; Li, P.; Wang, M.; Wang, L. Indium-Catalyzed Highly Efficient Three-Component Coupling of Aldehyde , Alkyne , and Amine via C - H Bond Activation In This Paper , Indium (III) Chloride Was Found to Be a Highly Effective Catalyst for the Three-Component Coupling Reactions of Aldehyd. *J. Org. Chem.* **2009**, *74*, 4364–4367.

(15) Samai, S.; Nandi, G. C.; Singh, M. S. An Efficient and Facile One-Pot Synthesis of Propargylamines by Three-Component Coupling of Aldehydes, Amines, and Alkynes via C-H Activation Catalyzed by $NiCl_2$. *Tetrahedron Lett.* **2010**, *51* (42), 5555–5558.

(16) Li, P. H.; Wang, L. Mercurous Chloride Catalyzed Mannich Condensation of Terminal Alkynes with Secondary Amines and Aldehydes. *Chinese J. Chem.* **2005**, *23* (8), 1076–1080.

(17) Rubio-Pérez, L.; Iglesias, M.; Munárriz, J.; Polo, V.; Pérez-Torrente, J. J.; Oro, L. A. Efficient Rhodium-Catalyzed Multicomponent Reaction for the Synthesis of Novel Propargylamines. *Chem. - A Eur. J.* **2015**, *21* (49), 17701–17707.
(18) Chen, W. W.; Bi, H. P.; Li, C. J. The First Cobalt-Catalyzed Transformation of Alkynyl C-H Bond: Aldehyde-Alkyne-Amine (A^3) Coupling. *Synlett* **2010**, 3, 475–479.
(19) dos Santos, G. C.; Moreno, V. F.; Oshiro, P. B.; da Silva-Filho, L. C. $NbCl_5$ a Multifunctional Reagent for the Synthesis of New Halogenated Aminoquinoline Compounds through Innovative One-Pot Reaction and the Acidochromism Effect. *Tetrahedron* **2018**, *74* (42), 6144–6149.
(20) Volkova, Y.; Baranin, S.; Zavarzin, I. A^3 Coupling Reaction in the Synthesis of Heterocyclic Compounds. *Adv. Synth. Catal.* **2021**, *363* (1), 40–61.
(21) Nasrollahzadeh, M.; Mohammad Sajadi, S.; Rostami-Vartooni, A. Green Synthesis of CuO Nanoparticles by Aqueous Extract of Anthemis Nobilis Flowers and Their Catalytic Activity for the A^3 Coupling Reaction. *J. Colloid Interface Sci.* **2015**, *459*, 183–188.
(22) Wang, D.; Astruc, D. The Recent Development of Efficient Earth-Abundant Transition-Metal Nanocatalysts. *Chem. Soc. Rev.* **2017**, *46* (3), 816–854.
(23) Bukowska, A.; Bukowski, W.; Bester, K.; Hus, K. Polymer Supported Copper(II) Amine-Imine Complexes in the C-N and A^3 Coupling Reactions. *Appl. Organomet. Chem.* **2017**, *31* (12), 1–15.
(24) Sadjadi, S.; Heravi, M. M.; Ebrahimizadeh, M. Synthesis of Cu@Fur-SBA-15 as a Novel Efficient and Heterogeneous Catalyst for Promoting A^3-Coupling under Green and Mild Reaction Conditions. *J. Porous Mater.* **2018**, *25* (3), 779–788.
(25) Ramu, V. G.; Bordoloi, A.; Nagaiah, T. C.; Schuhmann, W.; Muhler, M.; Cabrele, C. Copper Nanoparticles Stabilized on Nitrogen-Doped Carbon Nanotubes as Efficient and Recyclable Catalysts for Alkyne/Aldehyde/Cyclic Amine A^3-Type Coupling Reactions. *Appl. Catal. A Gen.* **2012**, *431–432*, 88–94.
(26) Cheng, S.; Shang, N.; Feng, C.; Gao, S.; Wang, C.; Wang, Z. Efficient Multicomponent Synthesis of Propargylamines Catalyzed by Copper Nanoparticles Supported on Metal-Organic Framework Derived Nanoporous Carbon. *Catal. Commun.* **2017**, *89*, 91–95.
(27) Sharma, S.; Kaur, M.; Sharma, C.; Choudhary, A.; Paul, S. Biomass-Derived Activated Carbon-Supported Copper Catalyst : An E Ffi Cient Heterogeneous Magnetic Catalyst for Base-Free Chan − Lam Coupling and Oxidations. **2021**.
(28) Tandon, R.; Tandon, N.; Patil, S. M. Overview on Magnetically Recyclable Ferrite Nanoparticles: Synthesis and Their Applications in Coupling and Multicomponent Reactions. *RSC Adv.* **2021**, *11* (47), 29333–29353.
(29) Zhang, F.; Jin, J.; Zhong, X.; Li, S.; Niu, J.; Li, R.; Ma, J. Pd Immobilized on Amine-Functionalized Magnetite Nanoparticles: A Novel and Highly Active Catalyst for Hydrogenation and Heck Reactions. *Green Chem.* **2011**, *13* (5), 1238–1243.
(30) Sharma, R. K.; Dutta, S.; Sharma, S. Quinoline-2-Carboimine Copper Complex Immobilized on Amine Functionalized Silica Coated Magnetite Nanoparticles: A Novel and Magnetically Retrievable Catalyst for the Synthesis of Carbamates via C-H Activation of Formamides. *Dalt. Trans.* **2014**, *44* (3), 1303–1316.
(31) Karimzadeh, I.; Aghazadeh, M.; Doroudi, T.; Ganjali, M. R.; Kolivand, P. H.; Gharailou, D. Amino Acid Coated Superparamagnetic Iron Oxide Nanoparticles for Biomedical Applications Through a Novel Efficient Preparation Method. *J. Clust. Sci.* **2017**, *28* (3), 1259–1271.
(32) Aoopngan, C.; Nonkumwong, J.; Phumying, S.; Promjantuek, W.; Maensiri, S.; Noisa, P.; Pinitsoontorn, S.; Ananta, S.; Srisombat, L. Amine-Functionalized and Hydroxyl-Functionalized Magnesium Ferrite Nanoparticles for Congo Red Adsorption. *ACS Appl. Nano Mater.* **2019**, *2* (8), 5329–5341.

(33) Alazemi, A. M.; Dawood, K. M.; Al-Matar, H. M.; Tohamy, W. M. Efficient and Recyclable Solid-Supported Pd(II) Catalyst for Microwave-Assisted Suzuki Cross-Coupling in Aqueous Medium. *ACS Omega* **2022**, *7* (33), 28831–28848.

(34) Terra, J. C. S.; Moores, A.; Moura, F. C. C. Amine-Functionalized Mesoporous Silica as a Support for on-Demand Release of Copper in the A^3-Coupling Reaction: Ultralow Concentration Catalysis and Confinement Effect. *ACS Sustain. Chem. Eng.* **2019**, *7* (9), 8696–8705.

(35) Salehzadeh, F.; Esmkhani, M.; Zallaghi, M.; Javanshir, S.; Dekamin, M. G. $CuFe_2O_4$@SiO_2@L-Arginine@Cu(I) as a New Magnetically Retrievable Heterogeneous Nanocatalyst with High Efficiency for 1,4-Disubstituted 1,2,3-Triazoles Synthesis. *Sci. Rep.* **2023**, *13* (1), 1–9.

(36) Xia, Q.; Zhang, S.; Zhang, Y.; Bai, R.; Li, S.; Zhang, J.; Chen, X. Few-Layered Metal-Organic Framework Nanosheets as Catalysts for the Synthesis of 2,3-Dihydroquinazolinone and Propargylamines. *ACS Appl. Nano Mater.* **2021**, *4* (11), 12108–12118.

(37) Mesguich, D.; Moumaneix, L.; Henri, V.; Legnani, M.; Collière, V.; Esvan, J.; Ouali, A.; Fau, P. Grafting Copper Atoms and Nanoparticles on Double-Walled Carbon Nanotubes: Application to Catalytic Synthesis of Propargylamine. *Langmuir* **2022**, *38* (28), 8545–8554.

(38) Piranloo, F. G.; Abharian, M. K.; Kavousi, F.; Luque, R. Copper Nanoparticles Decorated on Boron Nitride Nanoflakes as an Efficient Catalyst for the Synthesis of Propargylamines under Green Conditions. *Mol. Catal.* **2022**, *533* (October), 112687.

(39) Tarahomi, M.; Alinezhad, H.; Maleki, B. Immobilizing Pd Nanoparticles on the Ternary Hybrid System of Graphene Oxide, Fe_3O_4 Nanoparticles, and PAMAM Dendrimer as an Efficient Support for Catalyzing Sonogashira Coupling Reaction. *Appl. Organomet. Chem.* **2019**, *33* (11), 1–13.

(40) Kalbasi, R. J.; Khojastegi, A. Fabrication of Bimetallic Ag-Co Nanoparticle Deposited on Hierarchical ZSM-5 as a Selective Catalyst for Synthesis of Propargylamine in Water via Multicomponent A^3 Coupling. *ChemistrySelect* **2018**, *3* (44), 12666–12675.

(41) Veisi, H.; Sayadi, M.; Morakabati, N.; Tamoradi, T.; Karmakar, B. Au NPs Fabricated on Biguanidine-Modified Zr-UiO-66 MOFs: A Competent Reusable Heterogeneous Nanocatalyst in the Green Synthesis of Propargylamines. *New J. Chem.* **2022**, *46* (6), 2829–2836.

(42) Yesmin, S.; Abbas, S. J.; Ke, S. C. A Powerful and Multifunctional Catalyst for Organic Synthesis, Transformation, and Environmental Remediation: A PolyImidazole Supported Trimetallic Catalyst. *Appl. Catal. B Environ.* **2022**, *316* (March), 121629.

(43) Borah, B. J.; Borah, S. J.; Saikia, L.; Dutta, D. K. Efficient Three-Component Coupling Reactions Catalyzed by Cu0-Nanoparticles Stabilized on Modified Montmorillonite. *Catal. Sci. Technol.* **2014**, *4* (4), 1047–1054.

(44) Cirujano, F. G.; Dhakshinamoorthy, A. Supported Metals on Porous Solids as Heterogeneous Catalysts for the Synthesis of Propargylamines. *New J. Chem.* **2022**, *46* (4), 1469–1482.

(45) Aliaga-Lavrijsen, M.; Herrera, R. P.; Villacampa, M. D.; Concepción Gimeno, M. Efficient Gold(I) Acyclic Diaminocarbenes for the Synthesis of Propargylamines and Indolizines. *ACS Omega* **2018**, *3* (8), 9805–9813.

5.7. Selected NMR (^{1}H & ^{13}C) spectra of Products

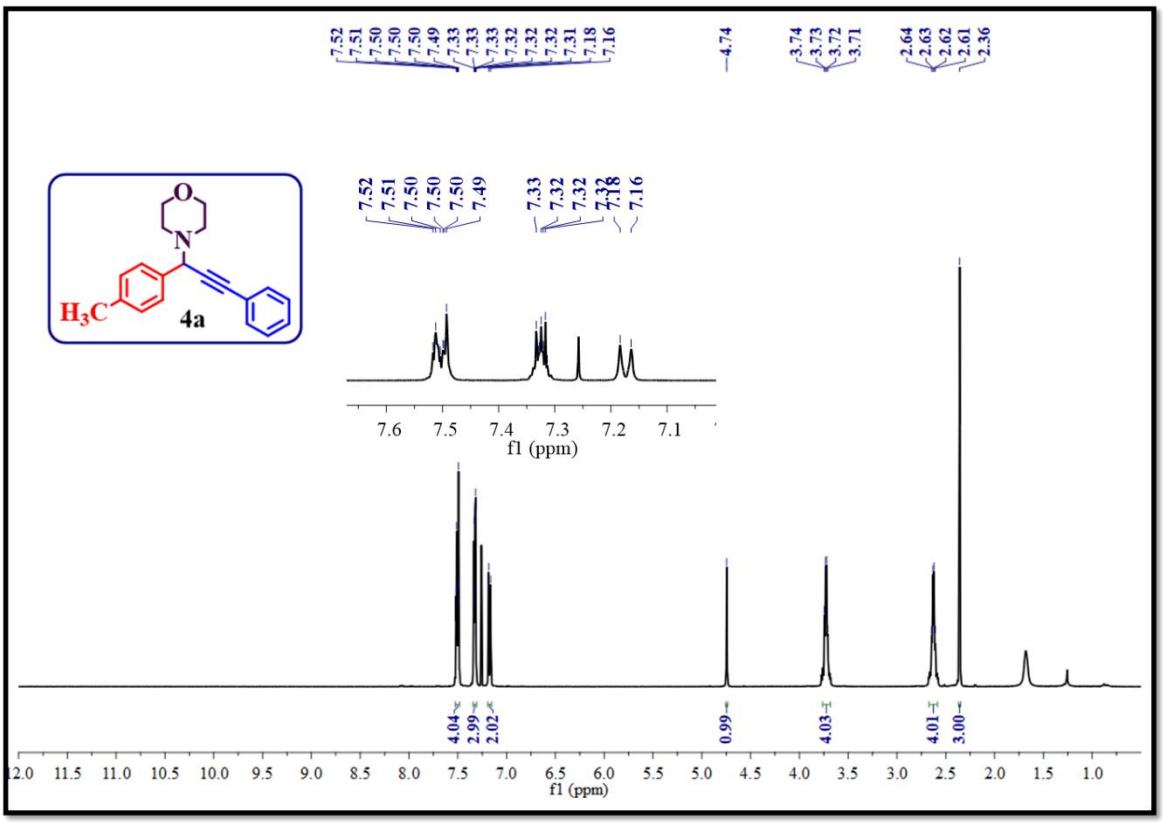

^{1}H NMR spectrum of the compound 4-(3-phenyl-1-(p-tolyl)prop-2-yn-1-yl)morpholine (4a).

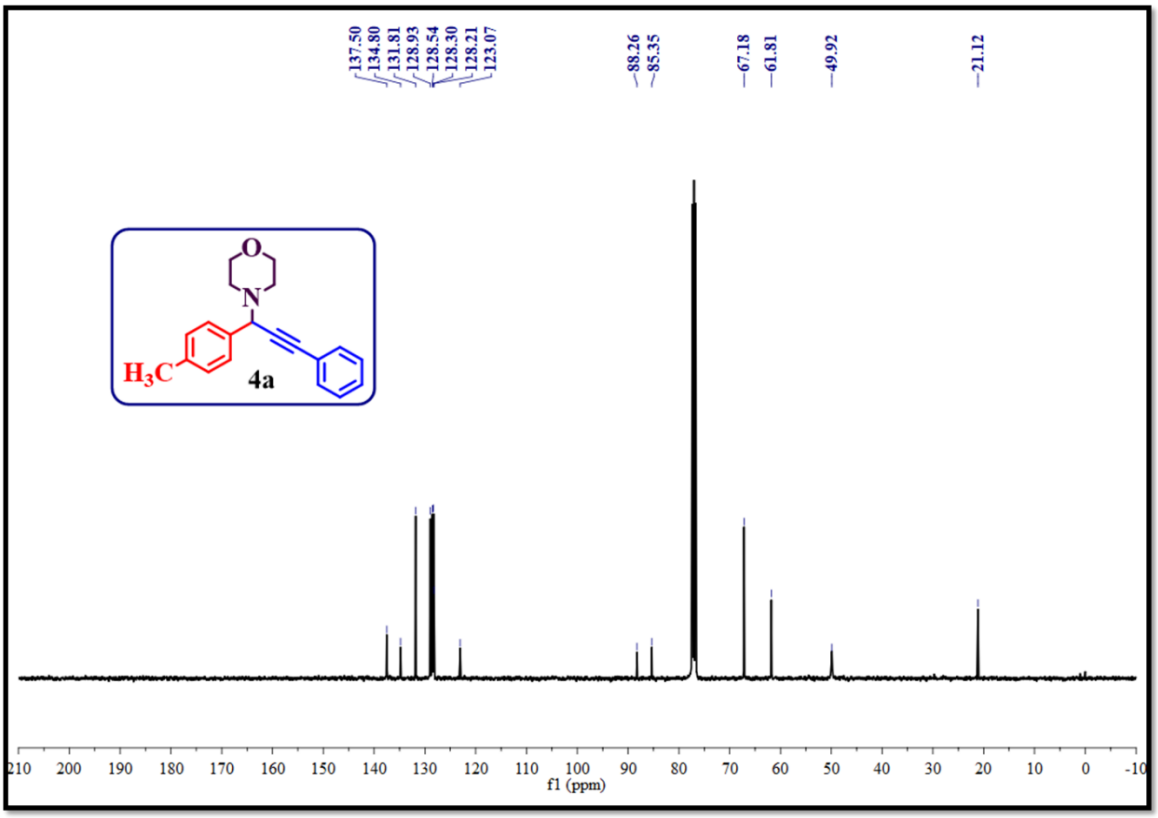

^{1}H NMR spectrum of the compound 4-(3-phenyl-1-(p-tolyl)prop-2-yn-1-yl)morpholine (4a).

CHAPTER-VI

Immobilization of Ag Nanoparticles on $NiFe_2O_4$@TiO_2@PDA for Reduction of Nitro Aromatic Compounds

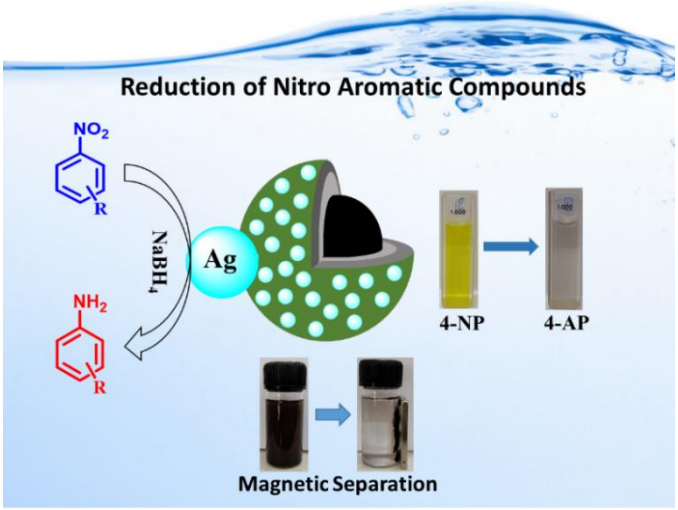

Chapter-VI

Immobilization of Ag Nanoparticles on $NiFe_2O_4$@TiO_2@PDA for Reduction of Nitro Aromatic Compounds

6.1. Introduction

Nitroarenes are specified as priority class of pollutants by USEA (United States Environmental Agency) that are let out from industrial effluents, agricultural waste and other sources.[1] Even low doses of nitroarenes have an impact on both anti-androgenic and estrogenic functions in living beings.[2] The acceptable limit of nitroarenes in water is 20 ppb as suggested by WHO and also it is very difficult to remove them by simple means owing to their good chemical stability and non-biodegradable nature.[3] Thus, significant research is necessary to reduce nitroarenes because of aforementioned harmful effects on the environment and human health and also due to associated stringent limits. 4-Nitrophenol (4-NP) among Nitroarenes is a pollutant of great concern as it is reported to be genotoxic, carcinogenic that cause serious harm to the human beings by affecting kidney, liver, respiratory, cardio vascular, central nervous system and lethal diseases in animal blood.[4] Simple degradation of 4-NP would merely remove the pollution, but reducing the nitro to an amino group would be more desirable because it would turn the hazardous pollutants into valuable industrial intermediates. Therefore, creating a straightforward and efficient process for converting such hazardous contaminants into safe chemicals remains a challenge. Nitrobenzene can be reduced to aniline which is an important and useful intermediates in the synthesis of food additives, medicines, agrochemicals, and other platform chemicals.[5]

Reduction of 4-NP demands catalytic and non-catalytic approach using different reducing agents.[6,7,8] The non-catalytic approach usually use either Bechamp or sulphide reduction technique which is associated with generation of enormous quantity of objectionable waste that is pernicious to the environment and moreover, reduction of 4-NP is a very slow process. On the other hand, the catalytic reduction technique for the reduction of 4-NP which needs catalyst give preference to the expensive metals such as Pd and Pt which are precious and sensitive to air and moisture.[9,10,11] However, metal NPs undergo agglomeration during the reaction process thus reducing their catalytic activity.[12] To overcome this, several matrices such as MOF's, rGO, WO_3, polydopamine (PDA) etc., have been reported to be used as solid supports for immobilising the metal NPs. Another limitation associated with metal NPs is the difficulty of their separation from the reaction mixture by simple means such as filtration or centrifugation. To overcome this, it was reported that magnetic component such as spinel ferrite

can be incorporated into the matrix due to its easy preparation, cost effectiveness and good stability to prepare a heterogeneous magnetically retrievable catalyst.[13] Thus, in spite of many reported catalysts, magnetically reusable catalysts with multifunctional behaviour are trending, owing to their sustainable approach. To address the need it is proposed to develop a magnetically reusable nanocatalyst in the present work for the reduction of 4-NP to from 4-amino phenol (4-AP) in the presence of $NaBH_4$ in water (green solvent). $NaBH_4$ was used as common reducing agent for the hydrogenation. When it was used as a reducing agent in the presence of transition metal catalyst, it was reported that large excess of $NaBH_4$ (~100-folds) was needed compared to substrate.[14,15] Thus it is challenging to design an appropriate catalyst that could enhance the catalytic activity and decrease the quantity of $NaBH_4$ required.[16]

To address the need, $NiFe_2O_4$ based core-shell type catalyst was developed in the current work for the reduction of 4-NP with a further scope of its multifunctional applications in photocatalysis. The catalyst was designed with $NiFe_2O_4$ as core and TiO_2 as shell whose surface was modified by Polydopamine (PDA) for effective immobilization of Ag NPs to result in magnetically reusable $NiFe_2O_4$@TiO_2@PDA-Ag catalyst for the reduction of 4-NP. Magnetic retrievability and reusability of the catalyst for more cycles was an added advantage of the catalyst. Besides all these facts, a simple methodology for the synthesis of the catalyst was adopted in this work. $NiFe_2O_4$ was synthesized via facile hydrothermal method in the first step. Preparation of $NiFe_2O_4$@TiO_2 (core@shell) nanostructure, PDA coating on $NiFe_2O_4$@TiO_2, and Ag immobilisation of PDA coated $NiFe_2O_4$@TiO_2 were performed in the subsequent steps by simple stirring at room temperature (RT). Among many synthesis methods for the synthesis of ferrite NPs, the hydrothermal method was preferred to synthesize $NiFe_2O_4$[17,18] because of its advantages.

Hence, based on all the aforementioned facts and in the process the development of novel ferrite based heterogeneous reusable nanocatalyst for various organic applications, the present catalyst was developed. Therefore, the present work reports the synthesis of Ag NPs immobilised, PDA coated $NiFe_2O_4$@TiO_2 (core@shell) heterogeneous magnetic nanocatalyst ($NiFe_2O_4$@TiO_2@PDA-Ag) *via* environmentally benign methodology with high efficiency for the aqueous phase chemical reduction of nitroarenes and heteronitroarenes to the corresponding amines in the presence of $NaBH_4$ as reducing agent in aqueous medium. The optimized conditions were used for the reduction of different substituted aromatic nitro arenes also. And also, multifunctional behaviour of the catalyst was explored for its photocatalytic applications.

6.2. Experimental Section

6.2.1. Materials

$Ni(NO_3)_2.6H_2O$ (Finar, 99%); $Fe(NO_3)_3.9H_2O$ (Finar, 99%); titanium tetraisopropoxide (TTIP) (Sigma-Aldrich, 99%); dopamine hydrochloride (98%); $AgNO_3$ (Sigma-Aldrich, 99%); $NaBH_4$ (Finar, 99%); HNO_3 (Finar, 69%); NaOH (Finar, 96%); ethanol (EtOH, Finar, 99%); methanol (MeOH, Finar, 99%), 4-NP (Sigma-Aldrich, 99%), MB (Sigma-Aldrich, 85%), CIP (TCI, 98%) were employed as starting materials and Double Distilled (DD) water was used during the course of the experiments.

6.2.2. Synthesis of $NiFe_2O_4$ NPs

The hydrothermal method was used to synthesize $NiFe_2O_4$ NPs. In this process, 40 mL of DD water was used to dissolve $Ni(NO_3)_2.6H_2O$ and $Fe(NO_3)_3.9H_2O$ in a 1:2 ratio. After 15 minutes of stirring at RT, a clear solution was attained. The pH of the solution was maintained at ~12 by using 2M NaOH solution and with continuous stirring for 30 minutes. The resultant mixture was positioned in a stainless steel autoclave and heated for 12 hours at 180 °C. It was then allowed to cool to RT. The obtained product was dried in an oven at 60 °C after washing with DD water and ethanol three times. It was then calcined for 2 h at 800 °C. In this way $NiFe_2O_4$ NPs were synthesized.

6.2.3. Synthesis of $NiFe_2O_4$@TiO_2 (core@shell) Nanostructure

50 mL of methanol was used to disperse 1 g of synthesized $NiFe_2O_4$. The mixture was magnetically stirred for 15 minutes. 2.5 g of (TTIP) [yield of TiO_2 (anatase): 1 g] was added into the mixture and stirred for 10 minutes followed by the addition of 10 mL DD water. After 10 minutes, HNO_3 was added slowly to maintain the solution pH at 2. The resulting mixture was vigorously stirred for 90 minutes at RT, resulting in a gel-like material. The gel was finely ground and calcined at 500 °C for 2 h after being dried in an oven at 60 °C for an hour. Thus, $NiFe_2O_4$@TiO_2 (core@shell) nanostructure was synthesized.

6.2.4. Surface Modification of $NiFe_2O_4$@TiO_2 with PDA

1g of prepared $NiFe_2O_4$@TiO_2 was mixed with Tris buffer in 500 mL (10 mM, pH 8.5). The resulting solution was mixed with 1g of dopamine hydrochloride (DA) followed by continuous stirring for 24 h at RT. Consequently, $NiFe_2O_4$@TiO_2 got coated by PDA via polymerisation of DA during the process. At the end, PDA-coated $NiFe_2O_4$@TiO_2 was easily separated using an external magnet and subsequently washed with DD water, ethanol and dried in an oven at 40 °C. This has led to the formation PDA coated $NiFe_2O_4$@TiO_2 (represented as $NiFe_2O_4$@TiO_2@PDA).

6.2.5. Synthesis of $NiFe_2O_4$@TiO_2@PDA-Ag Nanocatalyst

Dispersion of 1g of as prepared $NiFe_2O_4$@TiO_2@PDA in 200 mL of DD water was performed for 20 minutes. The reaction mixture was added with 0.05 g of $NaBH_4$ and vigorously stirred for 24 h at RT after the addition of 0.1 g of $AgNO_3$ in 20 mL of water. Ag (I) was converted during the process to Ag (0), which was then deposited on the $NiFe_2O_4$@TiO_2@PDA surface. Stirring was continued for 1 h and then the resulting Ag-immobilised $NiFe_2O_4$@TiO_2@PDA (represented as $NiFe_2O_4$@TiO_2@PDA-Ag) was set apart using an external magnet, washed exhaustively with DD water and ethanol with subsequent drying at 60 °C under vacuum for 12 h. This has led to the formation $NiFe_2O_4$@TiO_2@PDA-Ag nanocatalyst.

6.2.6. Reduction of nitro aromatic compounds

The $NaBH_4$ assisted conversion of nitro compounds has become a standard reaction to assess the activity of the nanocatalysts. Hence, the efficiency of the synthesized catalyst for the aforementioned reaction at RT was investigated. Nitro compounds (0.5 mmol) in water (10 ml) and $NaBH_4$ (5 mmol) were mixed together under magnetic stirring at RT. Consequently, 15 mg of the nanocatalyst ($NiFe_2O_4$@TiO_2@PDA-Ag) was added to the reaction mixture with constant stirring for 2 h. After the completion of the reaction (as tracked by TLC), the catalyst was readily isolated using an external magnet. Ethyl acetate was used twice to extract the desired products and purified on a microcolumn loaded with silica gel. Then, the products were examined using ^{1}H and ^{13}C NMR spectral analysis.

6.2.7. Characterization of Catalyst

The structural characteristics of the synthesized materials were characterised by Powder X-ray diffraction (PXRD) analysis on a PAN Analytical Advance X-ray diffractometer in a 2θ scan range between 10° and 60° using Ni-filtered Cu K (λ= 1.5406 Å) radiation. FT-IR spectrum for all of the materials were recorded using the PerkinElmer Spectrum with KBr pellet method, in the range of 4000 to 400 cm^{-1}. The surface morphology of the produced catalyst was investigated using Scanning Electron Microscopy (SEM, Carl Zeiss SMT Ltd., Zeiss EVO 18), Transmission Electron Microscopy (TEM), and Selected Area Electron Diffraction (SAED) (TEM, Jeol/JEM 2100 at 200 kV). The binding energies of the elements in the catalyst were confirmed using X-ray Photoelectron Spectroscopy (Kratos/Shimadzu Amicus, Model: ESCA 3400). UV-Vis diffuse reflectance spectra of all the materials was recorded at RT on an Analytik Jena SPECORD 210 PLUS. A Vibrating Sample Magnetometer (VSM) was used to record the catalyst's magnetic hysteresis curves (VSM, Lake Shore, Model: 8600 Series).

6.3. Results and Discussion

6.3.1. Preparation of $NiFe_2O_4$@TiO_2@PDA-Ag nanocatalyst

A multistep procedure was adopted to synthesize the $NiFe_2O_4$@TiO_2@PDA-Ag nanocatalyst as illustrated in **Scheme 6.1**. Step I was the synthesis of $NiFe_2O_4$ NPs via hydrothermal method and step II was the synthesis of *in situ* $NiFe_2O_4$@TiO_2 nanostructure by simple stirring. The surface of $NiFe_2O_4$@TiO_2 nanostructure was modified by PDA in step III. During this step, dopamine was continuously stirred in a Tris buffer solution (10 mM, pH 8.5) to polymerize to PDA. Lastly in step IV, Ag NPs were immobilized on PDA-coated $NiFe_2O_4$@TiO_2 by reduction of Ag(I) ions assisted by $NaBH_4$. This led to the synthesis $NiFe_2O_4$@TiO_2@PDA-Ag nanocatalyst. The synthesized catalyst was collected employing an external magnet and it was then dried under vacuum.

Scheme 6.1. *Preparation Path of the $NiFe_2O_4$@TiO_2@PDA-Ag Nanophotocatalyst*

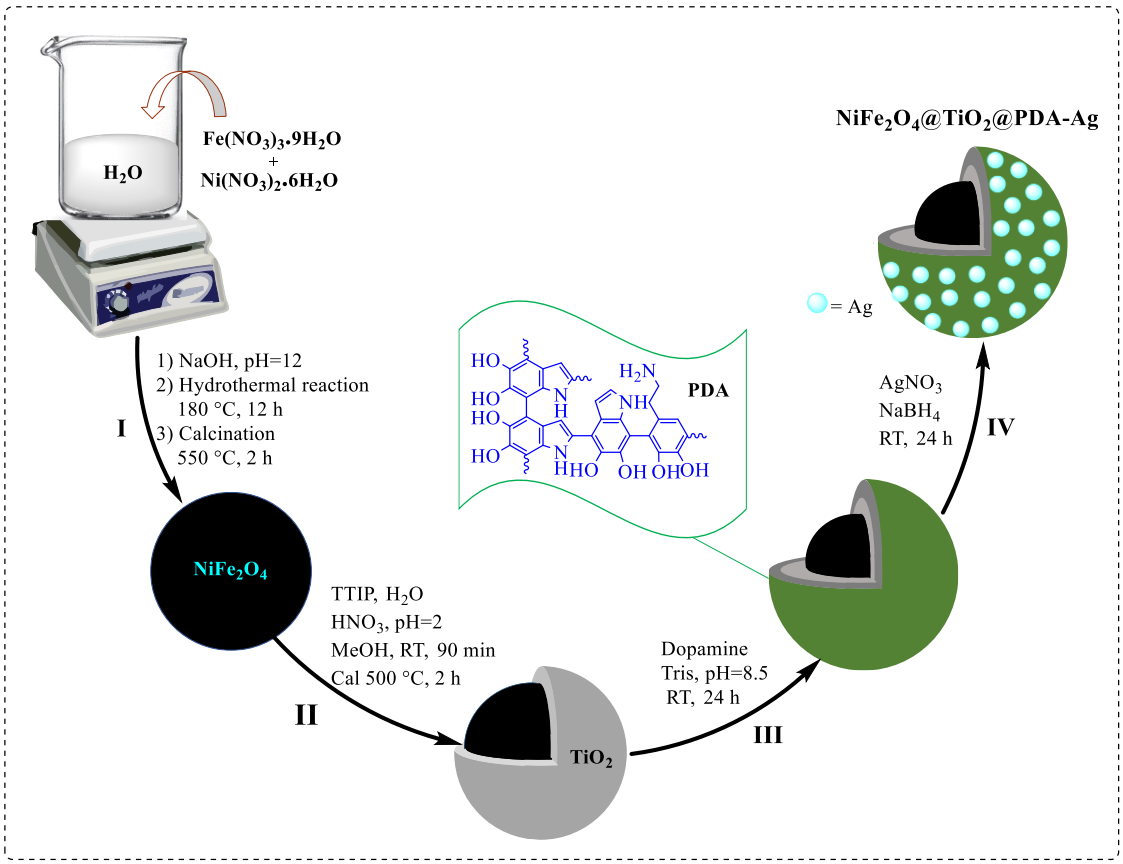

6.3.2. Characterization of $NiFe_2O_4$@TiO_2@PDA-Ag nanocatalyst

The indexed XRD patterns of the as-synthesized $NiFe_2O_4$, $NiFe_2O_4$@TiO_2, and $NiFe_2O_4$@TiO_2@PDA-Ag catalyst were shown in **Figure 6.1a.** The formation of particles in the nano-regime was confirmed by the broad peaks that appeared in the figure. From **Figure 6.1a(I),** it was clear that all the observed peaks coincide by all means with standard data of $NiFe_2O_4$ (ICDD card No. 10-0325). A very minor peak observed at 2θ of 33.2° for $NiFe_2O_4$

sample indicated the presence of the trivial amount of the impure phase of α-Fe_2O_3 that usually occurs as hematite (ICDD card 33-0664).[19] **Figure 6.1a(II)** revealed the appearance of additional peaks at 2θ of 25.3° and 48.1° together with the diffraction peaks of $NiFe_2O_4$. As confirmed by JCPDS card No. 78-2486, they were attributed to (101), (200) diffractions of anatase thus suggesting the formation of $NiFe_2O_4$@TiO_2 NPs.[20] The diffraction patterns of the synthesized catalyst $NiFe_2O_4$@TiO_2@PDA-Ag were represented in **Figure 6.1a(III)**. An additional new peak appeared at 38.1° in **Figure 6.1a(III)** along with diffraction peaks of $NiFe_2O_4$@TiO_2 attributed to (111) diffractions (JCPDS card no. 04-0783) corresponding to Ag thus inferred that $NiFe_2O_4$@TiO_2@PDA-Ag nanocatalyst was successfully synthesized.

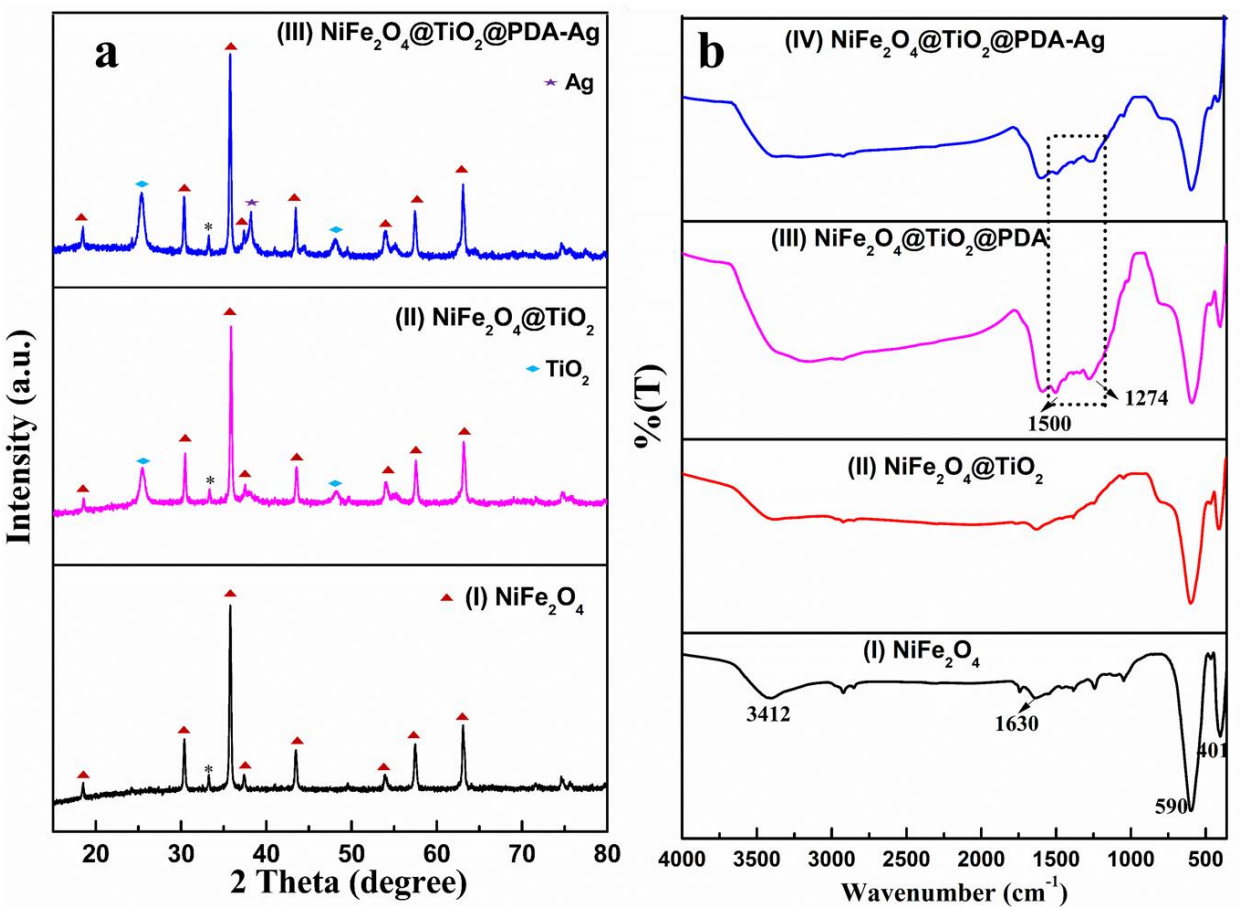

Figure 6.1. *a) XRD spectra b) FTIR spectra of the samples*

FT-IR spectra of the prepared samples were depicted in Figure 6.1b. For all samples, two prominent peaks were observed between 600 cm^{-1} and 400 cm^{-1} that were characteristic of spinel structure. The significant peaks observed at 406 cm^{-1} and 596 cm^{-1} were due to the intrinsic vibrations of M^{n+}-O bond in the octahedral and tetrahedral sites of the spinel structure, respectively. C=C and C-N stretching modes were ascribed to the observed peaks at 1500 cm^{-1} and 1274 cm^{-1} in **Figure 6.1b(III)** which were not noticed in **Figure 6.1b(II).** Thus, the presence of -C=C-NH groups in PDA was confirmed. The peak detected at ~3390 cm^{-1}

specified the existence of the -OH group of phenol in PDA. These findings concluded that PDA was effectively coated on the surface of $NiFe_2O_4@TiO_2$. No significant changes in the peaks were seen as evident from the keen observation of **Figure 6.1b(IV)** (FTIR spectrum of $NiFe_2O_4@TiO_2$@PDA-Ag nanocatalyst). A shift in the peak intensity to lower frequency from 1500 cm^{-1} and 1274 cm^{-1} was observed which might be due to the bonding interactions between the functional groups of PDA and the Ag NPs present at its surface.[21,22]

SEM images portrayed in **Figure 6.2(a, b)** depicted the surface morphologies of the synthesized $NiFe_2O_4@TiO_2$@PDA-Ag nanocatalyst. Near spherical cluster-like structure of the catalyst was apparent from the figure.

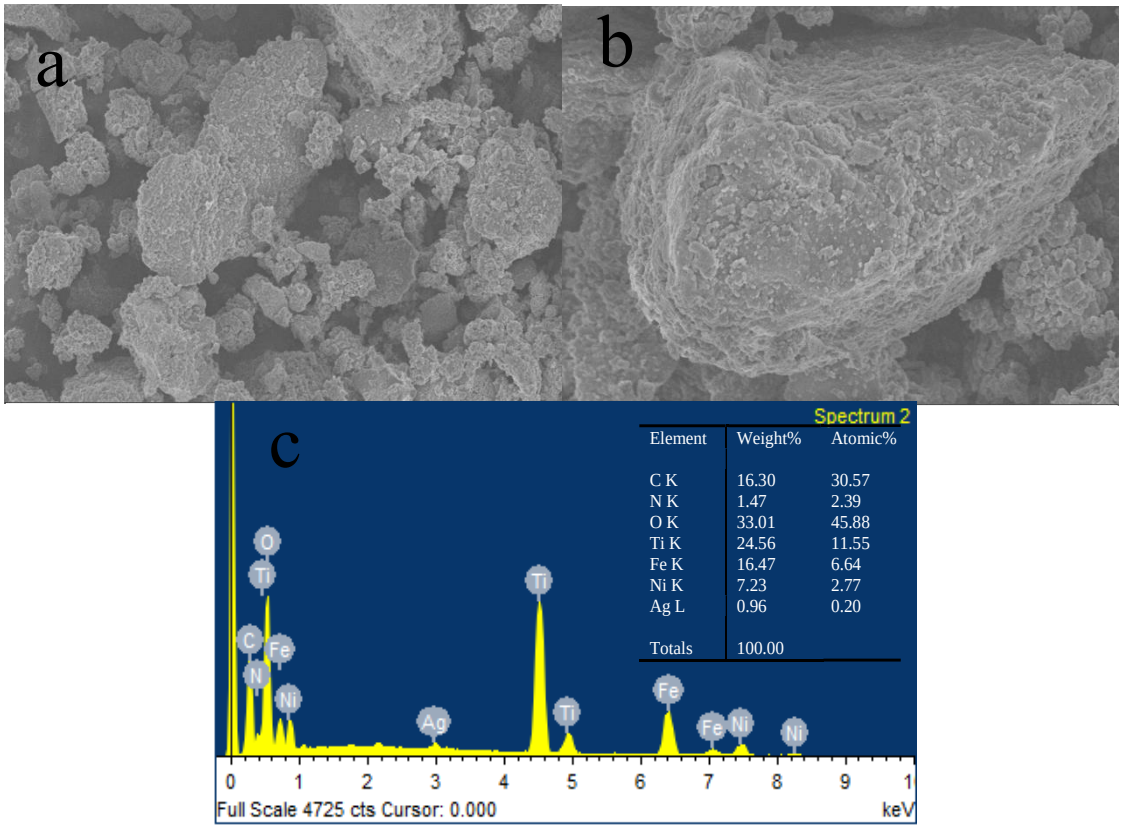

Figure 6.2. *(a,b) SEM images (c) EDAX of $NiFe_2O_4@TiO_2$@PDA-Ag nanocatalyst*

From the figure, it was evident that spherical Ag NPs were supported over a continuous PDA layer on the core-shell justifying the deposition of Ag NPs on PDA layer over the surface of $NiFe_2O_4@TiO_2$ (core@shell) nanostructure as $NiFe_2O_4@TiO_2$@PDA-Ag. The SEM-EDAX spectrum was shown in the inset of **Figure 6.2(c)** where **t**he elemental % composition was described**.** Accordingly, the SEM-EDAX images revealed the effective deposition of PDA on $NiFe_2O_4@TiO_2$ and also effective immobilisation of Ag over $NiFe_2O_4@TiO_2$@PDA surface.

Immobilisation of Ag NPs on the surface of the PDA in the catalyst was also established by TEM analysis. TEM images presented in **Figure 6.3(a, b)** prominently established that small, spherical Ag NPs were evenly distributed all over the surface of the PDA layer. It was evident from the magnified TEM image in **Figure 6.3a** that small silvery white spherical Ag NPs were deposited over the pale grey PDA layer on the jet black $NiFe_2O_4@TiO_2$ (core@shell) nanostructure. The TEM images in **Figure 6.3 (b, c)** at 20 nm and 10 nm, clearly depicted that Ag NPs were spherical and were evenly ornamented over the superficial surface of $NiFe_2O_4@TiO_2@PDA$. These images inferred that Ag NPs were well immobilised on the surface of PDA without large agglomeration. The particle size distribution histogram of the catalyst was presented in **Figure 6.3(d)**, from which the average size of the Ag NPs was estimated to be ~6.3 nm. The information obtained from TEM images was in accord with SEM information with regard to morphology.

Keen observation of the HRTEM image depicted in **Figure 6.3(e)** represented the layer like morphology of the catalyst. Several grains with various plane orientations for the catalyst were seen in HRTEM image **6.3(f).** Thus the polycrystalline nature of the catalyst was illustrated. The (111) crystal planes of Ag NPs observed in **Figure 6.3(f)** could be attributed to the lattice fringe spaces of 0.36 nm. The Selected Area Electron Diffraction (SAED) pattern of the catalyst was presented in **Figure 6.3(g)**. Diffraction rings containing bright spots having six-fold symmetry were displayed that revealed the polycrystalline behaviour of the catalyst.

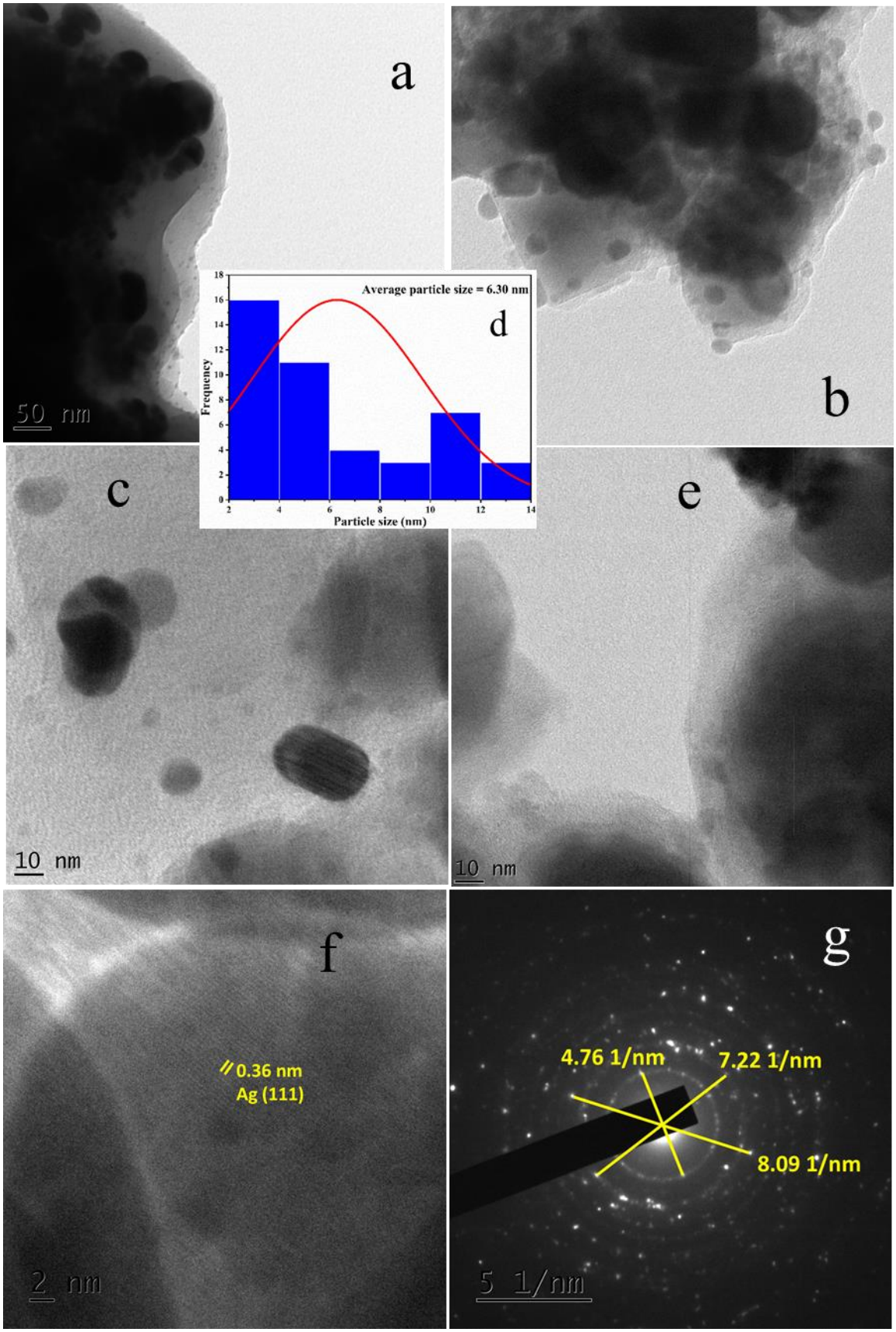

Figure 6.3 *(a,b) TEM images (d) Particle size distribution (c,e,f) HRTEM image (g) SAED pattern of* $NiFe_2O_4@TiO_2@PDA\text{-}Ag$

XPS is a robust tool for determining the binding energy, electron environment and chemical valence states of coordinated metal particles on the catalyst surface. The XPS spectra of the catalyst was presented in **Figure 6.4 (a, b, c)** which analysed the chemical valence states of Ti, N and Ag in the catalyst.

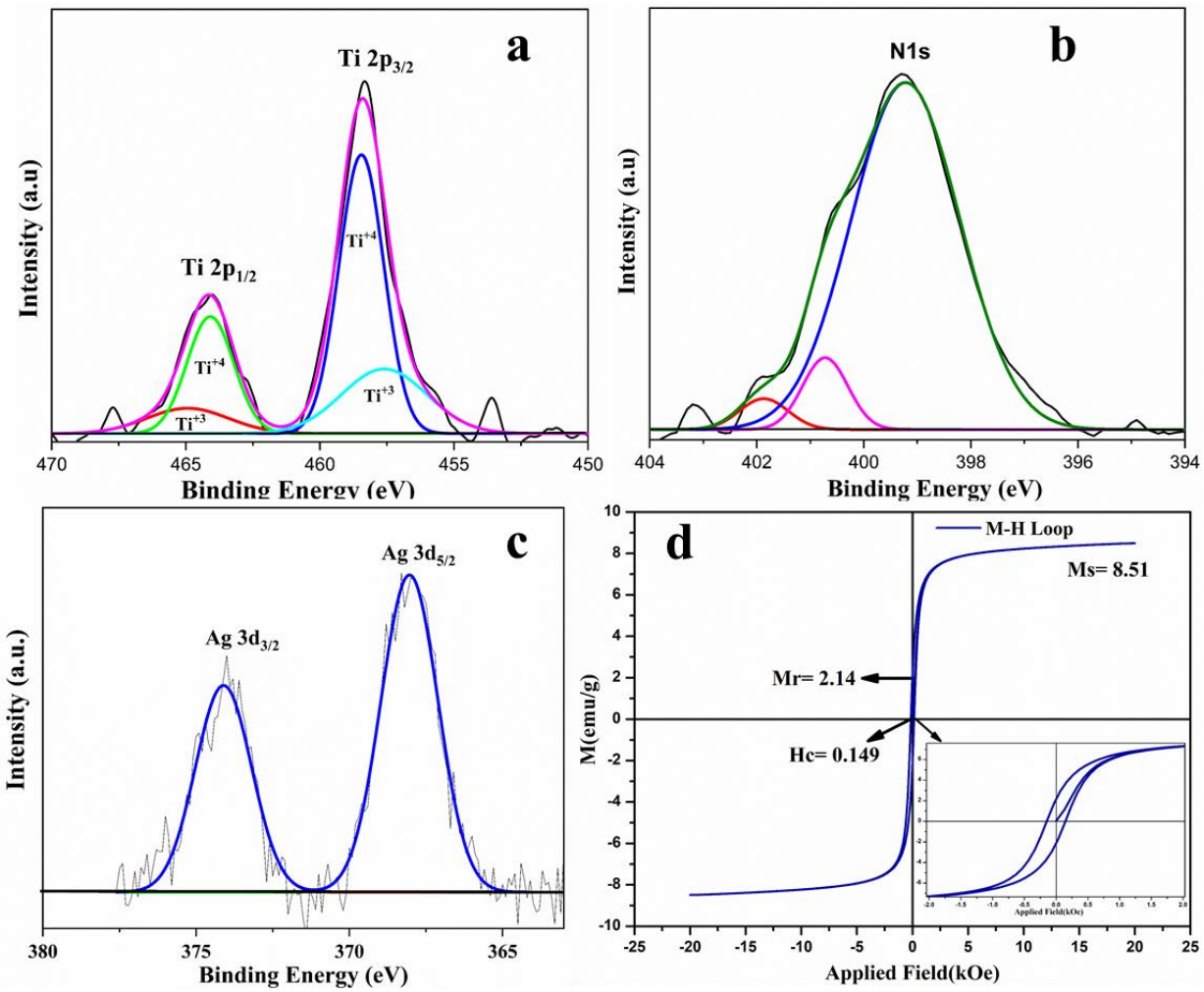

***Figure 6.4**. a) Ti 2p peaks b) N 1s peak c) Ag 3d peaks d) magnetisation curve of $NiFe_2O_4$@TiO_2@PDA-Ag nanocatalyst*

The two prominent bands observed in **Figure 6.4a** at binding energies 458.4 and 464.0 eV were ascribed to the Ti $2p_{3/2}$ and Ti $2p_{1/2}$ photoelectrons respectively in the Ti^{4+} chemical state whereas the two peaks at 457.6 and 465.0 eV were attributed to the Ti $2p_{3/2}$ and Ti $2p_{1/2}$ photoelectrons respectively in the Ti^{3+} state in the TiO_2 chemical state.[23] The N 1s photoelectrons of the NH group were identified at 399.2 eV as evident from the N 1s spectrum shown in **Figure 6.4b** which confirmed the successful coating of PDA on $NiFe_2O_4$@TiO_2 nanostructure. The binding of Ag in the catalyst was established from the **Figure 6.4c** where the two noticeable bands at binding energies 368.1 eV and 374.2 eV were indexed as Ag $3d_{5/2}$

and Ag $3d_{3/2}$ respectively. These results were in agreement with the binding energy values of metallic Ag.[24] The RT magnetization measurements were performed using VSM and the results were shown in the form of a magnetization curve in **Figure 6.4d** to establish the magnetic behaviour of the catalyst. The saturation magnetization (M_s), coercivity (H_c), and remanence magnetization (M_r) were found to be 8.51 emu/g, 0.149 kOe, and 2.14 emu/g respectively. Magnetic retrievability and reusability of the catalyst was supported by the evaluated magnetic parameters from the **Figure 6.4d** which manifested the notable magnetic performance of the synthesized catalyst.

The outcomes of recorded UV-Vis spectra of all the synthesised samples *viz.*, $NiFe_2O_4$, pure TiO_2, $NiFe_2O_4@TiO_2$, $NiFe_2O_4@TiO_2@PDA$ and $NiFe_2O_4@TiO_2@PDA$-Ag were described in **Figure 6.5a.** Two absorption bands were observed with absorption edges corresponding to pure TiO_2 at 400 nm (UV region) and $NiFe_2O_4$ at 700 nm (visible region) respectively as shown in **Figure 6.5a (I, II)**.

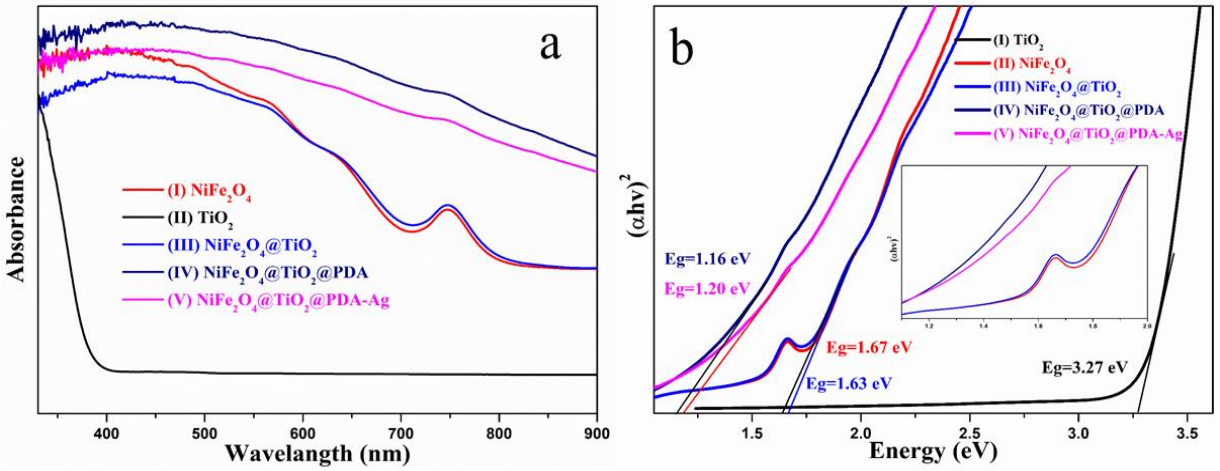

Figure 6.5. *a) UV-Vis absorption spectra b) band gap energies of the samples*

The formation of $NiFe_2O_4@TiO_2$ (core@shell) nanostructure exhibited the absorption in visible region as evident from **Figure 6.5a (III)**. Surface modified $NiFe_2O_4@TiO_2$ nanostructure with PDA and Ag immobilised $NiFe_2O_4@TiO_2@PDA$ nanocatalyst also have shown absorption in the visible region as clear from **Figure 6.5a (IV, V)**. Tauc plot of $(\alpha h\upsilon)^2$ vs $h\upsilon$, as presented in **Figure 6.5b** was used to estimate the band gap energy (E_g) of all the samples which was obtained by the extrapolation of $h\upsilon$ value to $\alpha = 0$. Evaluated E_g for the pure $NiFe_2O_4$ and TiO_2 as indicated in the figure was found to be in good agreement with the reported values.[25,26] $NiFe_2O_4@TiO_2$ nanostructure with measured band gap energy of 1.63 eV from the Tauc plot was confirmed to be visible light active. Surface modification by PDA with subsequent coating by Ag NPs over $NiFe_2O_4@TiO_2$ resulting in a catalyst had shown still

stronger visible region absorption as evident from the **Figure 6.5b**. Clear evidence of the band gap energies was observed in the inset of the Zoom in image of **Figure 6.5b**. Hence, the prepared catalyst could also be used as a photocatalyst for diverse applications.

6.3.3. Catalytic reduction of nitro aromatic compounds

The reduction of nitro aromatic compound to corresponding amine mediated by a catalyst has been considered as an eco-friendly remediation tool because of the less toxic nature of amine. Furthermore, numerous researchers have previously explored the activity of their synthesized nanostructured materials by performing the catalytic reduction of 4-NP as a model reaction.[27] In the current study, after the successful synthesis and characterization of $NiFe_2O_4$@TiO_2@PDA-Ag nanocatalyst, its activity was investigated for the reduction of 4-NP to 4-AP at RT with the assistance of $NaBH_4$. In order to establish the active species of the catalyst responsible for the activity in the reduction reaction, the reduction of 4-NP was performed in the presence of bare $NiFe_2O_4$, $NiFe_2O_4$@TiO_2, and $NiFe_2O_4$@TiO_2@PDA separately. Negligible yield of the product was observed. Whereas, the good yield of the product was observed when the reaction was performed in the presence of $NiFe_2O_4$@TiO_2@PDA-Ag inferring the fact that Ag was the active species in the reaction.

Several important reaction conditions for the reduction reaction of 0.5 mmol of 4-NP such as quantity of $NaBH_4$, temperature, amount of the catalyst (mg), reaction time and type of the solvent were optimized systematically. The effect of various solvents MeOH, EtOH and H_2O on the reduction reaction in the presence of 5 mmol of $NaBH_4$, 20 mg of the catalyst at RT for 5 h (**Table 6.1, entries 1,2,3)** was studied. However, the observed yield of the product in the presence of polar protic solvents such as MeOH and EtOH was 73 and 80% (**Table 6.1, entry 1,2)**. It was observed that 99% yield of the product was obtained in the presence of H_2O as a solvent (**Table 6.1, entry 3)**. Hence, H_2O was used as a solvent for the reduction reaction. To optimize the amount of $NaBH_4$, the reaction was carried out with different amounts of the $NaBH_4$ (1, 2, 3, 4, 5, 6 mmol) in H_2O at RT for 5h. Corresponding yield of the products were trace %, 24%, 60%, 87%, 99%, 99% (**Table 6.1, entry 4 to 9)** respectively and it was evident that there was no change in the yield beyond 5 mmol of $NaBH_4$. Thus, the optimum amount of the $NaBH_4$ used was 5 mmol. The effect of reaction time was also analysed on the reaction in the presence of 5 mmol of $NaBH_4$, 20 mg of the catalyst at RT for different time duration (1, 2, 3 h). It was observed that in 1 h, reasonable yield (76%) of the product was attained and in 2h, great yield of the product (99%) was achieved (**Table 6.1, entry 10,11)**. On increasing the time beyond 2h, there was no change in the yield (**Table 6.1, entry 12,8)**. Thus, optimum reaction time was 2h. Under these optimized conditions, as higher yield (99%) was obtained at

RT, there will not be any effect of higher temperature on the yield of the product. Thus, RT would be the optimum temperature. Further, the amount of the catalyst was optimized by considering 5, 10, 15 and 20 mg of the catalyst where 99% of the yield was obtained with 15 mg and 20 mg of catalyst (**Table 6.1, entry 13,14,15,11)**. Thus, optimum amount of the catalyst would be 15 mg.

Table 6.1. *Screening of Reaction Conditions for Reduction of Nitro compounds*[a]

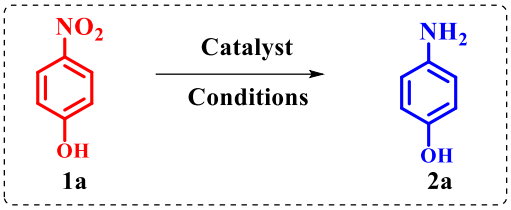

S.No	4-NP (mmol)	$NaBH_4$ (mmol)	Solvent	Time (h)	Yield(%)[b]
1	0.5	5	MeOH	5	73
2	0.5	5	EtOH	5	80
3	0.5	5	H_2O	5	99
4	0.5	1	H_2O	5	Trace
5	0.5	2	H_2O	5	24
6	0.5	3	H_2O	5	60
7	0.5	4	H_2O	5	87
8	0.5	5	H_2O	5	99
9	0.5	6	H_2O	5	99
10	0.5	5	H_2O	1	76
11	0.5	5	H_2O	2	99
12	0.5	5	H_2O	3	99
13	0.5	5	H_2O	2	42[c]
14	0.5	5	H_2O	2	78[d]
15	**0.5**	**5**	**H_2O**	**2**	**99[e]**

[a]**Reaction conditions:** 4-NP (0.5 mmol), sodium borohydride (5 mmol), $NiFe_2O_4$@TiO_2@PDA-Ag catalyst (20 mg) and in solvent (10 mL) at RT. [b]Isolated yields [c]5 mg catalyst [d]10 mg catalyst [e]15 mg catalyst.

Thus, the optimized reaction conditions for the reduction of nitroaromatic compounds to aromatic amines in the presence of $NiFe_2O_4$@TiO_2@PDA-Ag catalyst were 5 mmol of $NaBH_4$, 15 mg of the catalyst, H_2O as solvent, RT, 2h.

The activity and the substrate scope of the catalyst was explored by performing the reduction of a series of substituted nitroarenes using the optimized reaction conditions (0.5 mmol of nitroaromatic compound, 5 mmol of $NaBH_4$, 15 mg of the catalyst at RT for 2 h) as shown in **Table 6.2.** From the tabulated data, it was clear that substituted groups have little effect on the reaction yield. As observed from TLC in all the cases, the corresponding amines from the respective nitroarenes were found to be the exclusive reaction products and no indication of the formation of usual side products (azo, hydrazo and azoxy groups) of reduction reaction of nitroarenes.

Table 6.2 *Substrate Scope of the reduction of nitroaromatic compound catalyzed by* $NiFe_2O_4@TiO_2@PDA-Ag$ [a]

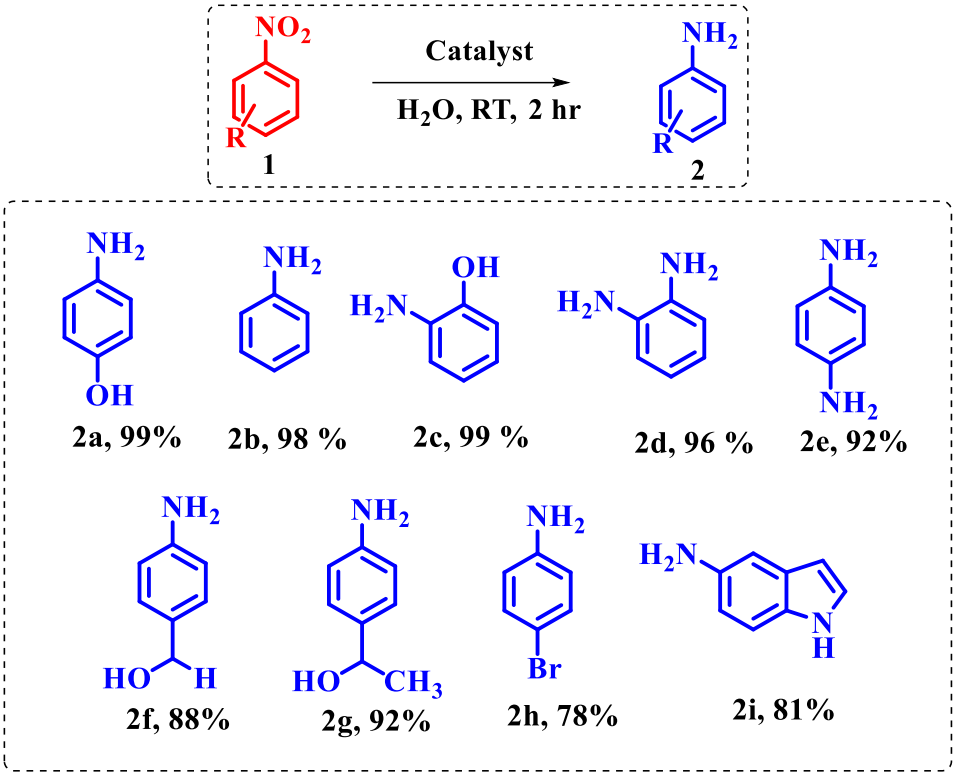

6.3.3.2. Kinetics study by UV-Vis. Spectra

The kinetics of the reduction of 4-NP in the presence of the catalyst was also studied using UV-Vis absorption spectroscopy as shown in **Figure 6.6a**. A solution of 4-NP in water (0.5 mL, 30 mM) was introduced into a glass vial containing 10 mL of deionized water under magnetic stirring followed by the addition of freshly prepared $NaBH_4$ solution (1 mL, 300 mM). Consequently, 5mg of the nanocatalyst ($NiFe_2O_4@TiO_2@PDA-Ag$) was added to the reaction mixture. The reaction mixture was collected at every oneminute time interval and monitored by UV−Vis absorption spectra till the solution becomes colourless which took 5 minutes. This indicated the complete catalytic reduction.

From the absorption spectra, the absorption peak intensity of 4-NP observed at 400 nm decreased and concomitantly a new absorption peak appeared at 297 nm and improved progressively in its intensity indicating the transformation of 4-NP to 4-AP. Furthermore, the reaction rate of the catalytic reduction could be evaluated by measuring the change in absorbance of the peak at 400 nm with respect to time. According to Beer Lambert's law, absorbance (A) of 4-NP is directly proportional to its concentration (C) in the solution. Hence, the 'A' at time t=0 (A_0) corresponds to 'C' at time t=0 (C_0) and the 'A' at time t (A_t) corresponds to 'C' at time t (C_t). From the **Figure 6.6b**, it was evident that the plot of $\ln(C_t/C_0)$ vs time (min) was linear which revealed that the reduction reaction followed pseudo first-order kinetics model which follows the equation[28]

$$\ln(C_t/C_0) = -kt$$

The rate constant as calculated from the slope of the straight line was 0.462 min^{-1}.

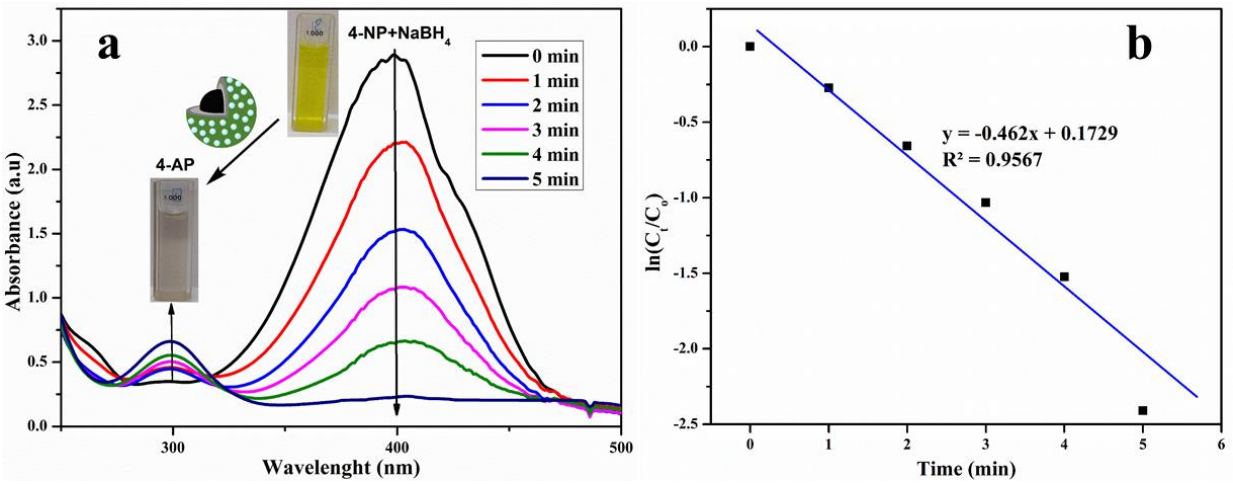

Figure 6.6: *a) UV-vis spectra of 4-NP to 4-AP b) Plot of $\ln(C_t/C_0)$ vs the reaction time (t) for reduction of 4-NP*

The comparison of the catalytic activity of $NiFe_2O_4$@TiO_2@PDA-Ag catalyst with other reported catalysts was portrayed in **Table 6.3**. From the represented data in the **Table 6.3,** it was prominent that all other catalysts (**S.No. 1to7**) were tested for their catalytic activity on low concentration of the pollutant 4-NP ranging from 0.1 to 3mM. Whereas, current catalyst was tested for its activity on a high concentration of the pollutant i.e. 30 mM under the similar conditions and it was observed that the catalyst was efficient in reducing 4-NP to 4-AP in just 5 minutes. Thus, current catalyst $NiFe_2O_4$@TiO_2@PDA-Ag exhibited superior ability compared to the previously reported catalysts.

***Table 6.3**: Comparison of the catalytic performances of $NiFe_2O_4$@TiO_2@PDA-Ag with other catalyst system over 4-NP reduction by $NaBH_4$*

S.No	Catalyst	4-NP (mM)	$NaBH_4$ (mM)	Time (min)	Ref.
1	Au-Ag nanocages/GO	0.1	10	7	[29]
2	BNNS/Ag-3 nanohybrids	0.4	400	10	[30]
3	PSMAA/Ag-3	0.1	60	3	[31]
4	Au@NiAg	0.12	100	2	[32]
5	GO-DAP-AgNPs	0.1	100	12	[33]
6	Fe_3O_4@MIL-100(Fe)/Ag	3	300	1	[34]
7	Fe_3O_4@PS@Ag	3	300	3	[35]
8	**Present work**	**30**	**300**	**5**	**This work**

From the data, it was evident that the $NiFe_2O_4$@TiO_2@PDA-Ag catalyst was superior in terms of its catalytic activity for the reduction of 4-NP. In order to show its industrial application, gram scale reaction was also performed with $NiFe_2O_4$@TiO_2@PDA-Ag catalyst. For this, 4-NP (10 mmol), $NaBH_4$ (100 mmol) were added in water (200 ml) followed by the addition of 0.3 g of the catalyst with constant stirring at RT for 2h. The catalyst was isolated from the reaction mixture after the completion of reaction (as tracked by TLC). Ethyl acetate was used twice to extract the desired products and purified on a microcolumn loaded with silica gel. Then, the products were examined using ^{1}H and ^{13}C NMR spectral analysis.

Based on the UV-Visible characterization, the catalyst was expected to have photocatalytic application as it was visible light active. Its photocatalytic applications were explored in the degradation of Methylene Blue (colored pollutant) and Ciprofloxacin (colourless pollutant) under direct sunlight.

6.3.3.3. Reusability and structural stability of the catalyst

The recycling ability of the $NiFe_2O_4$@TiO_2@PDA-Ag catalyst was investigated by performing the experiment with the same catalytic reaction conditions five times. In all these five cycles, the catalyst $NiFe_2O_4$@TiO_2@PDA-Ag was successfully retrieved from the reaction mix by employing an external magnet. The high catalytic activity of $NiFe_2O_4$@TiO_2@PDA-Ag up to 5 cycles was illustrated in **Figure 6.7**. Furthermore, the structural stability of the reused catalyst was confirmed by XRD and FTIR after five cycles. The XRD image of $NiFe_2O_4$@TiO_2@PDA-Ag catalyst after five runs of the experiment was shown in **Figure 6.8(I)**. The catalyst stability was confirmed by the observation that no impurity peaks were

seen in the XRD spectra of the reused catalyst. The catalyst was tested for FTIR spectral analysis after five cycles, which indicated that the absorption peaks of the recycled catalyst were similar to those of the fresh catalyst as shown in **Figure 6.8(II)** confirming the structural stability of the catalyst.

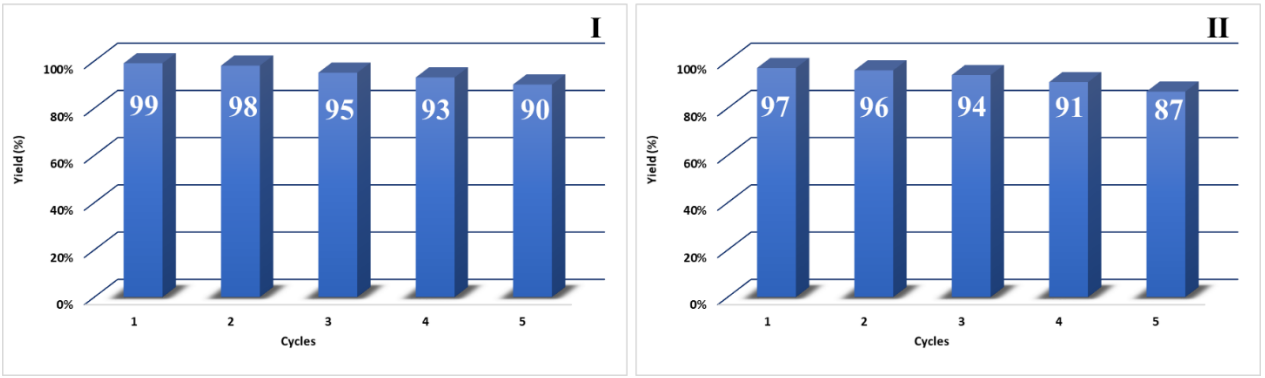

Figure 6.7: *Recyclability test of $NiFe_2O_4$@TiO_2@PDA-Ag nanocatalyst for I) Reduction of 4-NP reaction II) kinetic study 4-NP reaction*

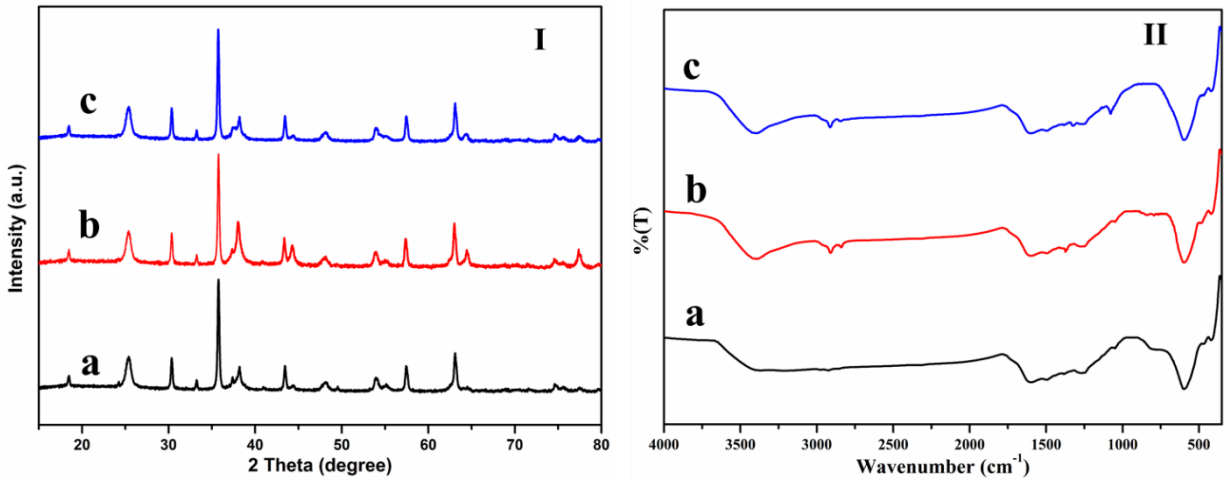

Figure 6.8. I) *XRD spectra* ***II)*** *FTIR spectra of (a) synthesized $NiFe_2O_4$@TiO_2@PDA-Ag nanocatalyst (b) used catalyst for Reduction of 4-NP reaction and (c) used catalyst for kinetic study 4-NP reaction after 5 cycles,*

6.3.3.4. Mechanism of reduction of nitro compounds

Based on the previously reported mechanisms and observed results, a plausible mechanism was proposed for the reduction of nitroarenes to corresponding amines with the assistance of $NaBH_4$ as source of hydrogen in the presence of the $NiFe_2O_4$@TiO_2@PDA-Ag nanocatalyst containing active Ag NP on its surface. The mechanism of this reaction could best be described via the Langmuir-Hinshelwood mechanism.[36] In this approach the reaction could proceed in two steps i. diffusion and adsorption of substrates on the catalyst's surface ii. transfer of electron from $NaBH_4$ to nitroarenes through the catalyst.[37] The catalytic reduction of

nitroarenes could occur over the Ag NPs present on the surface of the catalyst. As the catalyst was a solid material, it followed general heterogeneous catalysis mechanism. According to this approach, at first BH_4^- ion and nitroarene diffused through the solution and adsorbed on the catalyst surface. In the next step, BH_4^- ion acted as electron donor owing to its coordination with the metal. As a consequence, water was reduced to H_2 and finally active hydrogen species was formed on the catalyst's surface. These active hydrogen species reduced nitroarene to nitroso compounds, then to hydroxyl amines and finally on further reduction resulted in aromatic amines as a desired product. In the final step, desorption of aromatic amines from the surface of the catalyst occured.[38]

6.4. Conclusion

A highly efficient Ag immobilized polydopamine coated $NiFe_2O_4@TiO_2$ as a heterogeneous magnetic nanocatalyst ($NiFe_2O_4@TiO_2$@PDA-Ag) was developed for the catalytic reduction of nitro aromatic compounds to the corresponding amines using $NaBH_4$ in water as solvent with high product yield of 99 %. The catalyst exhibited good catalytic activity and high selectivity in the catalytic reduction of a series of substituted nitroaromatic compounds. The catalytic performance of the catalyst was explored in the reduction of 4-NP to 4-AP at room temperature in an aqueous medium in the presence of $NaBH_4$ as a reducing agent. The kinetic study of the reaction was performed by UV-Visible spectroscopy which confirmed the pseudo first order kinetics of the reaction with a rate constant of 0.462 min^{-1}. The unique characteristic features of the synthesized nanocatalyst were i) Effective performance of the catalyst under ambient conditions (RT and water as a solvent) ii) Magnetic recovery of the catalyst with the aid of an external magnet iii) Reusability of the recovered catalyst for five consecutive runs without significant loss in catalytic activity iv) Good structural stability of the catalyst as confirmed by XRD and FT-IR analysis of the recovered catalyst v) Use of the catalyst in a sustainable greener approach.

6.5. Spectral data of synthesized products nitro reduction 3a-3i

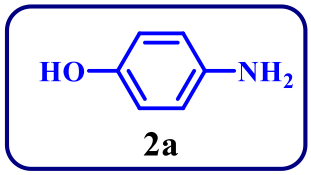

4-aminophenol

^{1}H NMR (400 MHz, DMSO): δ (ppm): 8.38 (s, 1H), 6.48 (d, J = 8.8 Hz, 2H), 6.42 (d, J = 8.8 Hz, 2H), 4.37 (brs, 2H); ^{13}C NMR (100 MHz, DMSO): δ (ppm): 148.69, 141.08, 116.00, 115.74.

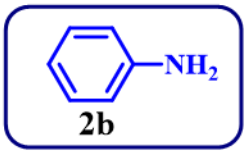

Aniline

^{1}H NMR (400 MHz, DMSO): δ (ppm): 7.14 (t, J = 8.4 Hz, 2H), 6.75 (t, J = 7.4 Hz, 1H), 6.66 (d, J = 7.4 Hz, 2H), 3.51 (brs, 2H); ^{13}C NMR (100 MHz, DMSO): δ (ppm): 146.45, 129.35, 118.59, 115.17.

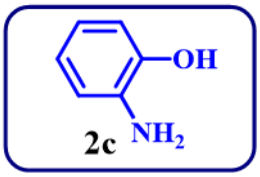

2-aminophenol

^{1}H NMR (400 MHz, DMSO): δ (ppm): 8.94 (s, 1H), 6.64 (d, J = 7.8 Hz, 1H), 6.59 – 6.52 (m, 2H), 6.39 (t, J = 7.4 Hz, 1H), 4.45 (brs, 2H).; ^{13}C NMR (100 MHz, DMSO): δ (ppm): 144.44, 136.97, 119.98, 116.92, 114.92, 114.92.

Benzene-1,2-diamine

^{1}H NMR (400 MHz, DMSO): δ (ppm): 6.55 – 6.51 (m, 2H), 6.43 – 6.38 (m, 2H), 4.39 (brs, 4H).; ^{13}C NMR (100 MHz, DMSO): δ (ppm): 135.39, 117.86, 115.10.

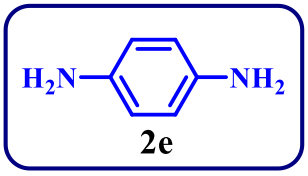

2e

Benzene-1,4-diamine

^{1}H NMR (400 MHz, $CDCl_3$): δ (ppm): 6.56 (s, 4H), 3.27 (s, 4H).; ^{13}C NMR (100 MHz, $CDCl_3$): δ (ppm): 138.60, 116.75.

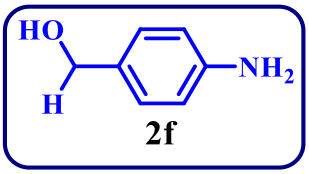

2f

(4-aminophenyl) methanol

^{1}H NMR (400 MHz, DMSO): δ (ppm): 6.94 (d, J = 8.2 Hz, 2H), 6.50 (d, J = 8.2 Hz, 2H), 4.93 (brs 2H), 4.24 (t, J = 6.6 Hz, 1H), 4.16 (d, J = 5.6 Hz, 2H); ^{13}C NMR (100 MHz, DMSO): δ (ppm):147.90, 130.09, 128.42, 114.03, 63.59.

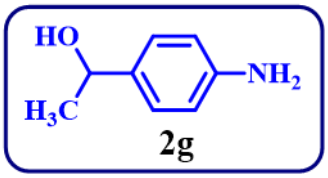

2g

1-(4-aminophenyl)ethan-1-ol

^{1}H NMR (400 MHz, DMSO): δ (ppm): 6.94 (d, J = 7.4 Hz, 2H), 6.37 (d, J = 6.8 Hz, 2H), 5.69 (s, 1H), 4.16 (brs 2H), 2.51 (dd, J = 3.6, 1.6 Hz, 1H), 1.27 (d, J = 4.4 Hz, 3H); ^{13}C NMR (100 MHz, DMSO): δ (ppm):147.60, 135.05, 126.48, 113.89, 68.41, 26.30

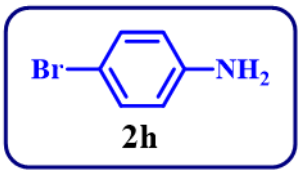

2h

4-bromoaniline

^{1}H NMR (400 MHz, DMSO): δ (ppm): 7.23 (d, J = 7.6 Hz, 2H), 6.56 (d, J = 7.8 Hz, 2H), 5.2 (brs, 2H); ^{13}C NMR (100 MHz, DMSO): δ (ppm): 145.58, 132.2, 116.78, 110.30.

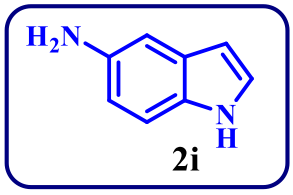

2i

1H-indol-5-amine

^{1}H NMR (400 MHz, DMSO): δ (ppm): 10.56 (s, 1H), 7.12 (d, J = 8.8 Hz, 1H), 7.08 (d, J = 8.6 Hz, 1H), 6.68 (s, 1H), 6.49 (d, J = 8.6 Hz, 1H), 6.12 (s, 1H), 4.25 (brs, 2H); ^{13}C NMR (100 MHz, DMSO): δ (ppm): 139.50, 130.70, 128.88, 124.67, 113.02, 111.49, 105.61, 101.56.

6.6. References

(1) Xiao, G, Yilin Zhao Y, Linghui Li, Jonathan O. Pratt, Haijia Su, Tianwei Tan, Facile synthesis of dispersed Ag nanoparticles on chitosan-TiO_2 composites as recyclable nanocatalysts for 4-nitrophenol reduction, *Mater. Nanotechnology*, **2018**, 0–23.

(2) Roy, S. Photocatalytic Materials for Reduction of Nitroarenes and Nitrates. *J. Phys. Chem. C* **2020**, *124* (52), 28345–28358.

(3) Wu, W.; Wu, Z.; Yu, T.; Jiang, C.; Kim, W. S. Recent Progress on Magnetic Iron Oxide Nanoparticles: Synthesis, Surface Functional Strategies and Biomedical Applications. *Sci. Technol. Adv. Mater.* **2015**, *16* (2), 23501.

(4) Sasmal, A. K.; Pal, J.; Sahoo, R.; Kartikeya, P.; Dutta, S.; Pal, T. Superb Dye Adsorption and Dye-Sensitized Change in Cu_2O-Ag Crystal Faces in the Dark. *J. Phys. Chem. C* **2016**, *120* (38), 21580–21588.

(5) Abdelhamid, H. N. High Performance and Ultrafast Reduction of 4-Nitrophenol Using Metal-Organic Frameworks. *J. Environ. Chem. Eng.* **2021**, *9* (1), 104404.

(6) Sorribes, I.; Wienhöfer, G.; Vicent, C.; Junge, K.; Llusar, R.; Beller, M. Chemoselective Transfer Hydrogenation to Nitroarenes Mediated by Cubane-Type Mo_3S_4 Cluster Catalysts . *Angew. Chemie* **2012**, *124* (31), 7914–7918.

(7) Cantillo, D.; Baghbanzadeh, M.; Kappe, C. O. In Situ Generated Iron Oxide Nanocrystals as Efficient and Selective Catalysts for the Reduction of Nitroarenes Using a Continuous Flow Method. *Angew. Chemie* **2012**, *124* (40), 10337–10340.

(8) Jagadeesh, R. V.; Wienhöfer, G.; Westerhaus, F. A.; Surkus, A. E.; Pohl, M. M.; Junge, H.; Junge, K.; Beller, M. Efficient and Highly Selective Iron-Catalyzed Reduction of Nitroarenes. *Chem. Commun.* **2011**, *47* (39), 10972–10974.

(9) Hudson, R.; Feng, Y.; Varma, R. S.; Moores, A. Bare Magnetic Nanoparticles: Sustainable Synthesis and Applications in Catalytic Organic Transformations. *Green Chem.* **2014**, *16* (10), 4493–4505.

(10) Li, M.; Hu, L.; Cao, X.; Hong, H.; Lu, J.; Gu, H. Direct Hydrogenation of Nitroaromatics and One-Pot Amidation with Carboxylic Acids over Platinum Nanowires. *Chem. - A Eur. J.* **2011**, *17* (9), 2763–2768.

(11) Amali, A. J.; Rana, R. K. Stabilisation of Pd(0) on Surface Functionalised Fe_3O_4 Nanoparticles: Magnetically Recoverable and Stable Recyclable Catalyst for Hydrogenation and Suzuki–Miyaura Reactions. *Green Chem.* **2009**, *11* (11), 1781–1786.

(12) Nasrollahzadeh, M.; Atarod, M.; Jaleh, B.; Gandomirouzbahani, M. In Situ Green Synthesis of Ag Nanoparticles on Graphene Oxide/TiO_2 Nanocomposite and Their Catalytic Activity for the Reduction of 4-Nitrophenol, Congo Red and Methylene Blue. *Ceram. Int.* **2016**, *42* (7), 8587–8596.

(13) Wang, Y.; He, L.; Li, Y.; Jing, L.; Wang, J.; Li, X. Ag NPs Supported on the Magnetic Al-MOF/PDA as Nanocatalyst for the Removal of Organic Pollutants in Water. *J. Alloys Compd.* **2020**, *828*, 154340.

(14) Wei, H.; Lu, Y. Catalysis of Gold Nanoparticles within Lysozyme Single Crystals. *Chem. - An Asian J.* **2012**, *7* (4), 680–683.

(15) Kuroda, K.; Ishida, T.; Haruta, M. Reduction of 4-Nitrophenol to 4-Aminophenol over Au Nanoparticles Deposited on PMMA. *J. Mol. Catal. A Chem.* **2009**, *298* (1–2), 7–11.

(16) Al-Shaal, M. G.; Wright, W. R. H.; Palkovits, R. Exploring the Ruthenium Catalysed Synthesis of γ-Valerolactone in Alcohols and Utilisation of Mild Solvent-Free Reaction Conditions. *Green Chem.* **2012**, *14* (5), 1260–1263.

(17) Kesavan, G.; Nataraj, N.; Chen, S. M.; Lin, L. H. Hydrothermal Synthesis of $NiFe_2O_4$

Nanoparticles as an Efficient Electrocatalyst for the Electrochemical Detection of Bisphenol A. *New J. Chem.* **2020**, *44* (19), 7698–7707.

(18) Majid, F.; Rauf, J.; Ata, S.; Bibi, I.; Malik, A.; Ibrahim, S. M.; Ali, A.; Iqbal, M. Synthesis and Characterization of $NiFe_2O_4$ Ferrite: Sol–Gel and Hydrothermal Synthesis Routes Effect on Magnetic, Structural and Dielectric Characteristics. *Mater. Chem. Phys.* **2021**, *258* (December 2019).

(19) Laokul, P.; Amornkitbamrung, V.; Seraphin, S.; Maensiri, S. Characterization and Magnetic Properties of Nanocrystalline $CuFe_2O_4$, $NiFe_2O_4$, $ZnFe_2O_4$ Powders Prepared by the Aloe Vera Extract Solution. *Curr. Appl. Phys.* **2011**, *11* (1), 101–108.

(20) Liu, Y.; Cherkasov, N.; Gao, P.; Fernández, J.; Lees, M. R.; Rebrov, E. V. The Enhancement of Direct Amide Synthesis Reaction Rate over TiO_2@SiO_2@$NiFe_2O_4$ Magnetic Catalysts in the Continuous Flow under Radiofrequency Heating. *J. Catal.* **2017**, *355*, 120–130.

(21) Farzad, E.; Veisi, H. Fe_3O_4/SiO_2 Nanoparticles Coated with Polydopamine as a Novel Magnetite Reductant and Stabilizer Sorbent for Palladium Ions: Synthetic Application of Fe_3O_4/SiO_2@PDA/Pd for Reduction of 4-Nitrophenol and Suzuki Reactions. *J. Ind. Eng. Chem.* **2018**, *60*, 114–124.

(22) Veisi, H.; Sarachegol, P.; Hemmati, S. Palladium(II) Anchored on Polydopamine Coated-Magnetic Nanoparticles (Fe_3O_4@PDA@Pd(II)): A Heterogeneous and Core–Shell Nanocatalyst in Buchwald–Hartwig C–N Cross Coupling Reactions. *Polyhedron* **2018**, *156*, 64–71.

(23) Rohani, S.; Ziarati, A.; Ziarani, G. M.; Badiei, A.; Burgi, T. Engineering of Highly Active Au/Pd Supported on Hydrogenated Urchin-like Yolk@shell TiO_2 for Visible Light Photocatalytic Suzuki Coupling. *Catal. Sci. Technol.* **2019**, *9* (14), 3820–3827.

(24) Xie, Y.; Yan, B.; Xu, H.; Chen, J.; Liu, Q.; Deng, Y.; Zeng, H. Highly Regenerable Mussel-Inspired Fe_3O_4@Polydopamine-Ag Core-Shell Microspheres as Catalyst and Adsorbent for Methylene Blue Removal. *ACS Appl. Mater. Interfaces* **2014**, *6* (11), 8845–8852.

(25) Babu, B.; Koutavarapu, R.; Shim, J.; Kim, J.; Yoo, K. Improved Sunlight-Driven Photocatalytic Abatement of Tetracycline and Photoelectrocatalytic Water Oxidation by Tin Oxide Quantum Dots Anchored on Nickel Ferrite Nanoplates. *J. Electroanal. Chem.* **2021**, *900* (July 2020), 115699.

(26) Tran, C. Van; La, D. D.; Thi Hoai, P. N.; Ninh, H. D.; Thi Hong, P. N.; Vu, T. H. T.; Nadda, A. K.; Nguyen, X. C.; Nguyen, D. D.; Ngo, H. H. New TiO_2-Doped Cu–Mg Spinel-Ferrite-Based Photocatalyst for Degrading Highly Toxic Rhodamine B Dye in Wastewater. *J. Hazard. Mater.* **2021**, *420* (April), 126636.

(27) Kumari, M.; Gupta, R.; Jain, Y. Fe_3O_4 –Glutathione Stabilized Ag Nanoparticles: A New Magnetically Separable Robust and Facile Catalyst for Aqueous Phase Reduction of Nitroarenes. *Appl. Organomet. Chem.* **2019**, *33* (11), 1–11.

(28) Dong, Z.; Le, X.; Li, X.; Zhang, W.; Dong, C.; Ma, J. Silver Nanoparticles Immobilized on Fibrous Nano-Silica as Highly Efficient and Recyclable Heterogeneous Catalyst for Reduction of 4-Nitrophenol and 2-Nitroaniline. *Appl. Catal. B Environ.* **2014**, *158–159*, 129–135.

(29) Hong, M.; Xu, L.; Wang, F.; Xu, S.; Li, H.; Li, C. Z.; Liu, J. In Situ Synthesized Au-Ag Nanocages on Graphene Oxide Nanosheets: A Highly Active and Recyclable Catalyst for the Reduction of 4-Nitrophenol. *New J. Chem.* **2016**, *40* (2), 1685–1692.

(30) Shen, H.; Duan, C.; Guo, J.; Zhao, N.; Xu, J. Facile in Situ Synthesis of Silver Nanoparticles on Boron Nitride Nanosheets with Enhanced Catalytic Performance. *J. Mater. Chem. A* **2015**, *3* (32), 16663–16669.

(31) Liao, G.; Chen, J.; Zeng, W.; Yu, C.; Yi, C.; Xu, Z. Facile Preparation of Uniform Nanocomposite Spheres with Loading Silver Nanoparticles on Polystyrene-Methyl Acrylic Acid Spheres for Catalytic Reduction of 4-Nitrophenol. *J. Phys. Chem. C* **2016**, *120* (45), 25935–

25944.

(32) Kulkarni, S.; Jadhav, M.; Raikar, P.; Raikar, S.; Raikar, U. Core-Shell Novel Composite Metal Nanoparticles for Hydrogenation and Dye Degradation Applications. *Ind. Eng. Chem. Res.* **2019**, *58* (9), 3630–3639.

(33) Nimita Jebaranjitham, J.; Mageshwari, C.; Saravanan, R.; Mu, N. Fabrication of Amine Functionalized Graphene Oxide – AgNPs Nanocomposite with Improved Dispersibility for Reduction of 4-Nitrophenol. *Compos. Part B Eng.* **2019**, *171* (February), 302–309.

(34) Chang, S.; Liu, C.; Sun, Y.; Yan, Z.; Zhang, X.; Hu, X.; Zhang, H. Fe_3O_4 Nanoparticles Coated with Ag-Nanoparticle-Embedded Metal-Organic Framework MIL-100(Fe) for the Catalytic Reduction of 4-Nitrophenol. *ACS Appl. Nano Mater.* **2020**, *3* (3), 2302–2309.

(35) Wang, Y.; Gao, P.; Wei, Y.; Jin, Y.; Sun, S.; Wang, Z.; Jiang, Y. Silver Nanoparticles Decorated Magnetic Polymer Composites (Fe_3O_4@PS@Ag) as Highly Efficient Reusable Catalyst for the Degradation of 4-Nitrophenol and Organic Dyes. *J. Environ. Manage.* **2021**, *278* (P1), 111473.

(36) Antonels, N. C.; Meijboom, R. Preparation of Well-Defined Dendrimer Encapsulated Ruthenium Nanoparticles and Their Evaluation in the Reduction of 4-Nitrophenol According to the Langmuir-Hinshelwood Approach. *Langmuir* **2013**, *29* (44), 13433–13442.

(37) Sravanthi, K.; Ayodhya, D.; Swamy, P. Y. Green Synthesis, Characterization and Catalytic Activity of 4-Nitrophenol Reduction and Formation of Benzimidazoles Using Bentonite Supported Zero Valent Iron Nanoparticles. *Mater. Sci. Energy Technol.* **2019**, *2* (2), 298–307.

(38) Bhaduri, B.; Dikshit, A. K.; Kim, T. Y.; Tripathi, K. M. Research Progress and Prospects of Spinel Ferrite Nanostructures for the Removal of Nitroaromatics from Wastewater. *ACS Appl. Nano Mater.* **2022**, *5* (11), 16000–16026.

6.7. Selected NMR (^{1}H & ^{13}C) spectra of product in Reduction of nitro compounds

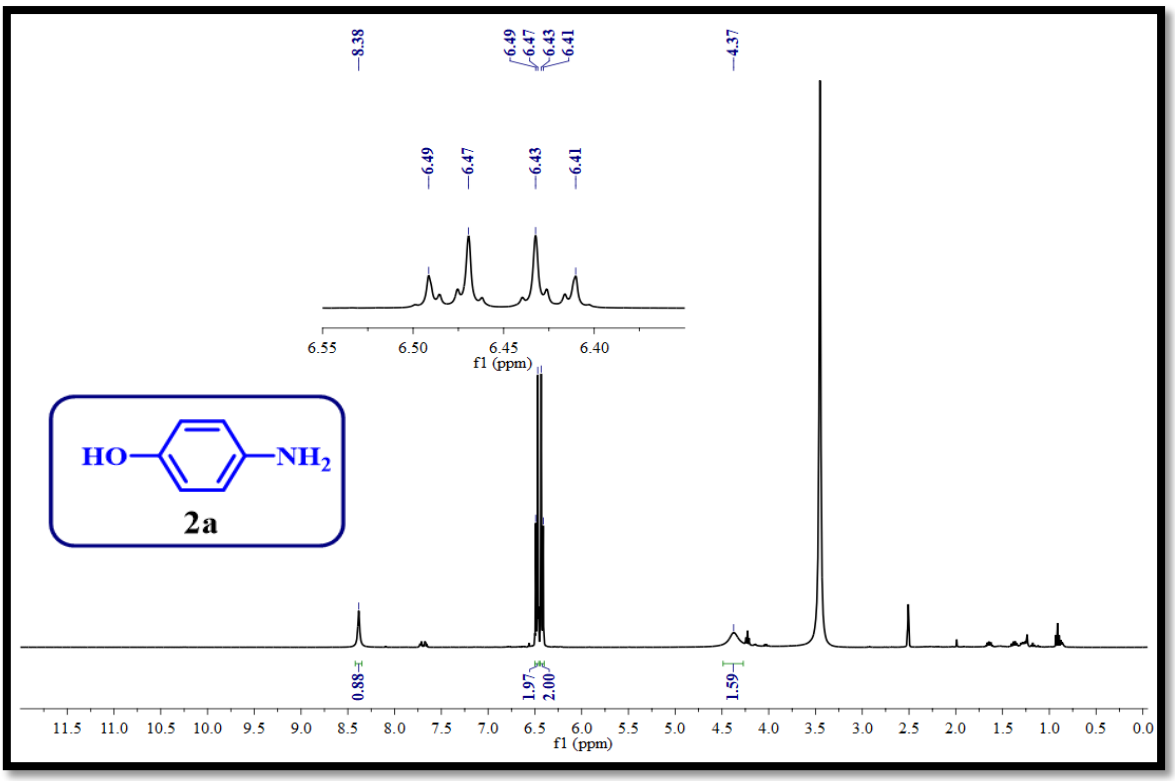

^{1}H NMR spectrum of the compound 4-aminophenol (2a)

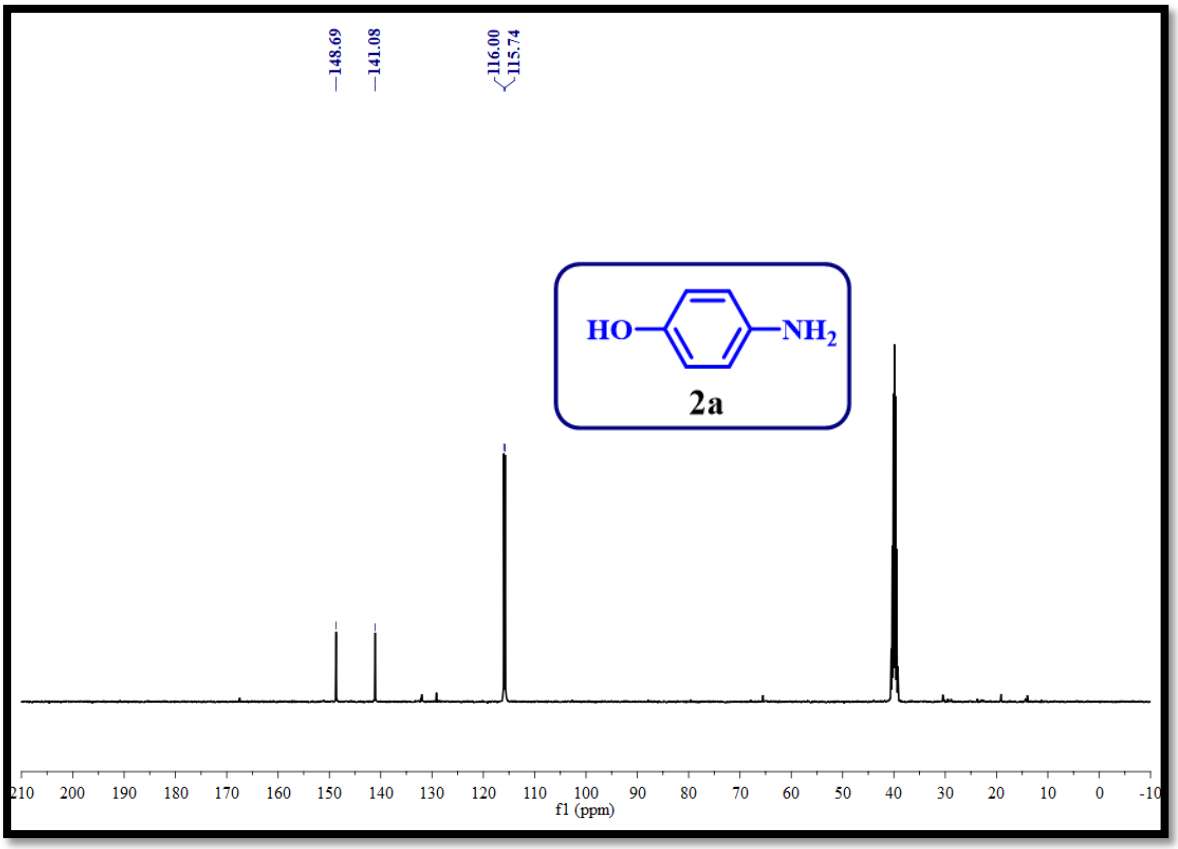

^{13}C NMR spectrum of the compound 4-aminophenol (2a)

CHAPTER-VII

Summary and Conclusions

Chapter-VII

Summary and Conclusions

7.1. Details of the Thesis work

This chapter consists of a summary and conclusion of the present research work and the thesis comprises seven chapters with the following details.

Chapter-I	:	General introduction, the background of the work, objectives, synthesis methods, and analytical techniques employed for the characterization of the synthesized materials
Chapters II to VI:		Original research work on the synthesis and systematic study and applications of various ferrites/ferrite-based reusable heterogeneous nanocatalysts for diverse organic transformations
Chapter-VII	:	Summary and Conclusions

7.2. Conclusions

During the course of this research work, numerous conclusions have been made with regard to the design and development of a variety of ferrite-based reusable heterogeneous nanocatalysts for different organic applications.

Chapter-I

This chapter dealt with the general background of the need for heterogeneous magnetic nanocatalysts,[1,2] development of ferrites/surface modified ferrite based heterogeneous nanocatalysts[3,4] for some important organic transformations. It described the advantages of surface modification of ferrites and their use in chemical catalysis, photocatalysis, and methods adopted for surface modification. It has described the literature review on surface functionalization of spinel ferrites, photocatalytic applications of spinel ferrites, and ferrite-based nanophotocatalyst in dye degradation and organic transformations. This chapter has presented the scope of the work and clear objectives of the research work. It has also described various synthesis methods used for the synthesis of nanoferrites, advantages and disadvantages associated with methods of synthesis of spinel ferrites so that the best suitable method can be chosen for the synthesis of spinel ferrites for a specific application with desired properties. This chapter has elaborated various analytical techniques used for the characterization of the synthesized materials. In specific, it has dealt with the significance, principle and procedure of variety of characterization techniques such as PXRD, FTIR, SEM, FESEM, TEM, EDAX, XPS, VSM, UV-Vis DRS, ICP-OES. Further, the mechanism of photocatalysis was also explained.

Chapter-II

Palladium-Supported Polydopamine-Coated $NiFe_2O_4@TiO_2$: A Sole Photocatalyst for Suzuki and Sonogashira Coupling Reactions under Sunlight Irradiation

Organic reactions involving C-C bond coupling (Suzuki and Sonogashira) are extremely significant with convenient approaches in synthetic organic chemistry in the preparation of natural products, pharmaceutical drugs and functional conjugated organic molecular materials etc.[5,6]

This chapter dealt with the synthesis of Palladium-Supported Polydopamine-coated $NiFe_2O_4@TiO_2$ as a sole photocatalyst ($NiFe_2O_4@TiO_2$@PDA-Pd) by a four-step procedure for Suzuki and Sonogashira Coupling Reactions under sunlight irradiation. This photocatalyst was synthesised, and analysed with various appropriate characterization techniques like PXRD, FT-IR, SEM, EDAX, TEM, XPS, VSM, UV–Vis DRS, ICP-OES. The photocatalytic activity of synthesised nanocatalyst under sunlight irradiation was investigated for both Suzuki and Sonogashira coupling reactions, where it worked excellently well with a high yield of the product up to 98% and 96% respectively.

Unique features of the synthesized catalyst were i) Its effective performance for both the aforesaid coupling reactions under ambient reaction conditions with a short reaction time in polar protic solvents (Ethanolic water/EtOH) with good yield without any byproduct ii) Magnetic retrieval of catalyst from the reaction mixture employing an external magnet iii) Reusability of the retrieved catalyst up to 5 consecutive runs without appreciable diminution of catalytic efficacy iv) Good stability with less leaching of the metal as confirmed by XRD, FT-IR and ICP-OES analysis of the recovered catalyst v) Use of the catalyst in a sustainable greener approach.

Application of the catalyst in Suzuki Coupling Reaction

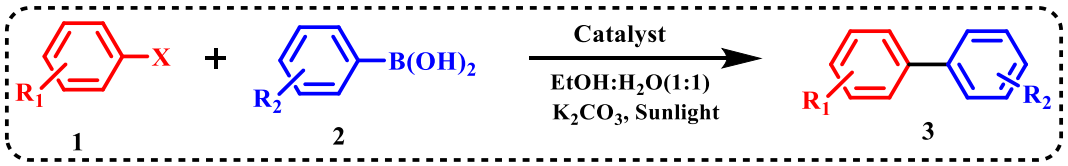

In Suzuki coupling reaction, the substrate scope was assessed by synthesizing 12 desired compounds (3a-l) using various aryl halides, and phenylboronic acids. The obtained yield of the compounds was in the range of 52-98%. Further, these synthesized compounds were well characterized using ^{1}H NMR, ^{13}C NMR spectral data.

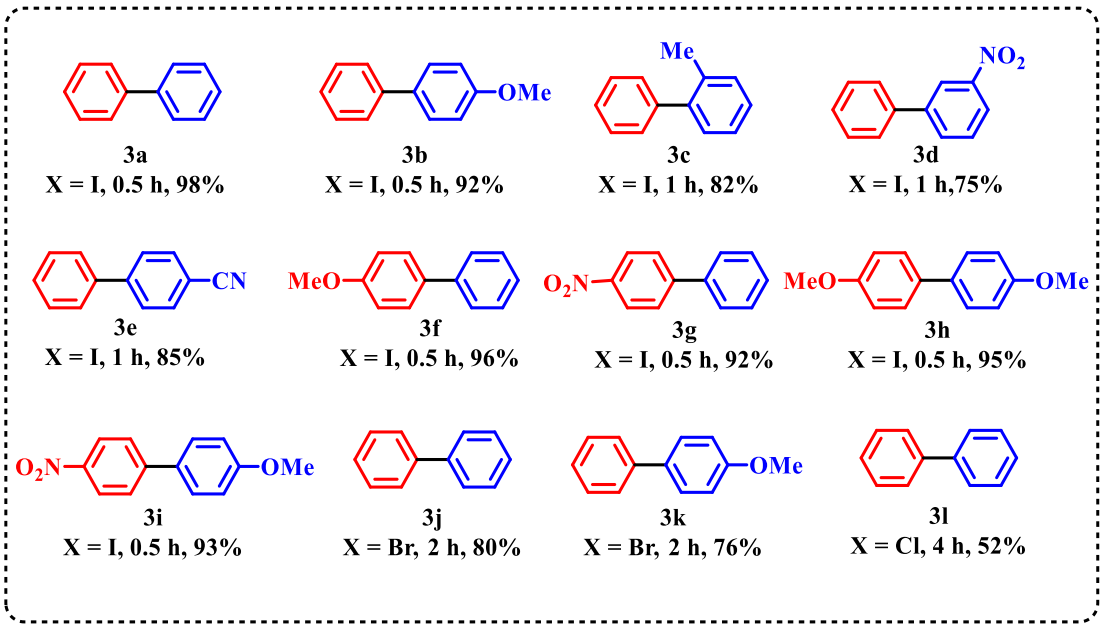

Reaction conditions: aryl halides (1.0 mmol), phenylboronic acids (1.5 mmol), $NiFe_2O_4$@TiO_2@PDA-Pd catalyst (5 mg), and K_2CO_3 (2.5 mmol) in EtOH:H_2O (3 mL) under direct sunlight at 30 °C.

Application of the catalyst in Sonagashira Coupling Reaction

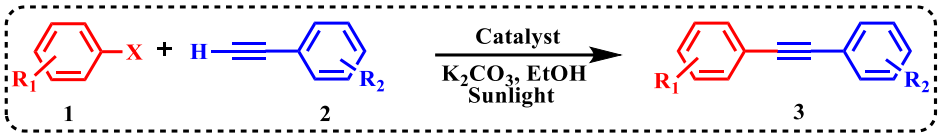

In the Sonogashira coupling reaction, the substrate scope was assessed by synthesizing 10 desired compounds (3a-j) using various aryl halides and phenyl acetylenes. The obtained yield of the compounds was in the range of 60-96%. Further, synthesized compounds were well characterized using ^{1}H NMR, ^{13}C NMR spectral data.

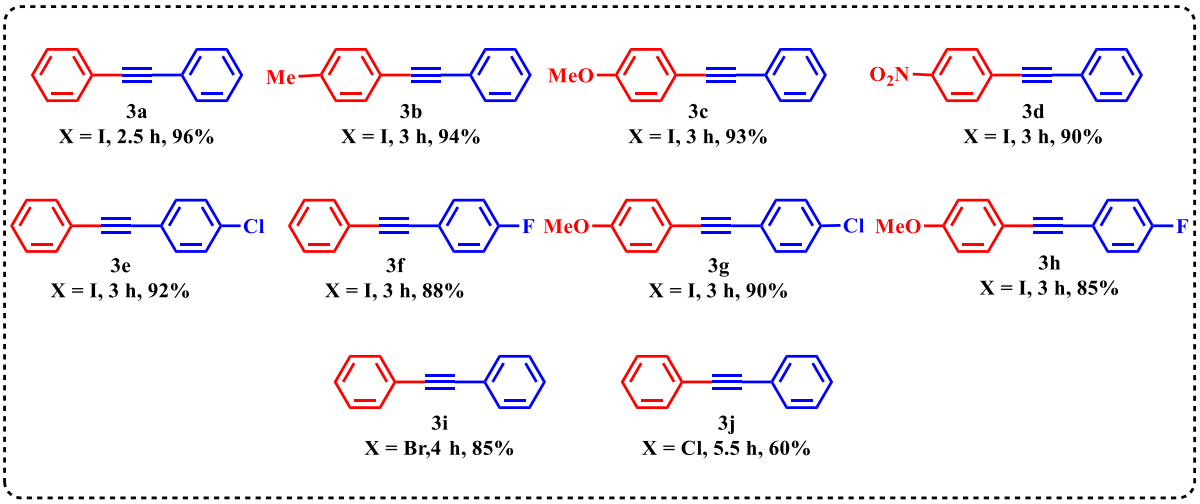

Reaction conditions: aryl halides (1.0 mmol), phenylacetylene (1.3 mmol), $NiFe_2O_4$@TiO_2@PDA-Pd catalyst (10 mg), and K_2CO_3 (2 mmol) in EtOH (3 mL) under direct sunlight at 30 °C.

Chapter-III

Direct Ortho-C-H Arylation of Benzamides/Benzoic Acids with Aryl halides Catalyzed by Pyridine-2-carboimine Pd-complex Immobilized on Amine Functionalized Magnetic Nanoparticles

The biaryl subunit is an important structural motif for the synthesis of a variety of natural products, biologically active pharmaceuticals, polymers, metal ligands for catalysis, and liquid crystals. The most efficient and well-known cross-coupling techniques used for creating aryl-aryl bonds usually require the pre-functionalized starting materials and auxiliary ligands that are often expensive or difficult to prepare. Recent years have seen a lot of interest in transition-metal-catalyzed direct arylation, which builds C-C bonds by cleaving aromatic C-H bonds. Compared to standard protocols, C-H arylation, which entails mixing an aryl halide (C_{Ar-X}) and an arene (C_{Ar-H}) to cause the cleavage of the sp2 C-H bond in order to create C-C bonds, is emerging as a more environmentally friendly, productive, and cost-effective methodology to make biaryls.[12,13,14,15] In the recent past, pyridyl,[16,17] acylamino,[18,19] oxazolyl,[20,21] carboxyl,[22,23] hydroxyl,[24,25] and oxime [26,27] were commonly employed as directing groups in the arene to facilitate C–H activation through intermolecular arylation in the formation of C–C bonds.

In this chapter, pyridine-2-carboimine Pd-complex immobilized on amine functionalized magnetic nanoparticles (Fe_3O_4-DA-2Py-Pd) as a magnetically recoverable catalyst was successfully synthesized for the first time for aromatic C-H activation by a four-step procedure. The synthesized catalyst was characterized by PXRD, FT-IR, FESEM-EDX, XPS, TEM, and VSM.

The unique features of the prepared catalyst were i) First magnetically recoverable nanocatalyst used for the direct ortho-C-H arylation of both benzoic acids and benzamides by aryl halides ii) An efficient and ligand free nanocatalyst iii) Magnetic retrieval of catalyst from the reaction mixture employing an external magnet iv) Reusability of the catalyst up to 5 consecutive runs after magnetic recovery without significant loss in catalytic activity v) Good structural stability of the catalyst as confirmed by XRD and FT-IR analysis of the recovered catalyst vi) Use of the catalyst in a sustainable greener approach.

Application of the catalyst for ortho-Arylation of Benzamide by Aryl halide

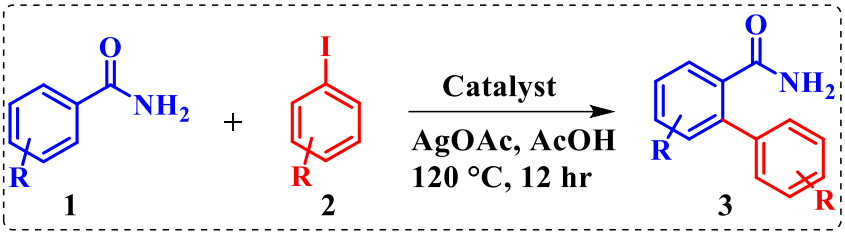

In the ortho-Arylation of benzamide, the substrate scope was assessed by synthesizing 10 desired compounds (3a-j) using various benzamides and aryl halides. The obtained yield of the compounds was in the range of 61-82%. Further, synthesized compounds were well characterized using ^{1}H NMR, ^{13}C NMR spectral data.

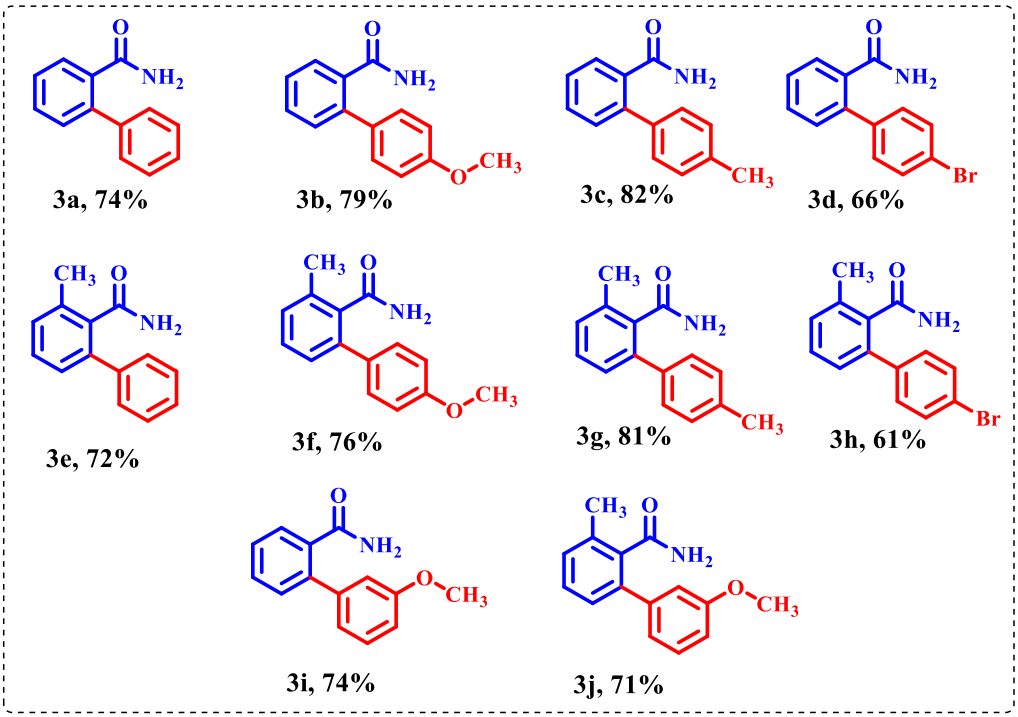

Reaction conditions: benzamides (1 mmol), aryl halides (2 mmol), AgOAc (2 mmol), catalyst (20 mg), and AcOH (3 mL) in 120 °C, 12 h.

Application of the catalyst for ortho-Arylation of Benzoic acid by Aryl halide

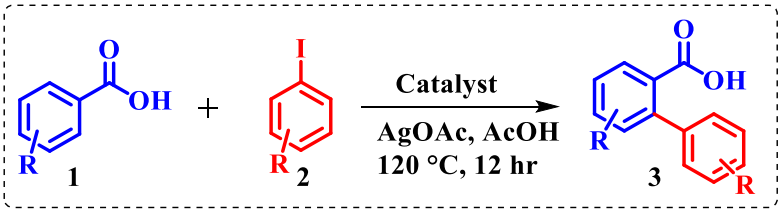

In the ortho-Arylation of benzoic acid, the substrate scope was assessed by synthesizing 10 desired compounds (3a-j) using various benzoic acids and aryl halides. The obtained yield

of the compounds was in the range of 72-88%. Further, synthesized compounds were well characterized using ^{1}H NMR, ^{13}C NMR spectral data.

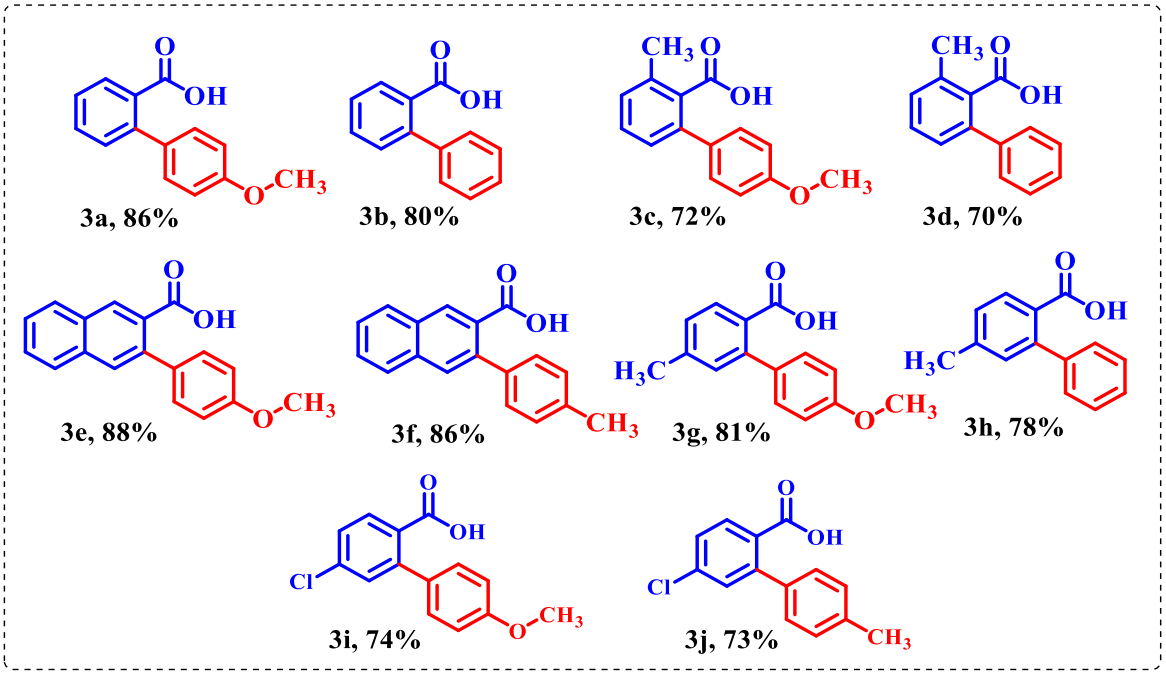

Reaction conditions: benzoic acids (1 mmol), aryl halides (2 mmol), AgOAc (2 mmol), catalyst (20 mg), and AcOH (3 mL) in 120 °C, 12 h.

Chapter-IV

Magnetically Reusable $CuFe_2O_4$ Nanocatalyst for its Dual Catalytic Action in Sonogashira and Chan-Lam Coupling Reactions

Reactions comprising of C-C and C-N bond development gained much attention owing to their significance in the synthetic organic chemistry for the generation of a wide range of complex compounds such as drugs, bioactive molecules, natural products, pharmaceuticals and so forth from simpler units. In C-C coupling, Sonogashira coupling reactions are extremely significant with convenient approaches in the preparation of natural products, pharmaceutical drugs and functional conjugated organic molecular materials etc.[5,6] Usually they demand Pd based catalysts for this purpose which are expensive.

C-N coupling reaction (Chan-Lam) involving arylamine synthesis by amination (N-arylation) is a significant research area in synthetic organic chemistry owing to their numerous uses in the generation of bioactive compounds, HIV-protease inhibitors, heterocycles, medicinally important compounds, and natural products, etc.[9,10] Usually copper based homogeneous catalysts are reported for this purpose which are not reusable.

In this chapter, magnetically recoverable $CuFe_2O_4$ nanocatalyst was successfully synthesized by co-precipitation method in single-step for both Sonogashira and Chan-Lam

coupling reactions with a good product yield up to 96% and 95% respectively. The synthesized catalyst was characterized by PXRD, FT-IR, SEM and VSM.

The unique characteristic features of the synthesized nanocatalyst were i) It is simple and effective for both Pd-free Sonogashira reaction and base-free Chan-Lam coupling reaction (dual application) under ambient reaction conditions in Green solvents such as EtOH and EtOH:H_2O (1:1) ii) Magnetic recovery of catalyst from the reaction mixture with the aid of an external magnet iii) Reusability of the recovered catalyst up to 5 consecutive runs without significant loss of catalytic efficacy iv) Good structural stability as confirmed by XRD and FT-IR analysis of the recovered catalyst v) Use of the catalyst in a sustainable greener approach.

Application of catalyst for Sonagashira Coupling Reaction

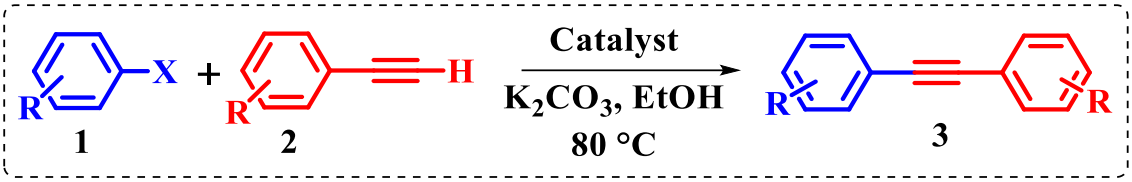

In the Sonogashira coupling reaction, the substrate scope of the catalyst was assessed by synthesizing 8 desired compounds (3a-h) using various aryl halides and phenyl acetylenes. The obtained yield of the compounds was in the range of 56-96%. Further, synthesized compounds were well characterized using ^{1}H NMR, ^{13}C NMR spectral data.

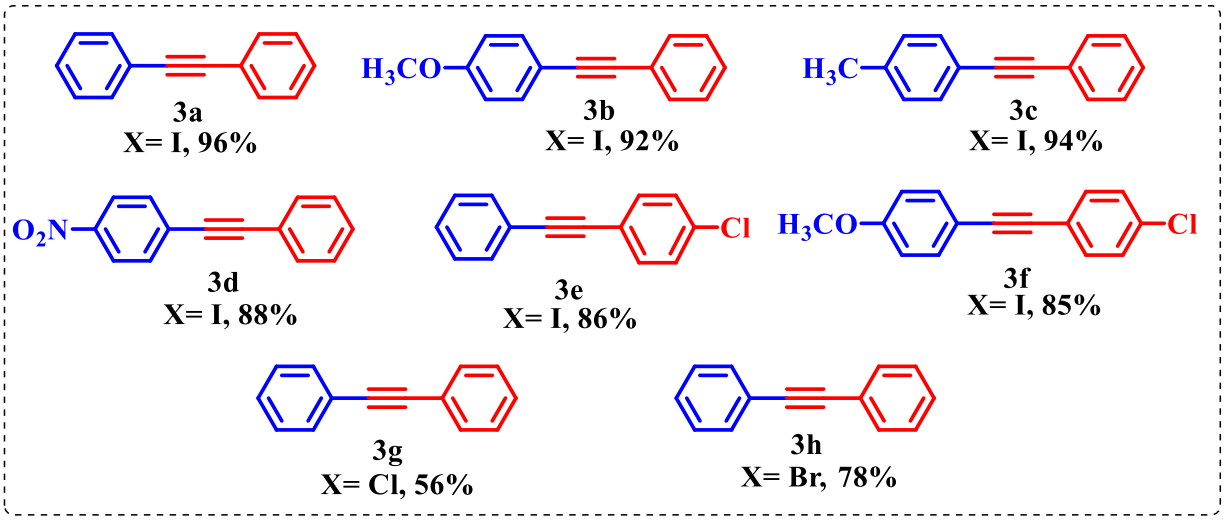

Reaction conditions: aryl halide (1.0 mmol), phenylacetylenes (1.5 mmol), $CuFe_2O_4$ catalyst (20 mg) and K_2CO_3 (2 mmol) in EtOH (3 mL)

Application of the catalyst for Chan-Lam Coupling Reaction

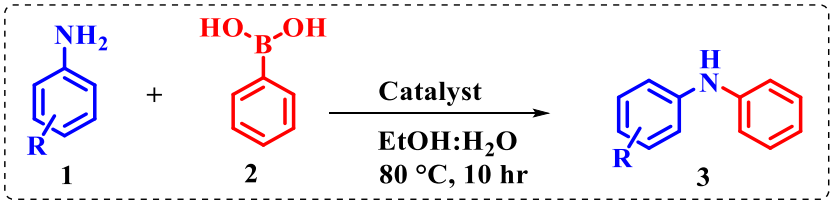

In the Chan-Lam coupling reaction, the substrate scope of the catalyst was assessed by synthesizing 8 desired compounds (3a-h) using various aryl amines, phenyl boronic acids. The obtained yield of the compounds was in the range of 82-95%. Further, synthesized compounds were well characterized using ^{1}H NMR, ^{13}C NMR spectral data.

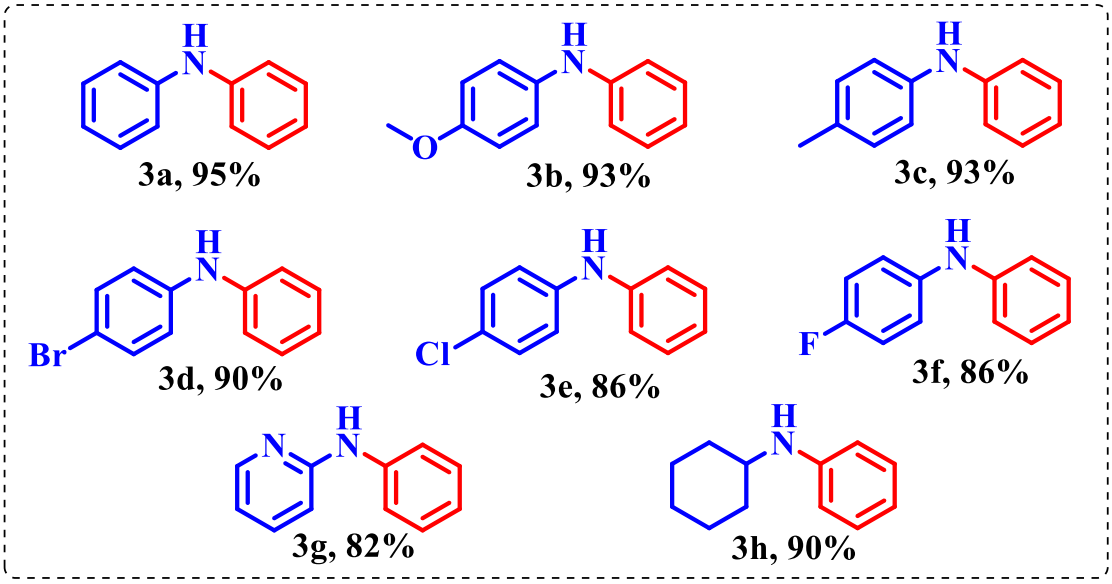

Reaction conditions: amine (1.0 mmol), phenylboronic acid (1.5 mmol), $CuFe_2O_4$ catalyst (25 mg) in EtOH:H_2O (3 mL)

Chapter-V

Synthesis of Cu Supported Fe_3O_4-NH_2 Nanocatalyst for One Pot Three-Component (A^3) Coupling Reaction

A^3 Coupling Reaction is a one-pot three-component condensation (Mannich type reaction) between an amine, an aldehyde and alkyne to produce Propargylamines with atom economy. Propargylamines are diverse substances that are widely used as intermediates for building nitrogen-containing heterocycles such as natural products and biologically active molecules. In the process of formation of the product, activation of alkyne C-H bond is an important step for which the selection of an appropriate catalyst is crucial.[11,12]

In this chapter, Cu supported amine functionalized ferrite nanocatalyst (Fe_3O_4-NH_2-Cu) was successfully synthesized by a two-step procedure for one-pot three component (A^3) coupling reaction with a good product yields of 97%. The synthesized catalyst was characterized by PXRD, FT-IR, FESEM-EDX, XPS, and VSM.

The unique characteristic features of the synthesized nanocatalyst were i) Effective performance of the catalyst under solvent free condition ii) Magnetic recovery of the catalyst with the aid of an external magnet iii) Reusability of the recovered catalyst for five consecutive runs without significant loss in catalytic activity iv) Good structural stability of the catalyst as confirmed by XRD and FT-IR analysis of the recovered catalyst v) Use of the catalyst in a sustainable greener approach.

Application of the catalyst for A^3 coupling reaction

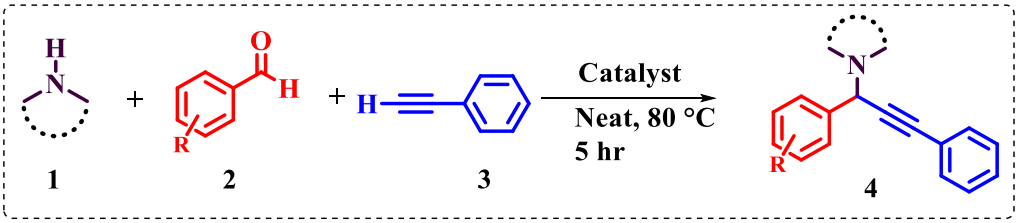

In this one pot three component (**A^3**) coupling reaction for the synthesis of propargylamines, the substrate scope of the catalyst was assessed by synthesizing 9 desired compounds (4a-i) using various amines, aryl benzaldehydes, phenyl acetylenes. The obtained yield of the compounds was in the range of 89-98% yields. Further, synthesized compounds were well characterized using ^{1}H NMR, ^{13}C NMR spectral data.

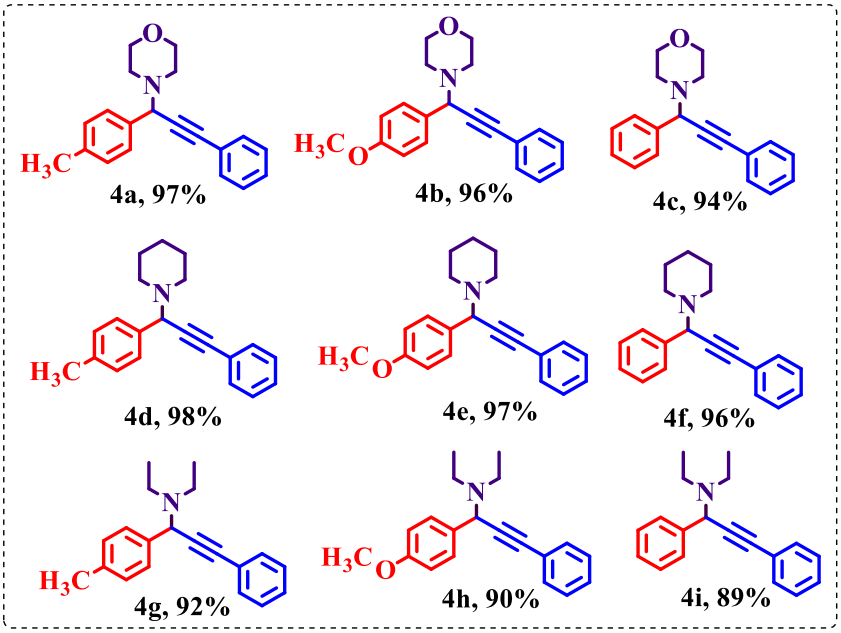

Reaction conditions: amines (1.0 mmol), aryl benzaldehyde (1.0 mmol), phenyl acetylene (1.5 mmol), Fe_3O_4-NH_2-Cu catalyst (15 mg), and solvent free condition, 80 °C temperature, 5 h

Chapter-VI

Immobilization of Ag Nanoparticles on $NiFe_2O_4$@TiO_2@PDA for Reduction of Nitro Aromatic Compounds

The reduction of nitro aromatic compounds to synthesize corresponding anilines has attracted a lot of interest because anilines are crucial intermediates in the production of drugs, dyes, polymers, and fine chemicals. Among nitro aromatic compounds, 4- nitrophenol (4-NP) is listed as 'priority toxic pollutant' by the United States Environmental Agency, because it will cause serious risk to both animal and human and can be hardly removed through natural degradation.[13,14]

In this chapter, a highly efficient Ag immobilized polydopamine coated $NiFe_2O_4$@TiO_2 as a heterogeneous magnetic nanocatalyst ($NiFe_2O_4$@TiO_2@PDA-Ag) was developed for the catalytic reduction of nitro aromatic compounds to the corresponding amines using $NaBH_4$ in water as solvent with high product yield of 99 %. A multistep procedure was adopted to synthesize the $NiFe_2O_4$@TiO_2@PDA-Ag nanocatalyst. The synthesized catalyst was characterized by PXRD, FT-IR, UV-Vis. DRS, SEM-EDX, TEM, XPS, and VSM.

The catalyst exhibited good catalytic activity and high selectivity in the catalytic reduction of a series of substituted nitroaromatic compounds. The catalytic performance of the catalyst has been explored in the reduction of 4-NP to 4-aminophenol (4-AP) at room temperature in an aqueous medium in the presence of $NaBH_4$ as a reducing agent. The kinetic study of the reaction was performed by UV-Visible spectroscopy which confirms the pseudo first order kinetics of the reaction with a rate constant of 0.462 min^{-1}.

The unique characteristic features of the synthesized nanocatalyst were i) Effective performance of the catalyst under ambient conditions (rt and water as a solvent) ii) Magnetic recovery of the catalyst with the aid of an external magnet iii) Reusability of the recovered catalyst for five consecutive runs without significant loss in catalytic activity iv) Good structural stability of the catalyst as confirmed by XRD and FT-IR analysis of the recovered catalyst v) Use of the catalyst in a sustainable greener approach

Application of the catalyst for Reduction of Nitroaromatic Compounds

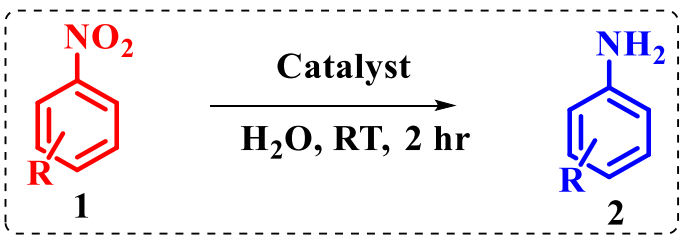

In the reduction reaction of nitroaromatic compound, the substrate scope of the catalyst was assessed by synthesizing 9 desired compounds (2a-i) using various nitro aromatic compounds. The obtained yield of the compounds was in the range of 78-96% yields. Further, synthesized compounds were well characterized using ^{1}H NMR, ^{13}C NMR spectral data.

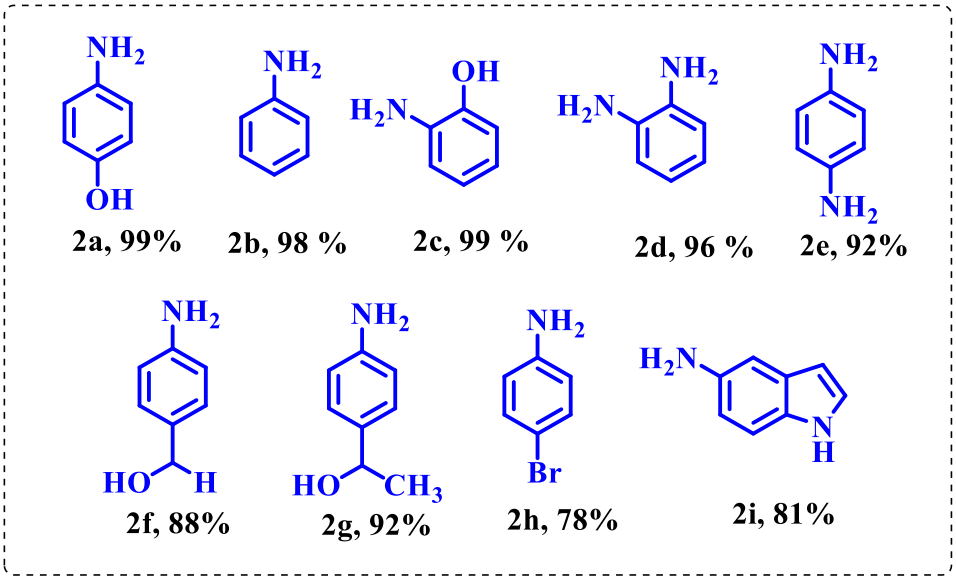

Reaction conditions: nitro compound (0.5 mmol), sodium borohydride (5 mmol), $NiFe_2O_4$@TiO_2@PDA-Ag catalyst (15 mg) Water 10 mL at rt, 2 h.

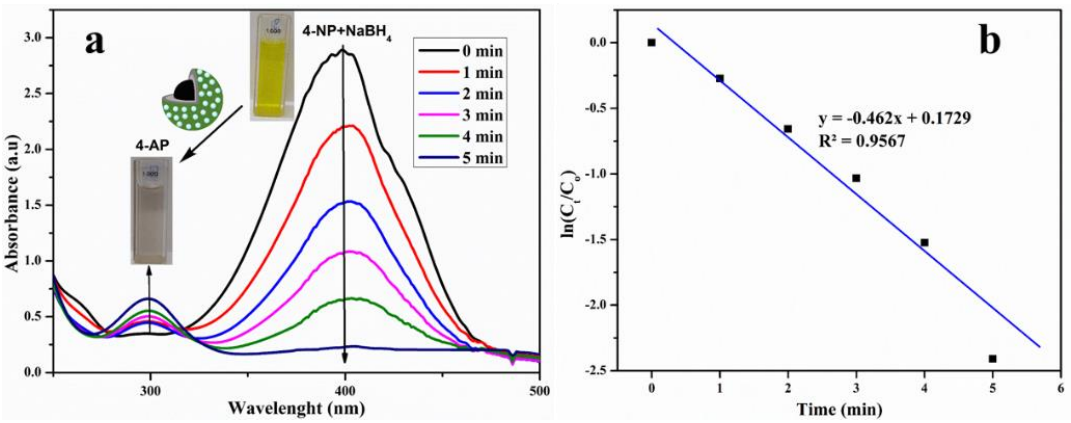

UV-Vis spectra for the reduction of 4-NP to 4-AP and plot of $ln(C_t/C_0)$ vs reaction time (t)

Reaction conditions: 4-NP (0.5 ml, 30 mM), sodium borohydride (1 mL, 300 mM), $NiFe_2O_4$@TiO_2@PDA-Ag catalyst (5 mg) Water 10 mL at rt 5min.

7.3. References

(1) Varma, R. S. Nano-Catalysts with Magnetic Core: Sustainable Options for Greener Synthesis. *Sustain. Chem. Process.* **2014**, *2* (1),

(2) Nasir Baig, R. B.; Varma, R. S. A Highly Active Magnetically Recoverable Nano Ferrite-Glutathione-Copper (Nano-FGT-Cu) Catalyst for Huisgen 1,3-Dipolar Cycloadditions. *Green Chem.* **2012**, *14* (3), 625–632.

(3) Baig, R. B. N.; Varma, R. S. A Facile One-Pot Synthesis of Ruthenium Hydroxide Nanoparticles on Magnetic Silica: Aqueous Hydration of Nitriles to Amides. *Chem. Commun.* **2012**, *48* (50), 6220–6222.

(4) Schneider, J.; Matsuoka, M.; Takeuchi, M.; Zhang, J.; Horiuchi, Y.; Anpo, M.; Bahnemann, D. W. Schneider et Al. - 2014 - Understanding TiO_2 Photocatalysis Mechanisms and Materials(2).Pdf. *Chem. Rev.* **2014**, *114* (9), 9919−9986.

(5) Elhage, A.; Lanterna, A. E.; Scaiano, J. C. Light-Induced Sonogashira C-C Coupling under Mild Conditions Using Supported Palladium Nanoparticles. *ACS Sustain. Chem. Eng.* **2018**, *6* (2), 1717–1722.

(6) Shafiei, N.; Nasrollahzadeh, M.; Baran, T.; Baran, N. Y.; Shokouhimehr, M. Pd Nanoparticles Loaded on Modified Chitosan-Unye Bentonite Microcapsules: A Reusable Nanocatalyst for Sonogashira Coupling Reaction. *Carbohydr. Polym.* **2021**, *262* (January), 117920.

(7) Li, D. D.; Yuan, T. T.; Wang, G. W. Palladium-Catalyzed Ortho-Arylation of Benzamides via Direct Sp2 C-H Bond Activation. *J. Org. Chem.* **2012**, *77* (7), 3341–3347.

(8) Parsharamulu, T.; Venkanna, D.; Lakshmi Kantam, M.; Bhargava, S. K.; Srinivasu, P. The First Example of Ortho -Arylation of Benzamides over Pd/Mesoporous Silica: A Novel Approach for Direct Sp2 C-H Bond Activation. *Ind. Eng. Chem. Res.* **2014**, *53* (52), 20075–20084.

(9) Kumari, S.; Pathak, D. D. Synthesis and Development of Chitosan Anchored Copper (II) Schiff Base Complexes as Heterogeneous Catalysts for N-Arylation of Amines. *Tetrahedron Lett.* **2015**, *56* (27), 4135–4142.

(10) Sanjeeva, K.; Wu, T. Chan e Lam Coupling Reactions : Synthesis of Heterocycles. *Tetrahedron* **2012**, *68* (38), 7735–7754.

(11) Terra, J. C. S.; Moores, A.; Moura, F. C. C. Amine-Functionalized Mesoporous Silica as a Support for on-Demand Release of Copper in the A^3-Coupling Reaction: Ultralow Concentration Catalysis and Confinement Effect. *ACS Sustain. Chem. Eng.* **2019**, *7* (9), 8696–8705.

(12) Chinna Rajesh, U.; Purohit, G.; Rawat, D. S. One-Pot Synthesis of Aminoindolizines and Chalcones Using CuI/CSP Nanocomposites with Anomalous Selectivity under Green Conditions. *ACS Sustain. Chem. Eng.* **2015**, *3* (10), 2397–2404.

(13) Kumari, M.; Gupta, R.; Jain, Y. Fe_3O_4 – Glutathione Stabilized Ag Nanoparticles: A New Magnetically Separable Robust and Facile Catalyst for Aqueous Phase Reduction of Nitroarenes. *Appl. Organomet. Chem.* **2019**, *33* (11), 1–11.

(14) Roy, S. Photocatalytic Materials for Reduction of Nitroarenes and Nitrates. *J. Phys. Chem. C* **2020**, *124* (52), 28345–28358.

List of Publications, Conferences, Workshops and Curriculum Vitae

List of Publications

Published

1. Palladium-Supported Polydopamine-Coated $NiFe_2O_4$@TiO_2: A Sole Photocatalyst for Suzuki and Sonogashira Coupling Reactions under Sunlight Irradiation
   Prashanth Goud Banda, Raghasudha Mucherla. *ACS Omega.* **2022**, *7*, 29356-29368.

2. Immobilization of Ag Nanoparticles on $NiFe_2O_4$@TiO_2@PDA: Multifunctional Catalytic Action toward the Reduction of 4-Nitrophenol, and Photodegradation of Methylene Blue and Ciprofloxacin
   Prashanth Goud Banda, Gayathri Bindu Kurup, Raghasudha Mucherla. *Journal of Physics and Chemistry of Solids.* **2022**,*181*, 111556.

3. Magnetically Reusable $CuFe_2O_4$ Nanocatalyst for its Dual Catalytic Action in Sonogashira and Chan-Lam Coupling Reactions,
   Prashanth Goud Banda, Gayathri Bindu Kurup, Raghasudha Mucherla (Under Review in Journal of Organometallic Chemistry)

4 Direct Ortho-C-H Arylation of Benzoic Acids/Benzamides with Aryl halides catalyzed by Pyridine-2-carboimine Pd-complex immobilized on amine functionalized magnetic nanoparticles
   Prashanth Goud Banda, Gayathri Bindu Kurup, Raghasudha Mucherla (Submitted to ACS Sustainable Chemistry and Engineering)

Manuscripts under preparation

1. Synthesis of Cu-Supported Fe_3O_4-NH_2 Nanocatalyst for One Pot Three-Component (A^3) Coupling Reaction
   Prashanth Goud Banda, Gayathri Bindu Kurup, Raghasudha Mucherla (Manuscript under preparation)

List of International, National Conferences and FDP Programs participated

1. ***International Conference on "Advances in Chemical Sciences and Technologies" (ACST-2019)*** organized by Department of Chemistry, NIT Warangal, during 23rd to 25th September 2019.
2. ***Teaching and learning of advances in physical chemistry through hands-on experiences*** organized by department of chemistry, NIT Warangal, during 17th to 22nd February 2020.
3. ***Teaching and learning of Modern Methods of Organic Chemistry through Hand-on Experience*** organized by department of chemistry NIT Warangal, during 24th to 29th February 2020.
4. Online Two-Day workshop for faculty development program on **"*Light Harvesting for Sustainable Energy*"** organized by Department of Chemistry, NIT Warangal, during 3rd to 4th March 2022.
5. ***National Conference on Recent Advances in Inorganic and Organometallic Chemistry (RADIOC-2023)*** organized by Department of Chemistry, NIT Warangal, during 24th to 25th February 2023.
6. ***International Conference On "Organic and Medicinal Chemistry" (ICOMC-2023)*** organized by Department of Chemistry, NIT Warangal, during 28th to 30th June 2023.

INFORMATION ABOUT THE AUTHOR

Mr. Banda Prashanth Goud
Doctoral Researcher
C/o Dr. M. Raghasudha
Assistant Professor
Department of Chemistry
National Institute of Technology Warangal (NITW)
Warangal-506004, Telangana
+91 - 9491228508
prashanthb@student.nitw.ac.in; prashanthgoudbanda@gmail.com
Gender: Male | Date of Birth: 16-03-1994 | Nationality: Indian |
Marital status: Single

OBJECTIVE:

To enhance my knowledge by being an integral part of a result oriented research team which will utilize my managerial and technical potentials, there by proving to be a productive and trust worthy professional in the advancements of the organization.

Education:

July 2019 – Present:

Doctoral Research Scholar (PhD Student)

Under the Supervision of **Dr. M. Raghasudha,**
Assistant Professor
Department of Chemistry,
National Institute of Technology Warangal,
Telangana, India.

Research Topic: "Development of Ferrite Based Heterogeneous Nanocatalysts for Organic Transformation".

Status: To be awarded (Thesis submitted).

July 2015 – June 2017:

Master of Science (Organic Chemistry)
Telangana University, Telangana, India
Percentage of Marks: **69.38**

June 2012 – June 2015:

Bachelor of Science (Maths, Physics and Chemistry)
Osmania University, Hyderabad, Telangana, India
Percentage of Marks: **77.60**

June 2010 – March 2012:

Intermediate (Maths, Physics, and Chemistry)
Board of Intermediate Education, Andhra Pradesh, India
Percentage of Marks: **68.60**

June 2009 – March 2010:

Secondary School Certificate (High School)
Board of Secondary Education, Andhra Pradesh, India
Percentage of Marks: **73.00**

RESEARCH INTERESTS

- Nanostructured Materials, synthesis and characterization
- Surface modified Ferrite based nanocatalysts
- Development of Ferrite based nanomaterials for diverse applications
- Heterogeneous catalysis
- Photocatalysis
- Organic transformations
- Organic synthesis

JOB-RELATED SKILLS

I am actively involved in innovative and quality research in the field of design and development of novel and efficient Ferrite based nanocatalysts for organic transformations during my doctoral and post-graduation studies. I acquired the following instrumental and computational expertise.

- FTIR Spectrophotometer, PerkinElmer.
- UV-Visible Spectrophotometers, Perkin Elmer, Analytik Jena Specord 205.
- Other small instruments relevant for materials characterization and analysis.
- NMR analysis.
- Origin, ChemDraw Ultra 14.0 etc.
- MENDELEY Reference Manager.

OTHER SKILLS

- Assisted my Research Supervisor and worked in several committees in various conferences and workshops organized by Department of Chemistry, Teaching Learning Centre, and Centre for Advanced Materials (NITW).
- Very good interpersonal and communication skills along with management skills.
- Good experience in writing technical papers, presentations and reports.
- Guided many post-graduate students for their projects.